VERSLAGEN EN VERHANDELINGEN

REPORTS AND TRANSACTIONS

NATIONAAL LUCHT- EN RUIMTEVAART-LABORATORIUM

NATIONAL AERO- AND ASTRONAUTICAL RESEARCH INSTITUTE

AMSTERDAM

*

XXXI - 1965

PREFACE

This volume of Reports and Transactions of the NLR contains a number of reports on crack propagation studies carried out under contract for the Netherlands Aircraft Development Board (NIV). The permission for publication is herewith acknowledged. In addition to the reports which are collected at more or less regular intervals in the volumes of Reports and Transactions, numerous others are published on subjects studied by the NLR. A complete list of publications issued from 1921 through 1963 is available upon request.

Amsterdam, November 1965

A. J. Marx

(Director)

CONTENTS

C. C. L. Class. G 042

REPORT NLR-TR M.2128

Fatigue crack propagation in unnotched and notched aluminium alloy specimens

by

J. SCHIJVE and F. A. JACOBS

Summary

The growth of fatigue cracks in unnotched and notched specimens of unclad 2024-T3 sheet material was observed through two microscopes during fatigue tests. Two types of notched specimens were used, which were geometrically similar ($K_t = 2.66$), having a ratio 1:2.5 of their dimensions. The results give information on the crack growth, mainly in the microcrack range, and the magnitudes of crack rates at low and high fatigue loads. The notch and the size effects are discussed and the significance of the test data for these problems is analysed. The difference between the theoretical and the empirical approaches of the problems is emphasized and some comments are presented on prospects for future developments.

Contents

This investigation has been performed under contract with the Netherlands Aircraft Development Board (N.I.V.)

List of symbols, units and nomenclature.

a — material constant
C_1, C_2 — constants
d — hole diameter
E — Young's modulus
E_s — secant modulus
k — stress intensity factor
K_f — fatigue notch factor
K_{fR} — K_f-value associated with certain R-value, see fig. 42a
K_{fS_m} — K_f-value associated with certain S_m-value, see fig. 42b
K_N — Neuber factor, eq. (6.5)
K_{pl} — plastic stress concentration factor, eq. (6.13)
K_t — elastic stress concentration factor
l — crack length
l_0 — see chapter 5
l_t — see chapter 5
n — number of cycles
Δn — number of cycles after detection of the crack
N — fatigue life
N_c — fatigue life at which crack(s) were detected
N_l — fatigue life to obtain a crack length l
P — load
q — notch sensitivity factor, eq. (6.7)
r — root radius

r,θ	— polar co-ordinates in eq. (6.15)		
R	— stress ratio $= S_{min}/S_{max}$		
S	— stress		
S_a	— stress amplitude		
S_f	— fatigue limit		
S_{f1}	— fatigue limit of unnotched specimen		
S_{fK}	— fatigue limit of notched specimen		
S_m	— mean stress		
S_{max}	— maximum stress	nominal stresses	
S_{min}	— minimum stress	on net area	
S_N	— fatigue strength associated with fatigue life N	(disregarding cracks)	
S_{N1}	— S_N for unnotched specimen		
S_{NK}	— S_N for notched specimen		
S_u	— ultimate tensile strength		
$S_{0.2}$	— yield strength		
w	— specimen width		
α,β,γ	— constants		
χ	— relative stress gradient, fig. 41		

mm = 10^{-3} meter = 0.04 inch; 1 inch = 25.4 mm.

μ = micron = 10^{-6} meter

1 kg/mm^2 = 1,422 psi = 0.635 tsi;
1000 psi = 0.703 kg/mm^2;
1 tsi = 1.574 kg/mm^2

cpm = cycles per minute

1 kc = 1 kilocycle = 1000 cycles

1 mm/kc = crack rate of 1 mm per kc = 1 μ/c

fatigue limit = highest S_a or S_{max}-value for infinite life

fatigue strength = S_a or S_{max}-value for finite life

NLR = Nationaal Lucht- en Ruimtevaartlaboratorium (National Aeronautical and Astronautical Research Institute, Amsterdam)

1 Introduction

Some years ago a literature review (ref. 28) led to the conclusion that reporting the fatigue load and the number of cycles to failure was giving an absolute minimum of information about what occurred in the specimen. Nevertheless, theories on several aspects of the fatigue problem were frequently based on this minimum, for instance for dealing with such problems as the notch effect, the size effect, the accumulation of fatigue damage, scatter etc. An exception was a cumulative damage rule proposed by Langer (ref. 20). He divided the fatigue life in a pre-crack stage and a crack stage and assumed that the cumulative damage rule, which is now known as the Palmgren-Miner rule, was valid for both stages separately. In ref. 28 (see also ref. 35) it was pointed out that several aspects of the fatigue problem could be qualitatively understood if the concept of a pre-crack stage followed by a crack stage was adopted, thus realizing that the two stages can be affected in different ways.

In ref. 28 it was pointed out that a division into a pre-crack stage and a crack stage was a simplification of the actual fatigue phenomenon. Microcracks are nucleated very early in the fatigue life and they are growing for a long time before becoming visible. The terminology could be improved by replacing pre-crack stage and crack stage by microcrack stage and macrocrack stage respectively. The problem of defining the boundary between the latter two stages is obvious and one might ask whether such a division is not somewhat artificial. Anyhow, to give theories on fatigue a more rational background the growth of microcracks to macrocracks and final failure should be incorporated. Since not too much is known quantitatively it was thought worthwhile to undertake an experimental study on the growth of microcracks to final failure. The present report gives the results of this study, the evaluation of the data obtained and their implications for the notch effect and the size effect under fatigue loading.

The following data apply to the tests. Unnotched and notched specimens of an aluminium sheet material (2024-T3) were tested in an axial-load fatigue machine. The notched specimens had a central hole and two sizes were employed, having a size ratio of 1:2.5 Tests were carried out with a zero minimum stress and with various values for the maximum stress in order to cover a large range of endurances. On the fatigue machine two microscopes were fitted for recording the crack growth during the tests.

Experimental details and results are presented in chapters 2 to 5. A discussion of the results and an account of relevant information from the literature are given in chapter 6, which deals with the subjects: (1) the fatigue phenomenon in aluminium alloys, (2) the notch effect and the size effect and (3) scatter, in separate sections. In chapter 7 a number of conclusions is summarized.

2 Specimens

The material of the specimens was 2024-T3 aluminium alloy sheet material in the unclad condition. The nominal composition is 4% Cu, 1.5% Mg, 0.6% Mn,

	Elastic limit	$S_{0.2}$	S_u	Young's modulus	Elongation (gage length 2″)
kg/mm^2	~30	41.6	50.6	7750	17%
ksi	~43	59.2	72.0	11000	

TABLE 1

Results of static tests

Type of specimen			Specimen	S_u kg/mm²	S_u ksi	$S_{0.2}$ kg/mm²	$S_{0.2}$ ksi	Elongation (%)
Tensile testing specimen, width 10 mm, gage length 50 mm (2″)			1A5	50.4	71.7	40.3	57.3	21
			1A5a	50.4	71.7	41.1	58.4	18
			3A46	50.9	72.4	42.1	59.9	16
			1B46	50.8	72.2	42.3	60.2	17
			5B5	51.0	72.5	42.1	59.9	15
			5B5a	50.2	71.4	41.6	59.2	13
			Mean	50.6	72.0	41.6	59.2	17
Fatigue specimens	Unnotched	—	1A42	51.3	72.9			
			1A37	51.3	72.9			
	Notched	Small	1A50	45.6	64.8			
			1A1*	45.8	65.1			
		Large	2A6	46.1	65.6			
			2B4**	46.8	66.5			

* Previously fatigue tested at $S_{max} = 12.5$ kg/mm² until $n = 10^7$ cycles.
** Previously fatigue tested at $S_{max} = 10.0$ kg/mm² until $n = 2.10^7$ cycles.

remainder Al. The sheet material was produced by the Netherlands Aluminium Company. The mechanical properties are given in the table on the previous page below as the mean results of 6 tests.

Detailed results are given in table 1, which also shows results of static tests on the fatigue specimens.

All specimens were cut from two sheets of the same batch. The nominal sheet thickness was 2 mm. Specimens were taken from the sheets in such a way as to exclude any bias on the results originating from the position of specimens in the sheets.

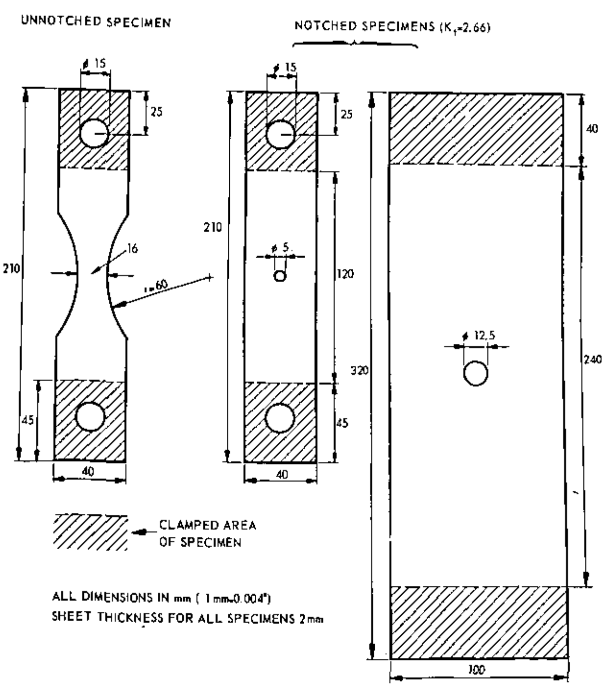

Fig. 1 Dimensions of the specimens.

The dimensions of the specimens are shown in fig. 1. The specimens were first cut to their rectangular form with a slight oversize. Then the edges were milled to the accurate width and length of the specimens. Before milling the reduced section in the unnotched specimens and drilling the holes in the notched specimens the sheets were electro-polished. This was mainly done to obtain a reflective surface, which is required for the observation of small cracks through the microscopes. The holes were drilled and subsequently reamed. The reduced section of the unnotched specimens was milled in such a way as to simulate the cutting action during the reaming of the holes as much as possible.

The ratio of the hole diameter and specimen width was the same for the small and the large notched specimen, being 0.125. According to fig. 69 of ref. 25 a theoretical stress concentration factor $K_t = 2.66$ is then obtained.

For recording the crack propagation after the crack has been detected the notched specimens were provided with very fine scribe-line markings as indicated in fig. 2.

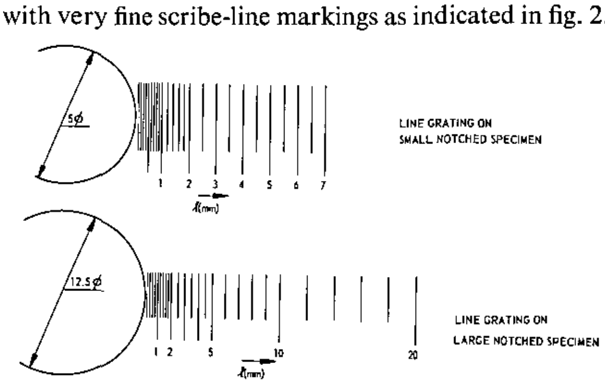

Fig. 2 Line gratings on the notched specimens for recording the crack propagation.

3 Experimental details

Almost all tests were performed on a 10-tons Amsler HFP (High Frequency Pulsator). This is an electromagnetic resonance fatigue machine which was described in ref. 27. The machine can be equipped with dynamometers of 2-tons, 5-tons and 10-tons capacity. For each test the most suitable one in view of the loading accuracy was used. The test frequency was about 4000 cpm. Some tests at high stress levels and short endurances were carried out on a horizontal Schenck-pulsator, type PPD6 with a maximum capacity of 6 tons. This machine is equipped with a high-frequency mechanical resonance system and a low-frequency mechanical screw-drive system. The low frequency drive was used, the loading rate being 15 cpm. On this machine a 2-tons or a 6-tons dynamometer can be installed.

The large notched specimens were clamped in grips belonging to the Amsler machine which do not require any holes in the clamping area of the specimen. A good central mounting of the specimens could be achieved. Mounting of the small notched specimens and the unnotched specimens in the smaller Amsler grips without introducing some bending was troublesome. A special end fixture was then made for this purpose which is shown in fig. 3. The ends of the specimen are clamped

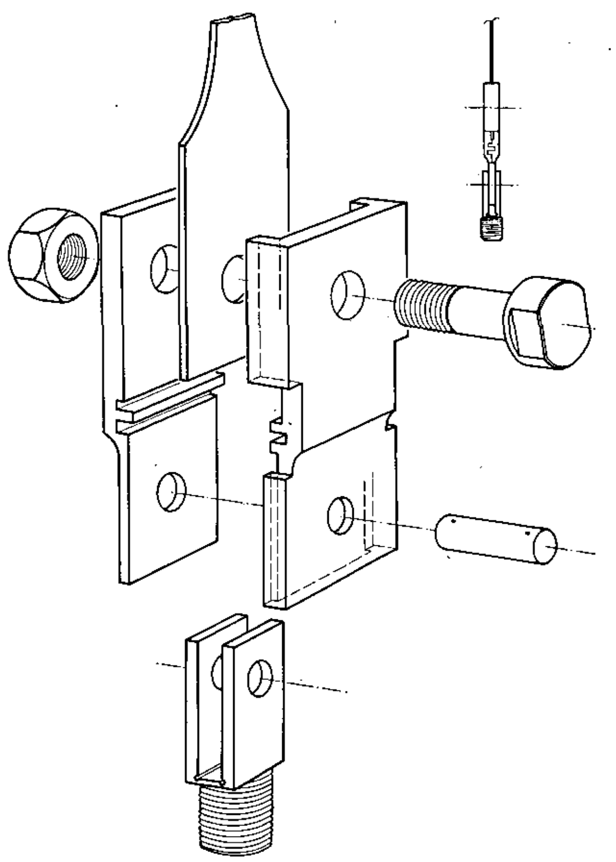

Fig. 3 End fixture for clamping a specimen in fork-ends (NLR-design).

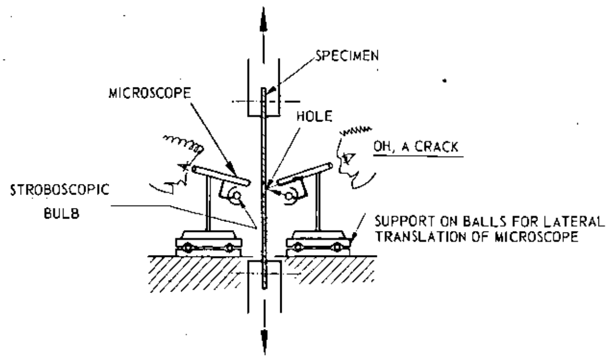

Fig. 4 Schematic view of test set up.

between two clamping plates which can neither rotate nor translate relative to one another. The clamping plates are bolted to the specimen outside the fatigue machine. The specimen with the end fixture is placed in the fatigue machine between two fork-ends. This clamping method proved to work very satisfactorily.

In all tests the minimum load P_{min} had a very small positive value. So the stress ratio $R = S_{min}/S_{max}$ was almost zero. P_{min} for the unnotched, the small notched and the large notched specimens was 20 kg, 20 kg and 50 kg respectively, corresponding to a net stress in the specimens of 0.6, 0.3 and 0.3 kg/mm^2 respectively. All maximum stresses quoted in this report are based on the differences between the maximum and the minimum load.

All tests were carried out with a constant load amplitude and the loading was maintained until complete failure of the specimen. Tests were carried out at several values of the maximum load in order to cover the complete S–N curve starting from very low endurances until $N = 10^7$ cycles. About 45 specimens of each type have been tested.

During the fatigue tests the specimens were continuously examined for cracks by two observers through Leitz stereoscopic binocular microscopes, one at each side of the specimen. A magnification of 30 times has been employed. A stroboscopic bulb was mounted on each microscope in such a way that its light was reflected by the specimen into the microscope. A small frequency shift between the fatigue loading and the stroboscopic light was maintained which introduces a slow breathing action of the cracks as watched through the microscope. This highly facilitates tracing the cracks when they are still very small. In the notched specimens the first crack could start at either the right-hand side or the left-hand side of the hole. Therefore an installation was made which allowed a lateral translation of the microscopes. Only one edge of the hole could be examined at a time and the two edges were examined alternately. A schematic view of the test set up is shown in fig. 4.

In the unnotched specimens the cracks were usually nucleated at the edges. In the vertical direction the length of the area in which the first cracking could occur is much larger than in the notched specimen. A vertical translation of the microscopes had to be made in order to cover the full area prone to crack nucleation. Since searching a specimen in two dimensions is fairly strenuous it was tried to detect the first stage of a crack in the specimen ultrasonically. The critical area of the specimen was automatically scanned by a surface wave probe. The ultrasonic frequency was 2.5 Mc/sec. Cracks were indicated as vertical pips on the screen of an ultrasonic apparatus. Cracks as small as 0.5 mm could be found in this way. Since smaller cracks could be found by the microscopes, the ultrasonic method was, however, dropped later on.

Recording of the crack propagation in the notched specimens was made by noting the number of load cycles at which the crack crossed the line markings on the specimen as shown in fig. 2. The number of cycles at intermediate values of the crack length was sometimes noted in the beginning of the crack propagation. At high values of the length, especially at a high stress, the crack rate became very high. Some automation in recording the number of load cycles was required. This was done by employing a Kelvin and Hughes recorder with four channels. Each observer, while looking through the microscope, pressed pushbuttons when a crack passed a line marking and this was shown on the recorder. Since each observer had to watch two edges of the hole four channels were required. A calibration was made to establish the correlation between 1 cm of the recording and the corresponding number of load cycles of the fatigue machine.

It was not feasible to make a line grating on the unnotched specimens in view of the slight curvature of the edges and the impossibility to predict in which section the crack would start. As soon as the first crack was detected a graduated scale on paper was bonded on the specimen just below the crack. The length of the crack was estimated from the scale which could easily be done with a sufficient accuracy.

4 Test results

4.1 *Endurances*

The applied maximum stresses and the corresponding endurances are presented in tables 2, 3 and 4 for

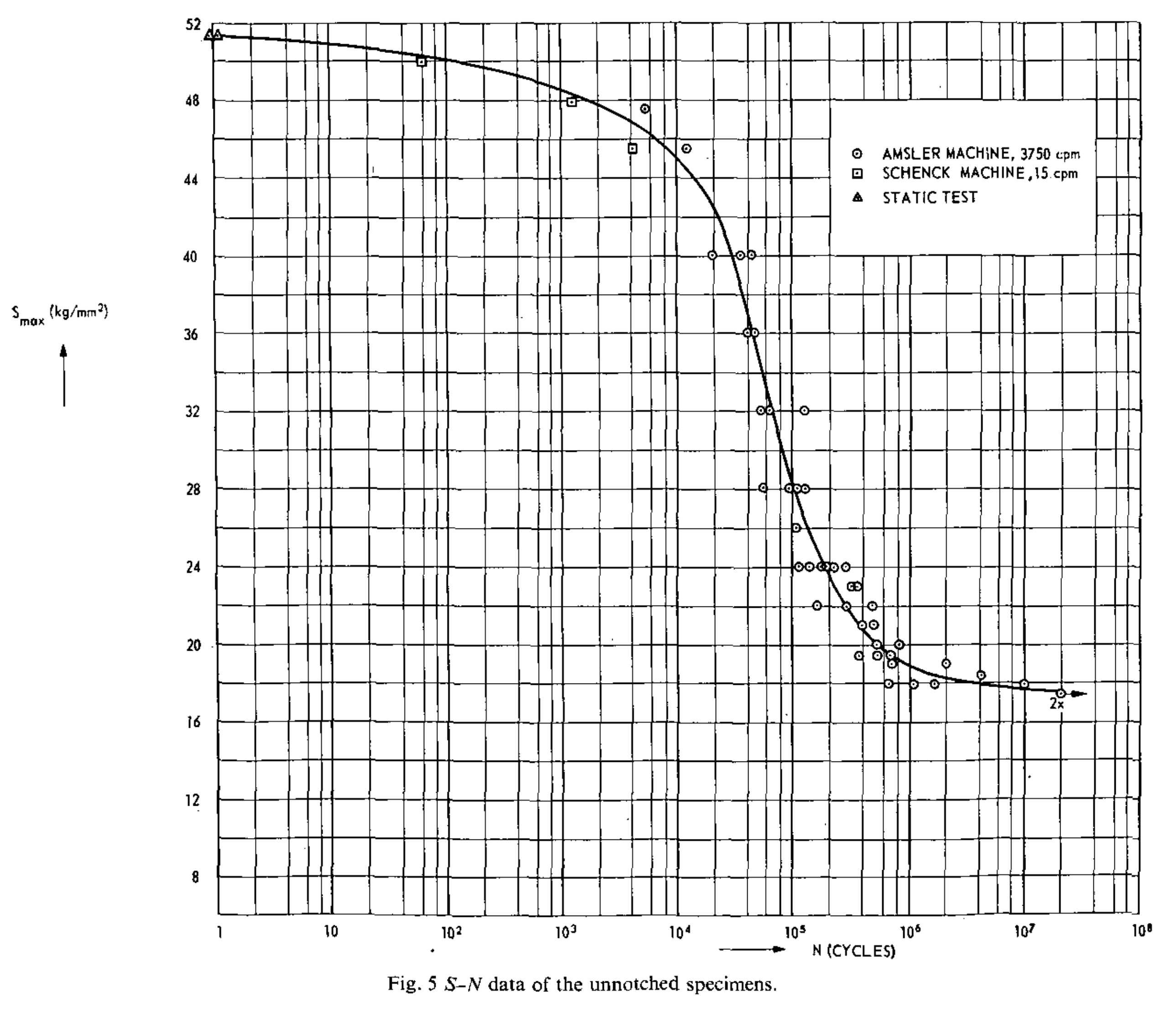

Fig. 5 *S–N* data of the unnotched specimens.

the three types of specimens. The S–N data have been plotted in figs. 5, 6 and 7. In these figures average S–N curves have been drawn through the data points. S_{max} in this report always indicates a nominal stress on the net area of the specimen (disregarding cracks).

4.2 *Crack propagation data*

The crack propagation data are very numerous and will not be given in full detail. The first treatment of these data was made as follows. The microscopical observations were plotted as the crack length l against the number of cycles n on a semi-log scale. Examples for an unnotched and a notched specimen are given in figs. 8 and 9. Curves were drawn through the plotted data points. Ordinates of these crack propagation curves have been compiled in tables 5, 6 and 7. Figs. 8 and 9 illustrate that this procedure implies some smoothing of the data since there are apparently slight irregularities in the crack propagation. Part of the irregularities stem from inaccurate observations of the tip of the crack. It was not always easy to decide whether a crack had reached a scribe line marking or not. On the other hand observation of crack growth through the microscope gave the impression that the crack rate is not always a monotonuosly increasing function of time. Obviously structural inhomogeneities in the material having a local character will affect the crack rate. Moreover it should not be overlooked that the microscope shows just one point of the crack front and will therefore not indicate the average crack rate along the whole crack front.

In general dormant periods were not observed. An exception should perhaps be made for very minute cracks. It was sometimes noticed that very minute grooves, which were suspected to be cracks did not propagate; they might have propagated if there had not been an overriding by another crack. The smoothing procedure is considered to be an elimination of the influence of microinhomogeneities and inaccuracies of the crack length observations.

Fig. 9 shows that in a notched specimen the growth of more than one crack was recorded. The main crack has started at point Al in fig. 11. The crack shape remains a quarter-circle for a considerable time. When

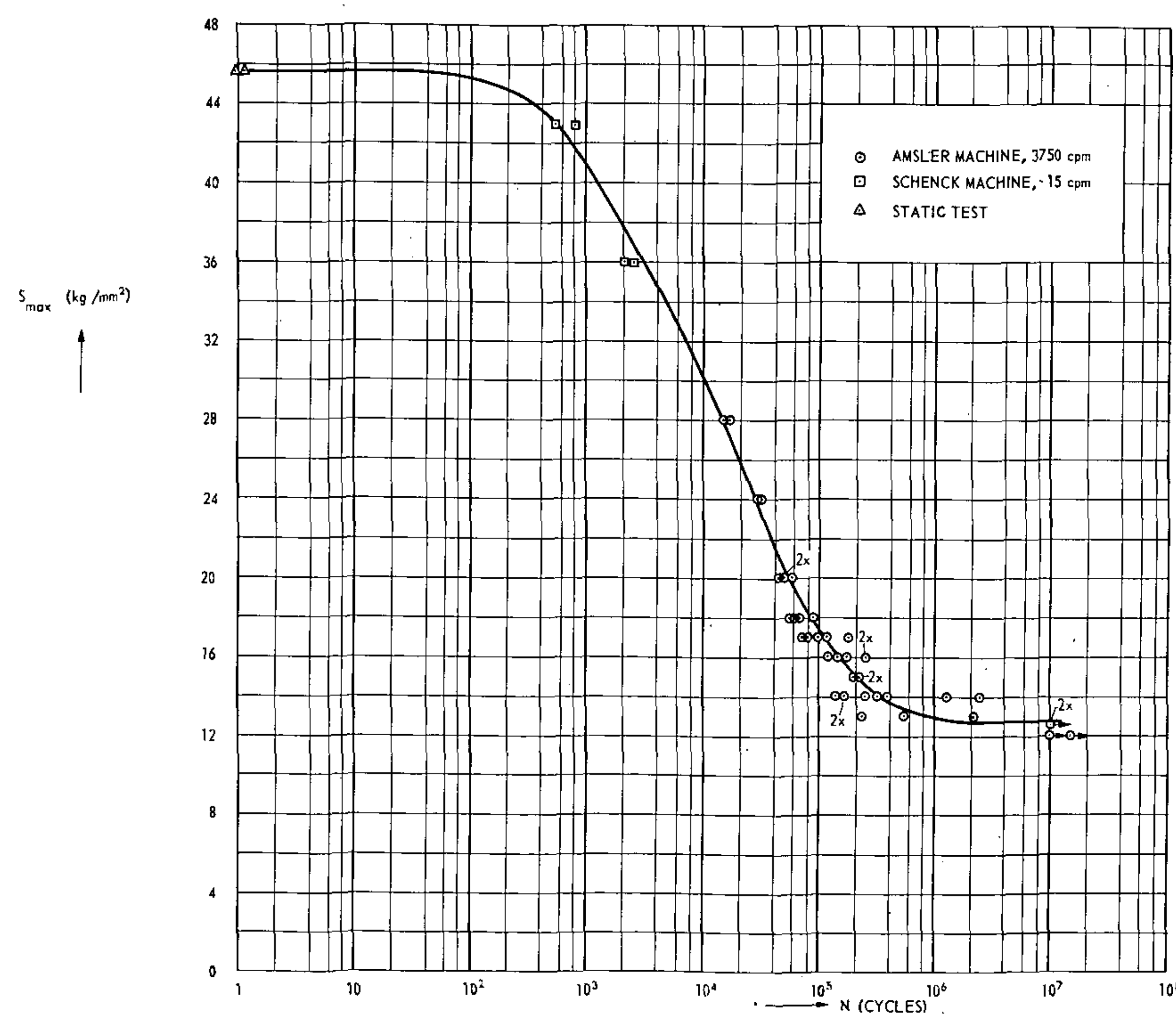

Fig. 6 S–N data of the small notched specimens.

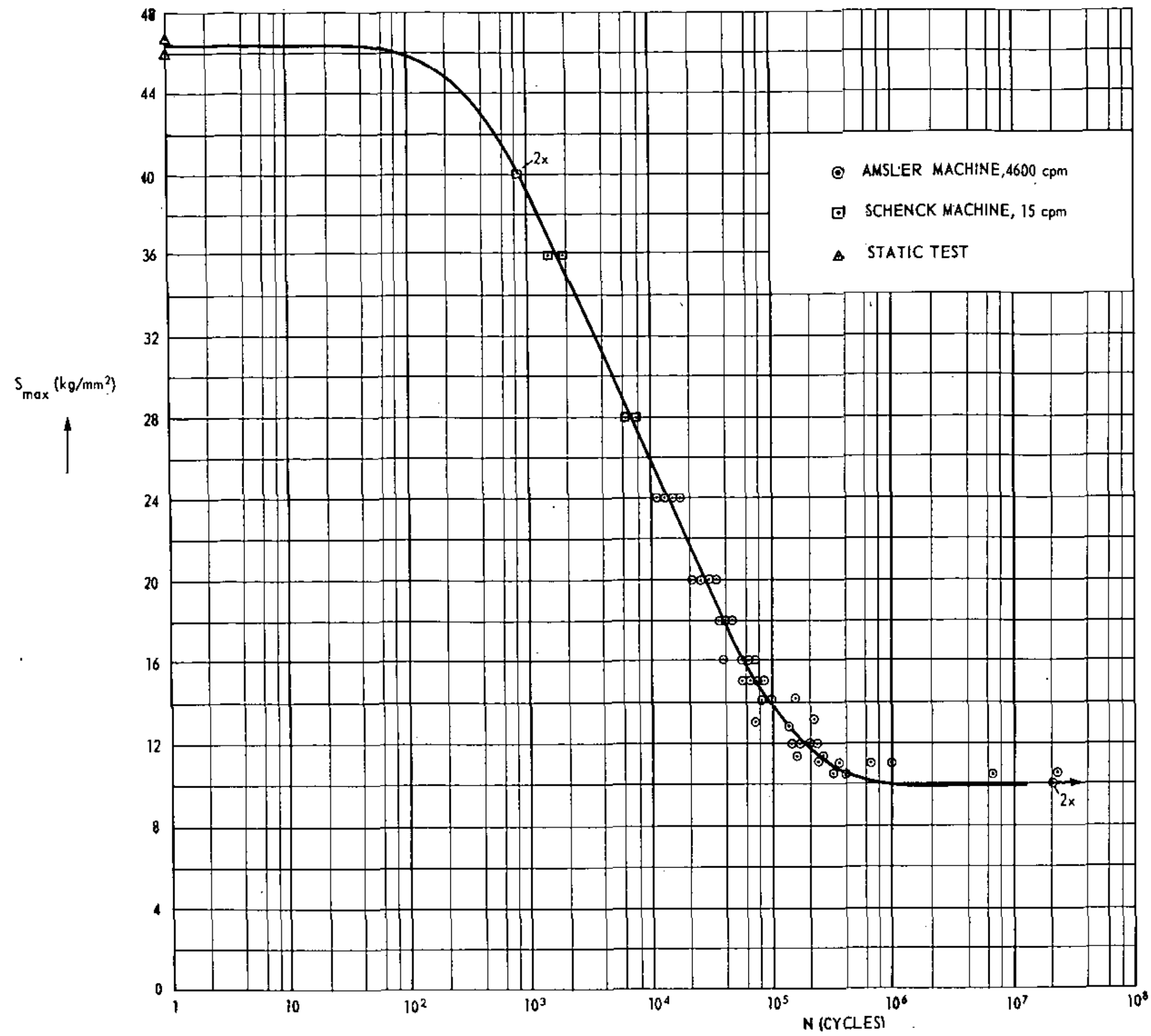

Fig. 7 *S–N* data of the large notched specimens.

the crack penetrates through the sheet at A2 the observed crack rate is originally very large there, see curve A2 in fig. 9, as this only requires a small rim of material to be disrupted. After a crack at one side of the hole (A1A2) has developed to a large extent cracks at the other side of the hole (A3A4) are observed, see figs. 9 and 11. Such a secondary crack is growing very fast due to the increased net stress induced by the main crack. The majority of the small notched specimens showed a sequence of cracking as described above. In a few specimens, mainly at the higher stress levels, two cracks of a comparable size developed simultaneously either at the same side of the hole (A1 and A2) or at different sides of the hole (A1 and A3 or A4). A systematic effect on the propagation of the largest crack due to the presence of the other crack was not apparent. Therefore the results of the dominating cracks were analysed only.

In several tests the crack growth recording was unsuccessful and therefore the number of tests which

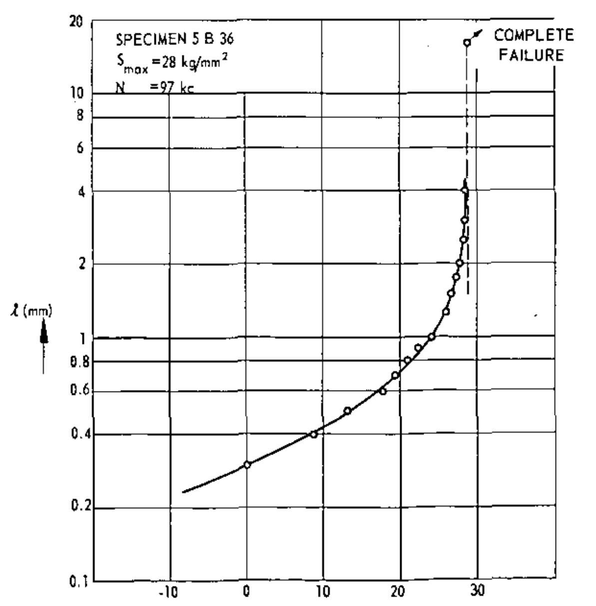

Fig. 8 Example of crack propagation curve for an unnotched specimen.

TABLE 2

Endurances of unnotched specimens

Specimen	S_{max} *(kg/mm²)*	*N* *(kc)*
5B37	50.0	0.058
1A30	48.0	1.164
3A37	45.4	4.117
1A12	47.0	5.5
3A35	45.5	13.5
5B48	40.0	19.4
3B29	40.0	35.0
3B48	40.0	44.8
1A48	36.0	39.9
3A48	36.0	47.1
5B42	32.0	54.0
3B37	32.0	62.6
3B42	32.0	126.0
1A 4	28.0	58.0
5B36	28.0	97.0
3B 4	28.0	107.5
3A 4	28.0	124.5
1A10	26.0	113.0
5B17	24.0	114.0
3B36	24.0	141.0
3A42	24.0	178.0
3B17	24.0	185.0
3A36	24.0	217.0
1A36	24.0	271.0
3A10	23.0	336.0
5B23	23.0	355.6
5B29	22.0	164.7
1A11	22.0	284.1
1A29	22.0	498.0
3A11	21.0	407.0
3B23	21.0	515.0
1A17	20.0	540.7
3B10	20.0	853.0
3A17	19.5	370.0
5B10	19.5	554.1
1A23	19.5	705.0
3B11	19.0	741.0
3A23	19.0	2125.0
5B11	18.5	4178.0
1A35	18.0	662.0
3A29	18.0	1104.0
5B35	18.0	1628.0
3B29	18.0	10107.0
3A35	17.5	> 20,000
3B35	17.5	> 20,000

The three specimens at the top of the table were tested on a Schenck machine at a speed of 15 cpm. All other specimens were tested on an Amsler machine at a speed of 3750 cpm.

TABLE 3

Endurances of small notched specimens

Specimen	S_{max} *(kg/mm²)*	*N(kc)*
1B48	43	0.53
1B42	43	0.85
5B50	36	2.06
3B25	36	2.48
3A44	28	15
3B44	28	17
3B38	24	29
3A38	24	31
1A38	20	44
5B25	20	51
5B32	20	52
3B32	20	58
5B 7	18	57
3A 7	18	64
3A50	18	67
3B 7	18	91
1A13	17	74
3B13	17	87
5B 1	17	90
1A19	17	100
5B13	17	114
3B 1	17	179
1B18	16	122
3B19	16	144
1B30	16	172
3A19	16	259
3B50	16	261
1B49	15	197
1A25	15	207
5B19	15	209
1B12	14	141
3B26	14	166
1A32	14	173
1A26	14	248
5B26	14	324
1B24	14	387
3A25	14	1294
3A32	14	2489
1B 5	13	225
1B43	13	559
1A 7	13	2208*
1A 1	12.5	> 10130
3A1	12.5	> 10404
1B37	12	> 10251
1B 6	12	> 14957

The four specimens at the top of the table were tested on a Schenck machine at a speed of 15 cpm. All other specimens were tested on an Amsler machine at a speed of 3750 cpm.

* Specimen failed at clamping.

TABLE 4

Endurances of large notched specimens

Specimen	S_{max} *(kg/mm²)*	*N(kc)*
2A 3	40	0.864
4A10	40	0.876
2A 7	36	1.430
2B10	36	1.765
4A 5	28	6.844
4B8	28	7.121
4B 9	24	10
2A10	24	12.2
4A11	24	14.5*
2B11	24	14.5
2A 1	20	21.5
4A 9	20	26
4B10	20	32.5
2B 6	20	34
4B 4	18	40.5
4A 4	18	42.6
2B 7	18	49.4
2A 4	16	36
4B 6	16	60.4
2B 1	16	69.5
4A 8	16	71
2A 9	15.2	51
2A 5	15.2	58.5
2B 8	15.2	64.5
4B 5	15.2	80.3
4B 2	14.2	90
4B12	14.2	98
4A 3	14.2	128.5
2A12	13	72
4A 2	13	148
2B 3	13.2	237
2B12	12	166
4B 7	12	192.5
4B 1	12	202
4A 7	12	230.2
4A 1	11.45	177
2B 2	11.4	245.5
2A 2	11	220
4A 6	11	328
4B11	11	625
2B 9	11	977
2A 8	10.5	300
4A12	10.5	383
2B 5	10.5	6549
4B 3	10.5	21338
2B 4	10	>20113
4A11	10	>20256

The six specimens at the top of the table were tested on a Schenck machine at a speed of 15 cpm. All other specimens were tested on an Amsler machine at a speed of 4600 cpm.

* Specimen previously tested at $S_{max} = 10$ kg/mm² for 20 million cycles.

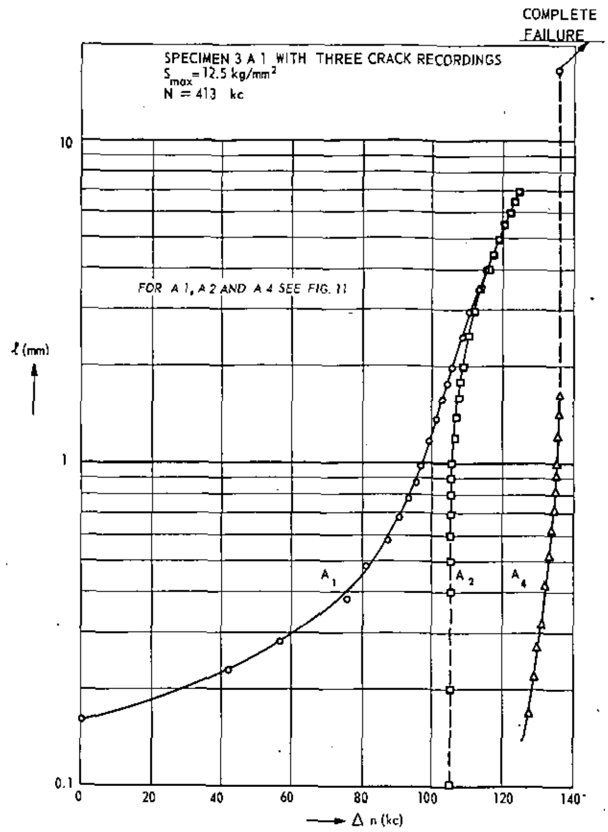

Fig. 9 Example of crack propagation curves for a small notched specimen.

supplied crack propagation data is smaller than the number of tests giving S–N data. This applied especially to the unnotched specimens. In the unnotched specimens the area to be searched for cracks was much larger than in the notched specimens. So cracks generally had a greater length at the moment of detection and sometimes they were too large then to yield useful propagation data. In other cases a certain groove was suspected to be a crack and attention was focussed on it. However, at a later stage it could turn out that it was not the dominant crack leading to ultimate failure. The latter especially applies to tests with a high maximum stress since many potential crack nuclei were formed then. For a low maximum stress, i.e. for high endurances, the microscopic examination of the unnotched specimens over a long period was very laborious and this somewhat impaired the success of the test. In general examination was stopped if no cracks were found at an endurance of $2 \cdot 10^6$ cycles. There was one serious phenomenon reducing the number of successful tests on unnotched specimens. Most cracks started at the edges of the specimen, point A in fig. 10, as should be expected. However, sometimes the cracks were nucleated at some distance from the edge at or perhaps slightly below the sheet surface, point D in fig. 10. Probably such cracks originate from inclusions. It is clear from fig. 10 that a crack length l' (or even $\frac{1}{2}l'$) cannot be directly compared with a

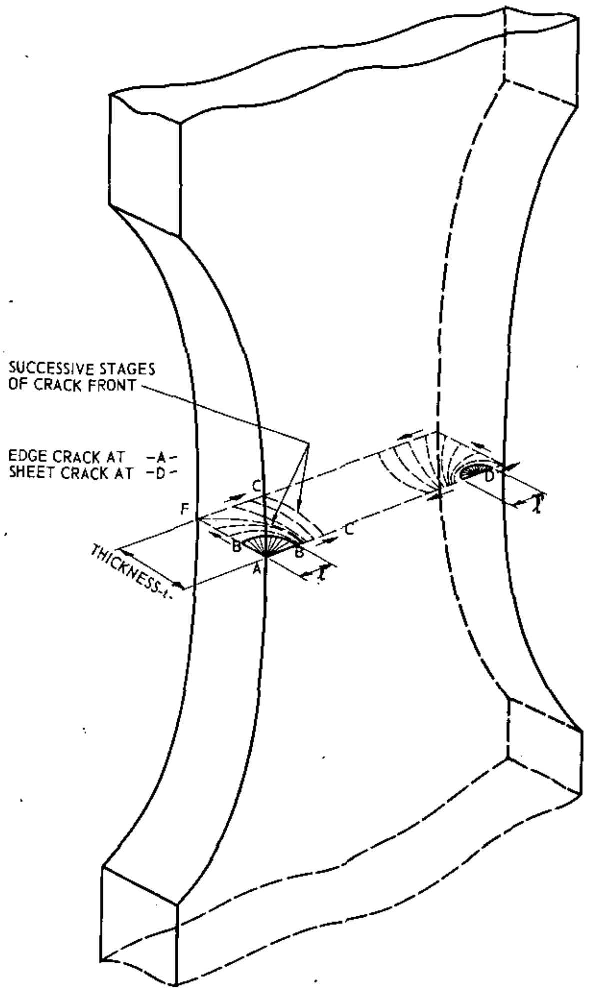

Fig. 10 Crack nucleation and propagation in the unnotched spemens (schematic view).

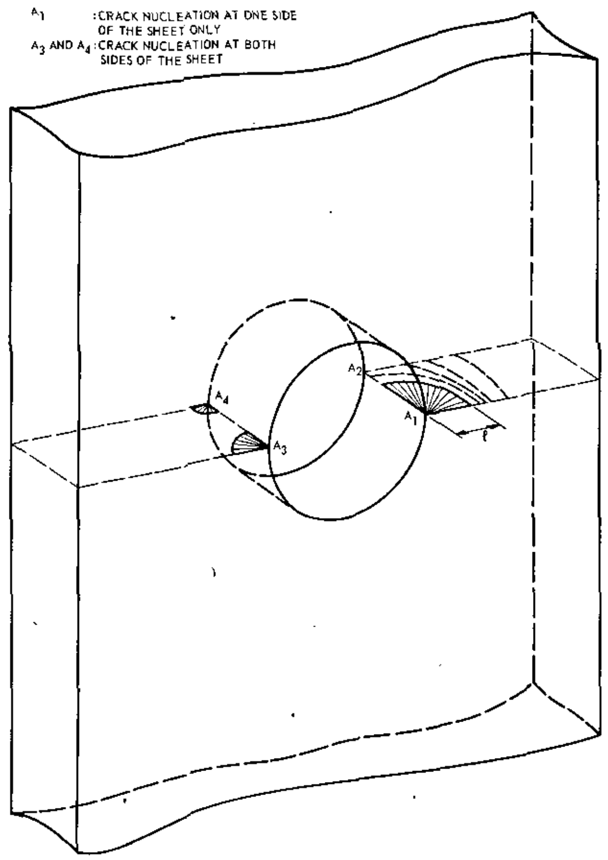

Fig. 11 Crack nucleation and propagation in the notched specimens (schematic view).

crack length l. In tests with cracks of the type D (called sheet cracks instead of edge cracks) some crack propagation observations were made, but their results were excluded from table 5. There was no systematic tendency for specimens with sheet cracks to yield shorter (or larger) endurances.

In some tests on the small notched specimens at low stress amplitudes the time to detection of the first crack was expected to be very long and no microscopic examinations were made. In other tests at the same stress amplitudes specimens were provided with a small artificial crack nucleus at the edge of the hole from which further crack growth started which was recorded.

In a few notched specimens sheet cracks instead of edge cracks occurred. Results of such tests have been omitted. Since the amount of highly stressed material is much smaller for notched specimens as compared with unnotched specimens it had to be expected that sheet cracks would occur rarely in the former ones.

5 Analysis of the crack propagation data

In this chapter the relation between the crack rate and the crack length is analysed. Secondly the percentage fatigue life covered by certain amounts of crack growth will be determined. Thirdly an estimate will be made of the minimum crack rates occurring in a test. Finally data will be presented to study the scatter.

The crack rate dl/dn has been calculated from the data compiled in tables 5, 6 and 7. For each interval of the crack length from l_i to l_{i+1} it is assumed that the crack rate in the middle of the interval, i.e. at $l=\frac{1}{2}(l_i+l_{i+1})$, is equal to the average crack rate in the interval

$$\frac{dl}{dn}=\frac{l_{i+1}-l_i}{\Delta n_{\text{interval}}} \quad \text{at} \quad l=\frac{l_i+l_{i+1}}{2}. \tag{5.1}$$

Crack rates obtained in this way have been plotted as a function of the crack length for all specimens. From such plots on a double logarithmic scale it was observed that log dl/dn was linearly related with log l for l-values up to 1 mm for all specimens. For the small and the large notched specimens this is shown in figs. 13 and 14. For the unnotched specimens the amount of crack propagation data for $l<1$ mm was more limited. Fig. 12 shows the data of the specimens with sufficient data points below $l=1$ mm for judging the validity of the linear relation. The linear relationship can be expressed as:

$$\frac{dl}{dn}=Cl^{\alpha}. \tag{5.2}$$

TABLE 5

Tabulated crack propagation curves for the unnotched specimens (edge cracks only)

Specimen	S_{max} *(kg/mm²)*	*Δn (kc)* *Crack length (mm)*										
		0.2	0.25	0.3	0.4	0.5	0.6	0.8	1.0	1.5	2.0	End
5B35	18						− 8.5	8.0	18.7	28.2	31.1	34.9
3A23	19					− 8.5	2.0	14.5	19.6	25.0	27.6	31.0
3B11	19					−18.0	− 7.5	7.5	16.8	23.3	25.3	28.3
1A23	19.5					5.5	17.3	33.5	40.2	46.6	48.8	52.0
5B10	19.5					0	9.0	19.5	26.0	31.7	34.2	37.5
3B10	20					0	7.0	16.7	22.0	27.0	28.8	31.3
1A17	20				0	12.3	19.7	30.6	37.2	43.6	45.6	48.2
1A29	22			−11.0	−1.5	4.2	7.5	11.8	14.3	17.0	18.5	19.8
5B29	22					− 7.5	− 3.8	1.5	5.0	10.2	12.9	15.2
3A10	23					−11.0	− 6.0	0	3.6	7.0	8.6	10.6
3B17	24					− 4.0	0	5.1	7.8	10.8	12.2	14.5
5B17	24						− 7.5	1.0	6.1	11.2	13.0	14.4
3B36	24	−15.5	−9.0	− 4.5	2.2	7.0	10.6	15.5	18.5	22.0	23.0	24.2
1A10	26				−0.5	2.8	5.2	8.5	10.3	12.0	12.8	13.2
1A 4	28			− 3.2	0	1.8	3.0	5.0	5.9	7.7	8.5	9.5
5B36	28		−5.6	0	8.6	13.5	17.3	21.4	24.1	26.7	27.6	28.8
3A48	36	− 8.0	−3.0	0.3	5.7	9.2	10.8	12.8	13.6	14.4	14.8	15.1

Δn is the number of cycles from the moment of crack detection.

This relation is used in this chapter for interpolation and extrapolation purposes. With the method of least squares values of C and α were calculated. The results are compiled in tables 8, 9 and 10. For the unnotched specimens there is some variability in α but a systematic trend to increase or decrease as a function of S_{max} cannot be observed. The average value of α is 2.0. For the small and the large notched specimens α has been plotted vs. S_{max} in figs. 15 and 16 as double logarithmic plots. For both types of specimens α is decreasing at increasing S_{max}. The values of C have been plotted in figs. 17, 18 and 19, again in a double logarithmic graph. C is increasing for increasing S_{max} as should be expected since from eq. (5.2) it follows that C is the crack rate at $l=1$ mm. For figs. 15 to 19 a linear regression line (method of least squares) was determined. These lines imply the following relations

$$C = C_1 S_{max}^{\beta} \qquad (5.3)$$

$$\alpha = C_2 S_{max}^{-\gamma} \qquad (5.4)$$

Substitution in eq. (5.2) gives

$$\frac{dl}{dn} = C_1 S_{max}^{\beta} \, l^{C_2 S_{max}^{-\gamma}} \qquad (5.5)$$

For the three types of specimens the following numerical results were obtained. Unnotched specimens:

$$\frac{dl}{dn} = 0.40 \times 10^{-6} S_{max}^{3.86} l^2 \qquad (5.6)$$

Small notched specimens:

$$\frac{dl}{dn} = 0.110 \times 10^{-3} S_{max}^{2.53} \, l^{16.6 S_{max}^{-0.83}} \qquad (5.7)$$

Large notched specimens:

$$\frac{dl}{dn} = 0.201 \times 10^{-3} S_{max}^{2.53} \, l^{3.30 S_{max}^{-0.31}} \qquad (5.8)$$

Values of dl/dn as a function of l have been plotted in figs. 20, 21 and 22 for the three types of specimens respectively. For $l < 1$ mm this has been done in accordance with the above equations, leading to straight lines. For $l > 1$ mm the linearity between $\log dl/dn$ and $\log l$ no longer holds and the following procedure was adopted. For several values of l the crack rate was plotted as a function of S_{max} and curves were faired through the data points. From such graphs the values of dl/dn plotted in figs. 20, 21 and 22 for $l > 1$ mm were obtained. Again this procedure implies a smoothing of scatter.

Integration of eq. (5.2) gives:

$$\frac{1}{l_1^{\alpha-1}} - \frac{1}{l_2^{\alpha-1}} = (\alpha - 1)\, C(N_{l_2} - N_{l_1}), \qquad (5.9)$$

N_{l_1} and N_{l_2} being the fatigue lives at a crack length of l_1 and l_2 respectively. Eq. (5.9) can be used as an extrapolation formula to estimate crack lengths and crack rates at numbers of applied cycles, N_l, before cracks were observed. For the unnotched specimen N_l was calculated for $l=0.2$ mm and $l=0.1$ mm with eq.(5.9) starting from N_l for $l=0.5$ as an experimental observation. The results are plotted in fig. 23 as a percentage of the fatigue life at failure. The figure also gives the experimental data for $l=0.5$ mm and $l=1$ mm. Although the results for $l=0.2$ mm were calculated with eq. (5.9) they still have a reasonable accuracy,

TABLE 6

Tabulated crack propagation curves for the small notched specimens

Specimen	S_{max}	Δn (kc)															
		Crack length (mm)															
	(kg/mm^2)	0.06	0.08	0.1	0.15	0.2	0.3	0.4	0.6	0.8	1.0	1.5	2.0	3.0	4.0	6.0	End.
3A 1*	12.5				—10.0	27.0	60.5	75.5	87.5	93.5	97.0	102.2	105.8	111.2	115.5	122.0	136.0
5B44*	12.5					—13.0	16.5	35.5	53.5	60.3	64.3	70.0	74.0	79.5	84.0	91.0	107.0
1A44*	13			—16.0	9.0	25.0	45.0	57.5	68.0	72.5	75.3	80.0	83.6	88.5	92.6	98.8	115.0
5B38*	13					—20.0	4.5	19.0	34.5	42.2	45.8	50.5	54.0	59.9	64.0	70.0	84.0
1A26	14	—10.0	8.0	21.0	42.0	56.0	73.3	84.0	96.3	101.7	104.6	109.0	111.7	116.3	120.2	125.8	138.1
3B26	14			3.5	9.1	13.4	18.6	22.5	28.0	31.3	33.8	38.0	41.0	45.5	48.9	54.0	64.1
5B26	14								15.5	32.5	37.0	42.5	45.2	50.0	53.7	60.0	70.9
1A32	14					4.0	27.5	36.5	42.7	46.5	48.7	52.8	55.3	60.0	63.4	69.0	82.8
3A32*	14					— 3.0	21.7	32.5	45.0	50.0	52.9	57.5	60.2	64.5	67.8	73.0	84.0
3A25	14										88.0	93.0	96.0	101.0	104.4	110.4	121.0
5B19	15				— 6.5	4.0	18.5	29.0	40.5	45.4	48.0	52.4	55.0	59.5	63.2	69.0	77.3
1A25	15					— 3.0	9.0	17.5	26.0	31.0	34.3	38.5	41.4	45.1	48.1	53.7	56.5
1	15					— 0.5	11.2	18.0	24.5	27.5	29.9	33.5	36.0	40.1	43.5	49.0	54.0
3A19	16						11.5	16.6	21.3	23.9	25.6	28.7	30.9	34.3	37.3	42.2	48.8
3B50	16					10.0	17.5	21.5	26.4	29.5	31.3	34.3	36.7	40.0	43.0	48.2	56.0
3B19	16								21.5	26.8	29.2	32.5	34.5	37.8	40.6	45.0	49.3
136	16		—2.5	3.5	12.0	18.0	26.0	30.8	36.5	39.8	41.7	45.0	47.2	51.0	54.0	59.3	63.0
1A13	17					— 2.0	6.1	8.9	11.7	13.7	15.1	17.3	18.9	21.5	23.6	27.3	31.9
3B13	17								13.2	15.9	17.4	20.3	22.2	25.0	27.1	30.9	34.0
5B13	17					3.9	10.7	14.4	18.5	20.9	22.7	25.6	27.6	30.4	32.5	36.1	39.0
1A19	17						13.0	15.7	19.1	21.7	23.6	26.4	28.5	31.6	34.6	40.0	46.0
151	17				— 1.4	5.1	12.6	16.4	20.5	22.6	24.1	26.9	28.8	31.3	32.9	35.2	36.0
3A50	18				— 0.8	4.1	10.2	14.2	17.7	19.8	21.2	23.5	25.2	27.5	29.2	30.8	32.0
3B·7	18			— 1.0	2.8	5.6	9.4	11.7	14.8	16.7	17.8	19.6	20.8	—	—	—	30.5
3A 7	18					— 1.4	2.2	4.5	7.0	8.5	9.6	11.7	12.9	15.2	17.3	—	21.8
5B 7	18								19.5	21.4	22.8	25.0	26.6	28.4	29.4	30.7	31.7
1A38	20			2.6	5.9	8.1	11.8	14.2	17.1	18.3	19.0	20.2	21.4	23.5	24.9	26.4	27.0
3B32	20								19.0	20.5	21.3	23.0	24.0	25.8	27.1	28.3	29.0
5B32	20		0.9	3.2	7.2	9.8	13.6	16.2	19.2	20.7	21.7	23.0	23.8	24.7	25.3	25.8	26.0
3B38	24	— 2.0	0.3	1.3	2.9	4.1	5.7	6.8	8.3	9.4	10.0	11.0	11.6	12.2	12.5	12.8	13.0
3A38	24				2.7	4.0	5.8	7.2	8.9	10.2	11.0	12.2	13.1	14.3	15.1	15.7	16.0
3B44	28					— 0.5	0.5	1.2	2.13	2.79	3.25	3.79	4.01	4.26	4.38	4.45	4.5
3A44	28						4.08	5.00	6.20	6.89	7.36	8.13	8.53	8.85	9.01	—	10.0
3B25	36						0.140	0.410	0.770	0.970	1.085	1.175	1.200	—	—	—	1.207

* specimens with a small artificial crack starter.

Δn is the number of cycles from the moment of crack detection.

TABLE 7

Tabulated crack propagation curves for the large notched specimens.

Specimen	S_{max} (kg/mm^2)	$\Delta n(kc)$ Crack length (mm) 0.08	0.1	0.15	0.2	0.3	0.4	0.6	0.8	1.0	1.5	2	3	4	6	8	10	15	20	End
4A12	10.5		0	9.2	16.0	25.5	32.3	41.0	45.5	48.4	52.8	55.4	59.1	62.2	68.2	76.0	83.0	94.8	103.5	112.0
2A 8	10.5			−2.8	9.0	23.3	31.4	40.1	44.8	47.6	51.7	54.1	58.1	61.4	67.0	72.6	77.4	86.8	93.0	100.0
4A 6	11			6.6	16.8	26.0	31.0	36.6	40.1	42.6	46.2	48.2	51.1	53.8	58.6	62.5	65.9	74.5	81.5	88.0
4B11	11							− 1.2	4.8	7.9	11.3	13.5	17.0	20.1	25.8	31.3	37.5	49.5	56.5	63.0
2B 9	11				0	13.5	19.7	25.5	28.6	30.8	34.4	36.6	40.0	42.7	48.7	54.7	60.4	71.5	77.7	83.0
2B 2	11.4			−1.8	6.5	16.5	22.5	29.0	32.6	34.6	37.6	39.8	42.8	45.5	51.9	57.4	62.0	71.0	76.1	81.5
4A 1	11.45			−4.2	1.0	7.7	12.2	17.7	21.2	23.5	26.8	28.7	31.4	33.6	37.7	41.6	45.3	53.2	59.0	65.0
2B12	12		−7.0	2.2	8.0	15.0	19.0	23.5	26.1	28.0	30.9	32.6	35.4	37.5	41.6	45.4	49.0	56.3	60.6	65.0
4B 7	12		−4.5	4.8	10.9	19.0	24.0	30.3	34.1	36.6	40.2	42.4	45.8	49.1	55.1	60.4	64.7	72.0	76.6	81.5
4B 1	12										9.5	11.4	14.3	16.7	21.0	25.2	28.1	31.4	33.0	35.0
4A 7	12									38.0	41.2	43.0	45.4	48.0	53.2	58.0	62.5	71.5	76.8	79.5
2A12	13				2.2	11.3	16.8	22.9	25.8	27.6	29.7	31.1	33.1	35.0	39.1	43.0	44.9	47.0	48.1	49.0
4A 2	13			7.0	13.0	20.0	23.0	26.3	28.5	30.0	32.6	34.0	36.2	38.3	42.2	45.6	48.5	54.2	57.8	62.0
2B 3	13.2				− 3.2	3.6	8.0	13.3	16.3	18.2	20.8	22.5	25.0	27.2	31.0	34.3	37.3	42.2	44.5	46.5
4A 3	14.2			0.6	3.5	7.2	9.6	12.5	14.2	15.4	17.2	18.2	19.6	20.8	23.3	25.3	26.5	29.7	31.9	33.5
4B 2	14.2							22.8	24.8	26.1	28.1	29.3	31.2	32.7	34.8	36.7	37.9	39.8	40.6	41.0
4B12	14.2											39.7	41.4	43.0	45.8	48.1	50.1	52.7	54.3	55.0
4B 5	15.2		−1.2	3.3	6.3	9.9	12.2	14.8	16.4	17.5	19.2	20.3	21.8	22.9	24.2	25.1	25.65	26.35	26.8	26.8
2B 8	15.2							17.3	19.0	20.1	21.9	23.1	24.6	25.7	27.1	28.4	29.4	31.3	32.5	34.0
2A 5	15.2											12.5	13.7	15.0	16.6	17.5	17.9	—	—	18.5
2A9	15.2											16.2	17.9	19.1	21.0	22.5	23.4	24.9	25.5	26.0
2B 1	16				5.0	8.8	11.2	14.1	15.8	17.0	18.6	19.55	20.7	21.6	23.1	24.2	25.1	26.5	27.15	27.5
4B 6	16						9.2	11.9	13.4	14.5	16.0	17.0	18.2	19.0	20.1	21.0	21.75	23.15	24.0	25.0
4A 8	16											15.8	17.2	18.2	19.8	21.0	21.7	23.0	23.8	24.4
2A 4	16							17.2	18.65	19.55	20.9	21.8	22.85	23.6	24.8	25.95	26.9	28.3	29.0	29.5
4A 4	18		−1.7	0.85	2.6	5	6.65	8.6	9.8	10.7	12.0	12.8	13.55	13.95	14.55	15.05	15.5	16.3	16.8	17.0
2B 7	18		0.8	3.35	5.15	7.7	9.45	12.0	13.75	14.95	16.7	17.5	17.95	18.2	18.6	18.85	19.05	19.45	19.8	19.9
4A 9	20		−1.25	0.25	1.3	2.75	3.8	5.25	6.3	7.05	8.05	8.6	9.05	9.27	9.5	—	—	—	—	11.0
2B 6	20		−2.0	−0.4	0.9	2.55	3.65	5.1	6.0	6.60	7.65	8.25	8.95	9.4	9.95	10.35	10.6	11.1	11.35	11.5
4B 9	24						− 0.17	0.97	1.76	2.40	3.01	3.30	3.48	3.56	3.70	3.82	3.90	4.09	—	4.2
2A10	24				2.05	3.55	4.55	5.85	6.65	7.05	7.68	8.06	8.30	8.48	8.72	9.00	9.11	9.25	—	9.4
4A11	24							1.00	1.60	2.05	2.66	2.93	3.22	3.40	3.60	3.72	3.85	—	—	5.5
4A 5	28				0	0.720	1.235	1.840	2.225	2.475	2.825	2.970	3.095	3.165	3.220	3.250	3.270	—	—	3.294
2A 7	36				− 0.003	0.128	0.221	0.350	0.440	0.504	0.598	0.628	0.649	0.658	0.676	0.687	0.693	—	—	0.695
2B10	36									0.394	0.484	0.518	0.550	0.566	0.588	0.600	—	—	—	0.607
4A10	40					0.023	0.116	0.208	0.254	0.282	0.316	0.332	0.343	0.352	0.356	—	—	—	—	0.359
2A 3	40											0.047	0.057	0.068	0.071	—	—	—	—	0.075

Δn is the number of cycles from the moment of crack detection

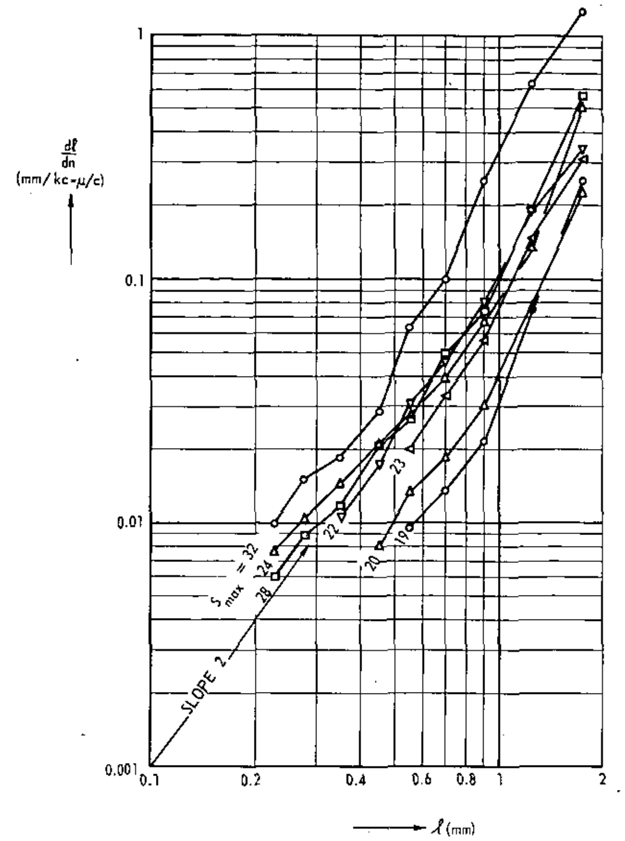

Fig. 12 Crack rate data for some unnotched specimens.

←

Fig. 13 The crack rate data for l < 1 mm for the small notched specimens.

↓

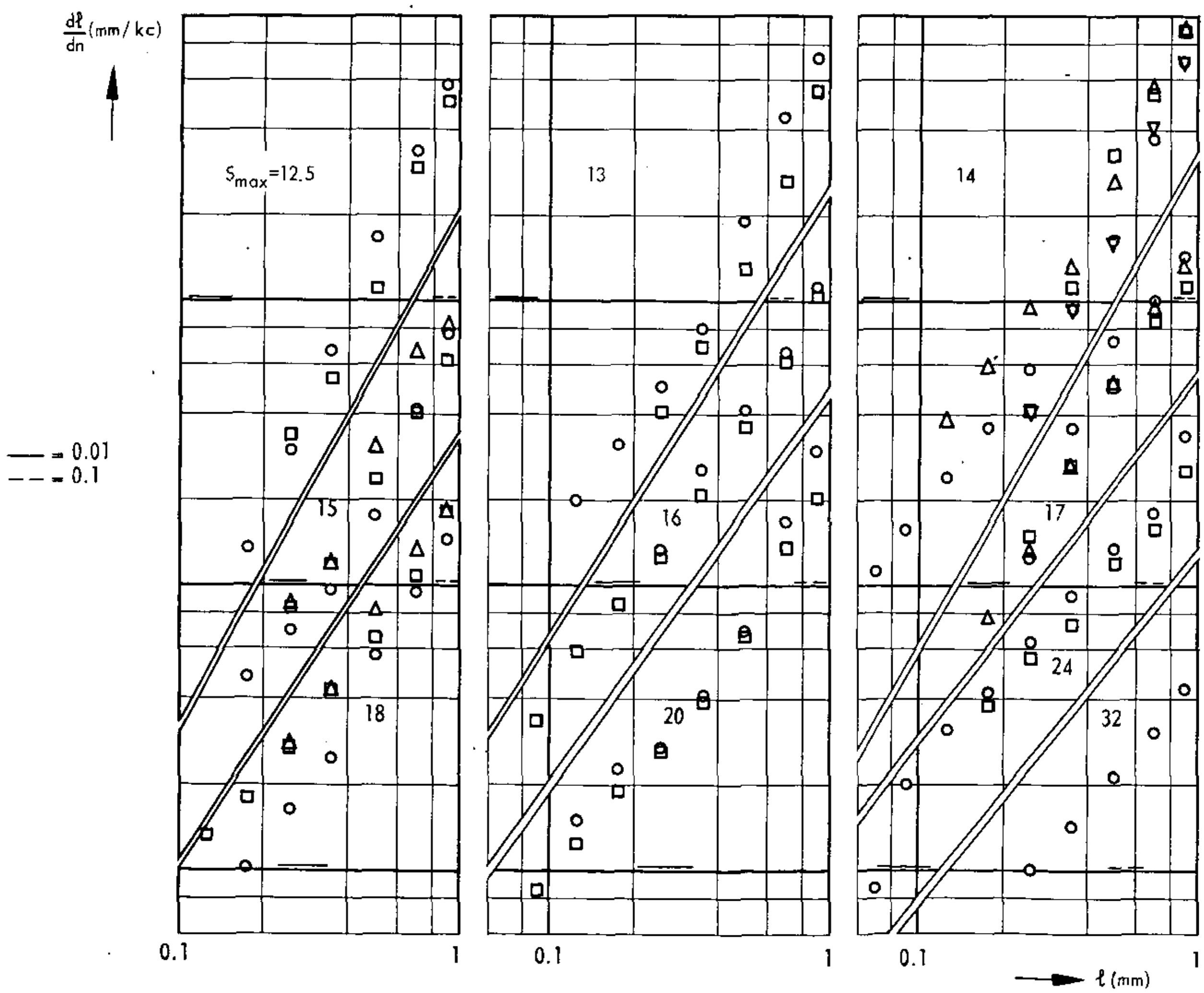

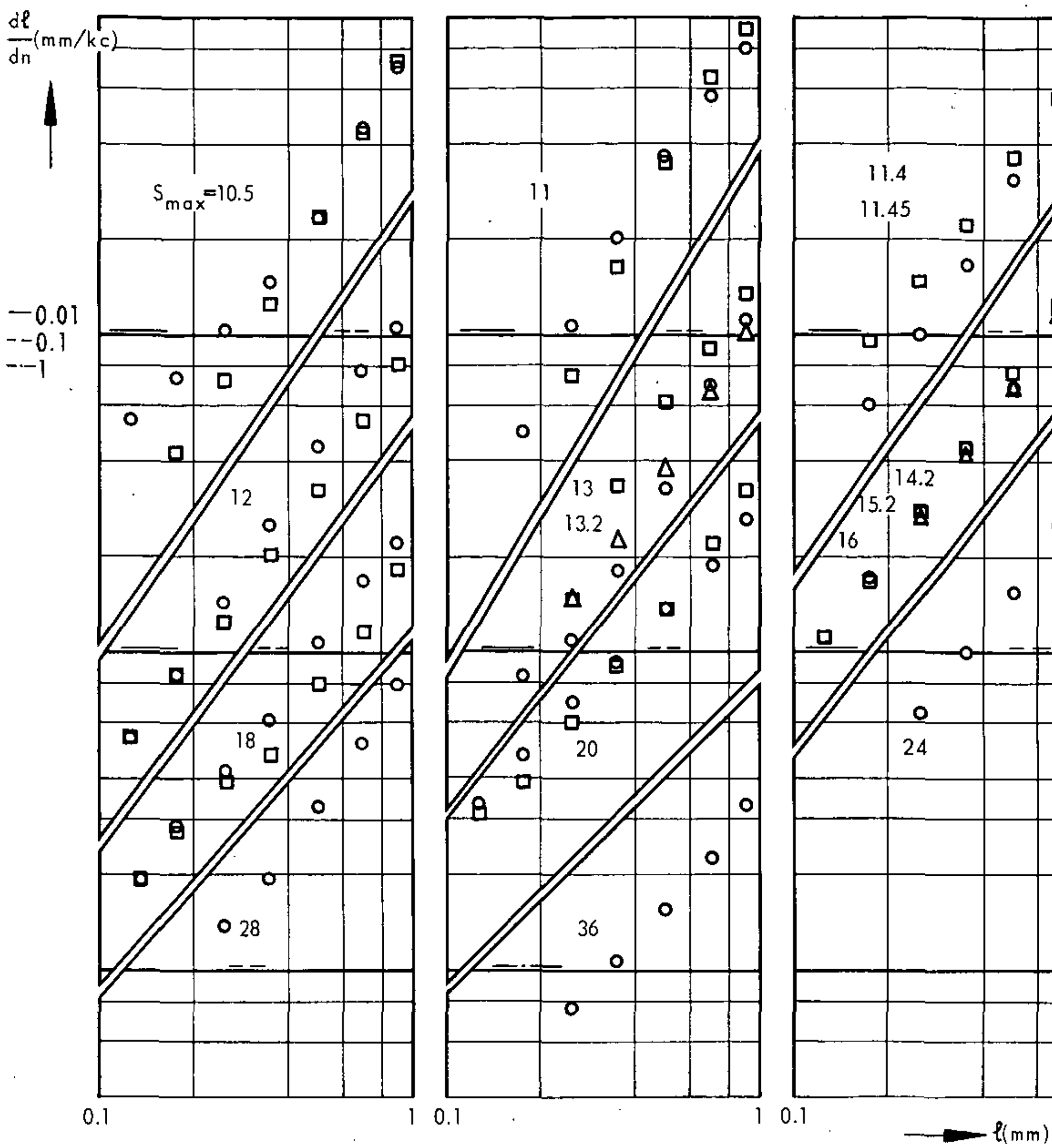

Fig. 14 The crack rate data for l < 1 mm for the large notched specimens.

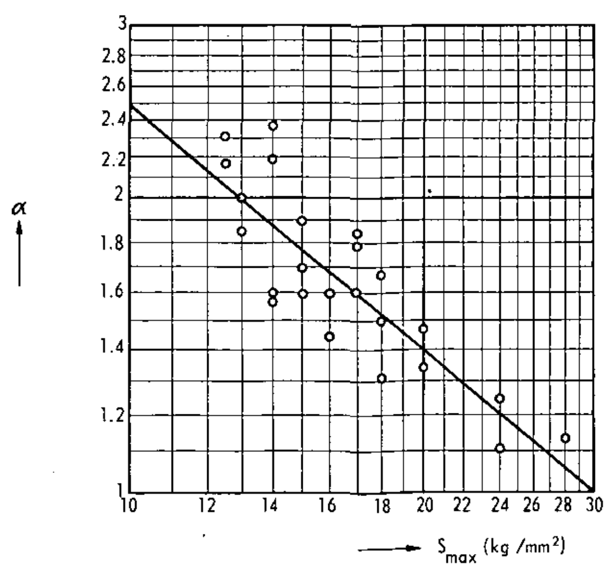

Fig. 15 The exponent α as a function of stress for the small notched specimens.

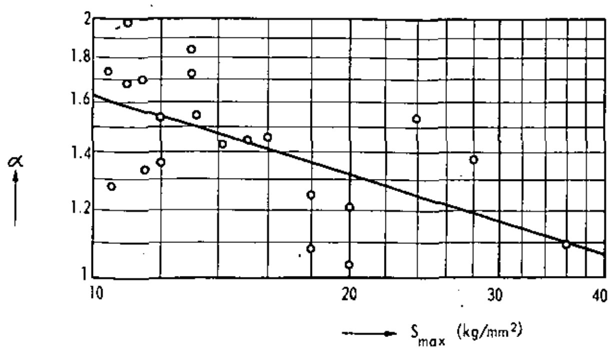

Fig. 16 The exponent α as a function of stress for the large notched specimens.

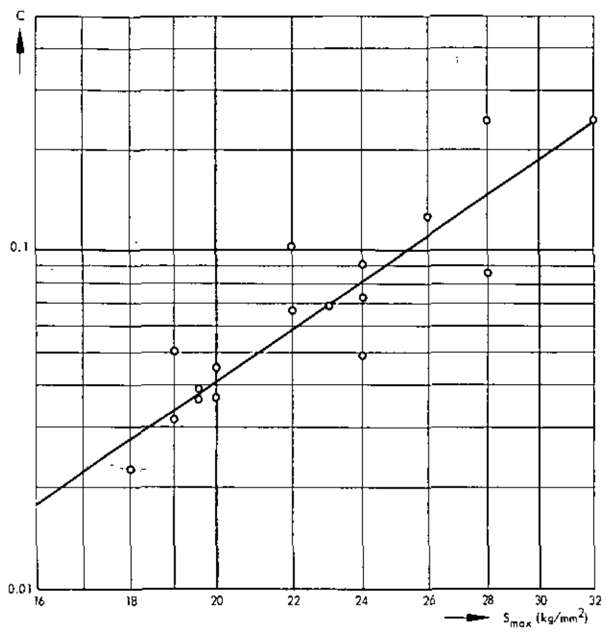

Fig. 17 The constant C as a function of stress for the unnotched specimens.

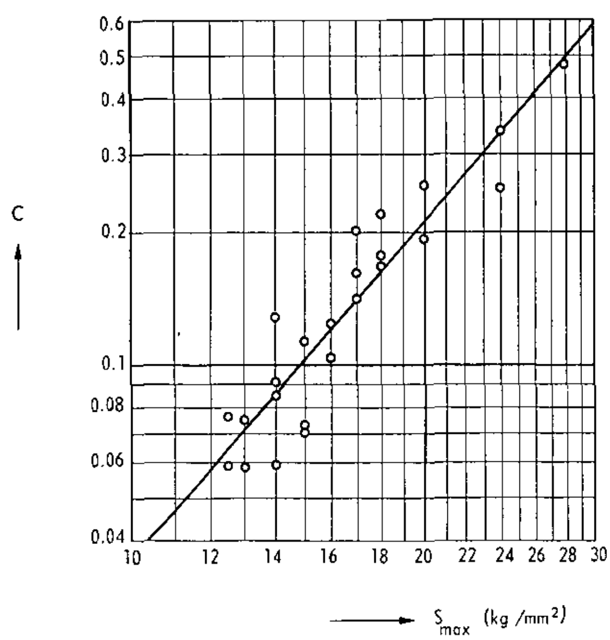

Fig. 18 The constant C as a function of stress for the small notched specimens.

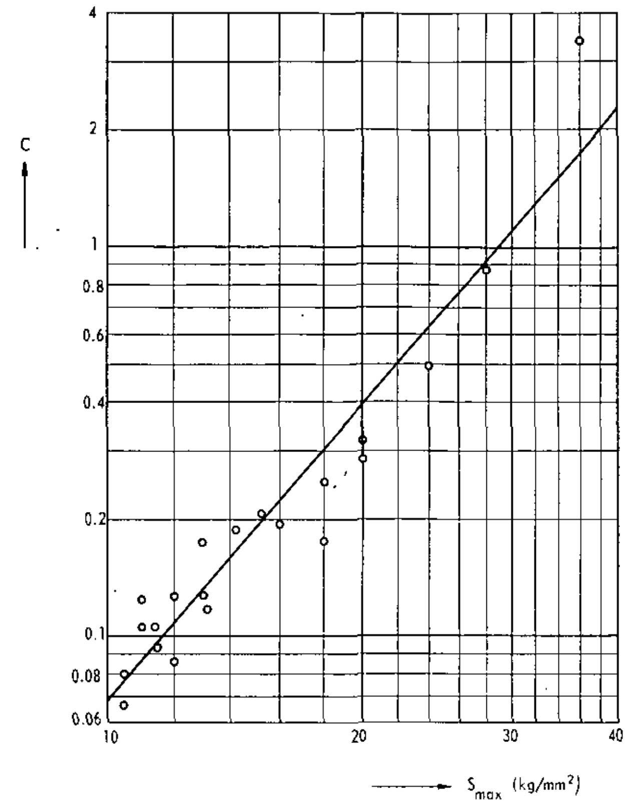

Fig. 19 The constant C as a function of stress for the large notched specimens.

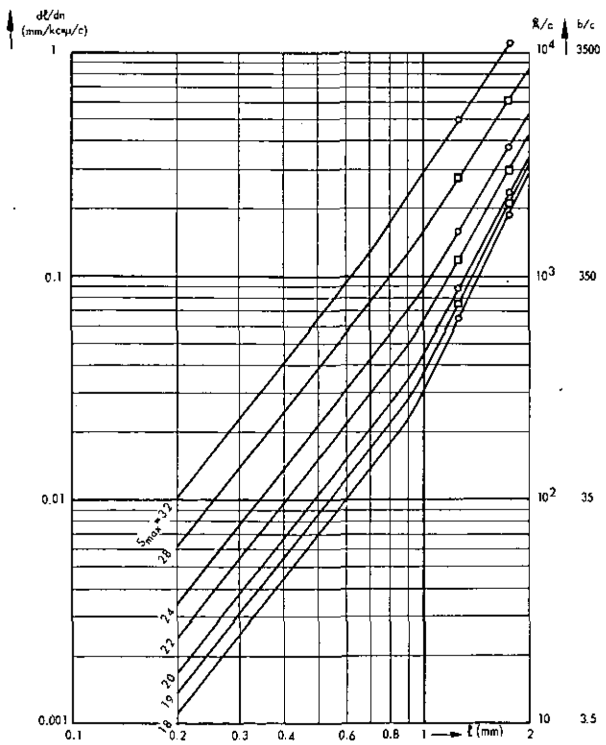

Fig. 20 The crack rate as a function of crack length for the unnotched specimens.

The plotted data were read from a graph in which dl/dn had been plotted vs. S_{max} for constant values of l ($l = 1.25$ mm and $= 1.75$ mm resp.). For $0.2 < l < 1.0$ mm curves were drawn in accordance with eq. (5.6).

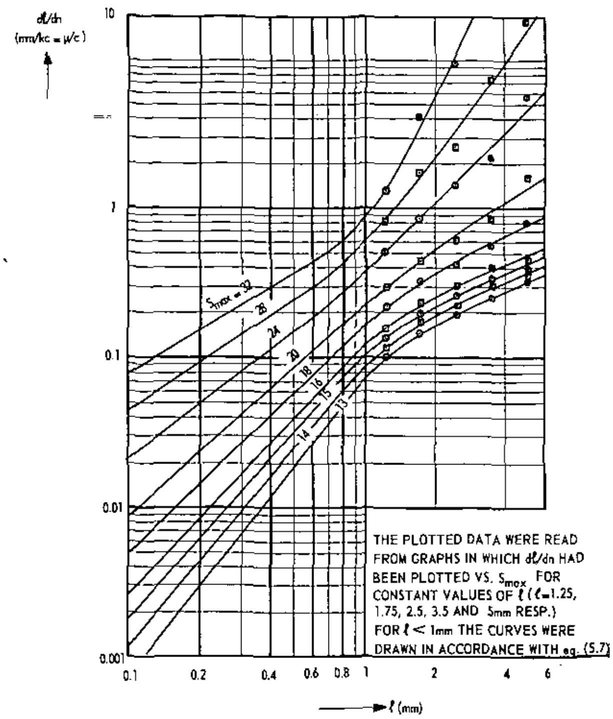

Fig. 21 The crack rate as a function of crack length for the small notched specimens.

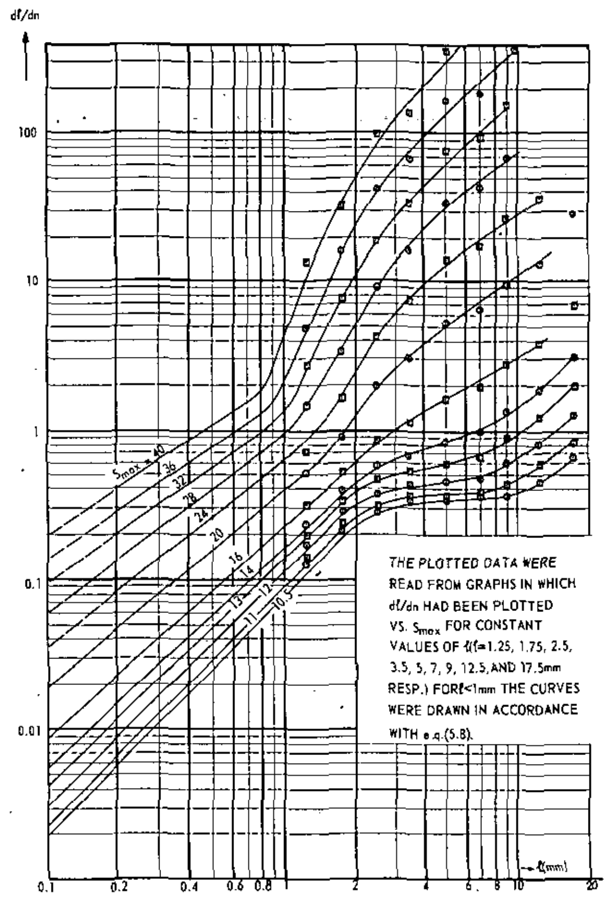

Fig. 22 The crack rate as a function of crack length for the large notched specimens.

TABLE 8

Calculated values of α and C in $dl/dn = Cl^{\alpha}$ for the unnotched specimens
The values of α and C were calculated (method of least squares) for a linear regression of log dl/dn on log l for $l \leq 1$ mm (see fig. 12)
The number of test data involved in each calculation is indicated between brackets

S_{max} (kg/mm^2)	32	28	26	24	23	22	20	19.5	19	18
Values* of α	2.26(7)	1.82(7) 1.94(5)	1.85(4)	1.50(4) 2.21(3) 2.04(2)	2.07(3)	2.16(5) 1.52(3)	1.98(3) 1.83(4)	2.55(3) 2.07(3)	2.88(3) 1.66(3)	1.73(2)
Weighted mean value of α	1.98 ~ 2.0									
Values* of C	0.242	0.0868 0.246	0.127	0.0721 0.0909 0.0486	0.0693	0.102 0.0663	0.0449 0.0368	0.0361 0.0389	0.0502 0.0316	0.0225

* Values were computed with l in mm and dl/dn in mm/kc (μ/c).

TABLE 9

Calculated values of α and C in $dl/dn = Cl^{\alpha}$ for the small notched specimens
The values of α and C were calculated (method of least squares) for a linear regression of log dl/dn on log l for $l < 1$ mm (see fig. 13)
The number of test data involved in each calculation varied from 5 to 9

S_{max} (kg/mm^2)	28	24	20	18	17	16	15	14	13	12.5
Values* of α	1.13	1.11 1.25	1.34 1.47	1.31 1.50 1.66	1.60 1.79 1.84	1.44 1.59	1.59 1.69 1.89	1.46 1.59 2.19 2.37	1.85 2.00	2.18 2.31
Values* of C	0.472	0.251 0.338	0.193 0.255	0.168 0.177 0.220	0.141 0.171 0.201	0.103 0.124	0.0702 0.0723 0.113	0.0590 0.0844 0.0906 0.1292	0.0585 0.0749	0.0591 0.0761

* Values were computed with l in mm and dl/dn in mm/kc (μ/c)

TABLE 10

Calculated values of α and C in $dl/dn = Cl^{\alpha}$ for the large notched specimens
The values of α and C were calculated (method of least squares) for a linear regression of log dl/dn on log l for $l < 1$ mm (see fig. 14). The number of test data involved in each calculation varied from 5 to 7.

S_{max} *(kg/mm²)*	36	28	24	20	18	16	15.2	14.2	13.2	13	12	11.45	11.4	11	10.5
Values* of α	1.09	1.37	1.53	1.21	1.08	1.46	1.43	1.40	1.54	1.72	1.36	1.33	1.70	1.98	1.73
				1.03	1.25					1.83	1.53			1.68	1.27
Values* of C	0.443	0.876	0.495	0.285	0.250	0.194	0.206	0.189	0.118	0.129	0.127	0.094	0.107	0.106	0.066
				0.337	0.174					0.175	0.086			0.124	0.080

* Values were computed with l in mm and dl/dn in mm/kc (μ/c).

since they involve only a small extrapolation of the available data. For $l=0.1$ mm the extrapolation is no longer small and this result depends entirely on the validity of eq. (5.2) at such a small crack length.

Similar figures have been prepared for the small and the large notched specimens, see figs. 24 and 25. However, in these cases no extrapolations were made since more experimental data for small cracks were available. N_l -data were read from S_{max}–N_l curves. For reasons to be discussed in section 6.1 both figures have been replotted in figs. 26 and 27 by using as an abscissa N_l/N_2 and $N_l/N_{2.5}$ respectively instead of N_l/N. Figs. 23, 24 and 25 show that a substantial part of the fatigue life is covered by cracking with crack sizes larger than 0.1 mm. This part is reduced at lower stress values near the fatigue limit.

Knowing that a large part of the fatigue life involves crack propagation with cracks larger than 0.1 mm one is tempted to extrapolate with eq. (5.2) or eq. (5.9) to still earlier stages of the fatigue life. If eq. (5.2) should hold from the beginning of the fatigue test eq. (5.9) implies that a crack of finite length should be present in a virgin specimen. Indicating this initial crack length by l_0 one can calculate its magnitude from eq. (5.9) by substituting $l_1=l_0$ and $N_{l_1}=0$. With $l_2=0.5$ mm the result is

$$\frac{1}{l_0^{\alpha-1}} = 2^{\alpha-1}+(\alpha-1)\,CN_{0.5}\,. \tag{5.10}$$

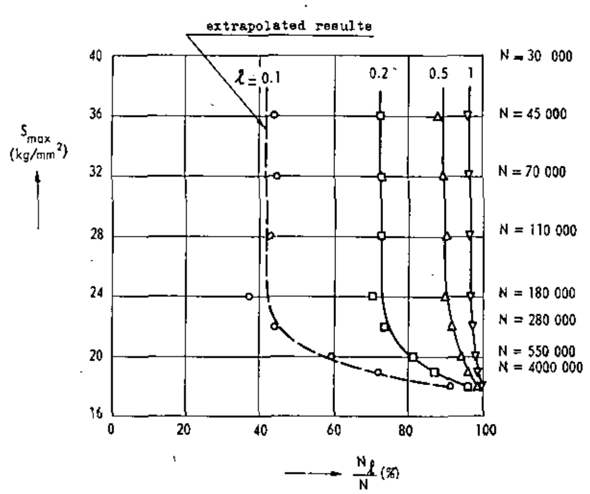

Fig. 23 Percentage of fatigue life covered by crack propagation in the unnotched specimens.

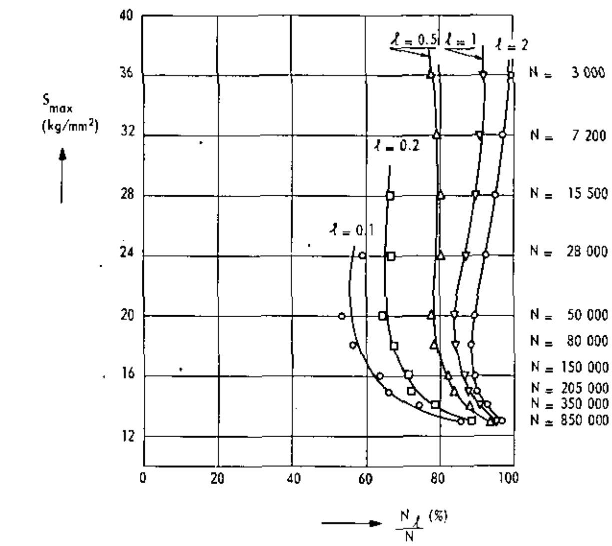

Fig. 24 Percentage of fatigue life N covered by crack propagation in the small notched specimens.

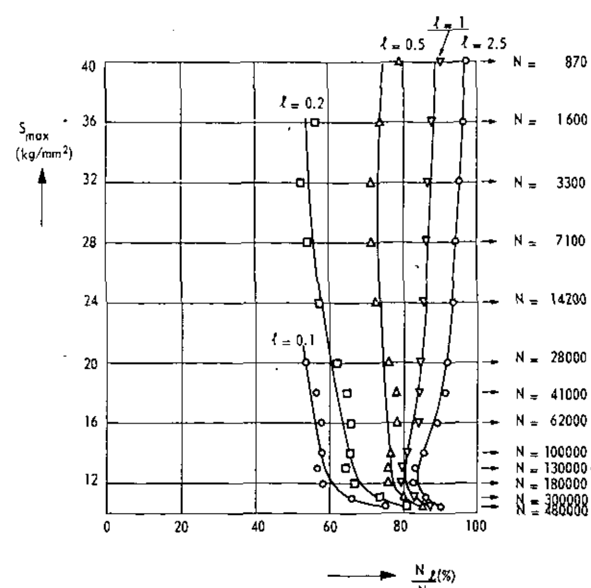

Fig. 25 Percentage of fatigue life N covered by crack propagation in the large notched specimens.

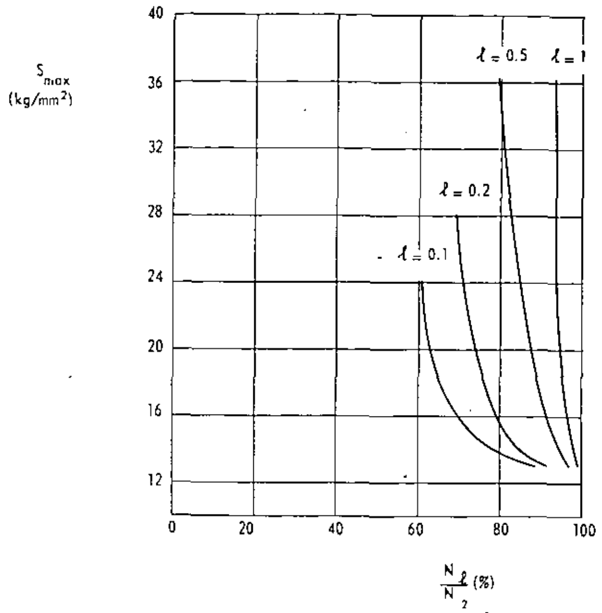

Fig. 26 Percentage of fatigue life N_2 covered by crack propagation in the small notched specimens.

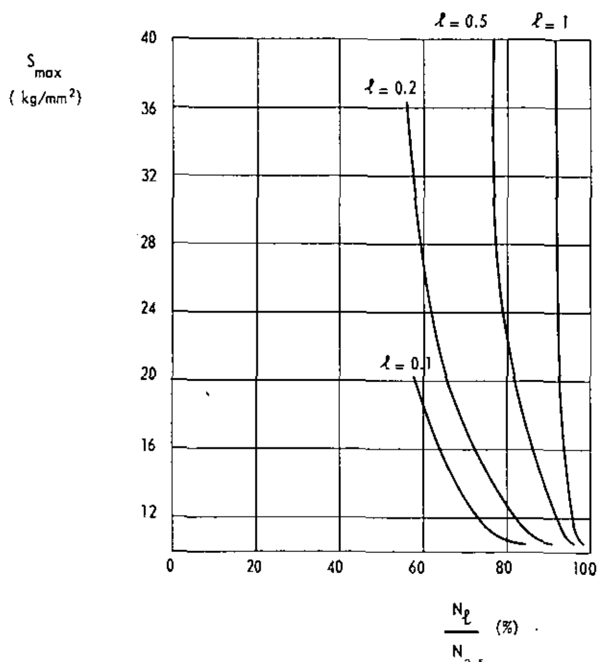

Fig. 27 Percentage of fatigue life $N_{2.5}$ covered by crack propagation in the large notched specimens.

With this relation l_0-values and the corresponding crack rates $(dl/dn)_0$ have been calculated and compiled in table 11.

Table 11 shows l_0 to depend on the stress level, which is unsatisfactory in itself. But moreover the idea that cracks are present in virgin specimens is probably not realistic. Some relevant evidence on micro cracking was recently published by de Lange (ref. 19). His results are analysed in Appendix A and further discussed in chapter 6. They give the impression that cracks start with a zero-crack length, the crack rate being approximately constant during the initial period of the fatigue test. At a certain length of the crack the growth accelerates in accordance with eq. (5.2). If it is assumed that de Lange's results also apply to the present tests, the constant crack rate at the beginning of the test $(dl/dn)_t$ and the crack length l_t at which the crack starts accelerating can be calculated from the following relations:

Firstly,
$$\frac{l_t}{\left(\dfrac{dl}{dn}\right)_t} = N_{l_t} \tag{5.11}$$

N_{l_t} is the number of cycles during which the crack rate remains constant. From eq. (5.9) with $l_1 = l_t$ and $N_{l_1} = N_{l_t}$

$$\frac{1}{l_t^{\alpha-1}} - \frac{1}{l_2^{\alpha-1}} = (\alpha-1)\,C(N_{l_2} - N_{l_t}) \tag{5.12}$$

and from eq. (5.2)

$$\left(\frac{dl}{dn}\right)_t = C l_t^{\alpha}\,. \tag{5.13}$$

With $l_2 = 0.5$ mm evaluation of eqs (5.11), (5.12) and (5.13) leads to

$$\frac{1}{l_t^{\alpha-1}} = \frac{1}{\alpha}\left[2^{\alpha-1} + (\alpha-1)\,C N_{0.5}\right]. \tag{5.14}$$

Values of $(dl/dn)_t$ and l_t have been calculated with eq. (5.13) and eq. (5.14) and the results are also compiled in table 11. It should be pointed out that if α is near to one the calculated results are very sensitive to small variations of α. In view of the scatter in α, see figs. 15 and 16, it cannot be said that α is accurately known. Since α-values near to one were obtained for high stress levels the corresponding values of l_t and $(dl/dn)_t$ are far from accurate.

To obtain an impression on the scatter in the fatigue life until visible cracking and the fatigue life covered by visible cracking the values of $N_{0.5}$ (fatigue life until $l=0.5$) and N–$N_{0.5}$ (fatigue life covered by cracking from $l=0.5$ to final failure) have been plotted as a function of S_{max} in figs. 28, 29 and 30 for the three types of specimens respectively. Scatter bands have been roughly indicated. The bands do not have a clearly statistical meaning, but their width might be associated with twice the standard deviation. For fatigue lives below 100,000 cycles the bands have an approximately constant width and the widths are almost equal for $N_{0.5}$ and N–$N_{0.5}$. If this width is equal to 2σ the following values for $\sigma_{\log N}$ are obtained: 0.18, 0.13 and 0.10 for the unnotched, the small notched and the large notched specimens respectively. At low stress values the scatter band for $N_{0.5}$ becomes broader for all three types of specimens, contrary to the scatter band for N–$N_{0.5}$.

It was checked whether a high $N_{0.5}$-value would

TABLE 11

Calculated values of crack lengths and crack rates

Type of specimen	S_{max} (kg/mm²)	N (kc)	l_0 (mm)	$(dl/dn)_0$ (mm/kc)	l_t (mm)	$(dl/dn)_t$ (mm/kc)	$(dl/dn)_t$ (Å/c)	N_t/N %
	36	45	0.058	0.0013	0.117	0.0052	52	50
	32	70	0.058	0.00081	0.115	0.0033	33	50
	28	110	0.060	0.00054	0.120	0.0021	21	51
Unnotched	24	180	0.065	0.00035	0.130	0.0014	14	52
specimens	22	280	0.058	0.00020	0.116	0.00080	8	52
	20	550	0.043	0.000075	0.085	0.00030	3	51
	19	970	0.030	0.000030	0.059	0.00012	1.2	51
	18	4000	0.009	0.000002	0.018	0.00001	0.1	50
	32	7.2	0.0045	0.0043	0.013	0.0112	112	16
	28	15.5	0.0028	0.00099	0.007	0.0028	28	17
	24	28	0.0073	0.00093	0.018	0.0028	28	24
Small notched	20	50	0.021	0.00098	0.049	0.0032	32	31
specimens	18	80	0.025	0.00061	0.057	0.0021	21	34
	16	150	0.026	0.00027	0.057	0.0010	10	38
	15	205	0.029	0.00019	0.061	0.0007	7	41
	14	350	0.025	0.00009	0.051	0.0003	3	44
	13	850	0.016	0.00002	0.033	0.0001	1	48
	40	0.87	0.121	0.24	0.32	0.67	6700	55
	36	1.6	0.088	0.12	0.23	0.34	3400	42
	32	3.3	0.049	0.041	0.12	0.12	1200	32
	28	7.1	0.024	0.011	0.060	0.033	330	26
Large notched	24	14.2	0.016	0.0063	0.039	0.011	110	25
specimens	20	28	0.014	0.0014	0.033	0.0044	44	27
	18	41	0.013	0.00086	0.032	0.0027	27	28
	16	62	0.014	0.00054	0.032	0.0018	18	30
	14	100	0.015	0.00035	0.035	0.0012	12	30
	13	130	0.016	0.00027	0.037	0.0009	9	31
	12	180	0.016	0.00018	0.035	0.0006	6	31
	11	300	0.011	0.00007	0.025	0.0003	3	33
	10.5	480	0.007	0.00003	0.015	0.0001	1	35

imply a high N–$N_{0.5}$-value, in other words whether there was a (positive) correlation between the fatigue life until visible cracks and the fatigue life covered by visible cracking. This has been done by adding numbers to the data points for $N_{0.5}$ indicating the sequence of increasing N–$N_{0.5}$-values of the corresponding test results. A sequence 1, 2, 3 implies a positive correlation and a sequence 3,2,1 a negative correlation. Figs. 28, 29 and 30 then show that no systematic correlation is present.

6 Discussion

The data obtained in this investigation have some relevance to three questions, viz.:

1. How does fatigue occur in a metallic material, in this case an aluminium alloy?
2. How is the correlation between the fatigue phenomenon in different types of specimens (notch and size effect)?
3. Which period of the fatigue life is most liable to scatter?

The first question is considered in section 6.1, in which some results of a more extensive study (ref. 30) on the fatigue phenomenon in aluminium alloys are briefly recapitulated. A summary of crack growth data from the literature is added. Macro-fractographic observations are summarized in section 6.2. Question no. 2 is dealt with in sections 6.3 and 6.4. In the former section the methods of analysis of the notch and size effect as given in the literature are broadly outlined and comments based on the implications of the present results are given. In section 6.4 the endurances obtained in the present investigation are compared with NASA results. Subsequently it is studied whether a correlation between the crack rate data for the three types of specimens tested could be indicated. The third question on scatter is briefly touched upon in section 6.5. Finally the salient aspects of this chapter are summarized in section 6.6, to which some comments on prospects for the future are added.

Test data drawn from the literature are mainly concerned with the same material as used in the present investigation, viz. 2024 material.

6.1 *The fatigue phenomenon in aluminium alloys*

The main purpose of this section is to study how the nucleation and propagation of fatigue cracks is affected by (1) the stress amplitude and (2) the presence of a notch. Before doing so a general summary of the fatigue phenomenon in aluminium alloys is presented which is largely based on ref. 30. Secondly the present investigation leads to an assessment of the orders of

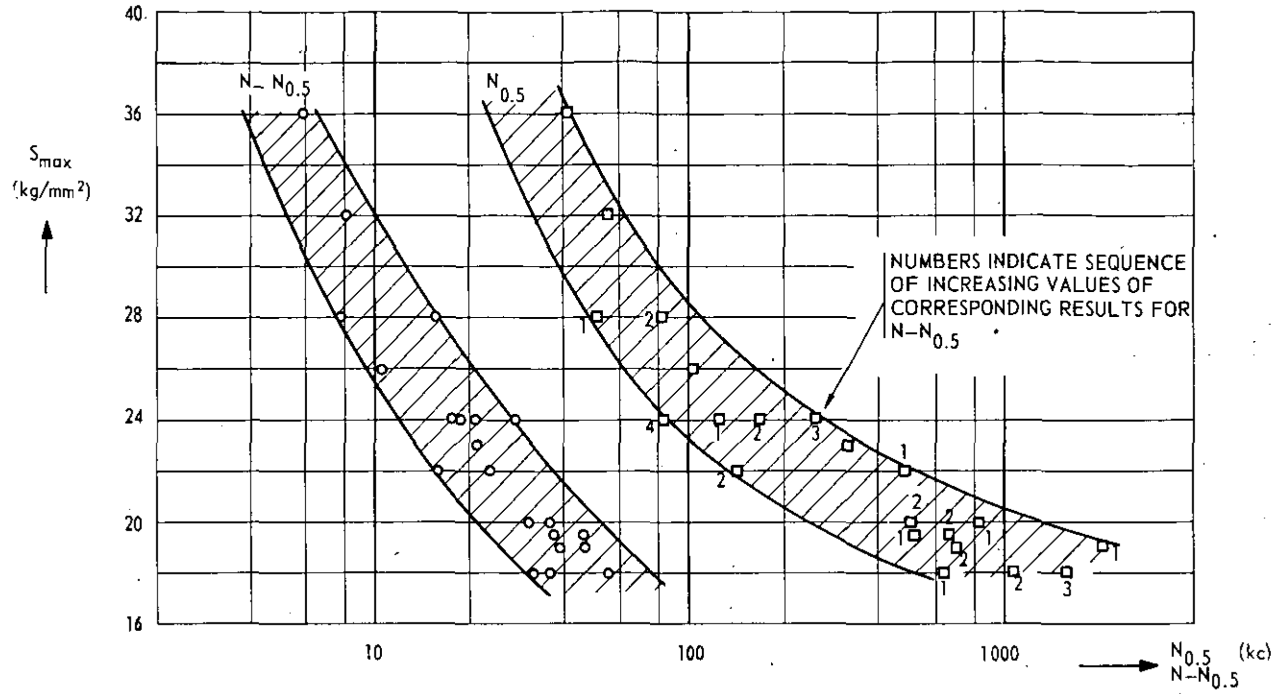

Fig. 28 Scatter in fatigue life until visible cracking ($N_{0.5}$) and the fatigue life covered by visible cracking (N–$N_{0.5}$) for unnotched specimens.

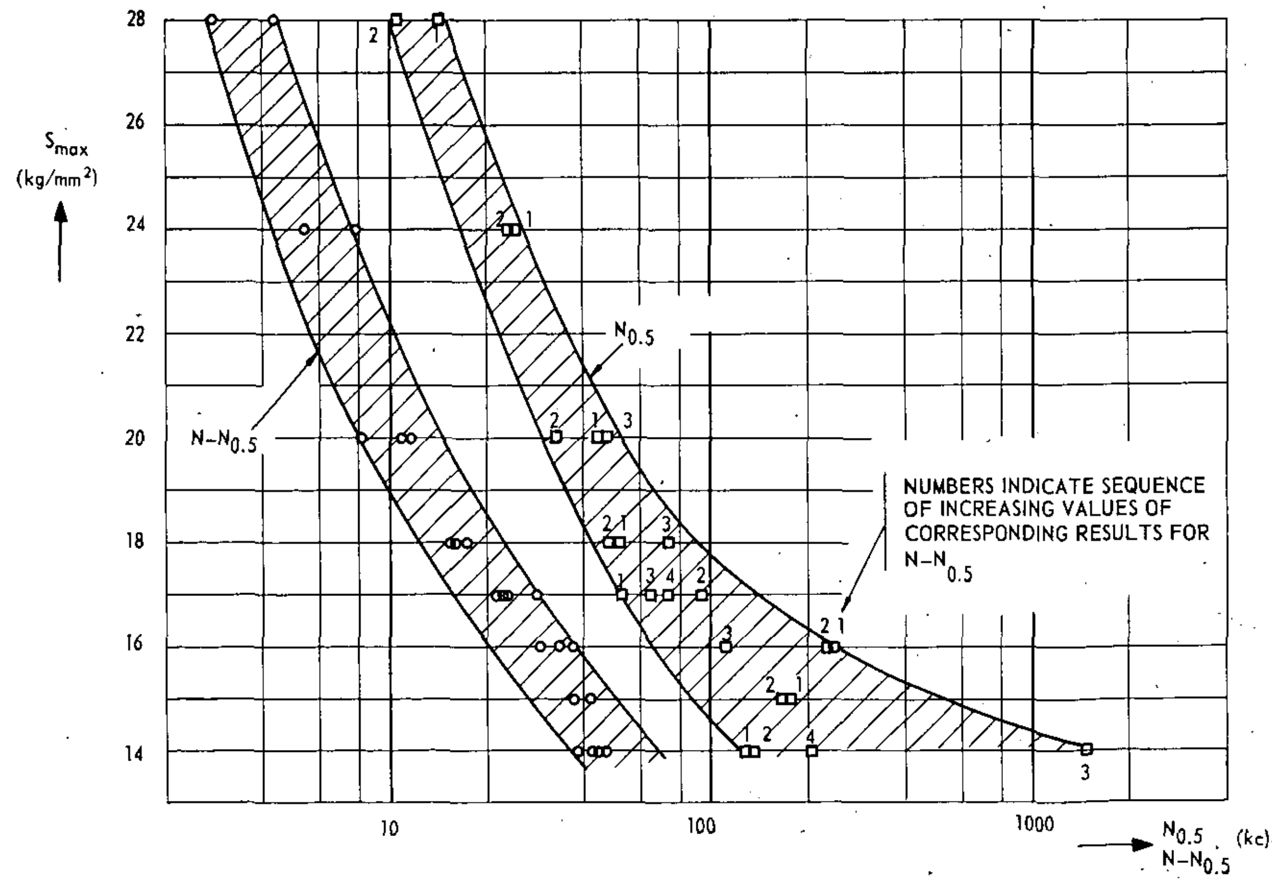

Fig. 29 Scatter in fatigue life until visible cracking ($N_{0.5}$) and the fatigue life covered by visible cracking (N–$N_{0.5}$) for the small notched specimens.

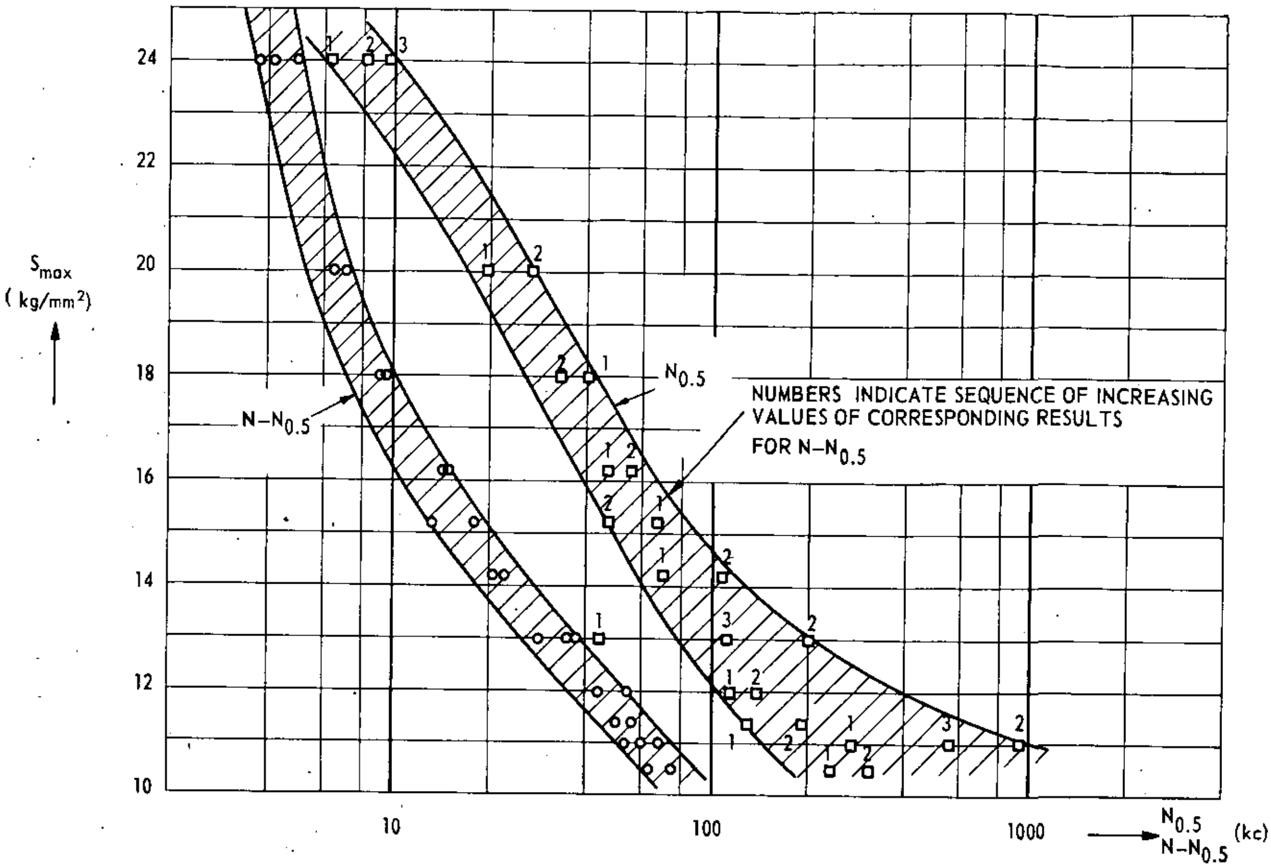

Fig. 30 Scatter in fatigue life until visible cracking ($N_{0.5}$) and the fatigue life covered by visible cracking (N–$N_{0.5}$) for the large notched specimens.

magnitude of the crack rate as occurring in aluminium alloy specimens. Such values have some meaning for a theory on the fatigue phenomenon, an aspect which is further explored in ref. 30.

During a fatigue test fatigue damage is accumulating. For a rational approach of several problems it is necessary to know how this occurs. The fatigue process can be schematically described by the following steps.

$\boxed{\text{Cyclic slip}} \longrightarrow \boxed{\text{microcrack}} \longrightarrow \boxed{\text{macrocrack}} \longrightarrow \boxed{\text{final failure}}$

From microscopical studies it is known that microcracks are present very early in the fatigue life. Secondly the growth of a microcrack to a macrocrack covers the major part of the fatigue life. The difference between microcracks and macrocracks cannot exactly be defined. Usually the term macrocrack is associated with cracks which are visible to the naked eye. The final failure occurs in the last cycle of the fatigue test. It is comparable to a static failure so far as it usually exhibits macro-plastic deformation.

The propagation of cracks depends on external factors, such as applied load, geometry of specimen, environment etc., and internal factors, such as the crack length, the strain-hardening in the specimen due to the fatigue load history and the residual stresses in the specimen. During crack propagation the zone ahead of the crack is subjected to cyclic strain-hardening (or softening) which will affect the amount of cyclic slip and thus the crack extension in subsequent cycles. Residual stresses are known to have some additive effect to the externally applied loads. Broadly speaking one can indicate three damage parameters: (1) crack length, (2) strain-hardening and (3) residual stress. It is difficult to describe quantitatively the second and the third parameter since both strain-hardening and residual stress will not be homogeneous through the specimen and moreover they may change form cycle to cycle. The crack length is the only parameter which can be easily defined. Moreover, it is the only one amenable to measurements. It was one of the purposes of the present study to obtain quantitative data on the microcrack propagation for various fatigue loads and three different types of specimen. Systematic studies on microcrack propagation giving quantitative data are scarce in the literature.

A restriction of the present study is the low magnification of the microscopes implying that in general cracks were not found before they had a length of 0.1 mm (100 μ). As a consequence crack propagation was not observed in the first part of the fatigue test. Recently some results were published by de Lange (ref. 19). Studying the possibilities of a new replica method for microscopical observations he also performed rotating beam tests on unnotched specimens of the 26 ST aluminium alloy, which is practically the same material as used for the present investigation. The replica method allowed large magnifications to be used and de Lange observed crack propagation from the beginning of the test. His tests are a welcome complement to the present study. A brief summary and an analysis of the results is presented in Appendix A. The main conclusion for the present purpose is that the crack rate is not increasing right at the beginning of the test. The crack rate shows a tendency to be approximately constant in the first part of the test after which acceleration of the growth occurs in the same way as for the unnotched specimens of the present investigation (see fig. A1 and compare this figure with fig. 12), i.e. in accordance with eq. 5.2, α being independent of S_a.

At first sight it might seem somewhat surprising that the crack rate is approximately constant during the nucleation period. However, there are some arguments to explain this feature qualitatively. Crack nucleation and propagation are closely associated with cyclic slip. At the start of a fatigue test cyclic slip will concentrate at the free surface even if the stress distribution is homogeneous. This is due to the lower restraint on slip movements at the free surface. Cracks are therefore nucleated at the free surface, apart from inclusions. If a crack nucleus has been formed, it will concentrate slip movements as a result of its stress raising effect and one would expect an increasing crack growth rate. However, if the crack penetrates into the material, the cyclic slip movements in the crack tip region will meet with an increasing restraint. In other words the state of stress in the critical region is changing from biaxial to triaxial. If there is a balance between the increasing stress raising and the increasing restraint on slip one might imagine that the crack rate remains approximately constant during the initial period of the test. When the crack is becoming larger the effect of the free surface vanishes and since the increasing stress concentration remains an acceleration of the crack growth will occur.

Based on the assumption that the crack rate is constant during the nucleation period until a crack length l_t has been reached, after which the propagation accelerates, the crack rate in the nucleation period was calculated from the present results as discussed in the previous chapter. Values were compiled in table 11. These values have been plotted in fig. 31. The results for high S_{max}-values for the notched specimens were omitted since they could not be determined accurately enough as pointed out in chapter 5. For low S_{max}-values $(dl/dn)_t$ is decreasing to very low values. It should be expected that the curves have a vertical

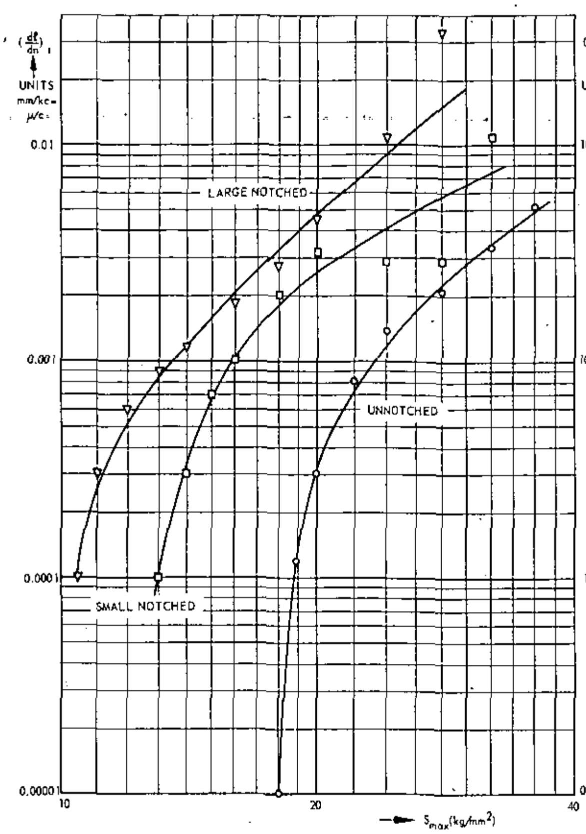

Fig. 31 Estimated minimum crack rates.

asymptote at the fatigue limit, unless non-propagating fatigue cracks could exist below the fatigue limit. However, Frost (ref. 8) has shown that this requires sharp notches which were not used in the present investigation. Although fig. 31 will not have a high accuracy it is thought that it reasonably represents the orders of magnitude of the minimum crack rates. Fig. 31 is then of importance for fundamental fatigue theories, since it gives quantitative indications of minimum values of crack rates to be considered.

A second result of the present study which is of importance for fatigue theories is that the observations point to a crack propagation during the complete fatigue life for low and high stress amplitudes and for unnotched and notched specimens. More particularly the opinion found in the literature, suggesting a fundamental difference between fatigue at high and low stress amplitudes seems not to be substantiated by the present observations on microcrack propagation.

Finally the crack growth, also in the micro-stage seems to be a continuous process. An elaboration of these three fundamental aspects is beyond the scope of this report. A further exploration is given in ref. 30.

The literature review presented in ref. 28 was a preliminary study for the present investigation. It was concluded there that the crack nucleation in unnotched specimens would cover a larger proportion of the fatigue life than in notched specimens. The conclusion was based on limited evidence that cracks in very severely notched specimens were observed very early in the fatigue life, whereas in unnotched specimens cracks were observed shortly before final failure. Some more evidence of this type has become available and will be briefly reviewed. The majority of the data of the literature is of a qualitative nature, i.e. the crack length at the moment of detection was not specified.

Bennett and Baker (ref. 1) performed tests on unnotched 2024-T3 sheet specimens in pulsating bending ($S_{min}=0$, $R=0$). From crack propagation data they derived the fatigue life N_l for a crack length $l=0.25$ mm. Their results are plotted in fig. 32 in the same way as for the unnotched specimens of the present study in fig. 23. The agreement between both figures is very good, even quantitatively.

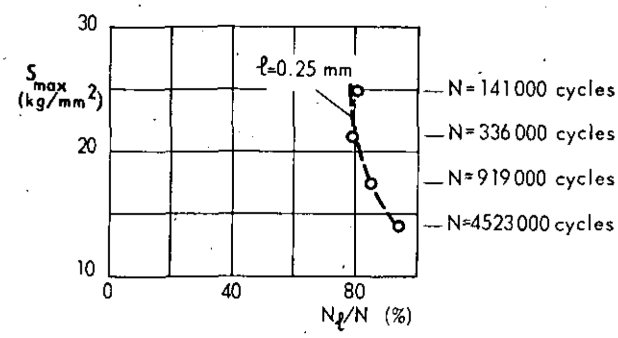

Unnotched sheet specimens of bare 2024-T3 material, sheet thickness 2 mm (0.08″) were loaded in pulsating bending ($R=0$, $S_{min}=0$). N_l = fatigue life at which the crack length was 0.25 mm (0.01″)

Fig. 32 The fatigue life at a small amount of cracking. Results of Bennett and Baker (ref. 1).

Similar results of Bennett and Weinberg (ref. 2) obtained with unnotched and mildly notched rotating beam specimens of 2024-T4 extruded material ($S_m=0$) are shown in fig. 33. Although the length of the crack at the moment of detection is not specified, it probably will have been in the order 0.25 to 0.5 mm. Fig. 33 then confirms that fatigue cracks are observed (1) at an earlier stage of the fatigue life at high stresses and (2) for the same fatigue life at an earlier stage in notched specimens as compared with unnotched specimens. The second trend is also observed by comparing figs. 23, 24 and 25 for $l=0.5$ mm. However, for smaller values of the crack length the picture is more complicated as will be discussed later.

Hunter and Fricke have made microscopical studies on the nucleation of microcracks in several aluminium alloys (refs. 12, 13 and 14). They do not specify the length of microcrack at the moment of detection. Results for 2024-T3 sheet material are shown in fig. 34 in a similar way as for the present study in fig. 23. Although the loading was alternating bending the trends are the same, i.e. (1) microcracks are observed

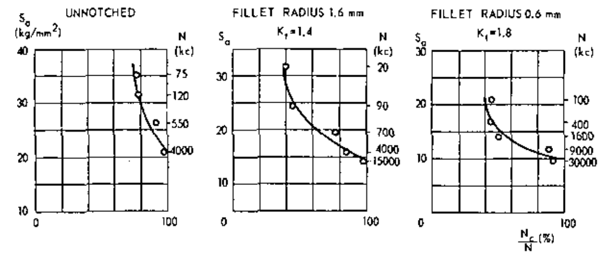

Unnotched and mildly notched rotating beam specimens ($S_m = 0$) were made of 2024-T4 extruded material. N_c = fatigue life at which cracks were detected. Crack length at the moment of detection was not specified.

Fig. 33 The fatigue life at detection of the first crack. Results of Bennett and Weinburg (ref. 2).

early in the fatigue life and (2) at lower stress amplitudes the moment of detection is shifted to a higher percentage of the fatigue life. They obtained similar results for 7075-T6 and Al–Mg alloys, also on sheet specimens loaded in alternating bending.

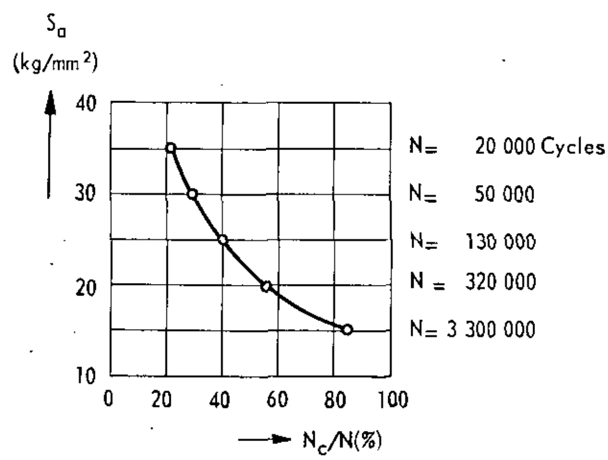

Unnotched sheet specimens of bare 2024-T3 material, sheet thickness 1.6 mm (0.64″) were loaded in alternating bending ($S_m = 0$). N_c is fatigue life at which cracks were observed with the microscope (replica technique). Crack length at the moment of detection was not specified.

Fig. 34 The fatigue life at detection of the first microcrack. Results of Hunter and Fricke (ref. 12).

In ref. 14 Hunter and Fricke suggest that log l was increasing as a linear function of the number of cycles in accordance with the following modified formula of Bennett, although they give no numerical data on the propagation.

$$\log l = an + b\ .$$

From this relation the following proportionality is easily deduced:

$$\frac{dl}{dn} \backsim l\ .$$

This result is in contradiction with the results of the present study, where it was found that $dl/dn \backsim l^2$ (see eq. 5.6). In other words, in the present study the crack rate is accelerating more quickly. This is not strange in view of the differences in test conditions. Note that de Lange found $dl/dn \propto l1\frac{1}{2}$ (see Appendix). Hunter and Fricke employed alternating bending ($S_m=0$) at constant deflection, de Lange applied rotating bending ($S_m=0$) and in the present study the loading was pulsating tension ($S_{min}\sim 0$, $R\sim 0$) and the specimens were axially loaded at a constant stress.

Axially loaded aluminium alloy specimens with very sharp notches were tested by Frost (refs. 7 and 8). The material was BS L65 (4.4% Cu, 0.7% Mg, remainder Al). Frost especially studied so-called non-propagating fatigue cracks. Such cracks are formed at stress levels below the fatigue limit. With very sharp notches fatigue cracks are observed almost immediately at the beginning of the test, even if the cracks become non-propagating. Frost has shown that non-propagating cracks require very sharp notches, i.e. $K_t > \sim 4$, and a low mean stress.

Fatigue crack propagation in severely notched rotating beam specimens ($S_m=0$) of 2024-T4 extruded material was studied by Hyler, Abraham and Grover (ref. 15). Root radii employed were 0.05 and 0.4 mm (0.002″ and 0.016″), K_t-values being 5.2 and 13.9. The depth of the crack was measured by sectioning of specimens at various values of the cycle ratio n/N. Although the available data is limited it shows that cracks were formed very early in the fatigue test even if the anticipated fatigue life was long. The crack was then growing extremely slowly for the major part of the fatigue life. Also fatigue cracks formed at a stress level below the fatigue limit were present after a relatively low number of cycles. The results confirm Frost's findings.

Demer (ref. 4) performed tests on unnotched and notched rotating beam specimens of 2024-T4 extruded material. He used somewhat unusual methods for crack detection. On the unnotched specimens cracks were indicated by a moisture coating method at 50 to 85% of the fatigue life, the higher values applying to higher endurances. In the specimens notched by a V-groove, top radius 0.25 mm (0.01″) and $K_t=3.9$, cracks were detected indirectly as an increase of the deflection of the cantilever specimen. In this way cracks were found very early in the fatigue life, viz. at 4% to 11% of the fatigue life, the higher values applying again to high fatigue lives. Sectioning of some specimens showed the method to be reliable. Below the fatigue limit the notched specimens revealed non-propagating cracks. With respect to the effect of stress amplitude Demer's results are qualitatively in agreement with the investigations discussed before and the present study.

Tests reported by Weibull (ref. 37) were carried out on 2024-T3 sheet specimens with a very sharp central notch ($K_t\sim 11.5$), the specimens being axially loaded with a zero minimum stress. In general visible cracks were found early in the fatigue life. The main purpose of these tests was to study the propagation of macro-cracks and the sharp notch was made to initiate cracks in a small number of cycles.

In the above review two trends were mentioned with respect to the moment of crack detection. (1) With a certain type of specimen cracks are observed at a lower percentage of the fatigue life for higher stress amplitudes. (2) If different types of specimens at the same fatigue life are compared cracks are observed at a lower number of cycles in the more severely notched specimens.

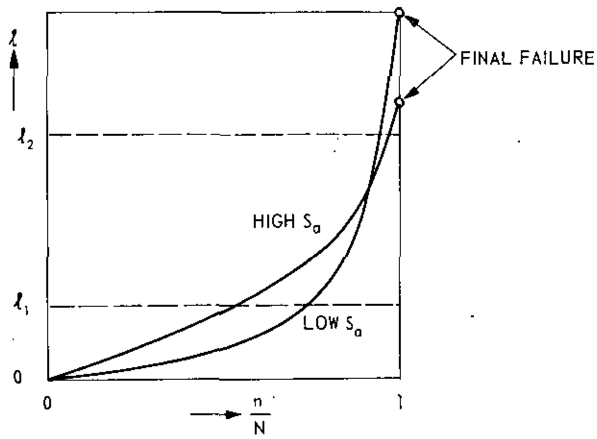

For the higher stress amplitude cracks detected at a length l_1 are observed at a lower percentage of the fatigue life. At a length l_2 the reverse is true.

Fig. 35 Schematic crack propagation curves at a high and a low stress amplitude for the same type of specimen.

The first trend is confirmed by all the investigations reviewed above. A schematic picture of the trend is shown in fig. 35. From this figure it will be clear that the trend will depend on the sensitivity of the crack detection method. If very minute cracks can be found they will be indicated in the very beginning of the test for both high and low stress amplitudes. If cracks of a length l_1 can be detected cracks will be found at an earlier stage of the fatigue tests with the higher stress amplitude. If the detection method is less sensitive and cracks of a length l_2 can be detected cracks will be observed at a later stage in the tests with the higher stress amplitude. The latter is illustrated in figs. 24 and 25 of the present study for $l \geqslant 1$ mm. It should be pointed out that the latter result is due to the fact that final failure occurs at a lower crack length for higher S_{max}-values. If the end of the test is defined at the moment that a certain crack length has been reached cracks are again found relatively earlier at the higher stress level, see figs. 26 and 27, for which the l-values defining the end of the test were $l=2$ mm and $l=2.5$ mm respectively. Figs. 24 and 25 show that for these values the maximum reductions of the fatigue life are 10 and 15% respectively. These data are of some importance for Valluri's criticism on the Palmgren-Miner rule $\Sigma n/N=1$. He says (ref. 36) that this rule is incorrect since N neglects that final failure does not occur at a constant crack length for all stress levels. This argument is correct, but the above results show that replacing in the Palmgren-Miner rule N by N_l (taking l as 2 or 2.5 mm for the present case) will affect $\Sigma n/N$ to a small extent and can therefore explain small deviations from this rule* only. It is thought that the deviations actually observed have other more important sources, such as residual stresses (ref. 32).

With regard to the second trend mentioned above, viz. that cracks are observed earlier in more severely notched specimens, it seems that the situation is somewhat more complicated than it was originally thought. The investigations reviewed above confirm that cracks are found earlier for increasing K_t-values. This also applies to the present investigation if a crack length $l \geqslant 0.5$ mm is considered. However, for very small cracks the trend need not apply. It is thought that the mean stress may have some effect on the picture. S_m was positive in the present investigation, but in the investigations on the effect of notches reviewed above a zero mean stress was applied (except for the tests of Weibull). Apart from the mean stress other factors, such as root radius, stress gradient and size may affect the trends. Some further thoughts on these aspects are given in section 6.3.

As a conclusion to this section it may be said that dividing a fatigue test in a pre-crack stage and a crack stage, as suggested in ref. 28, seems to be virtually impossible, also for unnotched specimens. It should be added that a complete picture of the crack growth has not yet been obtained. Especially the influence of the mean stress on crack nucleation and propagation (as a microcrack) is recommended for further microscopic studies.

6.2 *Macro-fractographic observations*

The fracture surface of a fatigue specimen can be divided in two parts, one being formed during crack propagation under cyclic loading, i.e. the fatigue part of the failure, and the other one being formed in the last cycle, i.e. the static part of the failure or the final failure. Apart from ring and river patterns the fatigue part generally shows the following characteristic features. (1) There is no plastic deformation on a macro scale contrary to the final failure. (2) The fatigue part is relatively flat in contrast with the final failure. (3) The fatigue part is in a plane perpendicular to the maximum principal stress (90°-mode of fatigue fracture), whereas the final failure in sheet material occurs in a plane rotated to an angle of 45° with the sheet surface.

* This conclusion is not necessarily valid under extreme conditions, such as an aircraft structure with poor fatigue properties (major part of life covered by macrocrack propagation) and poor residual strength characteristics (small cracks inducing a large reduction of strength).

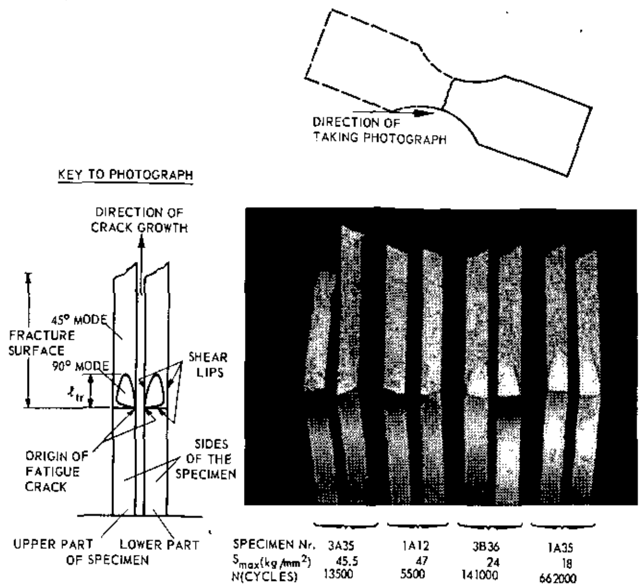

Fig. 36 Upper and lower fracture surfaces of four unnotched specimens tested at different stress levels.

The third feature requires some amplification. Although the 90°-mode is characteristic for the fatigue part of the fracture, it is not correct to assume that the 45°-mode of the fracture is completely caused during the final failure. It has been previously shown (refs. 3 and 29) that a rapidly growing fatigue crack exhibits the 45°-mode fracture.

Fig. 36 shows the fracture surfaces of four specimens. The following trends are observed. The 90°-mode area is larger for a lower value of S_{max}. The 45°-mode is gradually developing, starting as shear lips at the free surface of the specimens, see the fracture surfaces of specimens nrs. 3B36 and 1A35. In general this led to a single shear failure at the moment that the transition from the 90°-mode to the 45°-mode was completed. Sometimes a double shear failure originated then, see for instance specimen nr. 3A35 in fig. 36. If this occurred the direction of growing showed a tendency of deviating some 5 to 10° from being perpendicular to the specimen axis.

In fig. 37 the length of the crack, l_{tr}, at which the transition from the 90°-mode to the 45°-mode was completed has been plotted as a function of the applied stress. In the same graphs curves are shown which indicate the crack length until which crack observations were made. In view of the high crack rate towards the end of a test it is impossible to record the crack length at which the final failure occurs. This length will have been larger than indicated by the latter curves. Also from the fracture surfaces it could not be deduced at which crack length final failure occurred. Fig. 37 shows

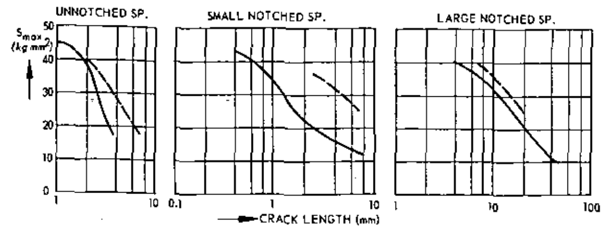

——— crack length l_{tr} (see fig. 36) at which the transition from the 90°-mode to the 45°-mode of fracture was completed. — — — crack length until which crack growth observations were made. For the small and the large notched specimens crack growth observations were not extended beyond $l = 7$ mm and $l = 20$ mm respectively.

Fig. 37 Length of the 90°-mode of the fatigue fracture.

that it is not correct to associate the 45°-mode of the fracture with the final failure.

Microscopical observations showed that the fatigue fracture was transcrystalline during both the 90° and the 45°-mode of fracturing. On the basis of an analysis of the shear stress distribution around the tip of a crack it was indicated in ref. 30 that the transition from one mode to the other one is associated with a transition from a state of plane strain to a state of plain stress. The transition need not be correlated with a change of the fracture mechanism.

6.3 *The notch effect and the size effect*

The notch effect under fatigue loading has puzzled a few generations of investigators. The stimulus for investigations on this problem is twofold: (1) On one hand there is the basic idea that there should be a correlation between the fatigue processes in a notched specimen and in an unnotched specimen. (2) On the other hand it is easily recognized that it would be of great value to the designer if he could calculate the S–N curves for a notched component from the fatigue data for the unnotched specimen, the latter being regarded as a material property. The problem is still far from a rigorous and generally accepted solution. Although the qualitative understanding of the problem has increased, this has revealed that the problem is more complex than was thought in previous days. At the same time several empirical rules have been postulated embedding the experience of numerous empirical data. In this chapter a brief review will be given of the knowledge of the problem and the background of some empirical solutions. Secondly the meaning of the results of the present investigation for this problem will be discussed in more detail.

The notch effect and the size effect are both discussed in this chapter since the size effect is so closely associated with the notch effect that a separate discussion is neither practical nor feasible. It is not the intention of this chapter to present a thorough review of these problems illustrated by empirical data from the literature. For such reviews the reader is referred to two recent textbooks by Heywood (ref. 11) and Forrest (ref. 6).

The simplest problem is a comparison of the fatigue limit, S_f, (i.e. the fatigue strength for infinite life) of a notched and an unnotched specimen at zero mean stress. In fact this is the problem dealt with in most publications on the notch effect. For components loaded in rotating bending for which an infinite life is required this is indeed the practical problem being frequently met in machinery. In aircraft structures positive mean stress and finite life are two rather common, complicating aspects.

The definition of the fatigue limit, S_f, given by the ASTM (ref. 38) is: S_f is the limiting value of the median fatigue strength as the fatigue life, N, becomes very large. For the present purpose it is more illustrative to read the definition as follows (omitting the statistical adjective): S_f is the highest stress amplitude which does not produce microcracks* and is therefore the highest stress amplitude still giving infinite life. Using the subscripts 1 and K for unnotched and notched specimens respectively, their fatigue limits are indicated by S_{f1} and S_{fK}. In the notched specimen the peak stress at the fatigue limit is $K_t S_{fK}$ assuming elastic behaviour. Since this stress is the maximum stress in the notched specimen unable of producing a microcrack and since S_{f1} is the maximum stress in the unnotched specimens unable of doing so, an obvious and simple assumption is:

$$K_t S_{fK} = S_{f1} \,. \tag{6.1}$$

The assumption is illustrated in fig. 38a and b. By definition the fatigue notch factor, K_f, is:

$$K_f = \frac{S_{f1}}{S_{fK}} \,. \tag{6.2}$$

Equation (6.1) then implies:

$$K_f = K_t \,. \qquad (6.3)^{**}$$

However, a general*** observation is:

$$K_f < K_t \,. \tag{6.4}$$

The explanation of this trend has been the subject of

---

* This definition is allowed only if non-propagating cracks will not occur. These cracks were extensively studied by Frost (refs. 7 and 8) who showed that the non-propagating cracks may occur at stress amplitudes below the fatigue limit in severely notched specimens. Frost's work was elucidatory for the notch effect for high K_t-values (say $K_t > 4$). This aspect, however, is not considered in this report.

** For round specimens with a notch the state of stress at the root of the notch is biaxial and this should be accounted for in K_t, which requires a yield criterion (see ref. 25).

*** The observation does not apply to bolt and rivet holes involving crack nucleation assisted by fretting corrosion.

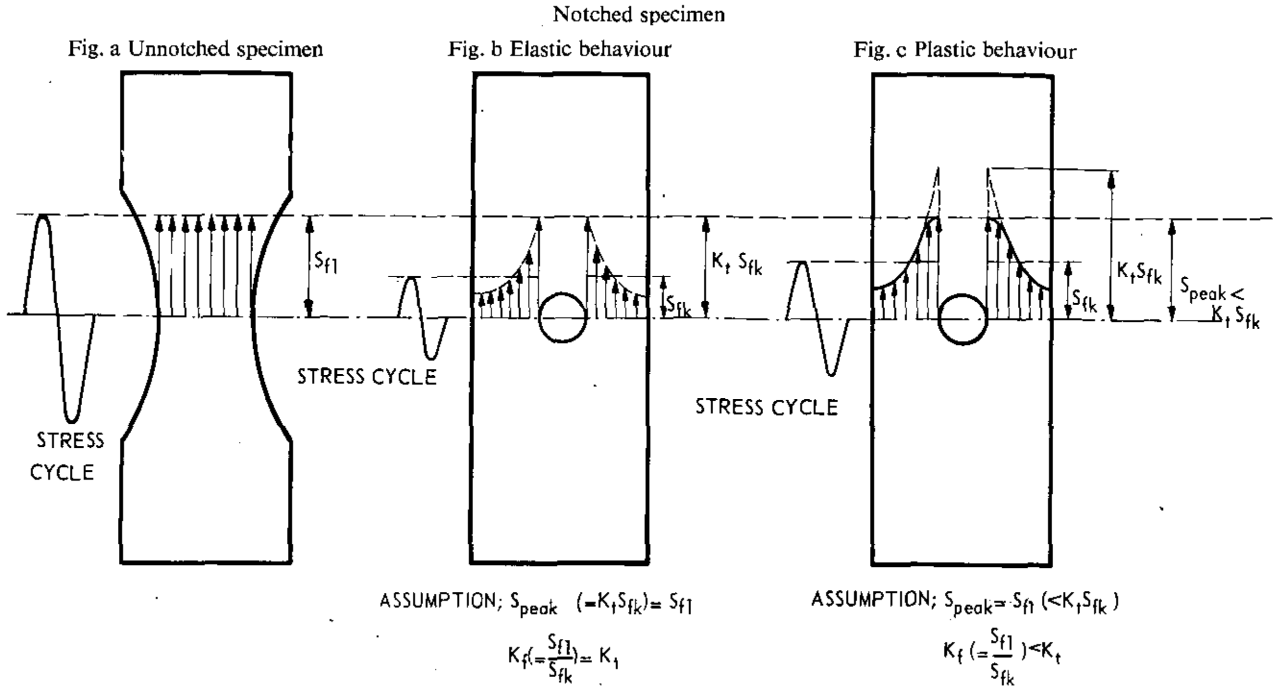

Fig. 38 Comparison of the stress distributions at the fatigue limit in an unnotched and a notched specimen ($S_m = 0$) assuming elastic and plastic behaviour.

many studies. The major aspects of such studies will be briefly summarized.

An obvious difference between figs. 38a and b is that the peak stress in the notched specimen occurs only locally, whereas in the unnotched specimen the stress S_{f1} is transmitted over the full cross section. In other words there is a stress gradient in the notched specimen which is absent in the unnotched specimen. A second difference to be considered is the possibility that the peak stress in the notched specimen will exceed the yield stress S_0, implying that the peak stress will be smaller than $K_t S_{fK}$, see fig. 38c.

These two differences have led to two different approaches of the notch problem. In one approach the stress gradient is considered as a second parameter on which S_{fK} will depend. In the second approach the plasticity is taken into account and it is tried to estimate the local peak stress, which then should be equal to S_{f1}. The first approach includes the size effect whereas the second does not.

The effect of a stress gradient at a notch on the strength of an element was already considered by Neuber (ref. 21). Based on the idea that the mean stress over a small "elementary particle" at the root of a notch was an important parameter for the strength, he developed the well known formula for an "effective stress concentration factor", K_N, sometimes indicated in the literature as the Neuber factor:

$$K_N = 1 + \frac{K_t - 1}{1 + \sqrt{\frac{a}{r}}} \qquad (6.5)$$

where r is the root radius and a is the half width of the elementary particle, also called Neuber constant. According to eq. (6.5) K_N is smaller than K_t, the more so for smaller values of r, i.e. for sharp notches. It should be pointed out that the formula is lacking a rigorous analytical background. Its usefulness for correlating fatigue data has been extensively checked at various laboratories, notably by Kuhn and Hardrath (refs. 16 and 17), starting from the assumption that

$$K_f = K_N . \qquad (6.6)$$

The quantity a was regarded as a material constant and values for steels and aluminium alloys were derived from available fatigue data. This approach is essentially empirical. Modifications of eq. (6.5) were proposed by Heywood (ref. 11) to improve its usefulness for limiting conditions.

Peterson (ref. 25) employed the notch sensitivity factor q defined by

$$q = \frac{K_f - 1}{K_t - 1} . \qquad (6.7)$$

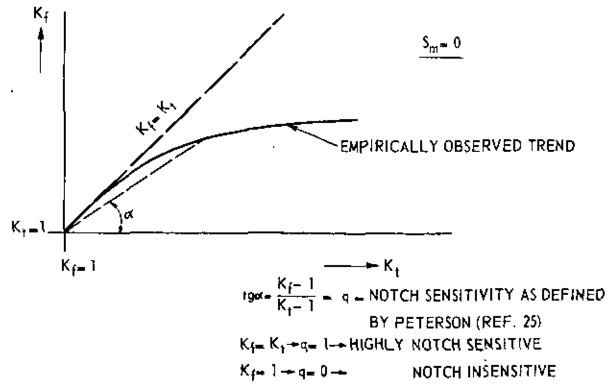

Fig. 39 Generally observed $K_f - K_t$ relation for $S_m = 0$.

For $K_f=1$ (notch insensitive), q is equal to zero and for $K_f=K_t$ (fully notch sensitive), q is equal to one. Increasing values of q from 0 to 1 indicate an increase of fatigue notch sensitivity, see fig. 39. Peterson has plotted q as a function of the root radius r and found such curves to depend on the type of material (refs. 25 and 26), see fig. 40 for an example. The material is now characterized by a curve. Peterson (ref. 26) feels that the q–r curves can be represented by the analytical relation

$$q = \frac{1}{1+\dfrac{a}{r}} \tag{6.8}$$

where a is again a material constant. The similarity (and the difference) with the approach of Kuhn and Hardrath is apparent since eqs. (6.5), (6.6) and (6.7) may be reduced to:

$$q = \frac{1}{1+\sqrt{\dfrac{a}{r}}}. \tag{6.9}$$

Peterson's approach as well as the Neuber formula are easily recognized as being associated with the effect of stress gradient, if it is realized that the relative stress gradient χ at the root of the notch is approximately inversely proportional to r. The relative stress gradient at the root of the notch is defined as the (absolute) value of the stress gradient of the normal stress at that location, divided by the peak stress ($K_t S_{\text{net}}$) at the same location, see fig. 41. For most notches (refs. 26 and 33):

$$\chi \approx \frac{2}{r}. \tag{6.10}$$

Siebel and Stieler (ref. 33) start from the idea that χ is a second parameter to K_t in predicting K_f-values. They proposed that the ratio K_t/K_f is a function of χ only, this function being characteristic for each material, see fig. 41. Since K_t/K_f cannot be written as a function of q only, there is again another empirical formula for the prediction of the notch effect.

It is not the purpose of the present study to compare the merits of the above methods. However, it may be

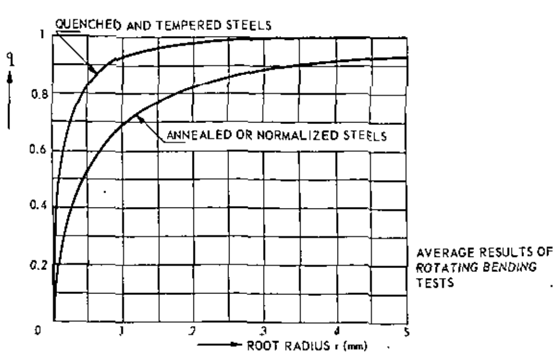

Fig. 40 The fatigue notch sensitivity factor as a function of the radius of the root of the notch according to Peterson (ref. 25).

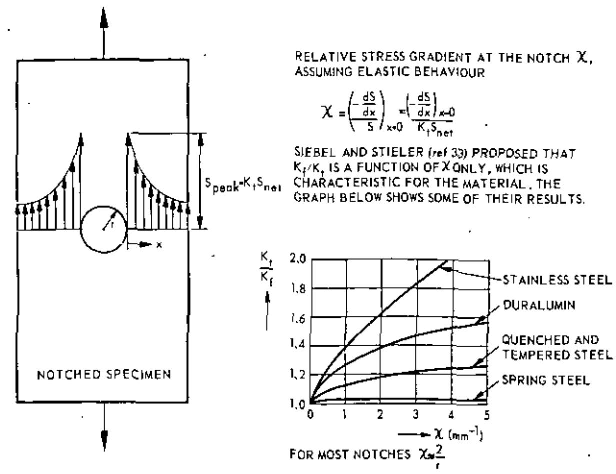

Fig. 41 The relative stress gradient χ as a second parameter to K_t for predicting K_f. Proposal of Siebel and Stieler (ref. 33).

pointed out that K_t alone is incapable of predicting the notch effect and even adding the relative stress gradient (i.e. some more information on the elastic stress distribution) is insufficient for doing so. The material has to enter the problem and in the above methods this occurred by an empirical material constant or an empirical curve, characteristic for the material.

Asking now for which physical reasons the stress gradient is important the explanation may be twofold. First the stress gradient is related to the volume of highly stressed material. Secondly the amount of plastic deformation at the root of the notch will depend on the stress gradient. These aspects will be discussed successively.

If the volume of the highly stressed material has some effect on the fatigue limit a statistical aspect is involved. In a larger volume there is an increased probability for weak spots being present. One may then be tempted to develop an analysis based on a weakest link concept. However, without a physical background this is virtually impossible. For instance, let it be assumed that the weak spots are inclusions, which according to Stulen, Cummings and Schulte (ref. 34) seems to apply to certain types of steel. Then an increase of all dimensions of a specimen with a factor k will increase the number of weak spots in the highly stressed volume k^3 times (statistical volume effect). However, if the weak spots are due to machining effects the number of weak spots will increase k^2 times (statistical surface effect). If the cross section of the specimen is not round but rectangular and cracks originate from the edges the number of weak spots has increased k times (statistical edge effect). In all cases the stress gradient has decreased k times. The problem may be even more complicated if more than one type of weak spots have to be considered. Let it be assumed that the type of weak spot is known, then its effect on the fatigue strength has to be considered. It has to be expected that the size or the severity of the weak spots obeys some statistical distribution law, which will be unknown. Since this law is required for the analysis it has to be determined indirectly from fatigue tests. This can only be successful if other sources of scatter can be excluded.

The foregoing gives a brief indication of the difficulties involved in arriving at the basic data for a weakest link analysis. The statistical aspect of the notch and the size effect certainly form a useful field for research studies, but the possibilities for arriving at a rational quantitative engineering theory are at the present time limited and one is forced to employ such empirical methods as discussed before. It would be of great advantage if basic studies could provide more information on the physical nature of weak spots or rather the sites at which cracks are nucleated. Such information for a variety of materials will be illuminating for technical problems, despite the qualitative character it will have.

With respect to the effect of plastic deformation at the root of the notch on the fatigue limit one might try to correlate this effect with the amount of plastic deformation. Consider a large and a small notched specimen which are geometrically similar. The size of the plastic zone and the plastic deformation integrated over the plastic zone will be larger for the larger specimen. However, the plastic strain at the root of the notch will be the same for both the large and the small specimen, provided the material is homogeneous. It is thought that the plastic strain rather than the integrated plastic deformation will be controlling the nucleation of a microcrack. At first sight this would outrule an influence of the stress gradient as caused by the plastic deformation. This is correct only if the material behaves as a homogeneous material, which need not apply for high stress gradients, i.e. small specimens with sharp notches. Under such conditions the size of the plastic zone may be of the same order or magnitude as the grain size or even smaller. The plastic strain may then depend on the stress gradient.

From the foregoing it will be recognized that it is very difficult to decide whether a stress gradient effect is associated with either statistical aspects (weak spots) or with plasticity. It is thought that in general the former aspect will dominate for large specimens, whereas for small specimens both may be active.

Irrespective of the size (or stress gradient) effect, plastic deformation at the root of the notch will cause a peak stress which is lower than $K_t S_{net}$. This can explain why $K_f < K_t$, see fig. 38c. (It may be repeated that the discussion is still restricted to $S_m = 0$). Defining now K_{pl} as the stress concentration factor in the presence of plastic deformation by:

$$S_{peak} = K_{pl} S_{net} \tag{6.11}$$

one might try to calculate K_{pl} and assume subsequently

$$K_f = K_{pl} \ (< K_t) . \tag{6.12}$$

Two noteworthy efforts may be mentioned here. Hardrath and Ohman (ref. 10) generalized a formula of Stowell for the estimation of K_{pl} for a circular hole in an infinite plate. Their solution was:

$$K_{pl} = 1 + (K_t - 1) \frac{E_s}{E} \tag{6.13}$$

where E is the elastic modulus and E_s the secant modulus in the stress-strain diagram corresponding to a stress $K_{pl} S_{net}$. Since E_s depends on K_{pl} a method of trial and error, requiring the static stress-strain diagram, has to be used for calculating K_{pl} with eq. (6.13). Hardrath and Ohman found K_{pl} to be in remarkably good agreement with strain measurements in static tests. Gunn (ref. 9) adopted K_{pl} for the fatigue notch problem of aluminium alloys and obtained a reasonable confirmation of eq. (6.12) in some cases, the agreement being less good in some other cases.

A second approach was published by Forrest (refs. 5 and 6). He assumed that the strain distribution obeys the elastic solution also after exceeding the elastic limit. From the strain distribution the stress distribution is derived by employing a dynamic stress-strain relation obtained with unnotched fatigue specimens and neglecting the biaxiality or triaxiality in the notched specimen. From this distribution K_{pl} ($= S_{peak}/S_{net}$) was deduced and the equality $K_f = K_{pl}$ (eq. (6.12)) was checked for a variety of materials. Although the agreement was much better than for $K_f = K_t$ a good agreement was obtained for some materials only. Probably the method breaks down for most materials since the stress distribution in a notched specimen, for which the peak stress exceeds the elastic limit will not remain constant during a fatigue test. Several materials show cyclic strain hardening or cyclic strain softening. Only those materials which rapidly stabilize to a constant stress amplitude under cyclic plastic strain with a constant amplitude may show some promise for Forrest's approach. The aluminium copper alloys seem to behave this way (summarized in ref. 30) and indeed Forrest found a good agreement between K_{pl} and K_f for these alloys. Still it should be kept in mind that a good agreement can only be expected if the material will not show a size effect. Gunn and Forrest both neglect the influence of the stress gradient at the root of the notch.

The foregoing discussion was concerned with estimating the fatigue limit of a notched specimen, S_{fK}, at $S_m = 0$, from the fatigue limit of an unnotched specimen S_{f1} also at $S_m = 0$. This problem is more complicated when $S_m \neq 0$, since then the definition of K_f as given in eq. (6.2) is not unambiguous. If the fatigue limit is understood to be the highest stress *amplitude* for infinite life, then S_{f1} and S_{fK} can be related either to the same mean stress (S_m) or to the same stress ratio (R), see fig. 42. Indicating the corresponding K_f-values by K_{fS_m} and K_{fR} respectively these factors will in general be functions of S_m and R respectively. For ductile materials it is frequently assumed (refs. 6 and 25) that K_{fS_m} is independent of S_m, or in fig. 42b: c/d is constant for all S_m-values. More complicated relations were proposed by Heywood (ref. 11).

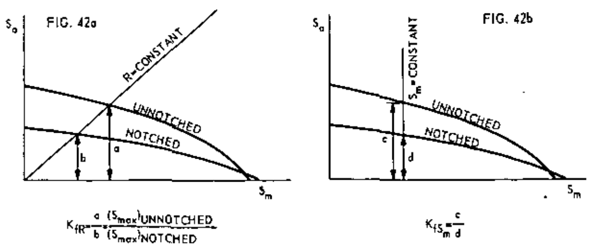

Fig. 42 The fatigue limit as a function of S_m and two definitions of the fatigue notch factor.

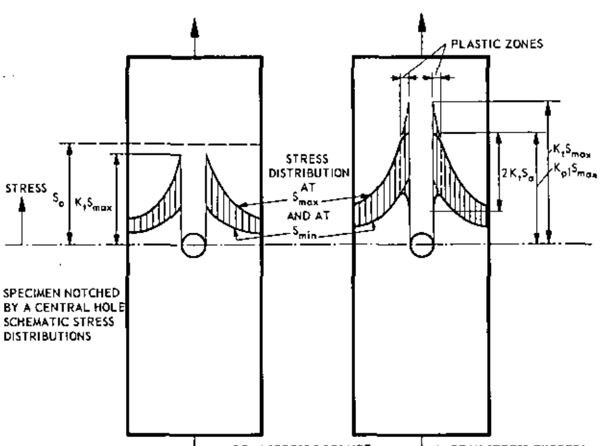

Fig. 43 The effect of plastic yielding on the maximum stress and the stress amplitude at the root of a notch according to Gunn (ref. 9).

A noteworthy evaluation is due to Gunn (ref. 9). He assumes that $K_{fR}=K_t$ if the peak stress in the notched specimen ($=K_tS_{max}$) does not exceed the yield limit. In that case the straining at the root of the notch would apparently be completely elastic (see fig. 43a) and it seems indeed appropriate to adopt K_{fR} for a correlation with K_t, since the stress ratios for the stress at the root of the notch and for the nominal stress on the specimen are the same. If K_tS_{max} exceeds the yield limit Gunn assumes that the maximum peak stress at the root of the notch is $K_{pl}S_{max}$ (K_{pl} according to eq. 6.13) and that the amplitude of the stress at the root of the notch is K_tS_a, see fig. 43b. In other words, the cyclic straining after the first load cycle is assumed to be elastic. With the above assumptions one can construct S_{fK} as a function of S_m if S_{f1} as a function of S_m is known. Gunn checked his method with some results from the literature and found a reasonable agreement in some cases, being less successful (although conservative) in other cases. Obviously the same problems arise as mentioned before, viz. K_{pl} is derived from a static test and the stress gradient effect is not accounted for. The former aspect may lead to even greater inaccuracies than for $S_m=0$ since for $S_m>0$ plastic shake down may occur.

In the previous paragraphs the relation between S_{fK} and S_{f1} was considered, first for $S_m=0$ and subsequently for $S_m\neq 0$. The final complication is to extend the problem to the fatigue strength, S_N, for a finite life, N. Usually the fatigue notch factor is then defined as the ratio between the fatigue strength of the unnotched specimen, S_{N1}, and the fatigue strength of the notched specimen S_{NK} or $K_f=S_{N1}/S_{NK}$. Since K_f for large values of N will be of the order of K_t and K_f for small values of N will be of the order of 1 it is clear that K_f will be a function of N. Further for $S_m\neq 0$ the ambiguity of defining K_f at the same value of R or the same value of S_m again arises.

For the case of infinite life, looking for a K_f–K_t relation seems reasonable since for both the unnotched and the notched specimen one compares the highest stress amplitudes which can be endured without the nucleation of a crack. However, for a finite life the fatigue strength cannot be defined in such a unique way. In fact, it is the cyclic stress which in N cycles leads to complete failure of the specimen. The present study has indicated that in both the unnotched and the notched specimen the fatigue life is occupied by crack propagation. It is difficult to see why crack propagation should occur at the same rate in unnotched and notched specimens if both yield the same fatigue life. This implies that looking for a K_f–K_t relation for finite life is not a rational procedure, the more so in view of the ambiguity of the K_f-definition. One could only hope that test results would lead to empirical relations with a reasonably general applicability. One such method consists of estimating S_{fK} and S_{uK} for the notched specimen and assuming an S-N relation satisfying S_{fK} for $N=\infty$ and S_{uK} for $N=1$ (ref. 11).

In ref. 28 it was suggested that dividing the fatigue life in a precrack stage and a crack stage might allow a better relation between the fatigue lives at the end of the precrack stage for the notched and the unnotched specimen. The results of the present study, however, indicate that a definition of the precrack stage is not easily done in a rational way. Some more thoughts on the relation between the crack propagation in unnotched and in notched specimens are presented in section 6.4.

It will now be tried to formulate some conclusions from the previous discussion.

1. *K_t–K_f relation.* Looking for a relation between K_t and K_f appears to be a rational approach for the fatigue limit S_f only. The problem is complicated by the occurrence of plastic yielding, especially if $S_m \neq 0$. An additional complication is the size effect, which for notched specimens is associated with the stress gradient. Unfortunately unnotched specimens may also exhibit a size effect which then implies that the fatigue limit cannot be a constant material property.

   For the fatigue strength S_N it will be difficult to arrive at a K_t–K_f relation on a rational basis in view of the occurrence of fatigue crack propagation in both the notched and unnotched specimens.

2. *Empirical solutions.* Tests with sharp notches and high K_f-values have certainly improved the understanding of the notch effect. Nevertheless it is thought to be unreasonable from an engineering point of view to require that an empirical K_t–K_f relation satisfies such extreme conditions which have no technical significance.

   Using empirical relations in fact implies an extrapolation of available experience. It is then always advisable to make an extrapolation as small as possible or, in other words, to start from fatigue data with a K_t-value and an r-value (radius of the notch) as nearby as possible to the case for which estimates of fatigue properties have to be made. This implies that starting from data for unnotched specimens will in general not be the most advisable method. It is suggested here that materials which in handbooks are frequently characterized by unnotched rotating beam specimen results should be better represented by data from mildly notched specimens (say $K_t = 2.5$) with not too small a radius of the notch and for aircraft materials by results of tests with a positive mean stress. Standardizing of one or a few notched specimens is to be advised.

3. *Research problems.* Two topics seem to offer fruitful fields for research efforts. First the correlation between crack propagation at various stress levels (S_m and S_a) and in various types of specimens should ultimately provide the answer to the question how fatigue lives for various stress levels and different specimens can be correlated. Some more thoughts to this problem are given in the following section.

   Secondly as has been indicated before, an improved understanding of the physical character of the sites at which cracks are nucleated is required to analyse the statistical aspect in a meaningful way. It is indeed surprising to see that in general only one macrocrack is observed in an unnotched specimen loaded just above its fatigue limit.

6.4 *Further evaluation of the present data*

In this chapter the fatigue life results of the present investigation are compared with NASA results. Secondly the crack rate data are further evaluated.

In ref. 18 Landers and Hardrath report a study on sheet specimens with central holes. Two materials were used, viz. 2024-T3 and 7075-T6 both in the bare condition, thickness 0.091″ (2.3 mm). Three values of the specimen width, w, were applied, viz. $w = 4''$ (102 mm), 2″ (51 mm) and 0.5″ (12.7 mm). The ratios between hole diameter, d, and the specimen width were $d/w = \frac{1}{32}, \frac{1}{16}, \frac{1}{8}, \frac{1}{4}$ and $\frac{1}{2}$ respectively, involving K_t-values varying between 2.9 and 2.16. S–N curves were determined for $R = 0 (S_{min} = 0)$ and $R = -1$ $(S_m = 0)$. Their tests at $R = 0$ and $d/w = \frac{1}{8}$ lend themselves for a direct comparison with the present investigation to which these values also apply. The comparison is made in fig. 44. The NASA results for $d = 12.7$ and $d = 6.3$ are almost coincident whereas the smallest specimen, $d = 1.6$ mm, gives a higher fatigue strength especially at high endurances. The latter could be the result of a size effect. The NLR results for $d = 5$ mm agrees reasonably with the NASA result for $d = 6.3$ mm, whereas the NLR curve for $d = 12.5$ mm has a somewhat lower position than the NASA result for $d = 12.7$ mm. Although both investigations indicate a higher fatigue strength for the smaller specimen fig. 44 shows that the two investigations do not show a completely

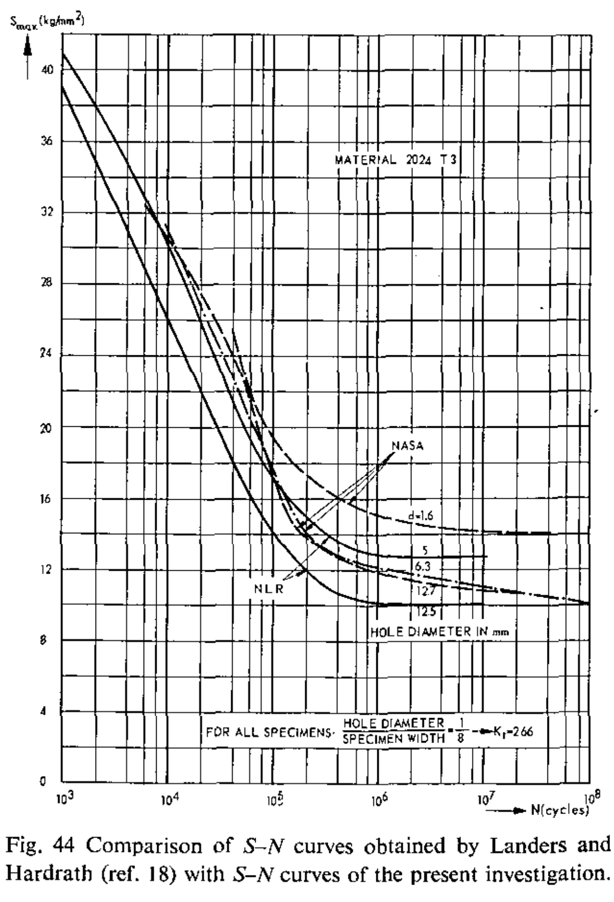

Fig. 44 Comparison of S–N curves obtained by Landers and Hardrath (ref. 18) with S–N curves of the present investigation.

consistent picture. It is poor comfort to conclude that this might have been caused by differences of the materials used. The static properties were approximately the same, but of course it is possible that there were differences in the impurity and inclusion contents which might be responsible for the differences of the test results.

In the NASA investigation a total of 46 S–N curves were produced, which led to the following conclusions. (1) For a constant value of d/w the fatigue strength decreases with increasing size of the specimen. (2) The difference between K_f and K_t became smaller for increasing d/w values. (3) At $R=-1$ ($S_m=0$ and $K_{fR}=K_{fS_m}$) there was a tendency for the specimens with the larger holes ($d=1''$ and $2''$) and for high fatigue lives towards $K_f=K_t$, as might be expected in view of the lower stress gradient. The results, however, were not sufficiently systematic to conclude that this equality was really obtained. For $R=0$ ($S_{\min}=0$ and $S_m>0$) this trend (for K_{fR}) was less marked.

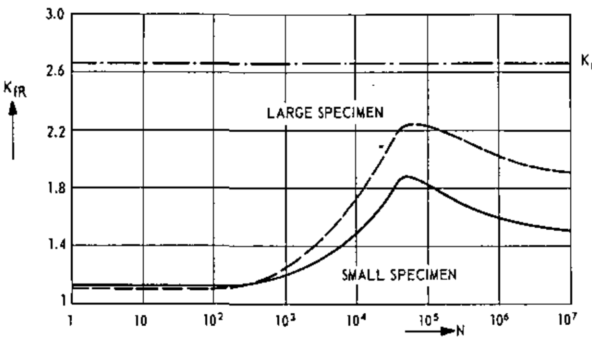

Fig. 45 The fatigue notch factor K_{fR} for the small and the large notched specimens of the present investigation.

For completeness the K_{fR}-values of the present investigation are shown in fig. 45. (For stress levels below the yield limit S_{N1} was corrected for $K_t=1.085$ for the unnotched specimen before calculating K_{fR}). The figure shows two usual features, viz. $K_f \sim 1$ for small N-values and K_f is increasing for higher N-values. The figure also shows a somewhat unusual feature, since the increase of K_f is followed by a smaller decrease at high N-values. Since the S–N curves for the notched specimens do not seem to be unusual as compared with the NASA data the cause of the decrease of K_f at high N-values should be mainly looked for in the S–N curve of the unnotched material. The fatigue limit of the unnotched material was indeed somewhat low, viz. $S_f=19.2$ kg/mm^2 ($S_{\max}$ at $R=0$ and $N=10^7$, corrected from $K_t=1.085$ to $K_t=1$) whereas the NASA arrived at $S_f=23.6$ kg/mm^2. A previous NLR study (ref. 31) on sheet material with a thickness of 5 mm yielded a value $S_f=22.5$ kg/mm^2. As pointed out in chapter 4 some cracks did not start at the edges, but away from the edges and probably from inclusions. It is not impossible that the fairly low fatigue limit has to be associated with an insufficient cleanness of the material. This would be consistent with the results of the large notched specimens being also somewhat lower than the NASA results (fig. 44) and it re-emphasizes the importance of a better understanding of the sites at which cracks are nucleated.

It will now be tried to correlate the crack rates in the three types of specimens. This will be done for two extreme conditions. First very small cracks will be considered, say $l<1$ mm. Such cracks have not yet penetrated through the thickness of the specimen and have approximately a quarter-circle form (figs. 10 and 11). Secondly relatively large cracks are considered which are growing through the full thickness of the specimen.

As long as the cracks are very small the stress distribution which applies in the absence of cracks will be affected by the cracks in a very small area only. One might hope that the stress distribution for the uncracked specimen could still be used for correlating the crack rates in different types of specimens. In fig. 46a the crack rate was plotted as a function of the crack length (results being read from figs. 20, 21 and 22) for the three types of specimens tested. The same stress at the edge of the specimens applies to all results, viz. 32 kg/mm^2, which implies that for the notched specimens a nominal stress level of $32/K_t=12$ kg/mm^2 was considered*. The stress level of 32 kg/mm^2, being the only one for which such a comparison could be made, is below the yield limit. Fig. 46a shows considerably different results for the three types of specimens, which

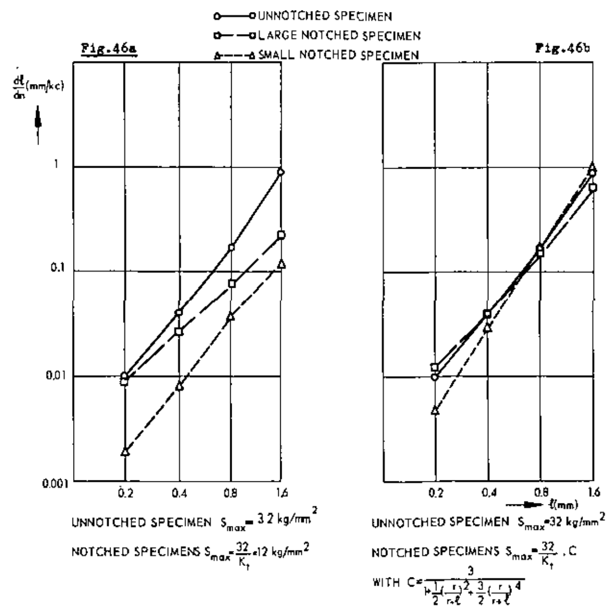

Fig. 46 Comparison of the crack rates in the unnotched and the notched specimens for small values of the crack length.

* For the small notched specimens the lowest $S_{\max}$-value in fig. 21 is 13 kg/mm^2, so that a small extrapolation was necessary.

is not unexpected in view of the stress gradients in the notched specimens. A second approach was made in fig. 46b, taking again $S_{max}=32$ kg/mm^2 for the un-

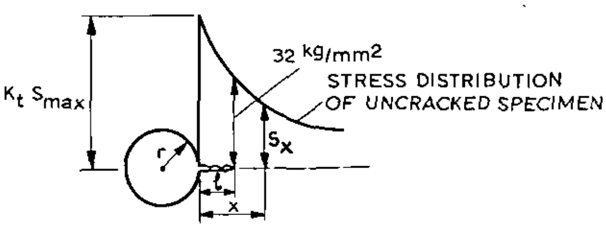

notched specimen and S_{max}-values (S_{max} is the nominal stress on the net area) for the notched specimens, such that the stress in the uncracked specimen for $x=l$ (see sketch) was also equal to 32 kg/mm^2. This procedure might yield a more characteristic nominal stress value for correlating the crack rates as long as the crack is small and has grown only partly through the sheet thickness (2 mm). For the procedure the stress distribution in the neighbourhood of the hole (uncracked specimen) is required. It was assumed that

$$S_x=S_{\max}\frac{K_t}{3}\left[1+\tfrac{1}{2}\left(\frac{r}{r+x}\right)^2+\tfrac{3}{2}\left(\frac{r}{r+x}\right)^4\right] \quad (6.14)$$

For an infinitely wide specimen ($K_t=3$) the relation is correct, whereas for a finite width S_x is reduced in the proportion $K_t/3$. Fig. 46b shows that in this way a reasonable agreement between the results of the three types of specimens was obtained. From the agreement one should not conclude that the above procedure is fully rational, however, it may be said that the agreement indicates that looking for a correlation of crack rates in different types of specimens is not an unrealistic approach.

In fig. 47 crack rate data for the small and the large notched specimens are compared for two stress levels, viz. 13 and 20 kg/mm^2. This has been done in three different ways (data read from figs. 21 and 22). Fig. 47a shows in a similar way as fig. 46a that the crack rate dl/dn as a function of l does depend on the type of specimen, i.e. on the size of the specimen in the case of fig. 47a. In fig. 47b the crack rate dl/dn was plotted as a function of the crack length, expressed as a fraction of the specimen width (l/w). For the same value of l/w the small and the large notched specimens are geometrically similar except for the sheet thickness which is 2 mm for both. The differences between the results of the large and the small notched specimens are large. If the cracks instead of having a quarter-circle shape had penetrated through the complete thickness of the specimens the theory of the stress intensity factor would have predicted the same result for the two specimens in fig. 47b. This theory is discussed hereafter

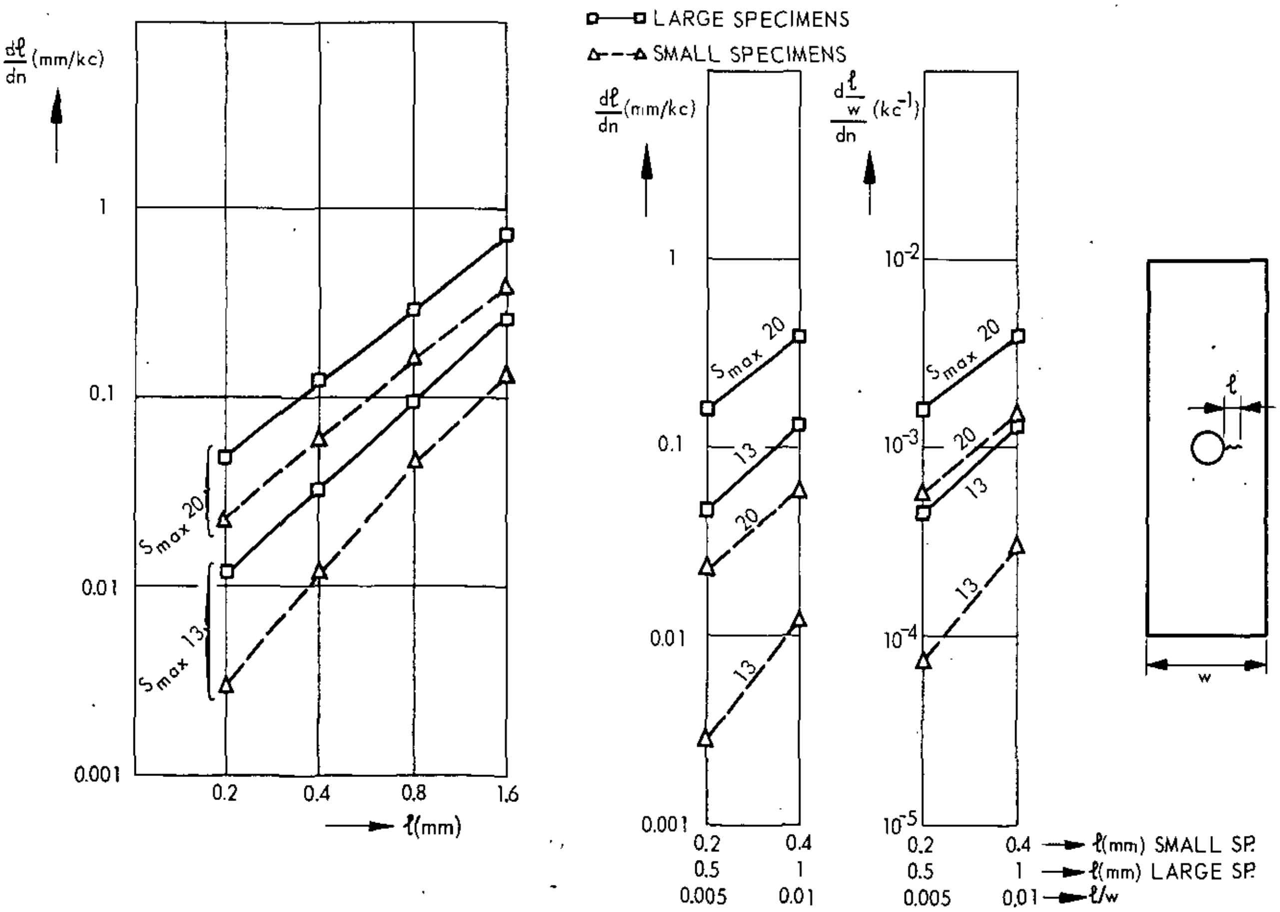

Fig. 47 Comparison of the crack rates in the large and the small notched specimens for small values of the crack length.

when considering larger crack length values. In fig. 47c both the crack rate and the crack length are related to the specimen width, viz. $\mathrm{d}\left(\frac{l}{w}\right)/\mathrm{d}n$ is plotted as a function of l/w. Also this does not lead to an agreement between the results of the large and the small notched specimens.

Now larger cracks are considered for which it is required that they have penetrated through the complete thickness of the sheet and that the crack front is perpendicular to the sheet. It is thought that this did occur for $l \geqslant 2$ mm (= sheet thickness). To such conditions the theory of the stress intensity factor applies as published by Paris et al. (ref. 23). For a specimen with a crack perpendicular to the loading direction the stresses in the neighbourhood of the crack tip (elastic theory) are approximately represented by:

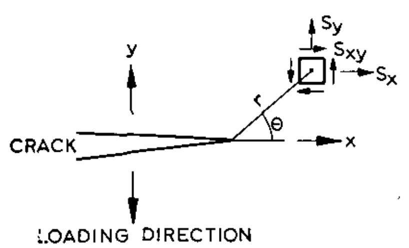

$$\left.\begin{aligned} S_y &= \frac{k}{\sqrt{2r}} \cos\frac{\theta}{2}\left(1+\sin\frac{\theta}{2}\sin\frac{3\theta}{2}\right) \\ S_x &= \frac{k}{\sqrt{2r}} \cos\frac{\theta}{2}\left(1-\sin\frac{\theta}{2}\sin\frac{3\theta}{2}\right) \\ S_{xy} &= \frac{k}{\sqrt{2r}} \cos\frac{\theta}{2}\sin\frac{\theta}{2}\cos\frac{3\theta}{2} \end{aligned}\right\} \qquad (6.15)$$

where r and θ are polar co-ordinates and k is the so-called stress intensity factor. For a central crack (length $2l$) and for an edge crack (length l) in an infinite sheet k follows from:

$$k = S\sqrt{l} \qquad (6.16)$$

where S is the stress loading the sheet. For a finite width, correction factors for k are available (ref. 22), but since the corrections are small (< 3 %) for the data to be discussed they will not be applied. The theory now predicts that the crack rate is a function of k only. Since k is defining the stress distribution around the crack tip this assumption has a rational background. The plasticity of the material does invalidate the elastic solution. However, if the material has a limited amount of ductility the plastic zone will be small. If it is assumed that the stress redistribution in the plastic zone will have a negligible influence on the stress distribution outside that zone, the location of the boundary and the stresses at the boundary of the plastic zone are correctly indicated by the elastic solution. It then seems reasonable to state that the elastic stress distribution is a basis for correlating crack data. The stress intensity factor being a parameter characterizing the elastic stress distribution could thus be used for the correlation. The crack rate for $l \geqslant 2$ mm has been plotted as a function of the stress intensity factor for the three types of specimens in figs. 48, 49 and 50 respectively. For the unnotched specimens crack rate data were available for $l = 2$ mm only. For the notched specimens a range of l-values could be used. For the notched specimens the hole and the crack were considered as a central crack with a length $2l'$ as defined in fig. 49. For the three types of specimens a number of S_{max}-values were considered so as to cover a large range of stress values. Each data point in figs. 48, 49 and 50 represents a single reading of figs. 20, 21 and 22 respectively. The figures show a consistent increase of $\mathrm{d}l/\mathrm{d}n$ as a function of k and as figs. 49 and 50 reveal, a single curve is obtained for the various values of l and S_{max}. In fig. 50 the results for $l = 2$ mm deviate from the results for the other l-values. This is not strange, since for $l = 2$ mm and a hole diameter of 12.5 mm the assumption of the crack and the hole being together a single crack with $2l' = 2 + 12.5$ mm is somewhat too drastic.

The curves of figs. 48, 49 and 50 were collected in fig. 51. Although the curve for the unnotched specimen suggests a somewhat different slope than the other two curves, it may be concluded that the agreement between the results of the three types of specimens is reasonable and indicates that the stress intensity factor can be a useful parameter for correlating crack rate data.

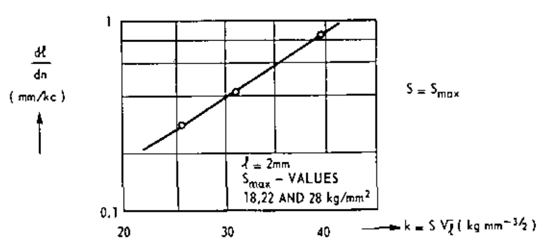

Fig. 48 The crack rate for the unnotched specimens as a function of the stress intensity factor $k(S\sqrt{l})$.

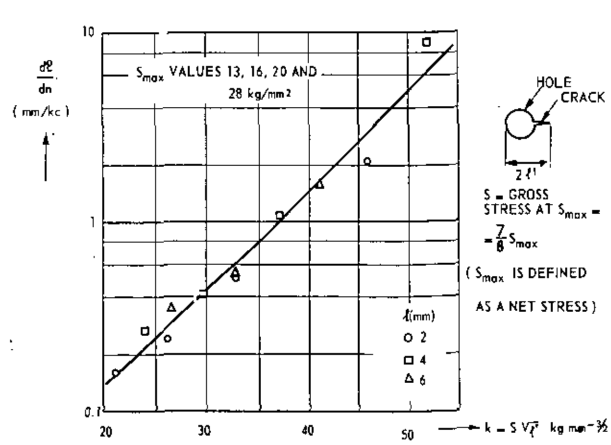

Fig. 49 The crack rate for the small notched specimens as a function of the stress intensity factor $k(S\sqrt{l'})$.

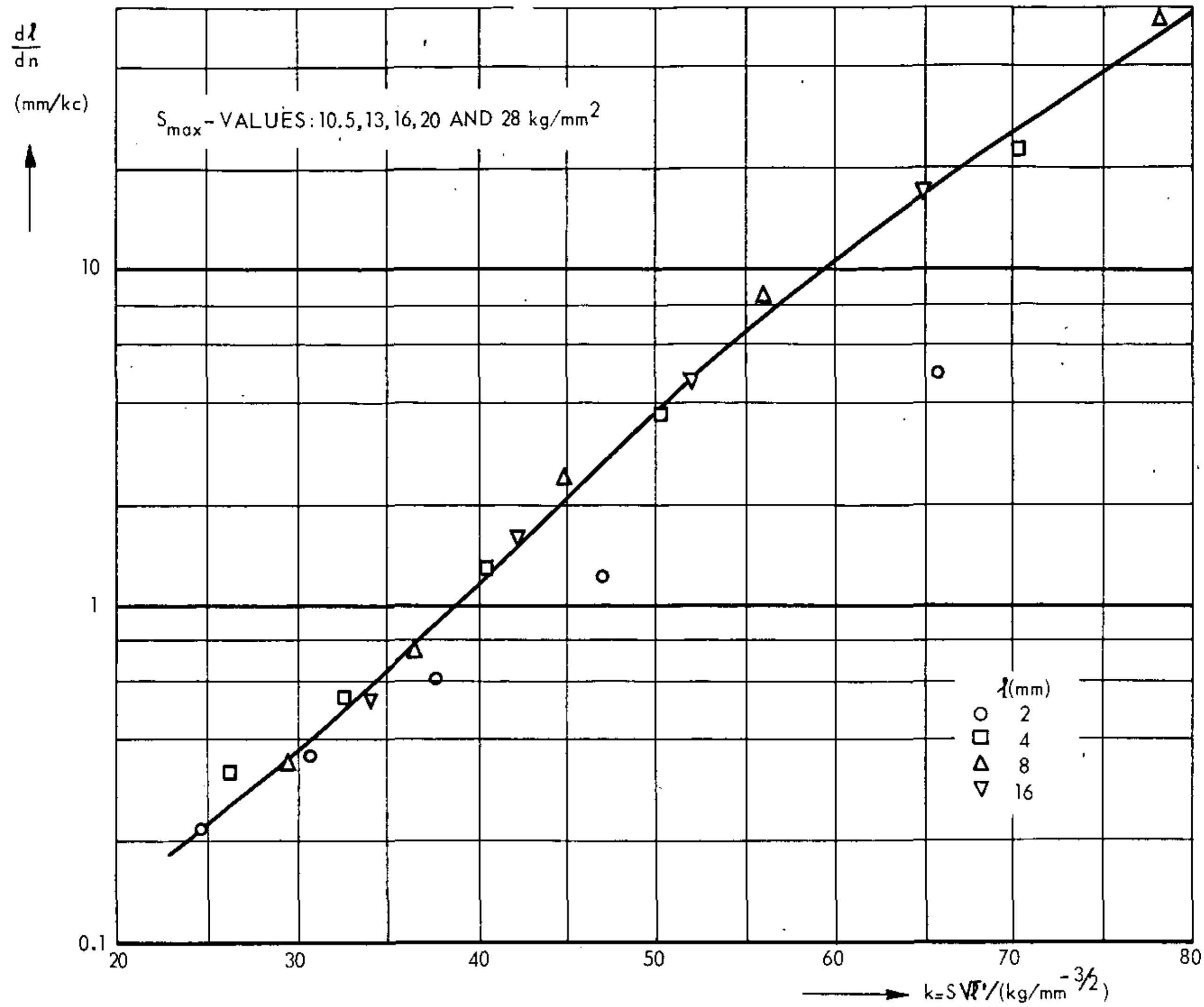

Fig. 50 The crack rate for the large notched specimens as a function of the stress intensity factor $k(S\sqrt{l'})$. l' and S are defined in fig. 49

For completeness a curve is shown in fig. 51 (dotted line) presented by Paris and Erdogan (ref. 24) for 2024-T3 sheet material as the average trend of American data of various sources. The differences with the present data may have several reasons, for instance small differences in the material. This will not be further analysed here.

For the study of the notch and the size effect as discussed in this chapter a possible applicability of the conception of the stress intensity factor for $l \geqslant 2$ mm would solve a minor part of the problem only, since a relatively short stage of the fatigue life is left if the crack length is larger than 2 mm, see figs. 23, 24 and 25. Nevertheless it is stimulating to see that a correlation of crack rate data for different types of specimens is not a priori impossible.

In ref. 37 Weibull proposes that $\mathrm{d}\left(\frac{l}{w}\right)/\mathrm{d}n$ as a function of l/w will be independent of the size of the specimen. For very small cracks fig. 47c showed this assumption to be incorrect. From fig. 52 it follows that also for large values of l the proposal is not confirmed by the present test results. It should be pointed out that Weibull was considering still larger values of l/w. The size effect on the propagation of macrocracks in large

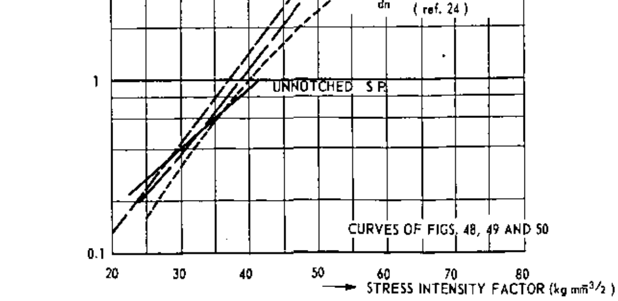

Fig. 51 Comparison of the crack rates for the three types of specimens as a function of the stress intensity factor, k.

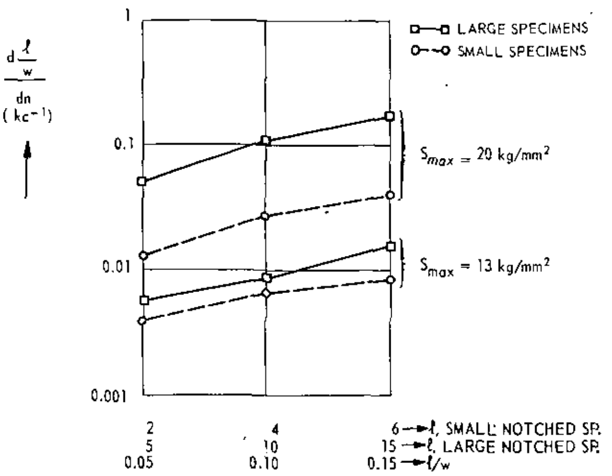

Fig. 52 Comparison of the crack rates in the large and the small notched specimens for large values of the crack length.

sheet specimens is studied in a current NLR test program which will be published in due course.

In conclusion to this section it may be repeated that the evaluation of the present data shows that the problems of the notch and the size effect for finite life are essentially problems of correlating crack rates in different types of specimens.

6.5 *Some remarks on scatter*

In the literature the idea that scatter in crack propagation is relatively low and scatter in crack nucleation is relatively larger has frequently been expressed. This idea has received confirmation from results on scatter of the propagation of macrocracks in large sheet specimens, which in general is low and much lower than is usual for fatigue lives of small specimens obtained in conventional fatigue tests. A second feature referred to in the literature is that scatter at high fatigue loads (standard deviation of log life) is smaller than at low fatigue loads.

The results of the present investigation (chapter 5) partly confirmed the second trend mentioned above. In figs. 28, 29 and 30 the scatterband for the fatigue life ($N_{0.5}$) until a small crack ($l=0.5$ mm) is broadening for fatigue lives beyond 10^5 cycles whereas the scatterband for the crack propagation period from $l=0.5$ mm to final failure (N-$N_{0.5}$) does not. As was pointed out in chapter 5 there was no obvious correlation between the magnitudes of $N_{0.5}$ and N-$N_{0.5}$. This suggests that the causes of scatter should be different for the crack growth until $l=0.5$ mm and for the remaining life until final fracture. In such a case one should look for causes in the specimen itself rather than in the procedure of testing. Such causes are (1) surface preparation, (2) impurities (inclusions) and (3) resistance against cyclic plastic deformation. The present results do not allow to discriminate definitively between these causes. In view of the occurrence of sheet cracks, see chapter 4, it is speculated that the scatter of the nucleation period was largely due to some type of inclusions, despite the lack of confirmation from microscopical indications. The scatter in the crack growth is thought to be related to inhomogeneities of the cyclic plastic behaviour of the material. Obviously a clear picture was not obtained. The scatter results re-emphasize that more should be known about the sites at which cracks are nucleated.

6.6 *Some concluding remarks and prospects for the future*

It seems to be fairly well established that microcracks are nucleated very early in the fatigue life. Only at stress levels just above the fatigue limit they can be made visible relatively late in the fatigue life. This confirms that the definition of the fatigue limit as being the highest stress amplitude which will not produce microcracks* is a useful one. As a consequence the problem of the notch effect and the size effect is different for the fatigue limit (infinite life) and the fatigue strength (finite life).

For the estimation of the fatigue limit of a notched element from the fatigue limit of the unnotched material the problem is how to account for the stress concentration at the root of the notch and for the stress gradient at the same location. The problem can be complicated by the presence of a non-zero mean stress and by the peak stress at the root of the notch exceeding the yield stress. A safe procedure is to apply K_t to both the mean stress and the stress amplitude. For ductile materials and for small notches this may involve a good deal of conservatism. Some methods are available which will lead to more accurate estimates and further improvements of these methods could be a goal for future research. An important difficulty is the statistical aspect which amongst other things may imply that the fatigue limit of the unnotched material is size-dependent.

Although the solution of the notch and size problem will see further improvements in the future it would be unrealistic to deny that for many materials the designer for several years will have to employ empirical rules for estimating fatigue properties. It therefore was proposed in section 6.3 that estimates should not be based on the fatigue data of unnotched material, but on fatigue data of notched specimens with values of K_t and the root radius close to those of the element for which estimates are required. In this way the extrapolation of the given data can be kept small and will involve less uncertainties. This implies that fatigue data of notched specimens with technically realistic values for K_t, root radius and S_m should be of greater value to the designer than

* Very sharp notches with high K_t-values, producing non-propagating cracks are not considered.

fatigue data of unnotched or notched rotating beam specimens, which, if notched, usually have an unrealistically small root radius. This especially applies to the aircraft designer, since his structures in general have no rotating parts, usually carry a positive mean stress (which in fact makes fatigue a problem) and where small root radii can generally be avoided. It may be pointed out here that it is not reasonable to require that empirical rules satisfy extreme conditions (high K_t-values, small root radii) which have no technical relevance.

The problem of estimating the fatigue strength (finite life) has a greater complexity for both the theoretical and the empirical approach. As a result of the previous section the impression was obtained that the crack growth in different types of specimens can be correlated on the basis of stress distributions. However, this is far from a solved problem. Moreover the complexity of this problem should depend on the plastic behaviour of the material under cyclic load. Some correlations indicated in the previous section were probably obtained by virtue of the low ductility of the aluminium alloy.

Further improvements of a rational treatment of the fatigue strength problem may certainly be anticipated, but also here the same remarks apply as made for the fatigue limit before, i.e. empirical rules cannot be missed. Since using such rules implies extrapolating from existing fatigue data it is again advisible to start from data of tests for which the circumstances are similar to those of the case for which estimates are to be made.

It has not been the purpose of the present study to give a thorough and complete treatment of the notch and size effect. It was thought, however, that the test results did justify a reconsideration of the present situation of approaching these problems, which revealed the duality of this situation. On the one hand there is an increasing understanding of these problems and on the other hand empirical rules are still indispensable. The understanding of the problem is largely qualitative in nature and to arrive at a rational quantitative theory will meet with rather complex problems. Nevertheless the qualitative understanding can be very useful also from a technical point of view. One aspect mentioned a few times before is the incomplete understanding of the sites at which cracks preferably nucleate. That such preferred sites do exist is obvious if one considers the small number of macrocracks occurring in a specimen. In general only one such a crack is observed at low stress amplitudes.

With respect to arriving at empirical rules it is reemphasized that such rules should primarily cover realistic values of the variables involved and that the classic approach of starting from unnotched specimen data as so-called fundamental material properties may seem attractive for sentimental reasons, but is a somewhat indirect method for practical reasons.

7 Conclusions

Unnotched and notched specimens of 2024-T3 sheet material were tested under an axial fatigue load. A zero minimum stress and various values of the maximum stress were applied. The notched specimens had a central hole and two geometrically similar sizes, having a size ratio of 2.5:1 were employed. Crack growth was recorded by using microscopes. A summary of conclusions is presented below.

1. The microscopical observations indicated that microcrack nucleation and growth started in the beginning of the fatigue test. The magnitudes of the crack rates were established. Probably the crack rate was approximately constant in the first stage of the fatigue tests, after which accelerating occurred. A division in a pre-crack stage and a crack stage as proposed earlier now seems to be somewhat artificial.
2. If $N_{0.5}$ and N indicate the fatigue life until a crack length $l=0.5$ mm (0.02 inch) and until final failure respectively, the scatter (standard deviation of log life) for $N_{0.5}$ increased for decreasing stress amplitudes, whereas for N–$N_{0.5}$ the scatter was approximately constant over the entire range of stress amplitudes. A correlation between $N_{0.5}$ and N–$N_{0.5}$ was not apparent.
3. Final failure occurs at a crack length depending on the applied fatigue load. The results indicated that in general this will account for minor deviations from the Palmgren-Miner rule only.
4. The fatigue strength for the large notched specimens was lower than for the small notched specimens, the difference being relatively larger for higher endurances.
5. For very small cracks (length smaller than the sheet thickness = 2 mm) a correlation of the crack rates in the unnotched and the notched specimens appeared to be present if comparisons were made on the basis of stress in the uncracked condition at the location of the tip of the actual crack. For relatively large cracks (length larger than the sheet thickness) such a correlation was most successful when using stress intensity factors. Further study of such correlations may yield valuable results.
6. If sharp notches and high K_t-values are disregarded the fatigue limit (infinite life) can be defined as the highest stress amplitude which does not produce microcracks. The fatigue strength (finite life) is essentially associated with (micro)crack propagation. For the fatigue limit the correlation for

different types of specimens is therefore a problem being essentially different from that for the fatigue strength.

7. Although the qualitative understanding of the notch and the size effect is increasing and further improvements may be expected empirical rules for estimating fatigue properties are indispensable for the time being. Usually such rules start from the unnotched material fatigue data. However, it is more expedient to employ fatigue data for which the stress concentration factor, the root radius of the notch and the mean stress have values comparable to those for the case for which fatigue properties have to be estimated. Fatigue data of mildly notched specimens are therefore of greater value than rotating beam data for unnotched or sharply notched specimens.
8. It is not necessary that empirical rules for estimating fatigue properties cover extreme conditions, which are lacking engineering significance.
9. Disregarding very sharp notches it is thought that the size effect in many cases will be a statistical effect associated with weak spots at which cracks are nucleated. Further study of this aspect is advisable.

8 List of references

[1] BENNETT, J. A. AND BAKER, J. L., Effects of prior static and dynamic stresses on the fatigue strength of aluminum alloys. J. of Research, N.B.S., Vol. 45, p. 449, 1950.

[2] BENNETT, J. A. AND WEINBERG, J. G., Fatigue notch sensitivity of some aluminum alloys. J. of Research, N.B.S., Vol. 52, p. 235, 1954.

[3] BROEK, D., DE RIJK, P. AND SEVENHUYSEN, P. J., The transition of fatigue cracks in alclad sheet. NLR Report M. 2100, Febr. 1962.

[4] DEMER, L. J., Interrelation of fatigue cracking, damping and notch sensitivity. WADC Tech. Report 56–408, 1957.

[5] FORREST, P. G., Influence of plastic deformation on notch sensitivity in fatigue. Proc. Int. Conf. on Fatigue of Metals, London, New York 1956, p. 171. Published by the Institution of Mech. Engrs, London.

[6] FORREST, P. G., Fatigue of metals. Pergamon Press, Oxford, 1962.

[7] FROST, N. E., Crack formation and stress concentration effect in direct stress fatigue. The Engineer, Vol. 200, p. 464 and p. 501, 1955.

[8] FROST, N. E., Notch effects and the critical alternating stress required to propagate a crack in an aluminium alloy subject to fatigue loading. J. Mech. Eng. Sc., Vol. 2, p. 109, 1960.

[9] GUNN, K., Effect of yielding on the fatigue properties of test pieces containing stress concentrations. The Aero. Quarterly, Vol. 6, p. 277, 1955.

[10] HARDRATH, H. F. AND OHMAN, L., A study of elastic and plastic stress concentration factors due to notches and fillets in flat plates. NACA TN 2566, Dec. 1951.

[11] HEYWOOD, R. B., Designing against fatigue. Chapman and Hall, London, 1962.

[12] HUNTER, M. S. AND FRICKE, W. G., Metallographic aspects of fatigue behaviour of aluminum. Proc. Am. Soc. Testing Mats, Vol. 54, p. 717, 1954.

[13] HUNTER, M. S. AND FRICKE, W. G., Effect of alloy content on the metallographic changes accompanying fatigue. Proc. Am. Soc. Testing Mats, Vol. 55, p. 942, 1955.

[14] HUNTER, M. S. AND FRICKE, W. G., Fatigue crack propagation in aluminum alloys. Proc. Am. Soc. Testing Mats, Vol. 56, p. 1038, 1956.

[15] HYLER, W. S., ABRAHAM, E. D. AND GROVER, H. J., Fatigue crack propagation in severely notched bars. NACA Tech. Note 3685, June 1956.

[16] KUHN, P., Effect of geometric size on notch fatigue. Colloquium on Fatigue, Stockholm 1955. Ed. by W. Weibull and F. K. G. Odquist, Springer, 1956.

[17] KUHN, P. AND HARDRATH, H. F., An engineering method for estimating notch-size effect in fatigue tests on steel. NACA Tech. Note 2805, Oct. 1952.

[18] LANDERS, C. B. AND HARDRATH, H. F., Results of axial-load fatigue tests on electropolished 2024-T3 and 7075-T6 aluminum-alloy-sheet specimens with central holes. NACA Tech. Note 3631, March 1956.

[19] DE LANGE, R. G., Plastic replica methods applied to a study of fatigue crack propagation in steel 35CD4 and 26ST aluminium alloy. To be published in Trans. Met. Soc. AIME.

[20] LANGER, B. F., Fatigue failure from stress cycles of varying amplitude. J. Appl. Mech., Vol. 4, 1937, p. A–160.

[21] NEUBER, H., Kerbspannungslehre. Springer, Berlin, 1937.

[22] PARIS, P., A handbook of crack tip stress intensity factors. Fracture Mechanics Research at Lehigh University, 1960–61, p. 39.

[23] PARIS, P., GOMEZ, M. P. AND ANDERSON, W. E., A rational analytic theory of fatigue. The Trend in Engineering, Vol. 13, p. 9, 1961.

[24] PARIS, P. AND ERDOGAN, F., A critical analysis of crack propagation laws. Trans. ASME, J. Basic Engineering, Vol. 85, Series D, p. 528, 1963.

[25] PETERSON, R. E., Stress Concentration Design Factors. John Wiley and Sons, Inc. 1953.

[26] PETERSON, R. E., Notch-sensitivity. Metal fatigue, p. 293. Ed. by G. Sines and J. L. Waisman, Mc Graw-Hill, 1959.

[27] RUSSENBERGER, M. AND FÖLDES, G., High-speed universal fatigue testing machine. Proc. of the Soc. of Exp. Stress Analysis, Vol. 12, no. 2, 1955, p. 9.

[28] SCHIJVE, J., Fatigue crack propagation in light alloys. NLL-TN M. 2010, Amsterdam, 1956.

[29] SCHIJVE, J., Fatigue crack propagation in light alloy sheet material. Advances in Aero. Sciences, Vol. 3, p. 387, Pergamon Press, 1960.

[30] SCHIJVE, J., Analysis of the fatigue phenomenon in aluminium alloys. NLR-Tech. Report M. 2122, April 1964.

[31] SCHIJVE, J. AND JACOBS, F. A., The fatigue strength of aluminium alloy lugs. NLR-Tech. Note M. 2024, Jan. 1957.

[32] SCHIJVE, J. AND JACOBS, F. A., Program-fatigue tests on notched light alloy specimens of 2024 and 7075 material. NLR-Tech. Report M. 2070, 1960.

[33] SIEBEL, E. AND STIELER, M., Ungleichförmige Spannungsverteilung bei schwingender Beanspruchung. Z.V.D.I., Vol. 79, p. 121, 1955.

[34] STULEN, F. B., CUMMINGS, H. N. AND SCHULTE, W. C., Relation of inclusions to the fatigue properties of high-strength steels. Proc. International Conf. on Fatigue of Metals, London, New York, 1956, p. 439. Publ. by The Institution of Mech. Engrs, London.

[35] THURSTON, R. C. A., Propagating and non-propagating fatigue cracks in metals. Dept. Mines and Tech. Surveys, Ottawa, Mines Branch IC 115, Jan. 1960.

[36] VALLURI, S. R., A unified engineering theory of high stress level fatigue. Aerospace Eng., Vol. 20, p. 18, 1961.

[37] WEIBULL, W., The effect of size and stress history on fatigue crack initiation and propagation. Proc. Crack Propagation Symposium, Cranfield 1961, Vol. 2, p. 271.

[38] WEIBULL, W., Definitions and symbols for fatigue testing. Proc. Am. Soc. for Testing and Materials, Vol. 59, p. 596, 1959.

APPENDIX A

Results of a crack propagation study carried out at the "Metaalinstituut TNO" at Delft, The Netherlands

An improved replica technique for a non-destructive study of the nucleation and growth of fatigue cracks was recently developed at the "Metaalinstituut TNO" at Delft. The technique is described by de Lange in a forthcoming publication (ref. 19), including results of fatigue tests on steel and the aluminium alloy 26 ST. He was so kind as to make available to the NLR his results in detail for an analysis similar to that applied to the results of the present investigation.

The material 26 ST corresponds to the AMS designation 2014-T4, which is almost similar to the 2024-T3 material of the present investigation. Unnotched specimens were tested in rotating bending. The tests were periodically interrupted for making replicas. The length of the fatigue cracks was measured from the replicas. The data on the crack length as a function of the number of load cycles were treated in the way as described in chapter 5 for the results of the present investigation. Crack propagation curves were drawn from which the average crack rate for a number of crack growth intervals was determined. In fig. A1 these calculated crack rates are plotted as a function of the crack length l. The first data point of each curve was not derived from the crack propagation curve, but directly from the data of de Lange, i.e. it gives the average crack rate until detection of the crack, assuming a zero crack length at the beginning of the test. These encircled data points are plotted in fig. A1 at half the length of the crack at the moment of detection.

For $l > 100\ \mu = 0.1$ mm $\log dl/dn$ is approximately a linear function of $\log l$ with a slope which seems to be independent of the stress amplitude. The same result was found for the unnotched specimens of the present

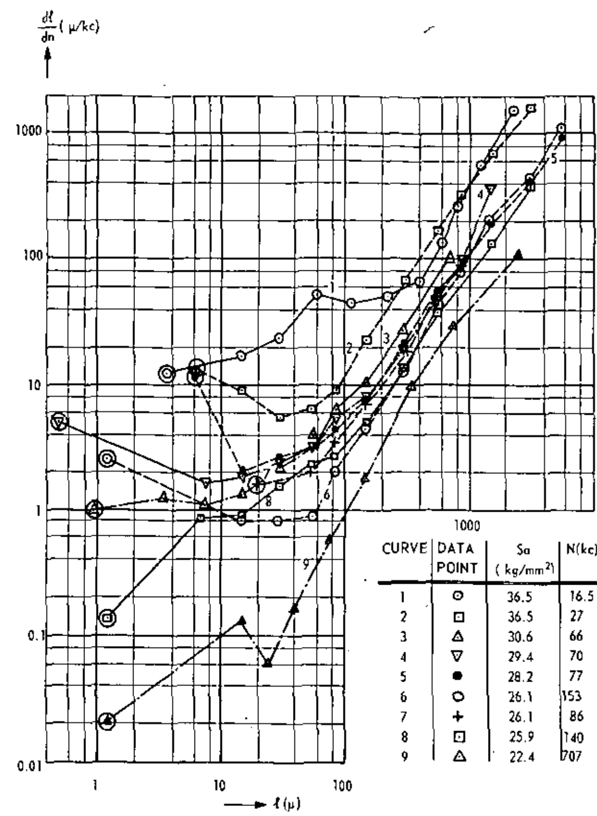

Fig. A1 The crack rate as a function of the crack length in unnotched rotating beam specimens of 26 ST material. Results of de Lange (ref. 19).

investigation, see fig. 12. In fig. A1 the slope is approximately 1.5 whereas in fig. 12 this value is about 2.

A second noteworthy result is that for decreasing values of $\log l$ (lower than say $l = 100\ \mu$) $\log dl/dn$ does not decrease much further. Although the data are somewhat unsystematic in this region there is a tendency towards an approximately constant crack rate in the first part of the fatigue test. Some of the cracks found by de Lange were initiated by inclusions. If this occurs just below the surface and there is a break through of the crack to the surface the initial value of the crack rate might have been enhanced. This could have been so for curve nr. 5.

Although the picture is still far from complete and more research of this type also for axially loaded specimens with a positive mean stress is needed an approximately constant crack rate during the nucleation period seems to be acceptable as a qualitative feature for the time being.

C. C. L. Class. G 042 : G 311 : G 331

REPORT NLR–TR M 2111

The influence of the mean stress on the propagation of fatigue cracks in aluminium alloy sheet

by

D. BROEK and J. SCHIJVE

Summary

Clad 2024-T3 and 7075-T6 sheet specimens were loaded at three different load amplitudes and three different mean loads. It turned out that the mean stress had an important influence on the crack rate. The test results suggest a relation to exist of the form

$$\frac{\mathrm{d}l}{\mathrm{d}n} = C_1 \mathrm{e}^{-C_2 R} S_{\max}^3 l^{3/2} \left(1 + 10 \frac{l^2}{w^2}\right)$$

The crack rate in the 7075 specimens was 3 to 4 times as large as in the 2024 specimens.

Existing crack propagation theories were checked by means of the present results. The theory of Paris gives some promise for further development.

Contents

This investigation has been performed under contract with the Netherlands Aircraft Development Board (N.I.V.).

Notations

A,B,C — constants

K — stress intensity factor; eq. (5) (kg/mm$^{3/2}$)

K_a — amplitude of stress intensity factor

$K_{\max}$ — maximum stress intensity factor in a cycle

K_E — stress concentration factor for an elliptical hole

K_H — stress concentration factor for a circular hole

l — half crack length (see fig. 1). (mm)

n — number of cycles

$n_z - n_y$ — number of cycles to extend a crack from $l=y$ mm to $l=z$ mm

$\mathrm{d}l/\mathrm{d}n$ — crack rate (mm/kc)

q — material parameter, constant

R — $S_{\min}/S_{\max}$

S — stress (kg/mm^2)

S_a — stress amplitude

S_m — mean stress

$S_{\max}$ — maximum stress in a cycle $= S_m + S_a$

$S_{\min}$ — minimum stress in a cycle $= S_m - S_a$

S_n — nett stress

S_u — ultimate tensile strength

$S_{0.2}$ — 0.2% yield strength
t — sheet thickness (mm)
w — half width of sheet (see fig. 1) (mm)
x — See fig. 1 (mm)
α,β,γ — constants
ρ_E — effective tip radius of crack
1 kc = 1000 cycles
1 inch = 25.4 mm
1 inch/cycle = 25.4 mm/kc
1 kg/mm^2 = 1,422 psi
1000 psi = 0.703 kg/mm^2

1 Introduction

In modern aircraft structures designed for finite fatigue life fatigue cracks may occur during service. These cracks should be detected and repaired early enough to prevent them from growing to catastrophic dimensions. Therefore the designer should be able to prescribe safe inspection periods, for which purpose he should avail himself of sufficient and reliable crack propagation data. At this moment already a large amount of crack-propagation data is available, but unfortunately most of these data were obtained from tests in repeated tension (minimum stress in a cycle zero). Therefore a test program has been carried out to investigate the influence of mean stress on fatigue crack propagation in two clad aluminum alloys (2024-T3 and 7075-T6).

In this report the test results are given and discussed. The results allow a more general verification of the theory of Paris on crack propagation. This results in some conclusions on the significance and practical value of the theory.

Some fractographical observations have been made on the transition of the fatigue crack. The relation of this phenomenon with the theory of Paris is discussed.

2 Experimental details

2.1 *Materials and specimens*

The specimens were cut from clad 2024-T3 and 7075-T6 sheet of 2 mm (0.08") thickness. Static properties of the materials were (averages of 8 tests).

Material	$S_{0.2}$ (kg/mm^2)	S_u (kg/mm^2)	Elongation (2" gage length)
2024-T3	37.1 (52.8 ksi)	48.3 (68.7 ksi)	18.9%
7075-T6	47.3 (67.3 ksi)	53.0 (75.4 ksi)	9.4%

The specimens (fig. 1) were cut to the same dimensions used in previous investigations (refs. 1–4) in order to facilitate comparison. The specimens were provided with a small severe central notch consisting of a drilled hole of 1 mm (0.04") diameter and two saw cuts of 1 mm (0.04") depth and 0.2 mm (0.008") width. These saw cuts were made by means of a jeweller's fret-saw. An enlarged view of the notch is given in fig. 1.

The area containing the notch was locally polished and provided with fine scribe line markings at spacings as illustrated in fig. 1.

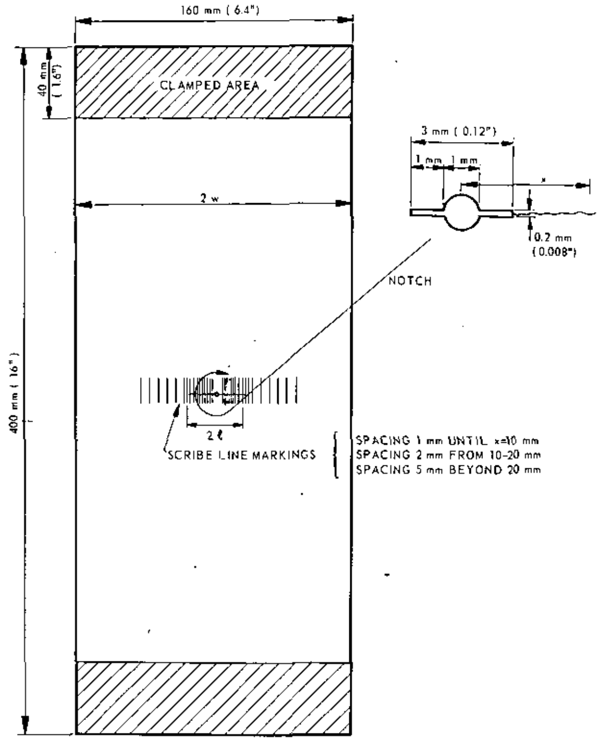

Fig. 1 Sheet specimen for crack propagation.

2.2 *Fatigue machine and testing technique*

The fatigue machine was a vertical Schenck pulsator type PVQ-002S with a maximum capacity of 6 tons, running at a frequency of approximately 2000 cycles per minute.

Recording of the crack growth occurred by counting the number of load cycles necessary to propagate the crack over the interval between two successive scribe-line markings. The tips of the crack could easily be

S_m		S_a		Number of tests
kg/mm^2	psi	kg/mm^2	psi	
12	17100	6.5	9200	3
		4	5700	3
		2.5	3600	3
9	12800	6.5	9200	3
		4	5700	3
		2.5	3600	3
4.5	6400	4	5700	3
		3.2	4600	3
		2.5	3600	3

observed with the aid of a spot light and a large magnifying glass of low magnification (2x).

2.3 *Stresses*

Three values of the mean stress have been investigated, viz. $S_m = 4.5$, 9 and 12 kg/mm^2. At each mean stress 9 tests were carried out at three different stress amplitudes. In order to prevent buckling of the specimen compressive stresses were avoided. The complete program is specified in the table on page 2.

All values are based on the gross sectional area, no allowance being made for the notch and the crack. Mean and alternating loads remained constant throughout a test.

3 Test results

The manufacturing procedure of the notch by means of sawing may produce (from a microscopical point of view) largely different notches in different specimens, which will influence the fatigue life until crack initiation and also the early crack-propagation. Therefore crack-propagation records were not started before the crack had escaped from the region in the immediate vicinity of the notch. The notch extends to $l \approx 1.5$ mm (see fig. 1). Crack-propagation records were started when the crack had reached $l = 2$ mm.

The crack length l is defined as half the total crack length from tip to tip; the crack-propagation life $n_l - n_2$ is the number of kilocycles (1 kc = 1000 cycles) necessary to extend the crack from a length of 2 mm to a length of l mm.

Numerical test results are given in tables 1 to 9 incl. The crack-propagation curves have been plotted in figs. 2–4 incl. for the 2024-T3 material and in figs. 5–7 incl. for the 7075-T6 material. The curves for $S_a = 3.2$ kg/mm^2, $S_m = 4.5$ kg/mm^2 are plotted in fig. 8 for both 2024 and 7075 material. Since scatter was low (see tables 1–9 incl.) only the mean curves of three tests have been plotted in order to avoid confusion by almost coinciding curves.

Figs. 2–7 incl. allow an immediate appreciation of the influence of the mean stress.

The crack rate dl/dn as a function of l has been calculated in tables 1–9 incl. as the linear average over the interval between two successive scribe-line-markings. The crack rate so obtained is assumed to be the crack rate at the middle of the interval. dl/dn has been plotted versus l on a double logarithmic scale in figs. 9–11 incl. The scatter around these curves must be due to small irregularities in crack growth and small errors in the measurements.

4 Comparison of the two alloys tested

Figs. 9 through 11 clearly demonstrate the superiori-

TABLE 1

Crack propagation records
$S_m = 12$ kg/mm^2; $S_a = 2.5$ kg/mm^2

	2024						7075					
	specimen			mean of three specimens			specimen			mean of three specimens		
	A92	A63	A14				A708	A731	A745			
l	n_l-n_2	n_l-n_2	n_l-n_2	n_l-n_2	Δn	dl/dn	n_l-n_2	n_l-n_2	n_l-n_2	n_l-n_2	Δn	dl/dn
mm	kc	kc	kc	kc	kc	mm/kc	kc	kc	kc	kc	kc	mm/kc
2	0	0	0	0			0	0	0	0		
3	89.25	88.50	93.40	90.38	90.38	0.0110	13.95	15.05	17.70	15.57	15.57	0.064
4	138.55	132.55	132.95	134.68	44.30	0.0226	21.90	23.35	28.25	24.50	8.93	0.112
5	167.70	162.45	162.15	164.10	29.42	0.0340	27.45	28.65	35.80	30.63	6.13	0.163
6	187.95	181.65	179.55	183.05	18.95	0.0528	30.70	32.45	39.60	34.25	3.62	0.276
7	200.20	198.10	194.00	197.43	14.38	0.0695	33.15	34.95	42.50	36.87	2.62	0.382
8	211.80	208.70	207.25	209.25	11.82	0.0845	35.65	37.25	45.50	39.47	2.60	0.384
9	221.65	221.35	217.15	220.05	10.80	0.0926	37.05	39.05	48.20	41.44	1.97	0.508
10	230.60	229.20	225.75	228.52	8.47	0.118	38.40	40.60	49.30	42.77	1.33	0.752
12	245.60	246.30	244.05	245.32	16.80	0.119	40.75	43.20	52.00	45.32	2.55	0.784
14	255.60	256.35	256.55	256.17	10.85	0.191	42.45	45.20	54.25	47.30	1.98	1.01
16	264.65	265.55	267.15	265.82	9.65	0.207	43.70	46.65	55.80	48.72	1.42	1.41
18	271.05	272.80	273.30	272.42	6.60	0.303	44.60	47.60	56.90	49.70	0.98	2.04
20	276.55	278.85	278.45	277.99	5.57	0.359	45.25	48.50	57.60	50.45	0.75	2.67
25	288.65	290.30	287.35	288.89	10.90	0.463	46.30	49.70	58.75	51.58	1.13	4.43
30	295.75	296.40	292.55	295.02	6.13	0.816	46.75	50.15	59.25	52.06	0.48	10.4
35	299.55	299.70	295.85	298.45	3.43	1.46	46.95	50.35	59.45	52.26	0.20	25.0
40	301.35	301.70	297.60	300.30	1.85	2.70		50.55	59.55	52.41	0.15	33.3
45	302.20	302.35	298.20	301.00	0.70	7.14			59.65	52.51	0.10	50.0

TABLE 2

Crack propagation records
$S_m = 12$ kg/mm^2; $S_a = 4$ kg/mm^2

	2024						7075					
	specimen			mean of three specimens			specimen			mean of three specimens		
	A6	A68	A111				A738	A725	A707			
l	n_l-n_2	n_l-n_2	n_l-n_2	n_l-n_2	Δn	dl/dn	n_l-n_2	n_l-n_2	n_l-n_2	n_l-n_2	Δn	dl/dn
mm	kc	kc	kc	kc	kc	mm/kc	kc	kc	kc	kc	kc	mm/kc
2	0	0	0	0			0	0	0	0		
3	18.50	15.80	18.90	17.70	17.70	0.0565	4.20	4.35	3.50	4.02	4.02	0.249
4	30.45	25.85	28.45	28.22	10.52	0.095	7.00	7.00	5.85	6.62	2.60	0.384
5	39.90	34.50	37.10	37.14	8.92	0.112	9.60	9.05	7.90	8.85	2.23	0.449
6	47.95	40.45	42.20	43.51	6.37	0.157	11.45	10.85	9.45	10.58	1.73	0.579
7	54.25	44.45	48.45	49.03	5.52	0.181	13.20	11.95	10.65	11.93	1.35	0.74
8	60.40	49.65	52.95	54.31	5.28	0.189	14.45	12.75	11.35	12.85	0.92	1.09
9	64.35	54.05	57.75	58.69	4.38	0.228	15.25	13.30	11.90	13.48	0.63	1.59
10	67.30	56.80	60.55	61.52	2.83	0.354	15.85	13.65	12.30	13.93	0.45	2.22
12	72.80	62.90	65.45	67.02	5.50	0.364	16.85	14.25	12.85	14.65	0.72	2.78
14	75.40	66.10	69.30	70.24	3.22	0.612	17.55	14.60	13.20	15.12	0.47	4.25
16	78.60	68.80	71.80	73.04	2.80	0.714	18.00	14.85	13.40	15.42	0.30	6.67
18	80.20	70.65	73.85	74.87	1.83	1.10	18.35	15.15	13.60	15.70	0.28	7.14
20	81.65	71.95	75.05	76.19	1.32	1.52	18.55	15.30	13.80	15.88	0.18	11.1
25	84.15	74.45	77.55	78.69	2.50	2.00	18.90	15.45	13.90	16.08	0.20	25.0
30	85.45	75.60	78.90	79.96	1.27	3.94	19.10			16.28	0.20	25.0
35	86.20	76.30	79.55	80.66	0.70	7.15	19.15			16.33	0.05	100
40	86.55	76.65	79.85	80.99	0.33	15.1						

TABLE 3

Crack propagation records
$S_m = 12$ kg/mm^2; $S_a = 6.5$ kg/mm^2

	2024						7075				
	specimen			mean of three specimens			specimen		mean of two specimens		
	A40	A28	A84				A724	A744			
l	n_l-n_2	n_l-n_2	n_l-n_2	n_l-n_2	Δn	dl/dn	n_l-n_2	n_l-n_2	n_l-n_2	Δn	dl/dn
mm	kc	kc	kc	kc	kc	mm/kc	kc	kc	kc	kc	mm/kc
2	0	0	0	0			0	0	0		
3	4.90	5.45	5.30	5.22	5.22	0.192	3.00	2.65	2.83	2.83	0.354
4	7.85	9.95	10.70	9.50	4.28	0.234	4.00	3.85	3.93	1.10	0.91
5	11.40	13.25	12.75	12.47	2.97	0.336	4.80	4.80	4.80	0.87	1.15
6	15.10	15.35	15.30	15.25	2.78	0.360	5.45	5.45	5.45	0.65	1.54
7	17.40	17.05	16.85	17.10	1.85	0.540	5.85	6.00	5.93	0.48	2.08
8	19.55	18.20	18.90	18.88	1.78	0.562	6.05	6.30	6.18	0.25	4.0
9	20.90	19.40	19.70	20.00	1.12	0.894	6.10	6.40	6.25	0.07	14.2
10	21.85	20.10	20.35	20.75	0.75	1.33	6.25	6.70	6.48	0.23	4.3
12	23.25	21.55	21.25	22.00	1.25	1.60	6.35	6.90	6.63	0.15	13.3
14	24.05	22.35	21.95	22.77	0.77	2.60	6.50	7.05	6.78	0.15	13.3
16	24.65	22.95	22.45	23.34	0.57	3.51		7.15	6.88	0.10	20.0
18	25.00	23.35	22.75	23.69	0.35	5.72					
20	25.30	23.65	23.00	23.97	0.28	7.14					
25	25.75	24.25	23.30	24.42	0.45	11.1					
30	26.00	24.45	23.40	24.62	0.20	25.0					
35	26.10	24.55		24.72	0.10	50.0					

TABLE 4

Crack propagation records

$S_m = 9$ kg/mm^2; $S_a = 2.5$ kg/mm^2

	2024						7075					
	specimen			mean of three specimens			specimen			mean of three specimens		
	A120	A41	A30				A704	A743	A722			
l	n_l-n_2	n_l-n_2	n_l-n_2	n_l-n_2	Δn	dl/dn	n_l-n_2	n_l-n_2	n_l-n_2	n_l-n_2	Δn	dl/dn
mm	kc	kc	kc	kc	kc	mm/kc	kc	kc	kc	kc	kc	mm/kc
2	0	0	0	0			0	0	0	0		
3	152.15	121.50	128.65	134.10	134.10	0.0075	26.80	21.25	18.60	22.22	22.22	0.045
4	230.60	194.30	210.85	211.92	77.82	0.0129	35.85	30.85	26.75	31.15	8.93	0.112
5	264.35	230.10	244.20	246.22	34.30	0.0292	42.15	39.55	32.75	38.15	7.00	0.143
6	290.60	250.50	266.50	269.20	22.98	0.0435	46.20	45.50	35.95	42.55	4.40	0.227
7	310.20	266.60	284.70	287.17	17.97	0.0557	49.45	49.65	39.00	46.03	3.48	0.287
8	326.30	281.30	301.60	303.07	15.90	0.0630	52.50	53.90	41.60	49.33	3.30	0.303
9	342.60	294.05	315.20	317.29	14.22	0.0703	55.00	56.75	43.95	51.90	2.57	0.389
10	353.40	306.25	327.10	328.92	11.63	0.0860	56.80	59.35	45.55	53.90	2.00	0.500
12	373.30	325.20	348.90	349.14	20.22	0.0990	60.55	64.25	48.85	57.95	4.05	0.494
14	387.35	338.45	361.70	362.61	13.47	0.149	63.55	68.20	51.35	61.07	3.12	0.641
16	399.75	350.30	374.30	374.89	12.28	0.163	65.60	70.65	53.15	63.17	2.10	0.952
18	409.90	360.80	385.30	385.44	10.55	0.190	67.15	72.85	54.55	64.89	1.72	1.16
20	419.35	369.70	393.75	394.37	8.93	0.224	68.30	74.35	55.75	66.17	1.28	1.56
25	433.85	386.45	407.80	409.47	15.10	0.331	69.95	76.85	57.65	68.19	2.02	2.48
30	444.10	397.30	416.90	419.54	10.07	0.497	70.85	78.20	58.70	69.29	1.10	4.54
35	449.95	403.35	422.10	425.24	5.70	0.878	71.35	78.80	59.30	69.86	0.57	8.78
40	453.70	406.95	425.40	428.79	3.55	1.41	71.60	79.25	59.75	70.23	0.37	13.5
45	455.95	409.15	427.70	431.04	2.25	2.22		79.45	59.95	70.43	0.20	25.0
50	457.10	410.05	428.70	432.06	1.02	4.90			60.05	70.53	0.10	50.0
55			428.80	432.16	0.10	50.0						

TABLE 5

Crack propagation records

$S_m = 9$ kg/mm^2; $S_a = 4$ kg/mm^2

	2024						7075					
	specimen			mean of three specimens			specimen			mean of three specimens		
	A86	A54	A17				A705	A737	A726			
l	n_l-n_2	n_l-n_2	n_l-n_2	n_l-n_2	Δn	dl/dn	n_l-n_2	n_l-n_2	n_l-n_2	n_l-n_2	Δn	dl/dn
mm	kc	kc	kc	kc	kc	mm/kc	kc	kc	kc	kc	kc	mm/kc
2	0	0	0	0			0	0	0	0		
3	26.20	25.70	33.90	28.60	28.60	0.0350	3.85	4.10	3.05	3.67	3.67	0.273
4	42.20	40.40	49.90	44.17	15.57	0.0642	6.40	7.40	5.55	6.45	2.78	0.360
5	52.70	49.30	61.95	54.65	10.48	0.0955	9.20	10.20	7.70	9.03	2.58	0.388
6	61.20	56.90	72.05	63.38	8.73	0.114	11.30	12.95	9.20	11.15	2.12	0.472
7	69.35	64.50	79.10	70.98	7.60	0.132	13.15	14.70	10.60	12.82	1.67	0.600
8	75.40	69.10	84.70	76.40	5.42	0.185	14.70	16.40	11.80	14.30	1.48	0.675
9	80.60	74.25	89.90	81.58	5.18	0.193	15.50	17.60	12.85	15.32	1.02	0.98
10	85.35	78.10	94.60	85.98	4.40	0.227	16.10	18.30	13.55	15.99	0.67	1.49
12	93.00	84.75	103.40	93.68	7.70	0.260	17.10	19.65	14.75	17.17	1.18	1.70
14	98.45	90.45	108.90	99.21	5.53	0.362	17.90	20.70	15.45	18.02	0.85	2.35
16	102.40	95.00	113.20	103.44	4.23	0.472	18.30	21.30	16.00	18.54	0.52	3.84
18	105.25	98.20	116.65	106.61	3.17	0.630	18.70	21.75	16.40	18.96	0.42	4.76
20	107.55	101.05	118.80	109.04	2.43	0.823	18.95	22.10	16.60	19.23	0.27	7.40
25	111.35	105.70	122.55	113.11	4.07	1.23	19.35	22.70	17.10	19.73	0.50	10.0
30	113.25	108.55	124.15	115.23	2.12	2.36	19.50	23.05	17.35	19.98	0.25	20.0
35	114.20	109.65	125.05	116.21	0.98	5.10	19.60	23.20	17.45	20.10	0.12	40.0
40	114.75	110.15	125.55	116.63	0.52	9.6						
45	115.05	110.45	125.75	116.90	0.27	18.5						

TABLE 6

Crack propagation records

$S_m = 9$ kg/mm^2; $S_a = 6.5$ kg/mm^2

	2024						7075					
	specimen			mean of three specimens			specimen			mean of three specimens		
	A22	A33	A100				A721	A710	A734			
l	$n_l - n_2$	$n_l - n_2$	$n_l - n_2$	$n_l - n_2$	Δn	dl/dn	$n_l - n_2$	$n_l - n_2$	$n_l - n_2$	$n_l - n_2$	Δn	dl/dn
mm	kc	kc	kc	kc	kc	mm/kc	kc	kc	kc	kc	kc	mm/kc
2	0	0	0	0			0	0	0	0		
3	7.63	6.25	9.00	7.63	7.63	0.131	2.15	2.40	5.60	3.38	3.38	0.296
4	13.28	11.00	14.10	12.80	5.17	0.194	3.65	3.35	7.25	4.75	1.37	0.730
5	17.68	14.60	18.60	16.97	4.17	0.240	4.50	4.60	8.60	5.90	1.15	0.869
6	21.73	18.00	22.80	20.85	3.88	0.258	5.55	5.20	9.45	6.73	0.83	1.21
7	25.06	20.40	25.30	23.58	2.73	0.367	6.20	5.60	9.90	7.23	0.50	2.00
8	27.76	22.05	27.55	25.78	2.20	0.455	6.65	6.00	10.40	7.68	0.45	2.22
9	30.36	23.85	29.40	27.86	2.08	0.481	6.85	6.10	10.65	7.86	0.18	5.55
10	31.36	25.40	30.80	29.18	1.32	0.757	7.00	6.30	10.85	8.04	0.18	5.55
12	33.76	27.25	33.10	31.36	2.18	0.917	7.25	6.50	11.25	8.32	0.28	7.14
14	35.06	28.60	34.70	32.78	1.42	1.41	7.45	6.70	11.40	8.50	0.18	11.1
16	36.01	29.25	35.95	33.73	0.95	2.10	7.60	6.80	11.60	8.65	0.15	13.3
18	36.61	29.70	36.60	34.30	0.57	3.51	7.70	6.90	11.70	8.75	0.10	20.0
20	37.11	30.10	36.95	34.72	0.42	4.76	7.80	7.00		8.85	0.10	20.0
25	37.76	30.65	37.55	35.32	0.60	8.33						
30	38.11	30.85	38.30	35.75	0.43	11.6						
35	38.51	31.15	38.60	36.08	0.33	15.2						
40	38.71			36.28	0.20	25.0						

TABLE 7

Crack propagation records

$S_m = 4.5$ kg/mm^2; $S_a = 2.5$ kg/mm^2

	2024						7075					
	specimen			mean of three specimens			specimen			mean of three specimens		
	A116	A59	A11				A739	A711	A727			
l	$n_l - n_2$	$n_l - n_2$	$n_l - n_2$	$n_l - n_2$	Δn	dl/dn	$n_l - n_2$	$n_l - n_2$	$n_l - n_2$	$n_l - n_2$	Δn	dl/dn
mm	kc	kc	kc	kc	kc	mm/kc	kc	kc	kc	kc	kc	mm/kc
2	0	0	0	0			0	0	0	0		
3	242.00	139.15	196.45	192.53	192.53	0.0052	104.40	59.10	49.10	70.87	70.87	0.0141
4	434.00	286.15	324.00	348.05	155.52	0.0064	141.25	83.60	69.25	98.04	27.17	0.0368
5	524.80	377.50	411.60	437.97	89.92	0.0111	156.15	92.85	79.55	109.52	11.48	0.0871
6	568.40	411.20	450.60	476.74	38.77	0.0258	166.35	99.45	85.55	117.12	7.60	0.132
7	597.05	422.05	479.40	506.17	29.43	0.0340	175.55	104.65	90.60	123.60	6.48	0.154
8	624.70	464.10	503.70	530.84	24.67	0.0405	180.90	109.50	95.10	128.50	4.90	0.204
9	640.15	483.00	525.05	549.41	18.57	0.0540	186.65	113.25	98.80	132.90	4.40	0.228
10	655.75	497.30	539.60	564.22	14.82	0.0675	191.45	116.65	101.65	136.58	3.68	0.272
12	685.00	529.00	570.00	594.68	30.45	0.0655	200.20	123.05	107.70	143.65	7.07	0.282
14	705.85	550.10	594.75	616.91	22.23	0.090	207.25	127.70	112.25	149.07	5.42	0.369
16	723.75	570.30	610.70	634.93	18.02	0.111	213.80	132.80	117.20	154.60	5.53	0.362
18	738.00	584.95	631.40	651.46	16.53	0.121	219.05	137.05	120.90	159.00	4.40	0.454
20	749.45	597.25	644.60	663.78	12.32	0.162	223.20	140.50	124.65	162.78	3.78	0.529
25	778.45	623.50	668.60	690.20	26.42	0.189	230.95	147.00	131.50	169.81	7.03	0.710
30	797.45	642.15	685.00	708.22	18.02	0.278	235.75	150.85	135.30	173.96	4.15	1.21
35	813.15	655.70	698.25	722.39	14.17	0.353	238.65	152.90	137.45	176.29	2.33	2.15
40	822.15	665.20	708.20	731.87	9.48	0.527	240.35	154.05	138.80	177.67	1.38	3.62
45	827.45	671.30	714.00	737.60	5.73	0.873	241.25	154.70	139.50	178.42	0.75	6.67
50	830.45	674.55	717.20	740.75	3.15	1.59	241.70	155.05	139.95	178.84	0.42	11.9
55	831.90	676.75	718.65	742.45	1.70	2.94	241.95	155.25	140.15	179.06	0.22	22.7
60	832.35	677.85	719.30	743.33	0.88	5.68						
65		678.25		743.73	0.40	12.50						

TABLE 8

Crack propagation records

$S_m = 4.5$ kg/mm^2; $S_a = 3.2$ kg/mm^2

	2024						7075					
	specimen			mean of three specimens			specimen			mean of three specimens		
	A23	A37	A103				A702	A723	A748			
l	n_l–n_2	n_l–n_2	n_l–n_2	n_l–n_2	Δn	dl/dn	n_l–n_2	n_l–n_2	n_l–n_2	n_l–n_2	Δn	dl/dn
mm	kc	kc	kc	kc	kc	mm/kc	kc	kc	kc	kc	kc	mm/kc
2	0	0	0	0			0	0	0	0		
3	106.35	151.55	139.55	132.48	132.48	0.0076	20.05	23.30	30.70	24.68	24.68	0.0405
4	170.10	218.00	181.70	189.93	57.45	0.0174	29.55	34.20	43.35	35.70	11.02	0.091
5	193.20	250.15	204.70	216.05	26.12	0.0383	36.05	40.50	50.85	42.47	6.77	0.148
6	212.05	267.80	230.20	236.72	20.67	0.0484	40.45	44.85	56.95	47.42	4.95	0.202
7	225.35	281.10	244.45	250.34	13.62	0.0735	44.45	48.60	61.40	51.49	4.07	0.246
8	238.75	293.80	259.95	265.21	13.87	0.0720	48.55	52.70	65.60	55.66	4.17	0.240
9	249.60	306.40	273.85	277.66	12.45	0.0804	51.55	55.60	69.25	58.84	3.18	0.314
10	261.50	315.60	283.40	287.88	10.22	0.098	54.70	58.50	72.60	61.97	3.13	0.319
12	278.50	335.20	305.60	307.48	19.60	0.102	60.60	64.40	79.05	68.05	6.08	0.328
14	293.45	350.75	321.05	322.80	15.32	0.130	65.20	68.65	83.75	72.57	4.52	0.442
16	307.70	362.90	333.85	335.87	13.07	0.153	68.35	72.85	87.10	76.14	3.57	0.560
18	316.85	371.65	343.45	345.04	9.17	0.218	71.00	75.95	90.25	79.11	2.97	0.673
20	325.90	379.65	350.65	353.12	8.08	0.248	73.10	78.30	92.60	81.38	2.27	0.881
25	341.75	396.40	365.80	369.04	15.92	0.314	76.45	82.50	96.70	85.26	3.88	1.29
30	351.15	409.15	378.20	380.56	11.52	0.433	78.00	84.55	98.90	87.19	1.93	2.59
35	358.10	417.15	386.60	388.34	7.78	0.643	78.85	85.75	100.05	88.29	1.10	4.54
40	362.40	422.15	391.85	393.19	4.85	1.03	79.30	86.45	100.70	88.89	0.60	8.3
45	365.15	424.75	394.85	395.97	2.78	1.80	79.55	86.80	101.15	89.24	0.35	14.3
50	366.60	426.00	396.50	397.42	1.45	3.45	79.75	87.00	101.45	89.51	0.27	18.5
55	367.20	426.55	397.10	398.00	0.58	8.63		87.10	101.65	89.66	0.15	33.3
60			397.30	398.20	0.20	25.0						

TABLE 9

Crack propagation records

$S_m = 4.5$ kg/mm^2; $S_a = 4$ kg/mm^2

	2024						7075					
	specimen			mean of three specimens			specimen			mean of three specimens		
	A72	A57	A4				A718	A742	A713			
l	n_l–n_2	n_l–n_2	n_l–n_2	n_l–n_2	Δn	dl/dn	n_l–n_2	n_l–n_2	n_l–n_2	n_l–n_2	Δn	dl/dn
mm	kc	kc	kc	kc	kc	mm/kc	kc	kc	kc	kc	kc	mm/kc
2	0	0	0	0			0	0	0	0		
3	38.80	42.95	46.85	42.87	42.87	0.0233	11.70	14.25	11.40	12.45	12.45	0.0804
4	62.10	70.50	68.50	67.04	24.17	0.0455	18.85	23.45	17.95	20.08	7.63	0.131
5	85.70	88.20	86.60	86.84	19.80	0.0505	24.20	29.10	23.40	25.56	5.48	0.183
6	96.20	100.10	98.60	98.31	11.47	0.0872	28.30	33.40	27.70	29.79	4.23	0.236
7	105.25	108.65	109.40	107.78	9.47	0.106	32.10	37.45	31.20	33.57	3.78	0.264
8	115.25	117.80	117.50	116.86	9.08	0.110	35.65	41.45	34.80	37.29	3.72	0.269
9	127.15	127.40	126.25	126.94	10.08	0.100	38.55	45.10	38.05	40.56	3.27	0.306
10	136.20	135.10	132.00	134.44	7.50	0.133	41.05	47.00	40.20	42.74	2.18	0.458
12	151.30	150.70	147.35	149.79	15.35	0.130	46.15	52.05	45.00	47.72	4.98	0.382
14	162.50	160.35	158.00	160.29	10.50	0.190	49.30	56.00	48.45	51.24	3.52	0.568
16	170.55	168.55	168.70	169.27	8.98	0.222	51.65	59.15	51.15	53.97	2.73	0.733
18	178.85	174.30	178.05	177.07	7.80	0.256	53.35	61.30	52.95	55.85	1.88	1.06
20	188.65	179.65	184.45	184.25	7.18	0.278	54.50	62.90	54.00	57.12	1.27	1.58
25	202.15	191.40	196.15	196.57	12.32	0.406	56.25	64.90	55.60	58.90	1.78	2.81
30	211.30	200.10	203.40	204.94	8.37	0.598	57.25	66.25	56.50	59.98	1.08	4.63
35	217.05	205.30	207.45	209.94	5.00	1.00	57.80	66.95	57.00	60.56	0.58	8.63
40	220.15	208.55	209.90	212.87	2.93	1.71	58.10	67.25	57.20	60.83	0.27	18.5
45	222.15	210.45	211.20	214.60	1.73	2.89	58.25	67.45	57.30	60.98	0.15	33.4
50	223.00	211.35	212.05	215.47	0.87	5.75		67.65		61.18	0.20	25.0
55	223.30	211.80	212.55	215.89	0.42	11.9						

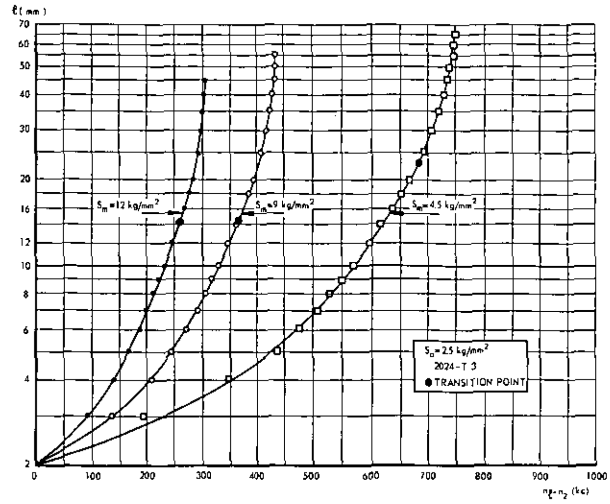

Fig. 2 Crack-propagation curves for 2024-T3 material at S_a = 2.5 kg/mm².

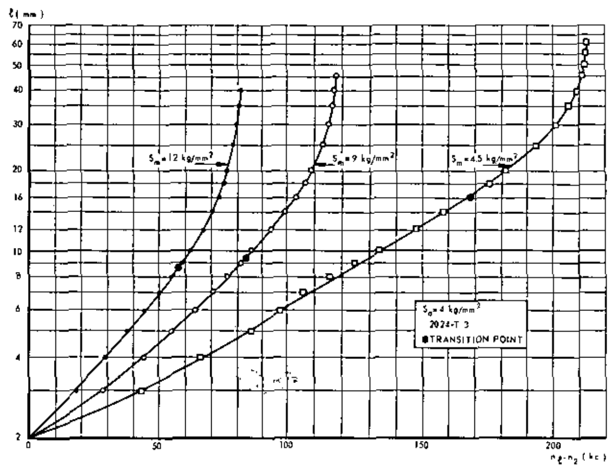

Fig. 3 Crack-propagation curves for 2024-T3 material at S_a = 4 kg/mm².

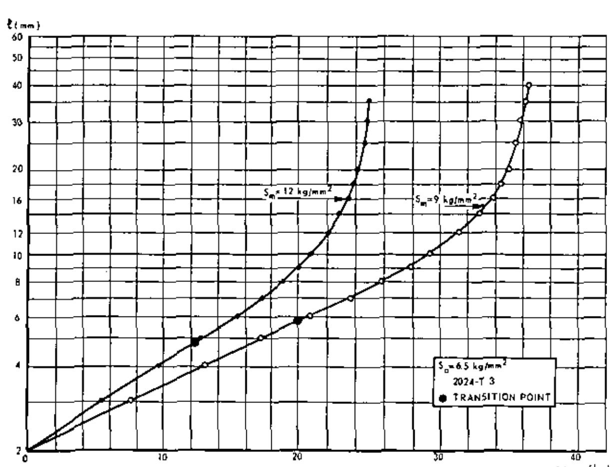

Fig. 4 Crack-propagation curves for 2024-T3 material at S_a = 6.5 kg/mm².

ty of the 2024 alloy above the 7075 alloy. The latter consistently shows a higher crack-rate and consequently a shorter crack-propagation life. These observations confirm those of other investigators (refs. 1 and 5–10 incl.).

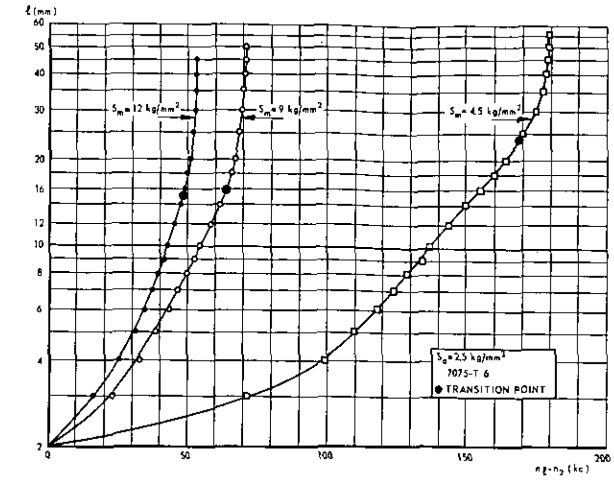

Fig. 5 Crack-propagation curves for 7075-T6 material at S_a = 2.5 kg/mm².

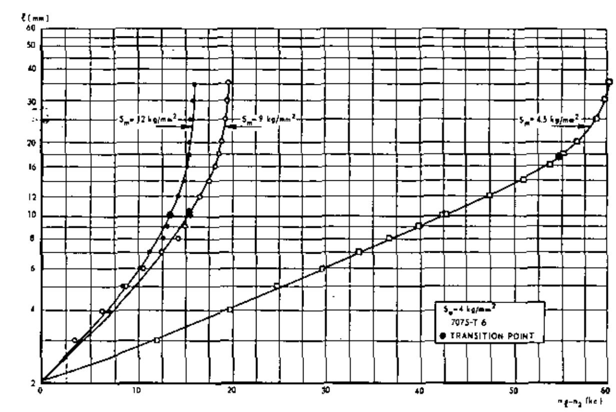

Fig. 6 Crack-propagation curves for 7075-T6 material at S_a = 4 kg/mm².

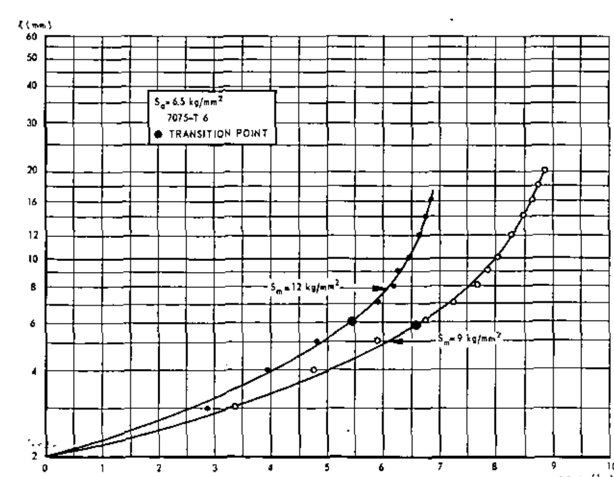

Fig. 7 Crack-propagation curves for 7075-T6 material at S_a = 6.5 kg/mm².

In table 10 the endurances $n_{30}-n_2$ for a crack extension from 2 through 30 mm are tabulated and the ratio of crack-propagation lives indicated. It appears that the crack-propagation life of the 7075 alloy on the average is only 25% of the corresponding life of the

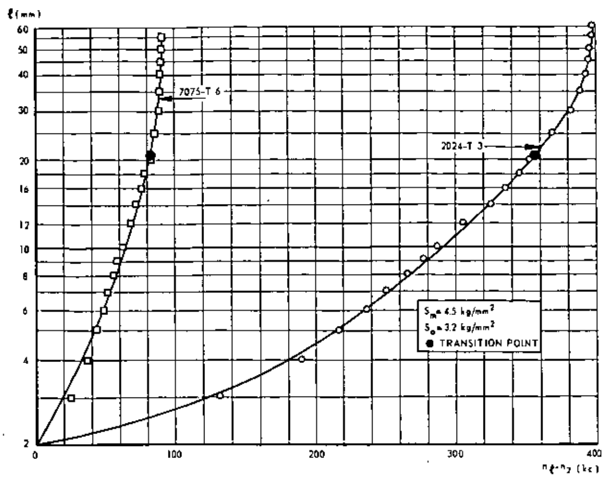

Fig. 8 Crack-propagation curves at S_a = 3.2 kg/mm².

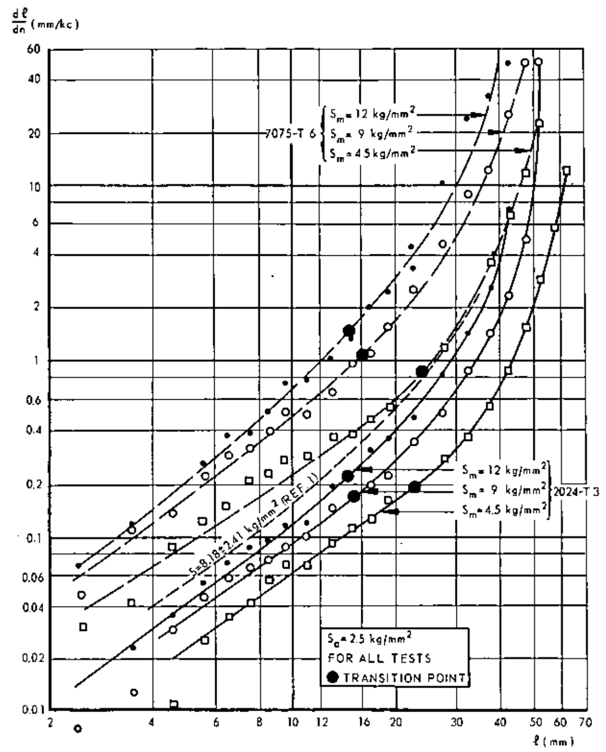

Fig. 9 The crack rate as a function of the crack length at S_a = 2.5 kg/mm².

2024 alloy. In table 11 results of McEvily and Illg (ref. 5) are given on an equivalent basis. Here the 7075 alloy shows relatively better properties giving an endurance in the order of 40% of that of the 2024 alloy. Results of Weibull (refs. 6,7) show about the same ratio; however, results from different investigators, collected in ref. 10 gave a ratio 0.1–0.3.

The 7075 alloy has a higher static strength, but it is unable to experience large plastic strains. Its ductility is low as compared with the 2024 alloy. This means that in the 7075 alloy there will be less stress relief by plastic flow in the vicinity of the crack tip. Therefore the actual stress concentration at the crack tip will be higher than in the 2024 alloy resulting in a higher crack rate.

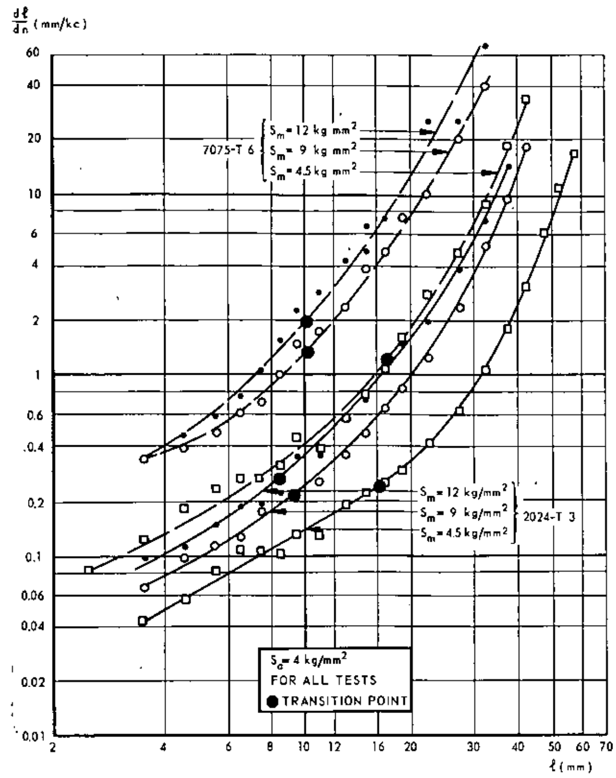

Fig. 10 The crack rate as a function of the crack length at $S_a = 4$ kg/mm².

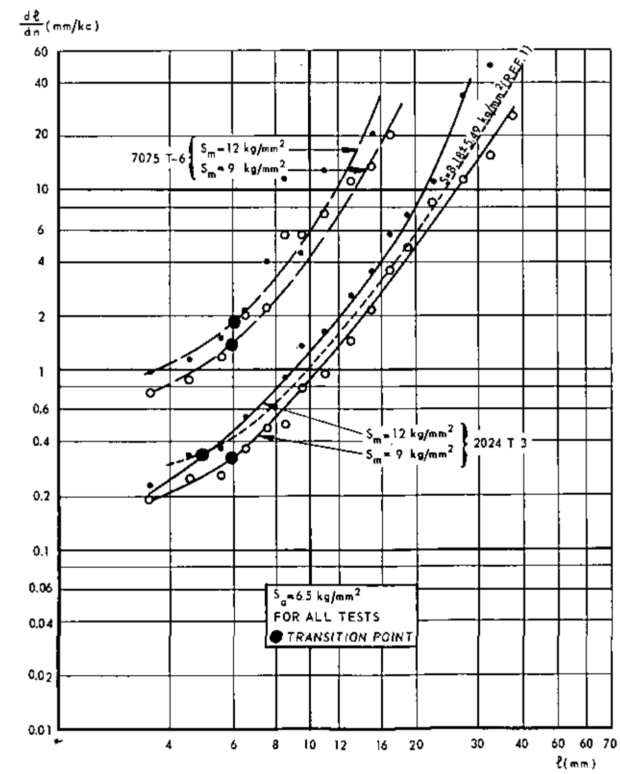

Fig. 11 The crack rate as a function of the crack length at $S_a = 6.5$ kg/mm².

The same reasoning may explain the fact that McEvily and Illg (ref. 5) found relatively better crack-propagation properties for the 7075 alloy than obtained in the present investigation, since the elongation of the material tested by them was 11.8%, whereas the

TABLE 10

Comparison of 2024 and 7075 alloy; present results

S_m (kg/mm²)	S_a (kg/mm²)	$n_{30}-n_2$ (kc)		ratio
		2024	7075	$\frac{(n_{30}-n_2)_{7075}}{(n_{30}-n_2)_{2024}}$
12	2.5	301	52.5	0.175
	4	81	16.3	0.201
	6.5	24.7	6.9	0.279
9	2.5	432	70.5	0.163
	4	117	20.1	0.172
	6.5	36.3	8.9	0.245
4.5	2.5	744	179	0.241
	3.2	398	89.7	0.226
	4	216	61.2	0.284
			Average	0.23

TABLE 11

Comparison of 2024 and 7075 alloy; results of McEvily and Illg (ref. 5)

specimen width (in)	max. stress in a cycle (min. stress zero; R=0) (ksi)	$n_{0.5''}-n_{0.2''}$ for 2″ specimens $n_{1''}-n_{0.2''}$ for 12″ specimens (kc)		ratio
		2024	7075	
2	7.1	841	265	0.315
	10	266	74.2	0.279
	14.5	40.6	14.3	0.352
	20	16.3	8.5	0.521
	25	9.3	5.1	0.548
	30	6.3	2.8	0.444
12	10	170	79.8	0.469
	14.5	50.3	24.8	0.493
	20	27.6	11.8	0.427
	25	14.4	6.0	0.416
			Average	0.43

alloy used in the present investigation showed an elongation of 9.4% (both based on a 2″ gage length).

In figs. 9 and 11 some results for a 2024-T3 alloy as obtained in ref. 1 are compared with the results of the present investigation. Clearly the crack rates in the alloy studied in ref. 1 were higher than the crack rates in the 2024-alloy studied here. The elongation of the material from ref. 1 was only 16%, whereas the present material showed an elongation of 18.9%. The yield stress and the ultimate-stress were practically the same for both materials.

Unfortunately most investigators which studied the crack propagation properties of the 7075-alloy do not give static properties in their reports: This makes a further comparison on the basis of ductility impossible. Still it is felt, that the ductility is a very important parameter for crack propagation properties.

5 The influence of mean stress; comparison with other investigations

5.1 *General*

The general trend revealed by figs. 9–11 incl. is an increasing crack rate with increasing mean stress, which consequently leads to shorter fatigue lives. This conclusion holds for both the 2024 and the 7075 alloy, the influence of the mean stress being very similar for both materials.

It is not unexpected that the mean stress affects crack propagation since it does affect the endurance in conventional fatigue tests. Some investigators (refs. 11, 12) argue that the influence of the mean stress is of minor importance as compared with the effect of stress amplitude. There are very few data available in the literature that may shed some light on this aspect. Frost and Dugdale (ref. 13) tested a mild steel at four values of the mean stress and did not find any influence indeed; on the other hand they found a definite influence of the mean stress for an aluminum alloy employing two values of the mean stress. In the following it will be shown that the test results of Frost and Dugdale are in agreement with the present results and that the crack rate is approximately proportional to the mean stress.

Some further data on the influence of mean stress are available. Due to the form in which these data are given the most convenient way to compare them with the present results is the indirect way via crack-propagation theories. Therefore it is necessary to give a short review of relevant theories, which will be done in the following section. In section 3 of this chapter it will be shown that the present results agree fairly well with those of other investigations.

5.2 *Summary of crack propagation theories*

In the past few years a number of crack-propagation theories were published. All these theories were discussed already in ref. 1 and therefore this will not be done again in detail here. In this section only those facts will be reviewed which are relevant for the discussion in this report.

In all theories it is tried to derive an analytical function for the relation

$$\frac{\mathrm{d}l}{\mathrm{d}n} = f(l, S) \qquad (1)$$

where $\mathrm{d}l/\mathrm{d}n$ is the crack rate, l the crack length and S some stress parameter. In ref. 1 a general formula for this relation was given:

$$\frac{\mathrm{d}l}{\mathrm{d}n} = p(S_m, \omega, t, q)\, S_a^{\beta} l^{\alpha} \qquad (2)$$

in which p is a function of mean stress S_m, testing frequency ω, sheet thickness t and some intrinsic material parameter q. Eq. (2) was arrived at as a summary of a number of theories, which all give values for the constants α and β. Values of these constants and the way in which they were obtained are tabulated below.

α	β	way in which constants were obtained	Investigators	ref.
1		dimensional analysis	Frost and	13
	3	empirical approach	Dugdale	13
1		dimensional analysis	Liu	14,11
	2	analysis of mechanical model		11
1,5		analysis of mechanical model	Head	15
	2,6	empirical approach	Weibull	16
1,5	2,6	empirical approach	Schijve, Broek and de Rijk	1

It should be noted that eq. (2) is correct only up till a crack length of 10–15% of the sheet width.

For the function p of eq. (2) several authors derived empirically a numerical value valid for their particular tests.

Two theories indirectly lead to a function for eq. (1), namely the theory of Paris et al. (refs. 12, 17, 18) and the theory of McEvily and Illg (ref. 5). Both theories are based on the same principle (refs. 18, 21); they were published independently at the same time.

The theory of McEvily and Illg states that the crack rate is a function of the stress at the tip of the crack only. This stress is assumed to be equal to the product of a stress-concentration factor K_E and the net stress for the cracked specimen, or

$$\frac{\mathrm{d}l}{\mathrm{d}n} = f(K_E \cdot S_n)\,. \tag{3}$$

K_E is defined as the theoretical stress concentration factor for an elliptical hole, representing the crack. The major axis is equal to $2l$ and the tip radius ρ is assumed to be a material constant. McEvily and Illg checked their theory by plotting their extensive test results at $R=0$ in terms of $K_E \cdot S_{an}$ versus the crack rate. All their test results fell within a narrow scatterband around a single curve, thus confirming eq. (3). McEvily and Illg derived empirically a rather complicated function for this curve.

The theory of Paris is based on more or less the same arguments. The crack is considered to be an elliptic hole in an infinite sheet with a zero minor axis and the major axis equal to the crack length. Formulas for the stresses at a point P in the crack tip region were given by Sneddon (ref. 19). The formulas are of the form:

$$\left.\begin{aligned} S_y &= S\sqrt{l}\cdot\sqrt{\frac{1}{2r}}\cos\frac{\theta}{2}\left[1+\sin\frac{\theta}{2}\sin\frac{3\theta}{2}\right] \\ S_x &= -S+S\sqrt{l}\cdot\sqrt{\frac{1}{2r}}\cos\frac{\theta}{2}\left[1-\sin\frac{\theta}{2}\sin\frac{3\theta}{2}\right] \\ S_{xy} &= S\sqrt{l}\cdot\sqrt{\frac{1}{2r}}\cos\frac{\theta}{2}\sin\frac{\theta}{2}\cos\frac{3\theta}{2} \end{aligned}\right\} \tag{4}$$

$$K = S\sqrt{l}\sqrt{\frac{2w}{\pi l}\tan\frac{\pi l}{2w}}\,. \tag{5}$$

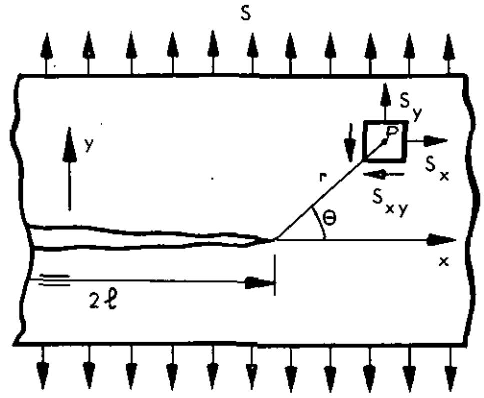

It appears from eqs. (4) that the stress field around the tip of the crack depends on the parameter $K'=S\sqrt{l}$ only, apart from the constant term S in the second relation of eqs. (4). The latter term, however, can be neglected for small values of r, i.e. in the region close to the tip of the crack. For a sheet of finite width $2w$ the factor K' can be corrected to (ref. 25)

K is known in the literature as the stress intensity factor.

Paris now argues that the crack rate is fully determined by the local stresses around the crack tip, and since K determines the stress field in the tip region, this parameter and only this governs the rate of crack growth. This means:

$$\frac{\mathrm{d}l}{\mathrm{d}n} = f(K)\,. \tag{6}$$

Paris checked his theory by plotting a large number of test results in terms of $\mathrm{d}l/\mathrm{d}n$ versus K and indeed all these tests results plotted on a single curve within a narrow scatterband. He also tried to give a relation for this curve in order to define $f(K)$ in eq. (6).

Originally Paris (ref. 17) claimed that K_{max} should be the important parameter (K_{max} is obtained if in eq. (5) S_{max} is substituted for S) but in his later work (ref. 12) he argues that K_a should be preferred (K_a is obtained if in eq. (5) S_a is substituted for S).

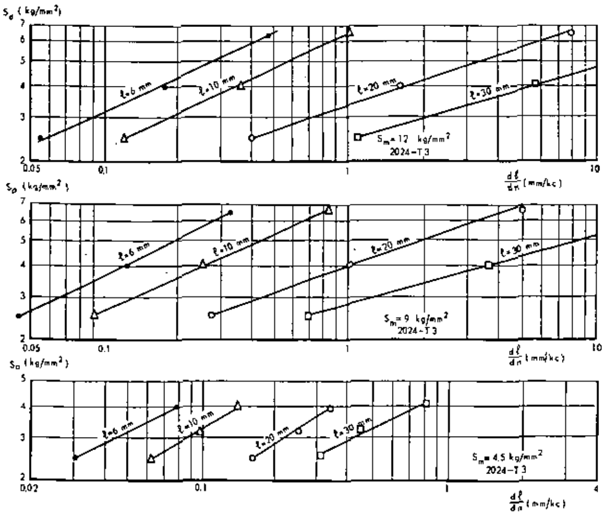

Fig. 12 The influence of the stress amplitude on the crack rate at different crack lengths and mean stresses. 2024-material.

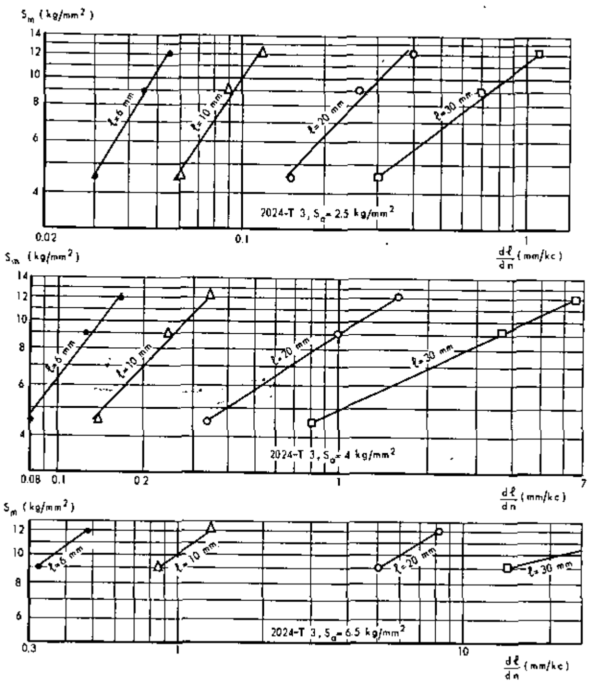

Fig. 13 The influence of the mean stress on the crack rate at different crack lengths and stress amplitudes; 2024-T3 material.

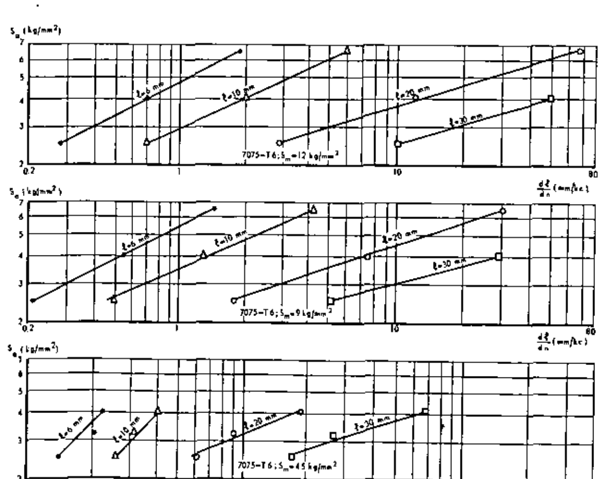

Fig. 14 The influence of the stress amplitude on the crack rate at different crack lengths and mean stresses; 7075-material.

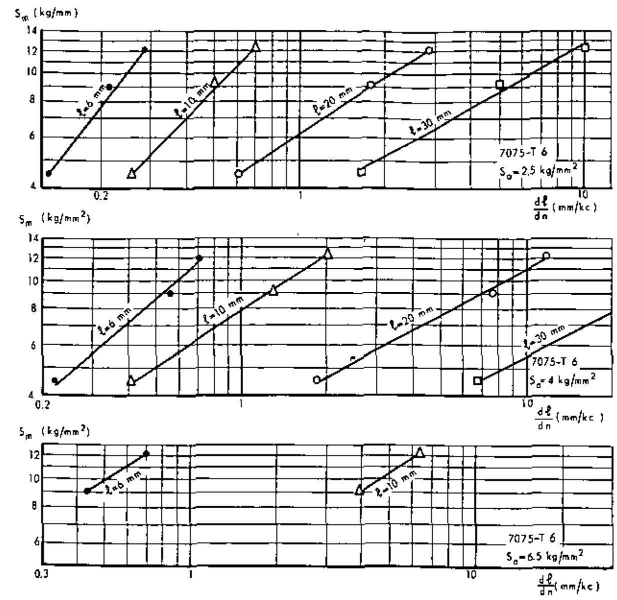

Fig. 15 The influence of the mean stress on the crack rate at different crack lengths and stress amplitudes 7075-T6 material.

5.3 *Application of the theories to the present results*

In figs. 12 through 15 the crack rate has been plotted versus stress amplitude and mean stress for both materials tested. The plots on a double logarithmic scale apparently lead to straight lines. This means that for a certain crack length eq. (2) can be written as:

$$\frac{\mathrm{d}l}{\mathrm{d}n} = C\,S_m^{\gamma}\,S_a^{\beta} \tag{7}$$

The exponents β and γ of equation (7) follow from figs. 12 through 15 as the slopes of the lines. Values of β and γ so obtained have been compiled in table 12. The upper part of table 12 giving values for β can be compared immediately with the table in section 2 of this chapter (page 42). It appears from table 12 that β is not a constant, but depends upon crack length and mean stress. The mean value for β in table 12 is 2.5, which is very close to the mean of the values given in the table on page 51. A close examination of the results of ref. 1 learns that also there β was not a constant, although this was less obvious. For 2024 and 7075 β appears to be almost the same.

The behaviour of the exponent γ is more or less analogous to that of β. The value of γ depends on l and on S_a. The values of γ can be compared with a result from ref. 13, where values for C in the relation:

$$\frac{\mathrm{d}l}{\mathrm{d}n} = C\,S_a^3\,l^{\alpha} \tag{8a}$$

have been derived. For a mild steel C appeared to be 0.086 for all (four) values of the mean stress. This leads to $\gamma=0$. However, for the aluminum alloy BS L 71 (almost the same as 2024) the following results were obtained:

$$S_m = 2\ \text{tons/in}^2; \quad C = 1.42$$

$$S_m = 4\ \text{tons/in}^2; \quad C = 3.02$$

TABLE 12

The exponents β and γ in the equation:
$dl/dn = CS_a^{\beta} S_m^{\gamma} l^{\alpha}$

	β at different values of S_m					
l	2024			7075		
(mm)	$S_m = 12$ kg/mm²	$S_m = 9$ kg/mm²	$S_m = 4.5$ kg/mm²	$S_m = 12$ kg/mm²	$S_m = 9$ kg/mm²	$S_m = 4.5$ kg/mm²
6	2.3	2.2	2.1	2.1	2.1	1.0
10	2.3	2.4	1.8	2.3	2.4	1.0
20	3.2	3.1	1.6	3.4	3.1	2.6
30	3.6	3.7	2.1	3.5	3.8	3.0

	γ at different values of S_a					
l	2024			7075		
(mm)	$S_a = 2.5$ kg/mm²	$S_a = 4.0$ kg/mm²	$S_a = 6.5$ kg/mm²	$S_a = 2.5$ kg/mm²	$S_a = 4.0$ kg/mm²	$S_a = 6.5$ kg/mm²
6	0.6	0.8	1.3	0.8	1.2	1.6
10	0.7	1.0	1.5	1.0	1.6	1.7
20	1.0	1.6	1.7	1.6	1.8	—
30	1.3	2.1	4.7	1.8	1.9	—

From these results it follows that $\gamma \approx 1$, which is in good agreement with the values obtained here for small cracks.

The value $\gamma = 1$ was also found by Frost in his later work (ref. 20), where for a large variety of materials Frost concludes from his test results that

$$\frac{dl}{dn} = (A + BS_m) S_a^3 l \tag{8b}$$

For a mild steel he again found that $B = 0$, but for an aluminium-copper alloy he concluded that $A \approx 0$.

In ref. 14 Liu determined values for the constant C in the equation

$$\frac{dl}{dn} = Cl\,. \tag{8c}$$

Liu called C the crack-propagation factor. If this factor for Liu's results on 2024 sheet specimens is plotted, versus the mean stress at constant S_a it appears that $C = cS_m$ for 2024 material. So here again a value $\gamma = 1$ is found.

The application of the theory of Paris to the present results was carried out for the 2024 alloy only, since the crack-propagation behaviour of the 7075 alloy is almost the same, apart from a nearly constant factor. This may imply that the results of the analysis will be valid also for the 7075 material, again apart from a nearly constant factor. The application of the theory was carried out in the following way. Six values of R ($= S_{min}/S_{max}$) were chosen arbitrarily, viz. $R = 0.1$, 0.2, 0.3, 0.4, 0.5 and 0.6, all between the two extreme R-values of the present tests. For each of the three values of S_a used in the present tests a certain value of S_m corresponds to each value of R. For these combinations of S_m and S_a the crack rate at different crack lengths can be read from fig. 13. On the other hand for each of the three S_m-values used in the present tests one value of S_a can be found for each value of R. For such combinations of S_a and S_m fig. 12 gives the crack rate. Figs. 12 and 13 were further completed with lines for a large number of crack lengths and from these figures dl/dn was derived as a function of l for the values of R given before. With the applicable values of S_a the values of K_a were calculated, using eq. (5). Then it was possible to compile a figure in which the crack rate is plotted for different values of R

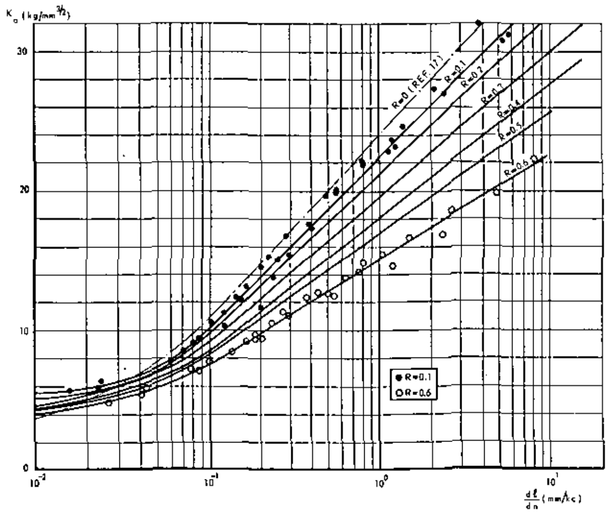

Fig. 16 The crack rate as a function of the stress intensity factor.

versus the stress-intensity factor K_a. This has been done in fig. 16. To avoid confusion by a great number of data points fig. 16 shows the individual points for the highest and lowest R-value only. This still allows an impression on the scatter. The scatterbands for the other values of R have a similar character. By plotting in fig. 16 also the curve for $R=0$ (as obtained in ref. 17 by treating results of refs. 5, 6, 7, 13, 16) a comparison can be made with results of other investigations. It is felt that a satisfactory agreement exists.

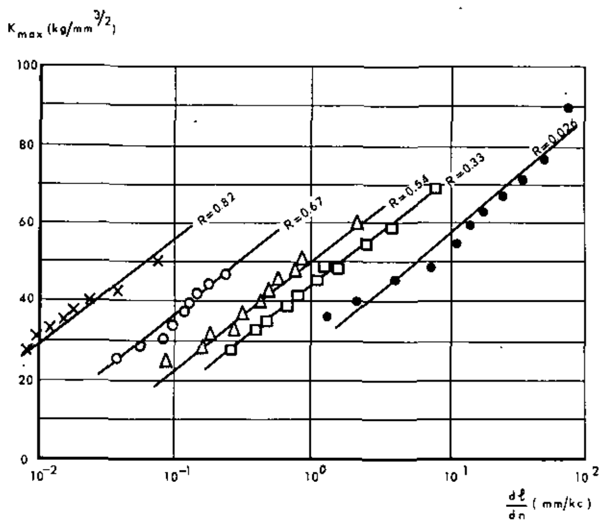

17a K_{max} versus dl/dn for different values of R (ref. 10).

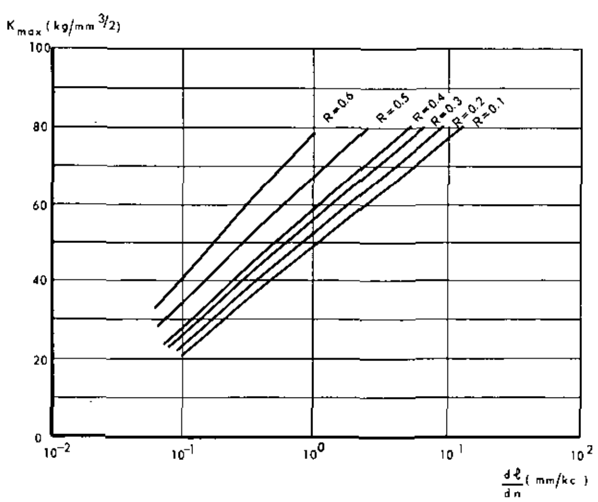

17b K_{max} versus dl/dn; present results.

Figs. 17a and b The crack rate as a function of the maximum stress intensity factor.

In ref. 10 results of several investigations were also analysed in order to determine the influence of R. For this purpose the crack rate was plotted versus K_{max}. The result obtained in ref. 10 is given here in fig. 17a. The present results were evaluated in the same way in fig. 17b. Comparison of figs. 17a and 17b learns that there is a fairly good agreement between both graphs.

5.4 *Discussion*

The influence of the mean stress is apparent from the present results.

It was already shown that the crack rate is proportional to a power of S_m, which varies from 0.6 to 2 depending on S_a and l. A further appreciation of the influence of S_m can also be obtained from the relation between the crack rate and the stress-intensity factor, as will be shown below.

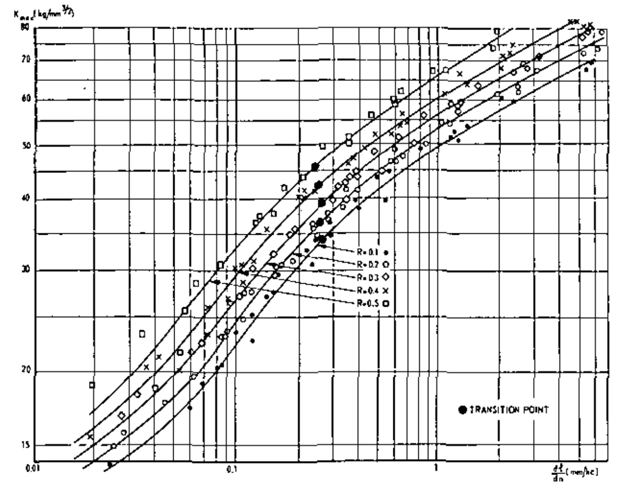

Fig. 18 K_{max} versus dl/dn on double-logarithmic scale.

In fig. 18 the maximum stress-intensity factor, K_{max}, has been plotted versus the crack rate on a double logarithmic scale. On this scale a set of nearly parallel curves is obtained. For the present purpose it is accurate enough to approximate these curves by a set of parallel straight lines. Then the following relation holds:

$$^{10}\log \frac{dl}{dn} = {}^{10}\log A + B\,{}^{10}\log K_{max}\,. \tag{9}$$

The constant B in eq. (9) is the same for all the lines, since they have the same slope. B appears to be approximately 3. The constant A is different for all lines. So, it is not a real constant but a function of R. This function can be determined as follows.

For $dl/dn=1$ mm/kc, or $\log dl/dn=0$ eq. (9) gives

$$^{10}\log A = -B\,{}^{10}\log(K_{max})_{dl/dn=1\ mm/kc} \tag{10}$$

or with $B=3$

$$A = (K_{max}^{-3})_{dl/dn=1\ mm/kc}\,. \tag{11}$$

In fig. 19a K_{max}^{-3} for $dl/dn=1$ mm/kc is plotted versus R on a semi-log scale. Fig. 18 suggests a constant vertical spacing between the lines of constant R-values, for which the difference in successive R-values is also constant. This is confirmed by the linear relation shown in fig. 19a. The analytical function for this relation is

$$-3\ {}^{10}\log K_{\max} = -R - {}^{10}\log 10^5 + {}^{10}\log 1.1\ . \quad (12)$$

Neglecting log 1.1 against log 10^5 the following relation is found for A:

$$A = K_{\max}^{-3} \approx 10^{-5}\ e^{-2.27R}\ . \qquad (13)$$

With $R = (S_m - S_a)/(S_m + S_a)$ and $K_{\max} = (S_m + S_a) l^{\frac{1}{2}}$ eq. (13) can be substituted in eq. (9) to give:

$$\frac{dl}{dn} = 10^{-5} \cdot (S_m + S_a)^3\, l^{\frac{3}{2}} \exp\left(-2.27\, \frac{S_m - S_a}{S_m + S_a}\right). \quad (14)$$

From eq. (14) it appears that the influence of S_m is somewhat more complicated than was predicted by eq. (7).

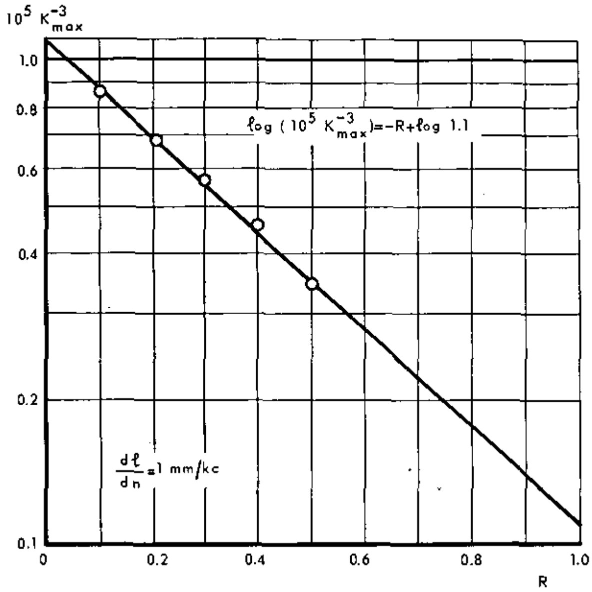

19a $K_{\max}$ versus R on semi-log scale

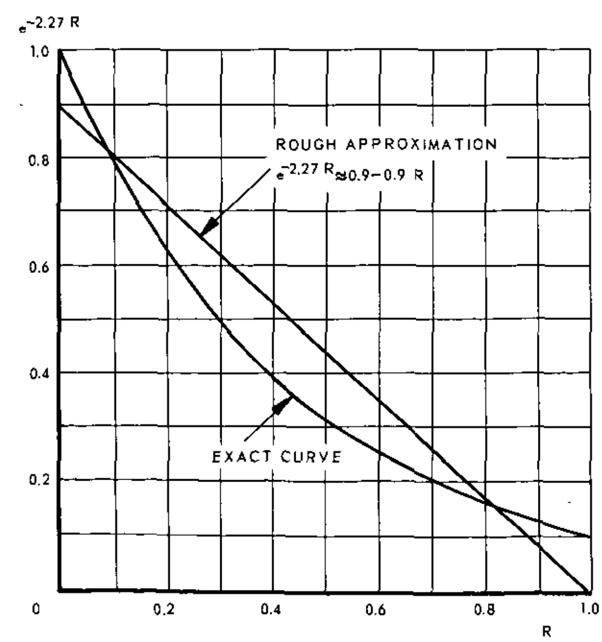

19b $e^{-2.27R}$ versus R

Figs. 19a and b $10^{-5} K_{max}^{-3}$ and $e^{-2.27R}$ as functions of R.

In ref. 13 no influence of the mean stress was found for mild steel; the following tentative explanation may be given. In the vicinity of the crack tip cyclic plastic straining will take place. If this occurs to a sufficient amount some relaxation of the mean stress in the tip region will occur. It is assumed that due to the typical straining behaviour of mild steel the relaxation will be practically complete. So even for a positive nominal mean stress S_m on the specimen the stress cycle in the tip region becomes symmetric around a zero mean value (plastic shake down). An effect of S_m on the crack rate should not be expected then. Apparently this reasoning does not apply to the aluminium alloys since there is a pronounced effect of S_m.

6 Crack propagation theories

6.1 *Comparison of theories*

The similarity of the theory of Paris and other crack-propagation theories has been shown in ref. 18. The theory of Paris states (see also fig. 16)

$$\frac{dl}{dn} = f(K) = f(S\sqrt{l}) \qquad (15)$$

if the correction for finite width is neglected. The crack-propagation theories as summarized in the table in the previous chapter can all be approximated by the formula

$$\frac{dl}{dn} = C \cdot S^{\beta} l^{\alpha}. \qquad (16)$$

For small cracks eqs. (15) and (16) are in agreement if

$$\beta = 2\alpha\ . \qquad (17)$$

The similarity of the theory of Paris and the theory of McEvily and Illg has been shown in refs. 18 and 21, where it was proved that the stress intensity factor is equal to the product of the stress-concentration factor of a crack as defined by McEvily and Illg and the nett stress, apart from a constant. The theory of Paris must be preferred, however, for its simplicity and for the fact that the stress intensity factor contains no constants to be derived from test results.

In fact none of the existing crack-propagation theories has a proper theoretical basis. It is felt that this basis should be a dislocation model. At this moment there is one theory available, based on a dislocation model, which was composed by Valluri (ref. 22). Although Valluri devoted a good deal of work to the analytical treatment of his theory, the equations he arrived at are very complicated and based on too many assumptions which are not supported by physical evidence. Nevertheless, further development and improvement of his theory seems to be worthwhile.

At this moment the theory that required the least assumptions and that agrees best with empirical evidence, should be preferred. The theory of Paris satisfies these requirements.

In fact the theory of Paris can hardly be appraised as a theory, since it is rather a hypothetical basis for comparison of crack rates. Its meaning and the results to which it leads will be discussed in the following section.

6.2 *Evaluation of the theory of Paris and its results*

As has been pointed out in sect. 5.4 the theory for 2024 material leads to (eq. 14)

$$\frac{dl}{dn} = 10^{-5}\, e^{-2.27R} S_{max}^{3}\, l^{\frac{3}{2}} \tag{18}$$

This relation was based on stress intensity factors which did not account for a finite width of the specimen. So the latter parameter does not enter into eq. (18). However, one should expect that for large cracks say larger than 25% of the specimen width, the effect of the finite width on the stress distribution can not longer be ignored. Comparison of the test data with calculated crack rates according to eq. (18) showed indeed an increasing discrepancy for larger cracks. The finite width correction given in eq. (5) hardly improved this. A better agreement was obtained by a correction of eq. (18) as given in the following relation

$$\frac{dl}{dn} = 10^{-5}\, e^{-2.27R} S_{max}^{3}\, l^{\frac{3}{2}} \left(1+10\,\frac{l^2}{w^2}\right). \tag{19}$$

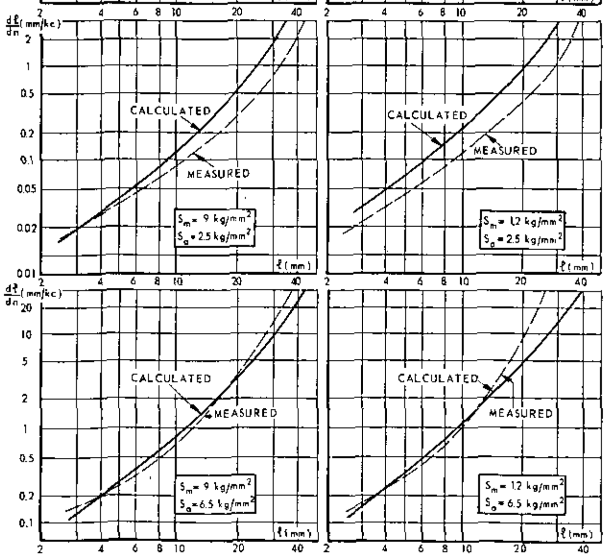

Fig. 20 Comparison of calculated and measured crack rates (2024-specimens).

The accuracy of eq. (19) is demonstrated in fig. 20, where crack propagation data as predicted by eq. (19) are compared with the actual results as obtained in the present investigation. For relatively small cracks there is practically no difference between eqs. (18) and (19).

To obtain a better understanding of the meaning of eq. (19) the function $e^{-2.27R}$ is plotted versus R in fig. 19b. The curve in fig. 19b can be roughly approximated by the straight line as shown. This allows to write for eq. (18):

$$\frac{dl}{dn} = 10^{-5}\left(0.9-0.9\,\frac{S_m-S_a}{S_m+S_a}\right)(S_m+S_a)^3\, l^{\frac{3}{2}} \tag{20}$$

or after rearranging terms

$$\frac{dl}{dn} = C\,S_{max}^{2}\,S_a\, l^{\frac{3}{2}} = C K_{max}^{2} K_a$$

Eq. (21) predicts the crack rate to be proportional to the square of the maximum stress in a cycle. It can be shown by substituting a yield criterion in eqs. (4) that the width of the plastic zone at the tip of the crack should also be proportional to the square of the maximum stress in a cycle. Then eq. (21) predicts the crack rate to be proportional to the width of the plastic zone at the tip of the crack. This result strongly appeals to intuitive feelings. According to eq. (21) the crack rate should also be proportional to the stress amplitude (or the stress range). Since the amplitude of the force F_a per unit length of the dislocation is

$$F_a = C \cdot S_a b \tag{22}$$

in which b is the Burger's vector and C is a constant, the crack rate should be proportional to the amount of cyclic plastic strain.

For short cracks eq. (21) predicts the crack rate to be proportional with $l^{\frac{3}{2}}$ which is in good agreement with a wide range of test results.

The conclusion to be drawn from the present discussion is that eq. (19) is a fairly accurate formula for the prediction of crack propagation properties. Eq. (19) is restricted to the 2024-T3 material used for the present investigation, but it is felt that a generalization is possible by writing:

$$\frac{dl}{dn} = C_1 e^{-C_2 R} S_{max}^{3}\, l^{\frac{3}{2}} \left(1+10\,\frac{l^2}{w^2}\right) \tag{23}$$

In principle it is possible to determine the constants C_1 and C_2 for any material by carrying out two tests at different values of R.

The crack rates of two other materials have been calculated with the aid of eq. (23), adapting C_1 and C_2 to the test data. The results are compared with the actual test results in figs. 21 and 22. These figures show that eq. (23) satisfies the results very well for the 2024 material (fig. 22). For the 7075 material the agreement on the average is fairly good if the crack length is not too large. For relatively large cracks eq. (23) gives unconservative results, especially for the 7075 alloy. It is felt that this is to be associated with the fact that the plastic zone at the tip of the crack becomes so large that a complete re-distribution of stresses takes place, which cannot be described any longer by means of a stress-intensity factor based on elastic calculations.

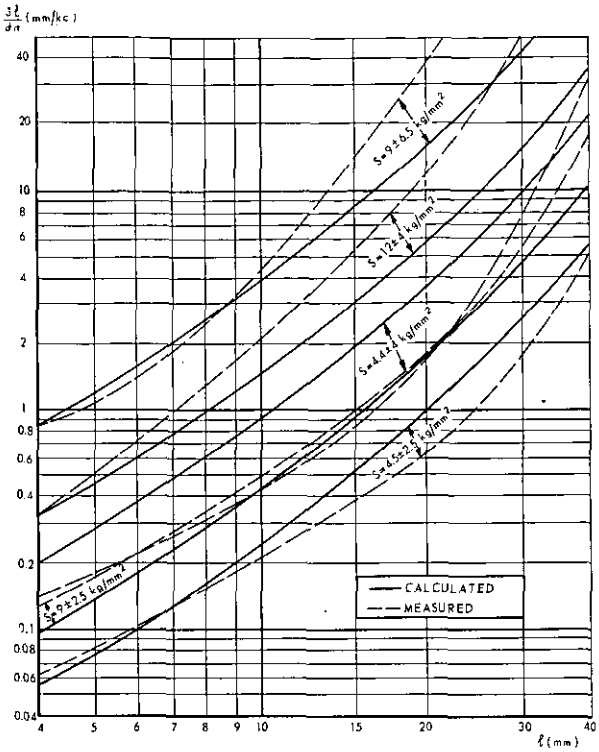

Fig. 21a Calculated crack rates compared with test data for the 7075-specimens.

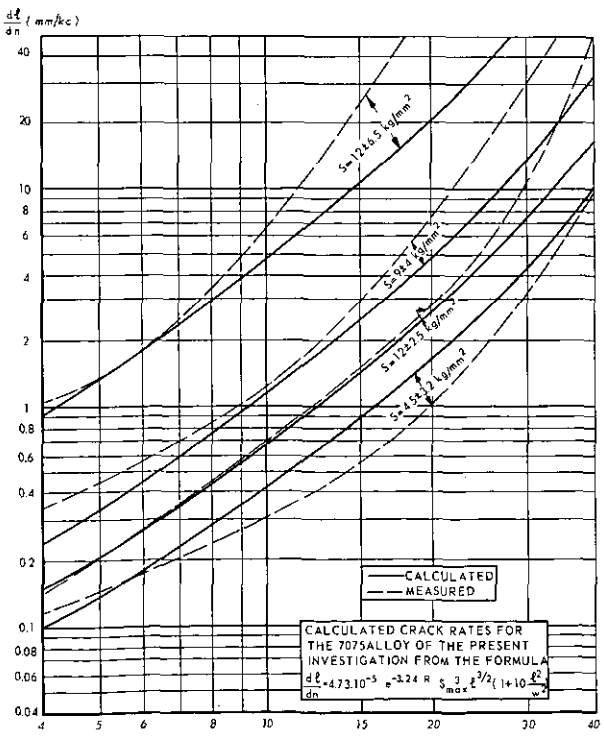

Fig. 21b Calculated crack rates compared with test data for the 7075-specimens.

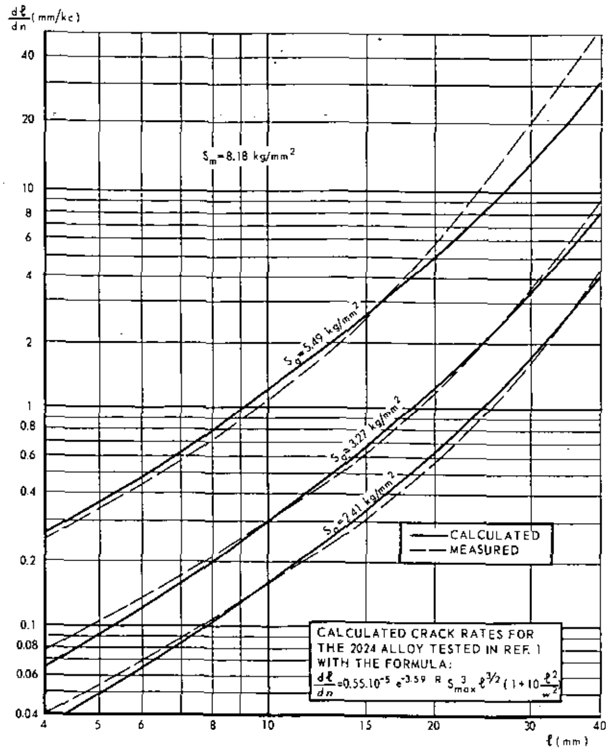

Fig. 22 Calculated crack rates compared with test data for the 2024-specimens from ref. 1.

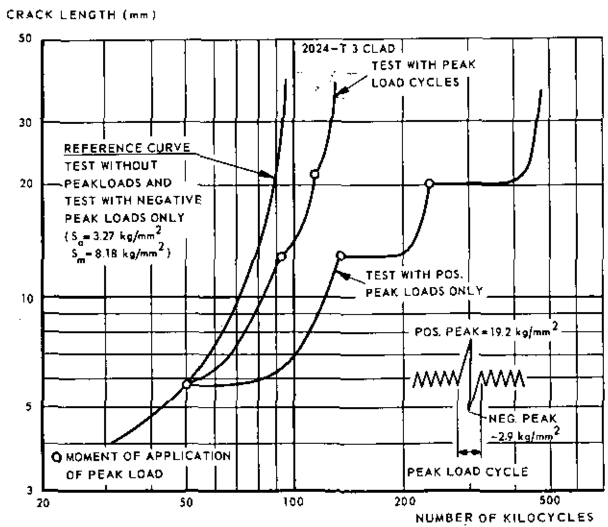

Fig. 23 Retardation of crack propagation due to peak loads. (refs. 3,4).

6.3 *Practical usefulness of the theory of Paris*

The theory of Paris was developed to correlate crack rate data of constant-amplitude tests. In service the loadings generally have a variable amplitude. Interaction effects on the crack propagation of loads with different amplitudes should be expected. Fortunately such effects are either negligible or favourable, see for instance refs. 3 and 4. Illustrations of favourable interactions are presented in figs. 23 and 24. Consequently crack rates under variable-amplitude loading are lower than predicted by the Palmgren-Miner rule. This rule being conservative for crack propagation, the major

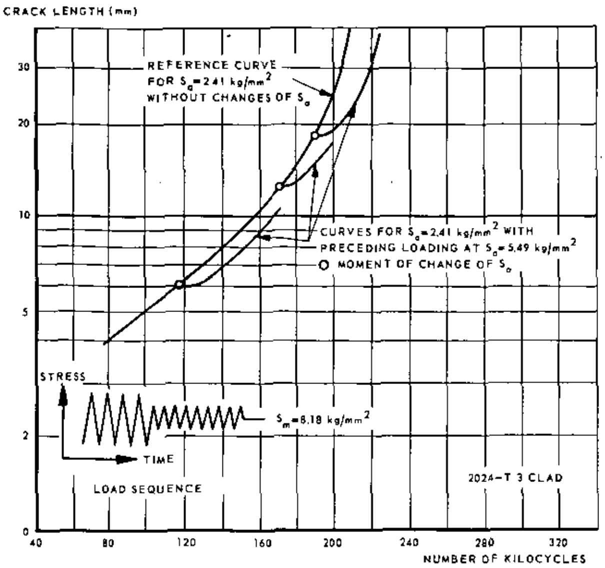

Fig. 24 The effect of preceding cycling at high amplitude on subsequent crack propagation at lower amplitudes. (refs. 3,4).

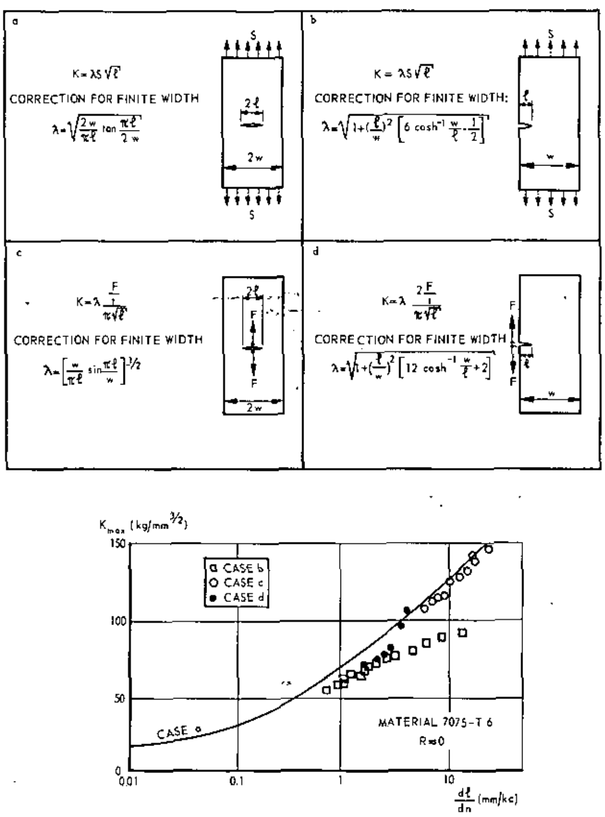

Fig. 25 Stress intensity factors and crack propagation for different configurations (results from refs. 10 and 24).

problem is to estimate reliable crack rate data for constant-amplitude loading. The problem to be considered here is whether a designer can use the theory of Paris for the latter purpose. Two pertinent questions have to be answered then.

(a) Has the theory a general validity also for other configurations? Cracks in service generally occur in more complicated parts than in a simple sheet specimen.

(b) Has the theory a general validity also for other materials?

The problem raised in the first question was recently discussed by Donaldson and Anderson (ref. 10). The stress intensity factor has been calculated for a number of configurations (ref. 24). A summary of some of these cases and the corresponding crack rate data as derived from ref. 10 is presented in fig. 25. The graph shows that the stress intensity factor offers some promise for correlating crack rate data for geometrically different configurations. It is hoped that a more general validity can be shown in the future.

The second question was also discussed in ref. 10 and it was shown for a large variety of materials that a relation between the stress intensity factor and the crack rate could be arrived at. Such a relation was found in the present investigation for sheet specimens with a central crack. Evaluation of the relation led to eq. (19) which proved to be useful for the 2024-alloy and the 7075-alloy. It was disappointing, however, to notice that the crack rates in the 2024-alloy in the present investigation were approximately two times lower than found in ref. 1 for exactly the same specimen of the same material, but from a different producer. So even in Al-Cu-Mg alloys no generalization of crack rate data seems to be allowed. This was also shown by Harpur (ref. 28). In a recent study of the N.L.R. on the effect of sheet thickness (not yet published) it was found that the sheet thickness also has a considerable and systematic effect on the crack rate. This emphasizes that one can not extrapolate data from one sheet material to another sheet material if only the chemical composition is the same.

As a consequence of the previous reasoning it has to be said that application of the theory of Paris requires a set of curves as shown in fig. 18 and it is not allowed to borrow such data from the literature. So crack propagation tests have to be performed. For sheet metals in an aircraft structure applied in an area which might be prone to fatigue cracking such tests are advised anyhow, since they will give the designer some indication of the crack-growth sensitivity of his material. If he performs two tests at different R-values on simple sheet specimens this will allow an assessment of C_1 and C_2 in the relation given before:

$$\frac{dl}{dn} = C_1 e^{-C_2 R} S^3_{max} l^{\frac{3}{2}} \left(1 + 10 \frac{l^2}{w^2}\right).$$

This relation was based on the theory of Paris. For small cracks in a structure the term $(1 + 10\ l^2/w^2)$ would be negligible and the only size parameter would be l, i.e. the absolute value of the crack length. In ref. 2 it was pointed out, that this view is probably correct. The above relation could then be used for a structure if relevant values of S_{max} can be indicated. In stiffened structures this will not be very simple and a rough indication can be obtained at most.

To get the theory of Paris accepted by designers it will be necessary:

1. To assess the stress intensity factor for configurations with the geometrical complexity as it occurs in real aircraft structures.
2. To show that such factors can be correlated with the crack rate in those structures and in simple specimens made from the same material as the structure itself.

Although it is clear that the crack rate is a function of the intensity of the stress field around the tip of the crack the application of the theory as advocated by Paris obviously requires much further research.

7 Fractographical observations

The fractures showed the usual characteristics. On a macro-scale all fatigue cracks started in a plane perpendicular to the direction of loading, but after a certain amount of crack extension the plane of the crack rotated around the direction of crack propagation as an axis until it made an angle of about 45 degrees with the loading direction and the sheet surface. This rotation is called the transition and the end of the transition is defined here as the transition point (see fig. 26a).

The moment of transition depends upon mean stress and stress amplitude. In the crack-propagation curves of figs. 2 through 8 the transition point has been indicated and also in figs. 9–11 where the crack rate is plotted versus the crack length. From figs. 9–11 it may be concluded that the transition occurs at a constant crack rate, which is in agreement with the results of refs. 1 and 26. The value of the crack rate for the transition in the 2024 alloy is the same as found in ref. 1. The crack rate for the transition appears to be different for the two alloys tested in the present investigation.

In order to be able to indicate the transition points also in fig. 18 the value of K_{max} at the transition was plotted versus R in fig. 26b. With the aid of this figure the transition points could be plotted in fig. 18. Again the transition is found to occur at constant crack rate.

In ref. 27 Liu states that the transition takes place when the plastic zone at the crack tip reaches a width equal to half the thickness of the specimen. Since the specimens in the present investigation were of the same thickness and since the plastic-zone width is proportional to S_{max}^2 and l, the transition should take place at a constant value of $S_{max}^2 \cdot l$. This has been checked in fig. 27 for both alloys tested, but the results are negative. For the 2024 alloy this result was already shown by fig. 26b, since $S_{max}^2 l = K_{max}^2$. From figs. 9, 10 and 11 it is easily deduced that neither does the

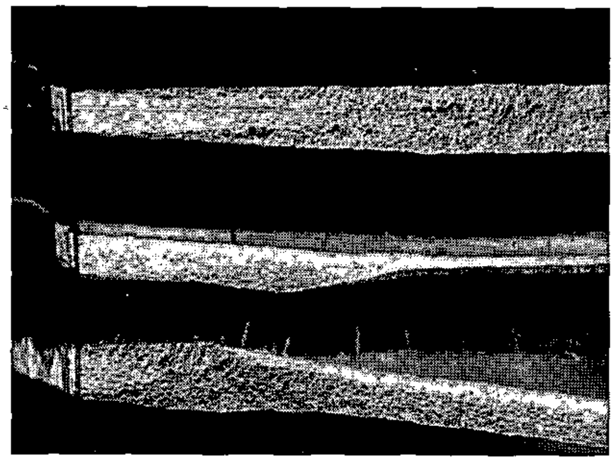

Specimens are from the investigation of ref. 1

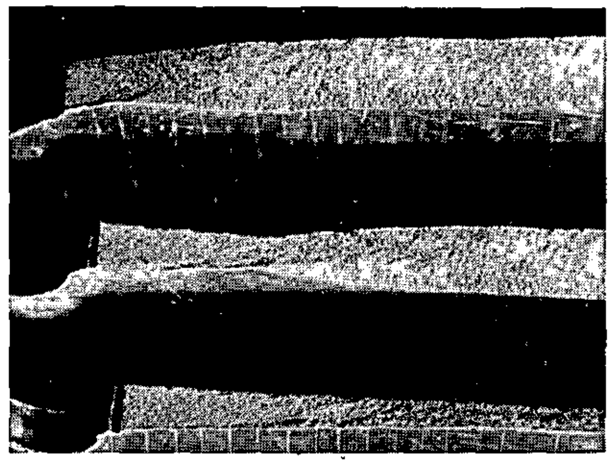

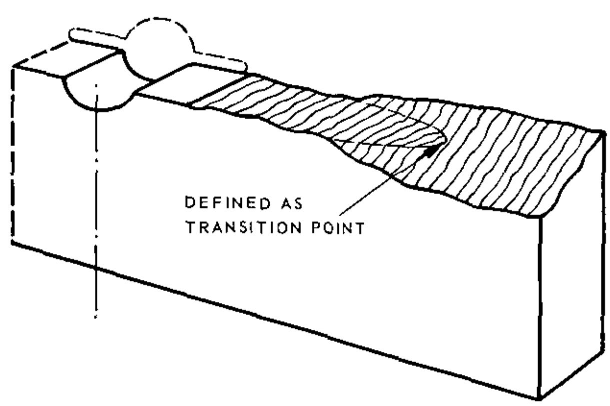

Fig. 26a The transition.

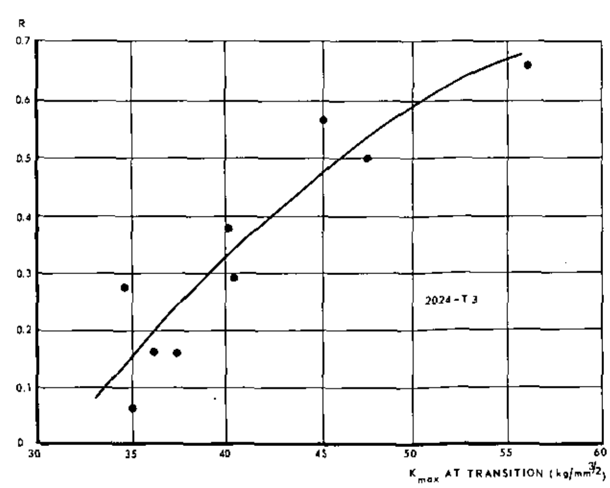

Fig. 26b K_{max} at the transition.

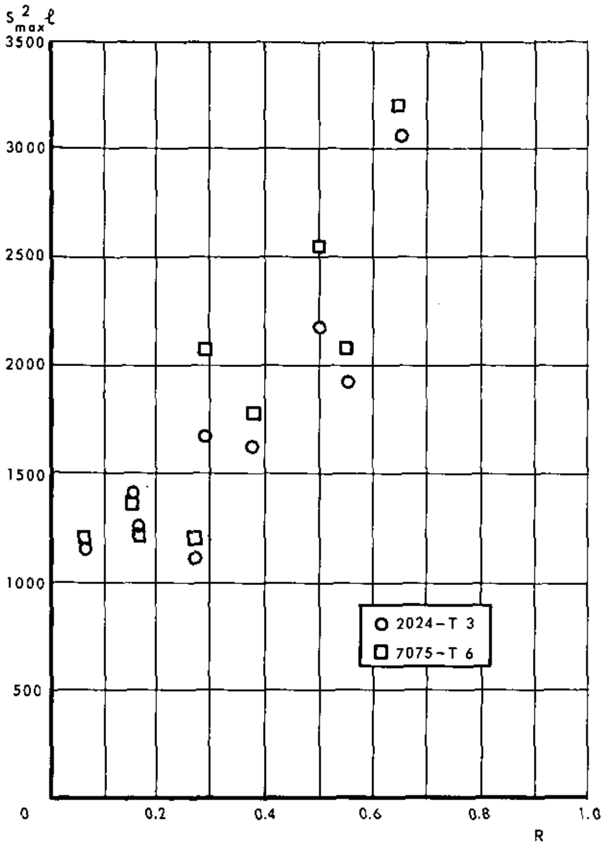

Fig. 27 $S^2_{max}\,l$ at the transition.

rotation occur at a constant value of $S_a^2 l$ since these figures apply to constant S_a-values and the transition does not occur at a constant l-value.

8 Conclusions

From an experimental investigation on the influence of the mean stress on the propagation of fatigue cracks in light alloy sheet and a discussion on crack-propagation theories, the following conclusions may be drawn.

1. The influence of the mean stress is evident, but rather complicated. The test-results suggest a relation between crack rate and stresses of the form:

$$\frac{dl}{dn} = C_1 e^{-C_2 R} S^3_{max} l^{\frac{3}{2}} \left(1 + 10\,\frac{l^2}{w^2}\right)$$

in which

$$R = \frac{S_m - S_a}{S_m + S_a} \quad \text{and} \quad S_{max} = S_m + S_a\,.$$

This relation holds both for 2024 and 7075 material.

2. The crack rate in the 7075 material was about 3 to 4 times as large as in the 2024 material under the same conditions (as for geometry and stress).
3. For sheet materials of the same type of alloy (i.e. similar chemical composition) the crack rate depends on the ductility of the material and is higher for a lower ductility.
4. The application of the stress intensity factor to predict crack rate data for design problems requires further research.
5. The transition of the fatigue crack appears to occur at a constant crack-rate, independent of mean stress and stress amplitude.

9 References

[1] Schijve, J., Broek, D., de Rijk, P., The effect of the frequency of an alternating load on the crack rate in a light alloy sheet. N.L.R. report M. 2092, Sept. 1961.

[2] Schijve, J., Fatigue crack propagation in light alloy sheet material and structures. Advances in Aeronautical Sciences. Vol. 3, pp. 387–408. Pergamon Press Ltd., 1961. Also N.L.R. rep. MP. 195, Aug. 1960.

[3] Schijve, J., Broek, D., de Rijk, P., Fatigue-crack propagation under variable-amplitude loading. N.L.R.-report M. 2094, Dec. 1961.

[4] Schijve, J., Broek, D., Crack-propagation under variable amplitude loading. Aircraft Engineering, Vol. 34, (Nov. 1962) pp. 314–316. Also N.L.R. rep. MP. 208, Dec. 1961.

[5] McEvily, A. J., Illg, W., The rate of fatigue-crack propagation in two aluminum alloys. NACA TN 4394, Sept. 1958.

[6] Weibull, W., Effect of crack length and stress amplitude on growth of fatigue cracks. FFA Rep. 65, May 1956.

[7] Weibull, W., Size effects on fatigue-crack initiation and propagation in aluminium sheet specimens subjected to stresses of nearly constant amplitude. FFA Rep. 86, June 1960.

[8] Raithby, K. D., Bebb, M. E., Propagation of fatigue cracks in wide unstiffened aluminium alloy sheets. R.A.E. TN Structures 305, Sept. 1961.

[9] Roberts, R. G., An experimental investigation into the crack propagation characteristics of sheet materials used in aircraft construction. Bristol Aircraft Ltd. Rep. 2/335/1, Nov. 1960.

[10] Donaldson, D. R., Anderson, W. E., Crack propagation behaviour of some airframe materials. Proceedings of the crack propagation symposium, Cranfield, 1961. Vol. II, pp. 375–441.

[11] Liu, H. W., Fatigue-crack propagation and applied stress range. An energy-approach-ASME paper No. 62-Met-2, 1962.

[12] Paris, P. C., The growth of fatigue cracks due to variations in load. Doctor Thesis, Lehigh University, 1962.

[13] Frost, N. E., Dugdale, D. S., The propagation of fatigue cracks in sheet specimens. Journal of the Mechanics and Physics of Solids. Vol. 6, 1958, pp. 92–110.

[14] Liu, H. W., Crack propagation in thin metal sheet under repeated loading. Journal of Basic Engng., Trans. ASME, Series D, Vol. 83, 1961, pp. 23–31.

[15] Head, A. K., The growth of fatigue cracks. Report A.R.L./Met 5, Melbourne, July 1954.

[16] Weibull, W., The propagation of fatigue cracks in light alloy plates. SAAB TN 25. January 1954.

[17] Paris, P. C., Gomez, M. P., Anderson, W. E., A rational analytic theory of fatigue. The Trend in Engineering. Vol. 13, 1961, pp. 9–14.

[18] Paris, P. C., Erdogan, F., A critical analysis of crack propagation laws. ASME paper 62-WA-234, 1962.

[19] Sneddon, I. N., The distribution of stress in the neighbourhood of a crack in an elastic solid. Proc. of the Royal Soc. of London, Series A, Vol. 187, 1946, pp. 229–260.

[20] Frost, N. E., Effect of mean stress on the rate of growth of fatigue cracks in sheet materials. Journal Mechanical Engineering Science, Vol. 4, 1962, pp. 22–35.

[21] Barrois, W., Etude documentaire critique sur la propagation

des fissures de fatigue. Paper presented at the 14th Meeting of the AGARD Structures and Materials Panel, Paris 3–10 July 1962.

[22] VALLURI, S. R., A unified engineering theory of high stress level fatigue. Aerospace Engineering, Vol. 20, 1961, p. 10.

[23] HUDSON, C. M., HARDRATH, H. F., Effects of changing stress amplitude on the rate of fatigue-crack propagation in two aluminum alloys. NASA TN-D-960, Sept. 1961.

[24] BAHAR, L. Y., BEER, F. P., ERDOGAN, F., PARIS, P. C., SIT, G. C., TUNCEL, O., Fracture mechanics research at Lehigh University, 1960–'61. Inst. of research, Lehigh Un., Bethlehem, Penns. Paper D-6-7960, 1962.

[25] WESTERGAARD, H. M., Bearing pressure and cracks. Journal of Applied Mechanics. Trans. ASME, Vol. 61, 1939, pp. A 49–53.

[26] BROEK, D., DE RIJK, P., SEVENHUYSEN, P. J., The transition of fatigue cracks in alclad sheet. N.L.R. report TN-M. 2100, Febr. 1962.

[27] LIU, H. W., Discussion in Proceedings of the Crack-Propagation Symposium, Cranfield 1961. Vol. II, pp. 514–517.

[28] HARPUR, N. F., Material selection for crack resistance. Proc. of the Crack Propagation Symposium, Cranfield 1961. Vol. II, pp. 442–466.

C.C.L. Class. G 042

REPORT NLR-TR M.2129

The effect of sheet thickness on the fatigue-crack propagation in 2024-T3 Alclad sheet material

by

D. BROEK and J. SCHIJVE

Summary

The influence of the sheet thickness on fatigue-crack propagation was studied on specimens of 2024-T3 alclad sheet of five thicknesses, viz. 0.6, 1, 2, 3 and 4 mm. It turned out that cracks grow faster in thicker sheets.

The different states of stress at the crack tip probably cause the thickness effect. The transition from the tensile mode fatigue fracture to the shear mode fatigue fracture and its relation with crack propagation are also discussed.

Contents

List of symbols

C	— constant
$2l$	— length of crack from tip to tip (mm)
l_{tr}	— crack length (mm) at the transition from tensile mode to shear mode of fracture
n	— number of cycles
n_y–n_x	— number of cycles to extend the crack from $l=x$ mm to $l=y$ mm
dl/dn	— rate of crack propagation (mm/kc; 1 kc=1000 cycles)
p	— width of plastic zone at tip of crack (mm)
S	— stress (kg/mm^2)
S_a	— stress amplitude
S_m	— mean stress
S_u	— ultimate tensile strength
S_y	— yield stress
$S_{0.2}$	— 0.2% yield strength
t	— sheet thickness (mm)
$2w$	— sheet width (mm)
δ	— elongation (% of 2″ gage length)
S_{max}	— S_m+S_a

This investigation has been performed under contract with the Netherlands Aircraft Development Board (N.I.V.).

1 Introduction

In recent years fatigue-crack propagation in aircraft sheet materials has drawn more and more attention. Although a fairly large amount of crack propagation data has become available there is still a lack of systematical data on the effect of different parameters influencing the crack-propagation rate. One of these parameters is the thickness of the sheet. Since the static residual strength of cracked sheets depends upon sheet thickness, it might be expected that also the rate of crack propagation under alternating load should be affected by the sheet thickness.

The aim of this investigation was to study by experiments whether such an influence exists and to determine its magnitude. Five values of the sheet thickness were investigated in test series on 2024-T3 alclad sheet. It turned out that crack propagation is faster in sheets with larger thickness.

In this report the test results are given and discussed. It is tried to give a qualitative explanation for the trends revealed by the experiments. Some fractographical observations are an essential part of the explanations and conclusions.

2 Experimental details

2.1 *Material tested*

The material tested was 2024-T3 alclad sheet. Five different sheet thicknesses were investigated, viz. $t=$ 0.6, 1, 2, 3 and 4 mm. The static properties of the sheets are given in the table 1. The table gives average results of four tests except for the 3 and 4 mm gauges where only two static specimens were employed.

TABLE 1

Static properties of sheets

Sheet thickness t		$S_{0.2}$		S_u		δ
mm	inch	kg/mm²	ksi	kg/mm²	ksi	% of 2″ gage length
0.6	0.024	35.9	51.1	46.0	65.5	16
1	0.04	36.8	52.3	47.2	67.1	16.5
2	0.08	37.0	52.6	48.0	68.3	18
3	0.12	37.7	53.6	48.1	68.4	18.5
4	0.16	40.4	57.4	49.3	70.1	17

The 2 mm sheet material was the same as that used in a previous investigation on the influence of the mean stress on crack propagation (ref. 1).

2.2 *Specimens and testing technique*

The specimens were cut to a size of 100 × 280 mm and provided with a sharp central notch as shown in fig. 1. The notch consisted of a drilled hole of 1 mm diameter and two saw cuts of 1 mm length and 0.3 mm width made by means of a jeweller's fret saw.

Fine line markings inscribed in the surface of the specimen at spacings as indicated in fig. 1 facilitated recording of the crack growth.

Crack growth records were made by counting the number of cycles applied each time the tips of the crack had grown to the successive line markings.

The specimens were loaded in tension in a horizontal Schenck pulsator type PP6D of six tons capacity. The machine can be equipped with either a 2-tons or a 6-tons dynamometer. For part of the tests (on specimens of 0.6 mm and 1 mm thickness) the 2-tons dynamometer was used in view of the low loads involved.

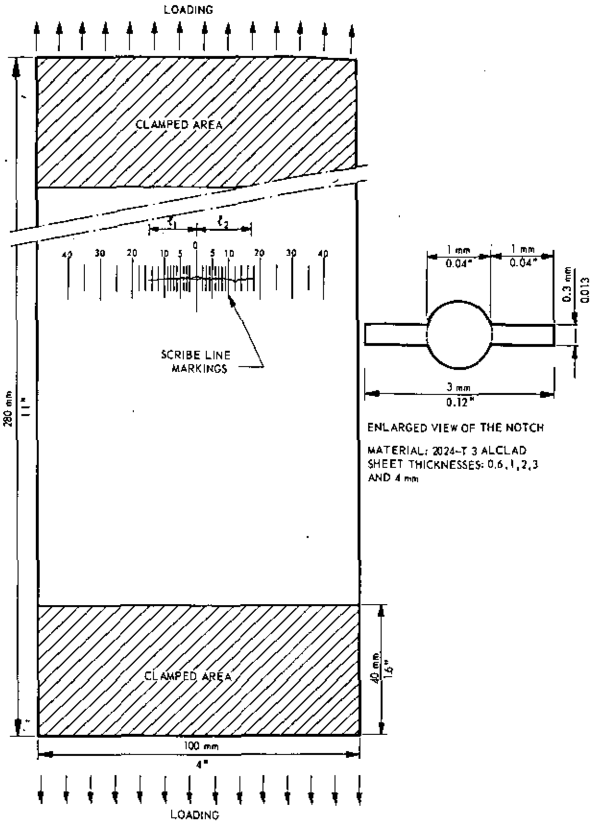

Fig. 1 Dimensions of sheet specimens.

The fatigue machine is of the resonance type (mechanical excitation) and loading frequency depends slightly upon specimen thickness and stress amplitude. The frequency was between 1700 and 2300 cycles per minute.

2.3 *Stresses*

All tests were performed at a positive mean stress $S_m = 8$ kg/mm² (11,400 psi). Three values of the alternating stress were used, viz. $S_a = 2.5$ kg/mm², 4 kg/mm² and 6.5 kg/mm² (3,570 psi, 5,690 and 9,250 psi respectively). All stresses are based on the specimen gross section disregarding the notch and the crack.

TABLE 2

Loading frequencies

Sheet thickness		Frequency (c.p.m.) at		
mm	inch	$S_a =$ 2.5 kg/mm² (3,570 psi)	$S_a =$ 4 kg/mm² (5,690 psi)	$S_a =$ 6.5 kg/mm² (9,250 psi)
0.6	0.024	1700	1800	1900
1	0.04	2050	2100	2150
2	0.08	2100	2150	2200
3	0.12	2150	2200	2250
4	0.16	2200	2250	2275

Both the mean load and the load amplitude were kept constant throughout a test. At each stress amplitude three tests were carried out for the five sheet thicknesses, leading to a number of $3 \times 3 \times 5 = 45$ tests.

Nominal values of the loading frequency are given in table 2.

3 Test results

Crack-propagation records were started as the crack had reached a length of 3 mm. So the influences of the notch on crack initiation and the early crack-propagation were eliminated. The crack length is defined as the average value of l_1 and l_2, see fig. 1. There is no objection against this procedure since all cracks grew almost perfectly symmetrically.

The crack-propagation data thus obtained are given in tables 3 through 5. The tables show that scatter was low. Therefore only the average results of three similar tests were plotted for drawing the crack-propagation curves in figs. 2–4.

From the average results in tables 3–5 for each group of three tests the crack rate dl/dn was calculated as a linear average between two successive l-values indicated in the table:

$$\frac{dl}{dn} = \frac{l_{i+1} - l_i}{n_{i+1} - n_i}.$$

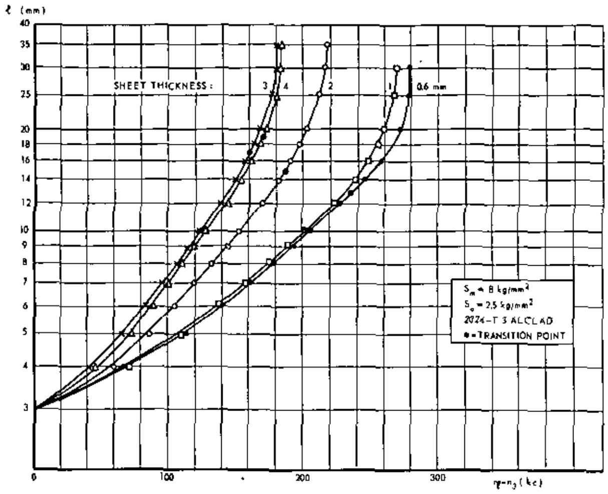

Fig. 2 Influence of the sheet thickness on the crack propagation ($S_a = 2.5$ kg/mm²).

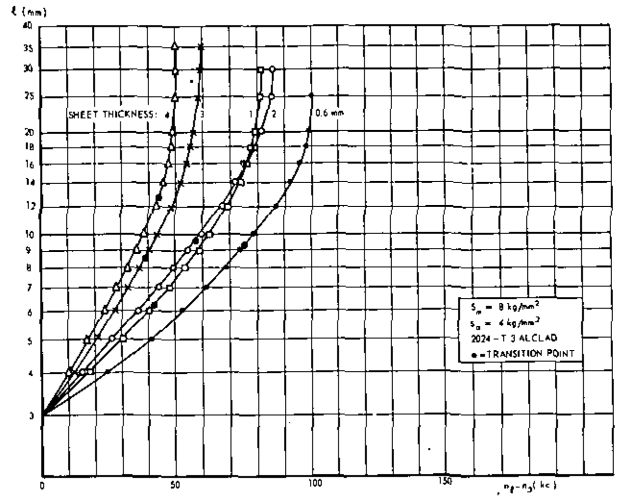

Fig. 3 Influence of the sheet thickness on the crack propagation ($S_a = 4$ kg/mm²).

TABLE 3

Crack propagation records

Figures in table represent number of kilocycles necessary to extend the crack from $l = 3$ mm to a length l mm

$S_m = 8$ kg/mm²; $S_a = 2.5$ kg/mm²

	0.6 mm thickness			1 mm thickness			2 mm thickness			3 mm thickness			4 mm thickness		
Spec. no. / l(mm)	B32	B38	B27	B52	B59	B45	B21	B17	B4	4	7	9	3	5	7
3	0	0	0	0	0	0	0	0	0	0	0	0	0	0	0
4	71.00	79.40	69.00	71.00	81.75	57.05	62.75	58.75	60.75	35.80	27.80	53.00	64.45	36.05	45.05
5	118.50	123.15	102.60	110.50	129.75	85.85	89.50	85.45	78.10	60.10	51.75	79.65	92.50	59.95	67.85
6	139.35	149.85	127.00	144.75	161.25	109.65	107.45	104.80	99.75	74.90	171.00	98.10	108.30	70.35	81.50
7	160.15	174.15	147.00	167.25	183.50	123.80	124.70	119.00	116.00	86.55	182.30	113.80	119.85	90.75	92.35
8	169.10	191.50	165.20	186.30	202.25	139.70	137.65	134.30	125.40	97.45	192.90	124.95	132.30	98.60	100.80
9	192.55	211.05	182.70	204.85	215.00	152.25	148.70	145.10	138.85	106.65	203.15	137.75	139.75	108.55	108.55
10	203.20	222.45	192.10	218.40	226.25	161.80	156.65	154.60	149.05	115.65	209.55	144.35	143.95	119.65	116.00
12	219.55	248.30	212.75	239.75	246.00	179.20	172.70	171.45	162.45	129.95	125.05	160.05	162.00	136.10	130.90
14	235.75	265.10	228.40	257.65	260.75	192.60	187.35	183.05	174.65	138.70	134.60	174.05	172.80	146.80	139.80
16	249.95	277.55	241.60	270.30	271.00	200.10	197.95	193.50	184.05	146.75	142.25	184.15	181.75	155.00	148.25
18	258.85	288.15	251.05	280.35	276.00	205.05	205.25	200.10	189.10	152.20	148.80	190.35	189.80	162.45	152.95
20	264.90	294.95	256.70	287.30	279.90	209.70	212.60	206.10	192.75	156.70	153.65	195.15	195.20	167.55	155.60
25	269.95	300.55	261.20	295.30	287.75	216.55	220.50	216.00	203.55	164.00	161.30	204.15	202.35	173.60	160.95
30	271.00	401.70	262.10	298.15	288.50	218.25	224.60	220.00	206.55	166.75	164.25	207.50	205.00	175.75	163.60
35				298.45			225.90	221.40		167.60	165.15	208.40	205.80	176.55	164.25

TABLE 4

Crack propagation records

Figures in table represent number of kilocycles necessary to extend the crack from $l = 3$ mm to a length l mm.

$S_m = 8$ kg/mm^2; $S_a = 4$ kg/mm^2

	0.6 mm thickness			1 mm thickness			2 mm thickness			3 mm thickness			4 mm thickness		
Spec. no. / l (mm)	B38	B29	B43	B58	B47	B65	B6	B11	B18	5	2	12	9	2	4
3	0	0	0	0	0	0	0	0	0	0	0	0	0	0	0
4	25.60	20.35	26.20	18.60	15.65	17.95	13.85	15.95	13.85	12.30	10.20	14.25	10.40	10.90	9.05
5	39.90	38.55	44.30	31.85	27.35	29.40	23.95	28.95	25.50	20.95	18.35	23.70	16.35	18.80	16.30
6	52.85	47.10	55.35	40.25	34.75	41.35	31.70	40.65	34.35	26.65	25.55	30.45	21.50	24.80	23.05
7	61.85	52.40	66.35	49.45	40.85	50.20	40.00	49.85	39.70	32.50	29.65	34.90	29.35	27.60	27.45
8	69.55	59.45	73.20	54.95	46.70	57.65	46.25	57.05	45.90	37.35	33.60	39.80	34.35	31.15	31.95
9	74.80	64.70	79.80	59.40	51.10	63.20	50.60	63.60	51.25	41.00	37.25	43.55	37.85	34.35	35.25
10	81.35	68.80	84.55	63.80	54.35	67.40	54.35	69.25	55.75	44.00	40.20	46.05	39.60	36.60	38.45
12	88.75	77.15	92.15	70.20	59.75	75.00	62.50	76.60	63.95	49.30	44.25	51.30	43.05	41.05	42.30
14	93.60	81.75	97.10	74.50	64.10	79.75	68.95	82.60	69.60	52.90	48.10	54.30	45.25	44.65	45.00
16	97.25	85.40	100.90	77.35	67.15	83.45	71.20	86.30	73.85	55.65	50.65	56.90	47.05	46.50	47.70
18	99.70	87.50	103.00	79.35	69.20	85.70	72.95	89.60	76.75	57.40	52.10	58.65	48.05	47.60	48.65
20	100.70	88.55	104.25	80.70	70.30	87.20	74.95	92.55	79.05	58.65	53.15	59.85	48.80	48.40	49.35
25	101.50	89.20	105.20	82.40	71.75	89.00	76.85	97.15	82.05	60.45	54.55	61.35	49.80	49.40	50.35
30				83.10	72.15	89.30	77.65	98.65	82.90	61.05	55.05	61.95	50.20	49.90	50.85
35								99.50	83.10	61.30	55.20	62.25	50.30	50.10	50.95

TABLE 5

Crack propagation records

Figures in table represent number of kilocycles necessary to extend the crack from l=3 mm to a length l mm

$S_m = 8$ kg/mm^2; $S_a = 6.5$ kg/mm^2

	0.6 mm thickness			1 mm thickness			2 mm thickness			3 mm thickness			4 mm thickness		
Spec. no. / l (mm)	B34	B41	B44	B54	B61	B66	B1	B23	B68	1	10	8	6	8	1
3	0	0	0	0	0	0	0	0	0	0	0	0	0	0	0
4	9.20	10.40	10.85	7.05	6.90	6.85	4.40	4.65	5.35	3.20	3.35	4.05	3.10	3.85	3.80
5	14.70	17.15	17.70	10.50	11.65	11.35	8.60	9.55	10.60	6.60	6.50	7.25	5.45	6.40	6.20
6	19.70	20.45	21.95	14.35	15.00	14.70	12.10	13.80	15.20	8.90	9.65	9.95	6.95	8.05	8.75
7	22.50	23.35	25.15	16.85	17.40	17.45	16.40	16.60	19.90	10.90	12.35	11.70	8.50	9.85	10.50
8	25.35	25.65	27.90	18.60	19.40	19.40	19.00	19.05	23.00	12.50	14.55	13.75	9.75	11.00	11.95
9	26.95	27.70	29.65	20.00	21.05	20.35	20.80	21.30	25.95	13.90	16.45	15.10	10.70	12.05	13.45
10	28.40	28.75	30.70	21.45	22.35	21.95	22.05	23.15	27.95	14.65	17.35	15.90	11.65	12.75	14.30
12	30.30	30.45	32.60	23.05	24.20	23.30		25.50	30.25	16.00	18.70	17.45	12.75	13.65	15.35
14	31.10	31.55	33.50	24.25	25.15	24.45		26.75	31.10	16.85	19.30	18.20	13.15	14.15	15.95
16	31.65	32.15	34.05	24.85	25.80	24.70		27.50	31.90	17.45	19.75	18.75	13.65	14.50	16.20
18	31.90	32.35	34.30	25.10	26.05	25.10		27.90	32.35	17.65	20.10	19.15	13.95	14.70	16.50
20	32.00	32.50	34.40	25.35	26.30	25.50		28.15	32.70	17.85	20.35	19.30	14.10	14.90	16.90
25				25.50	26.50			28.55	32.90	18.15	20.65	19.65	14.30	15.10	16.90
30													14.40	15.20	17.10

Crack rates so obtained are plotted in figs. 5–7 at a crack length $l = \frac{1}{2}(l_i + l_{i+1})$.

4 Discussion

4.1 *Influence of sheet thickness as found in the present and in other investigations*

Figs. 2–4 incl. show that there is a noticeable effect of sheet thickness. As a general trend cracks grow faster when the sheet is thicker.

The effect of sheet thickness as found in this investigation is confirmed by the work of Raithby and Bebb (ref. 2). Results of Raithby and Bebb on 1200 × 2400 mm (48 × 96 inch) specimens are given here in

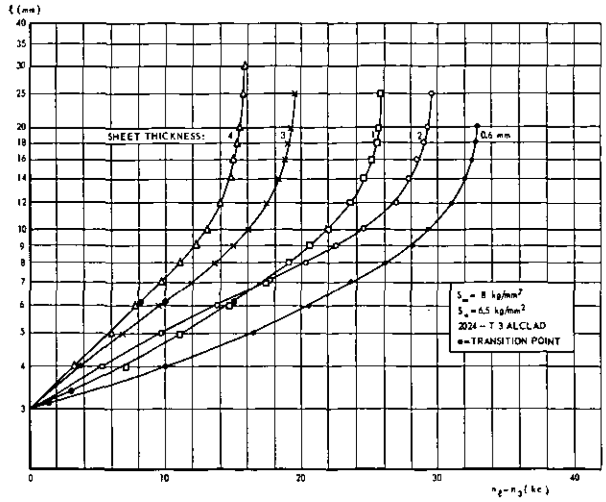

Fig. 4 Influence of the sheet thickness on the crack propagation ($S_a = 6.5$ kg/mm²).

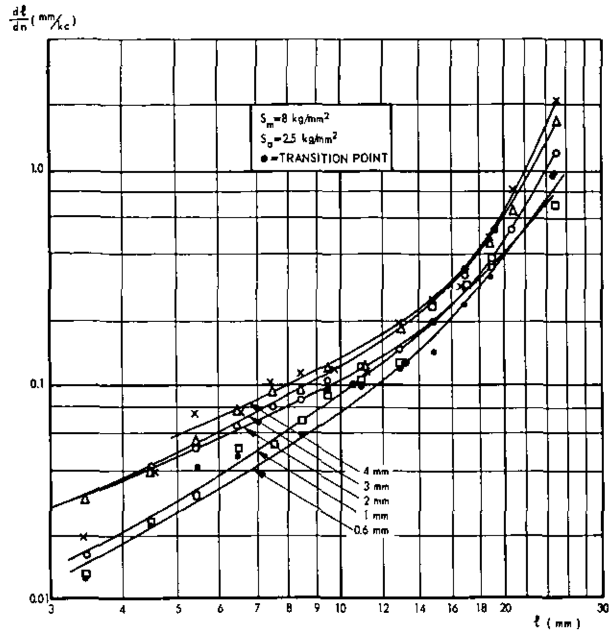

Fig. 5 The crack rate as a function of crack length.

table 6. Their crack-growth records are plotted in figs. 8–10. In these figures the early part of the crack propagation has been omitted (initial half length of the notch was 19 mm or 0.75 inch) in the same way as for the present results. The results of Raithby and Bebb in most cases show the same trends as found in the present test series, although there are a few exceptions.

Another systematical study on the influence of sheet thickness was published by Frost and Denton (ref. 3). This investigation was performed on mild steel specimens and no effect of sheet thickness was found from a comparison of three thicknesses viz. 3.2, 7.5 and 25 mm (0.128, 0.3 and 1 inch respectively). It is known that crack-propagation properties of mild steel show important differences with aluminium alloys. For example in ref. 1 a pronounced influence of the mean stress was found on crack propagation in two aluminium alloys. A similar trend was found by Frost (ref. 4) for different materials except for mild steel, which showed no influence of mean stress. The thicknesses of the sheets tested by Frost and Denton are relatively high as compared with those of the present test series. It may be that a thickness effect vanishes at these large thicknesses as will be discussed in the following section.

More systematic investigations on the influence of

TABLE 6

The effect of sheet thickness as found by Raithby and Bebb (ref. 2) compared with the present results

Material	S_m		S_a		Number of kilocycles for a crack extension of 30 mm[1]			
	ksi	kg/mm²	ksi	kg/mm²	thickness 0.04″ = 1 mm	thickness 0.08″ = 2 mm	thickness 0.16″ = 4 mm	Source
DTD 546	10	7	6	4.2	13.7	8.6	3.2	
(2024-T6	12	8.4	4	2.8	15.5	—	8.7	
artificially aged)	14	9.8	2	1.4	—	82	47	ref. 2
	14	9.8	4	2.8	13.9	9.6	—	
	14	9.8	6	4.2	8.3	4.1	—	
DTD 610	14	9.8	2	1.4	—	158	163 [2]	
(2024-T3	14	9.8	4	2.8	30	25	—	ref. 2
naturally aged)	14	9.8	6	4.2	10.8	12.8[2]	—	
DTD 687	14	9.8	2	1.4	—	16.5	21.3[2]	
(7075-T6	14	9.8	4	2.8	13.7	5.3	—	ref. 2
artificially aged)	14	9.8	6	4.2	1.8	0.3	—	
	11.4	8.0	3.6	2.5	375	328	300	Present
2024-T3	11.4	8.0	5.7	4.0	109	111 [2]	67	investi-
	11.4	8.0	9.3	6.5	32	35 [2]	21	gation

[1] $n_{50}-n_{20}$ for results of ref. 2; $n_{33}-n_3$ for the present results.

[2] Inconsistent results.

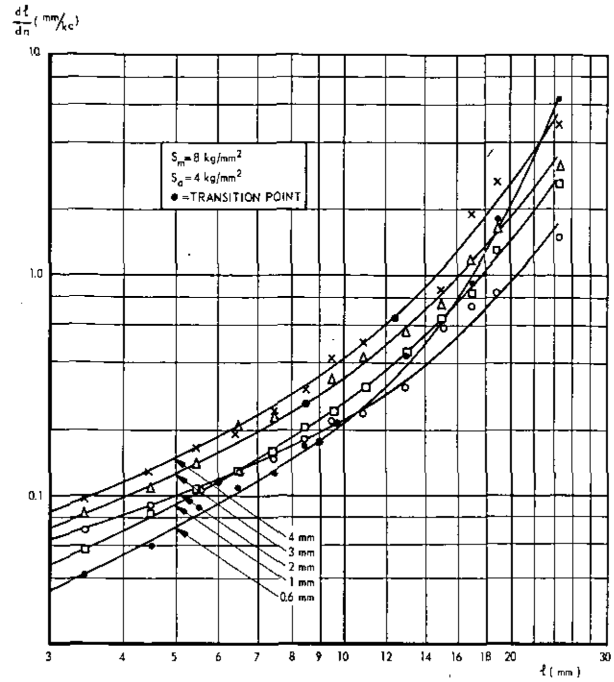

Fig. 6 The crack rate as a function of crack length.

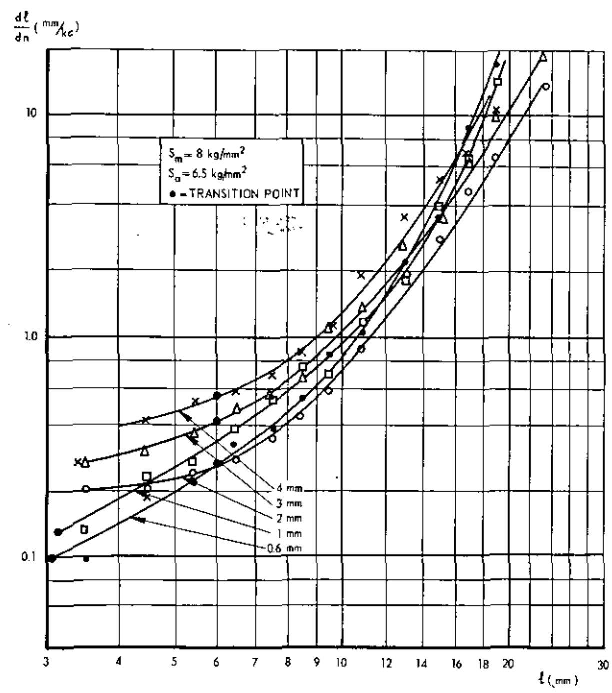

Fig. 7 The crack rate as a function of crack length.

sheet thickness could not be found. There are some incidental results in a review on crack propagation by Donaldson and Anderson (ref. 5). Based on the results collected they concluded that a thickness effect is completely absent. Reconsideration of these results, however, learns that the conclusion was mainly based on a comparison of crack-propagation records of specimens of different widths. This means that a thickness effect might have been obscured by the influence of sheet width. Donaldson and Anderson evaluated the results in terms of dl/dn as a function of the stress-intensity factor $K = S_a\sqrt{l}$ and made a correc-

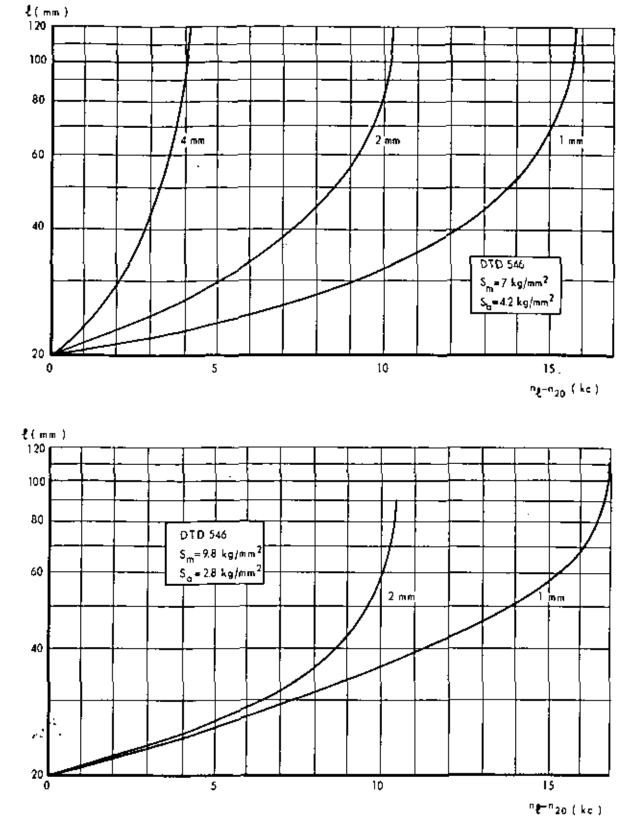

Fig. 8 Influence of sheet thickness as found by Raithby and Bebb (ref. 2) for the DTD 546 alloy (2024-T6; artificially aged).

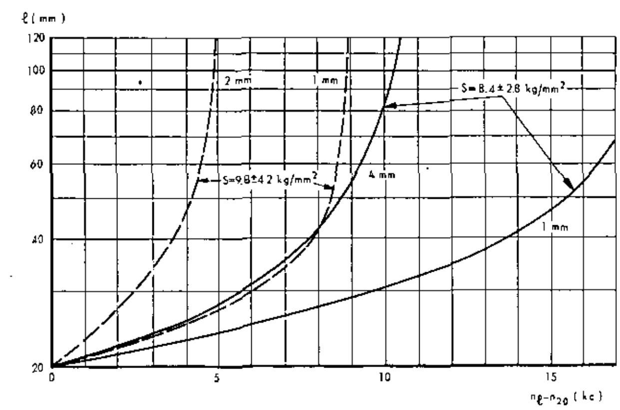

a) DTD 546 alloy (≈ 2024-T6, artificially aged)

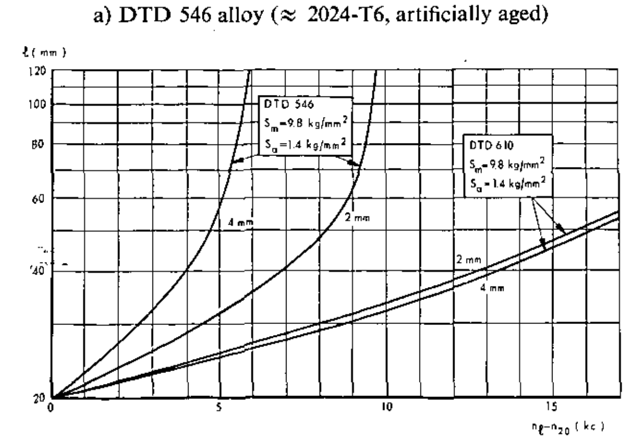

b) DTD 546 alloy and DTD 610 alloy (≈ 2024-T3, naturally aged)

Fig. 9 Influence of sheet thickness as found by Raithby and Bebb (ref. 2).

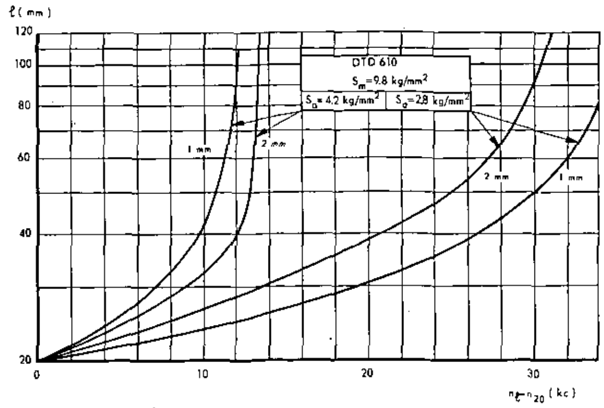

a) DTD 687 alloy (≈ 7075-T6; artificially aged)

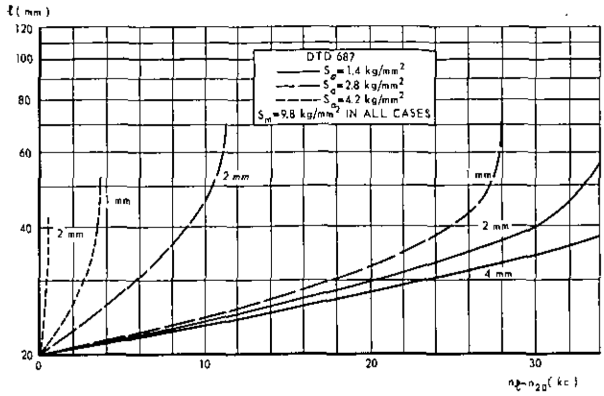

b) DTD 687 alloy (≈ 7075-T6; artificially aged)

Fig. 10 The influence of sheet thickness as found by Raithby and Bebb (ref. 2).

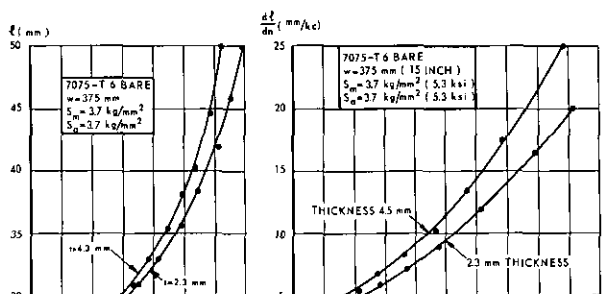

Fig. 11 Sheet thickness effect in 7075-T6 Bare (ref. 5).

tion for finite width w by multiplying K with a factor

$$\left(\frac{2w}{\pi l}\ tan\ \frac{\pi l}{2w}\right)^{\frac{1}{2}}$$

which should make the results of specimens of different widths comparable. Plots of K versus dl/dn generally show a wide scatterband and crack rate results for the same K-value may differ by a factor of 2. The scatter in the present investigation was low (compare in tables 3–5 the number of cycles necessary for a crack extension between two successive records) and consideration of figs. 5–7 learns that in a plot with such a relatively wide scatterband the thickness effect

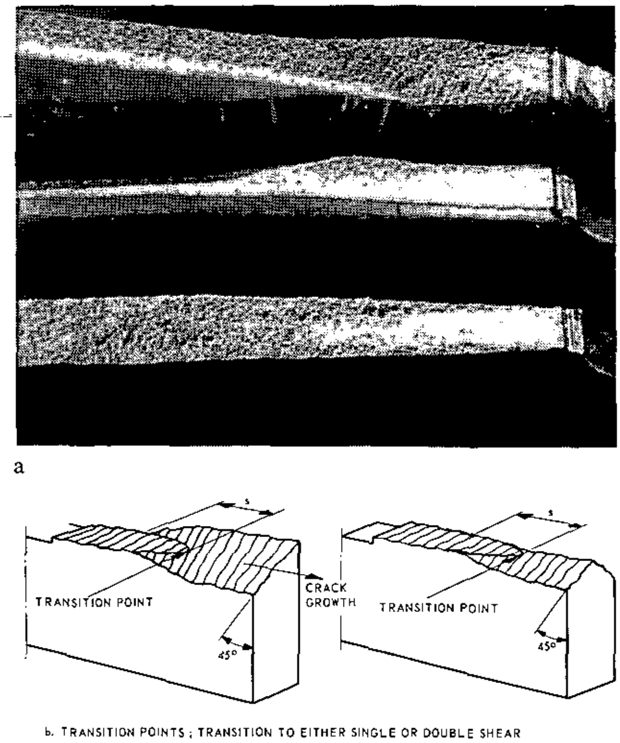

Fig. 12 The transition from the tensile mode to the shear mode.

may easily be obscured. There are two test series given by Donaldson and Anderson for which the effect of sheet thickness can be studied without confusion by other parameters. Tests on four sheet thicknesses of a Nickel alloy RENE 41 showed no systematical influence of sheet thickness. Two test records on 7075-T6 bare material are plotted here in fig. 11. From these tests a small but consistent thickness effect is apparent.

In conclusion it can be stated that for aluminium alloys there is an influence of sheet thickness leading to higher crack rates in sheet of larger thickness, whereas this conclusion need not necessarily apply to other materials.

4.2 *Transition of the fracture from the tensile mode to the shear mode*

The fracture surfaces of the specimens showed the usual characteristics. All cracks started in a plane *perpendicular to the loading direction*, which in the literature is called the tensile mode of the fatigue fracture. At high crack rates, however, the crack is *growing in a plane at 45° to both the loading direction* and the sheet surface, see fig. 12, which is called the shear mode. The transition from the tensile mode to the shear mode occurs *in a gradual way, starting with* shear lips at the two surfaces. When these lips cover half the sheet thickness the transition has been completed and the corresponding crack length is defining the "transition point", see fig. 12, a conception used in previous publications (refs. 1 and 6). If the shear lips do not occur in parallel planes and persist in this after the transition a double shear fracture is the result (see fig. 12). The single shear failure occurs more frequently than the double shear fracture.

In previous investigations (refs. 1, 6 and 7) the crack rate at the transition point was approximately constant. This trend is confirmed by the present results if a certain thickness is considered. Fig. 13 shows, however, that the crack rate at the transition point is a function of the sheet thickness, t, being larger for higher t-values. The values for $t=2$ mm, viz. 0.2 mm/kc is the same as found in refs. 1, 6 and 7 for the same material of that thickness.

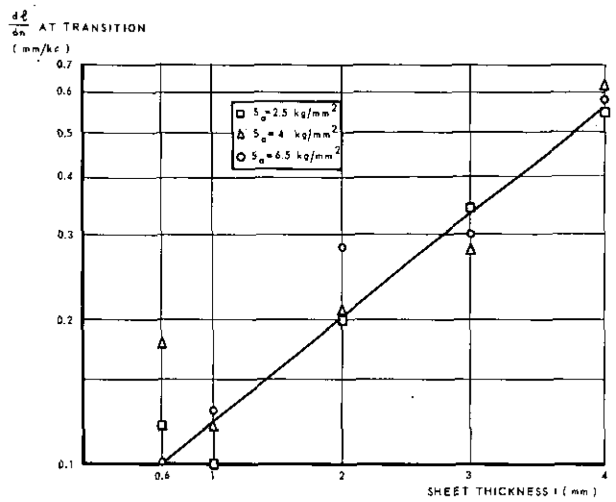

Fig. 13 The crack rate at the transition.

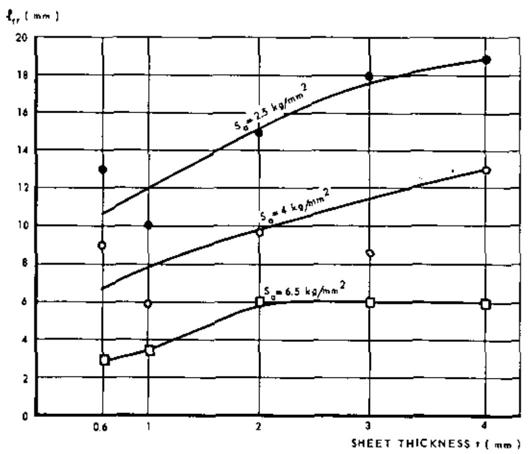

Fig. 14 Crack length at the transition point.

In fig. 14 the crack length l_{tr} at the transition point has been plotted as a function of the sheet thickness. It appears to depend upon sheet thickness. Average values of l_{tr} as determined from fig. 14 are $l_{tr}=5$ mm, 10 mm and 16 mm for stress amplitudes $S_a=6{,}5$ kg/mm^2, 4 kg/mm^2 and 2,5 kg/mm^2 respectively. With these average values of l_{tr} it was checked whether the effect of thickness on crack propagation is the same before and after the transition. This check has been carried out in fig. 15 by plotting the crack propagation life from $l=3$ mm to $l=l_{tr}$ and the crack propagation life from $l=l_{tr}$ to $l=30$ mm both as a function of the

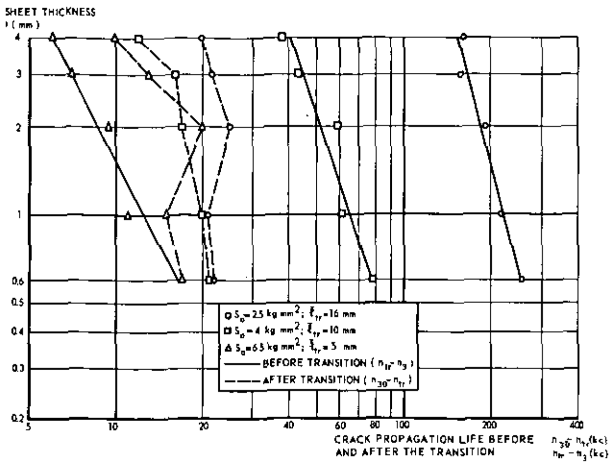

Fig. 15 The influence of sheet thickness on the crack propagation life before and after the transition.

sheet thickness. From fig. 15 it appears that the thickness effect is significant and systematical before the transition, i.e. the crack propagation life until a crack length l_{tr} decreases with increasing sheet thickness. The thickness effect is less pronounced and not systematical after the transition, i.e. the number of cycles to extend the crack from l_{tr} to a length of 30 mm is not systematically influenced by the sheet thickness. Although the results are not completely consistent it is tentatively concluded that a thickness effect exists for pre-transition cracks and that after the transition the influence of sheet thickness is not significant. The same conclusion can in fact be drawn from figs. 5, 6 and 7, which also show that the results after the transition are not fully systematical.

Some micrographs of the transition (fig. 16) show that the change in fracture direction is very abrupt. Also on a microscale the crack surface is almost perpendicular to the sheet surface in the pre-transition region whereas after the transition evidently the direction of the largest macro-shear stress is followed. The fracture path does not follow the slip line directions. In ref. 8 this is explained by the fact that in the interior of the specimen several slip systems are activated due to constraint by the surrounding material and hence the fracture may follow a path which is apparently uncorrelated with slip directions.

4.3 *Further considerations on the thickness effect and the transition phenomenon*

If the extent of the fatigue damage could be fully represented by the crack length l, i.e. by one dimension, one would not expect a thickness effect on the crack rate. Moreover l does not indicate whether the transition of the tensile mode to the shear mode fracture has occurred or not. It seems reasonable to assume that the transition and the effect of thickness on the crack rate are related phenomena. This is further analysed in this section. First it should be pointed out that the thick-

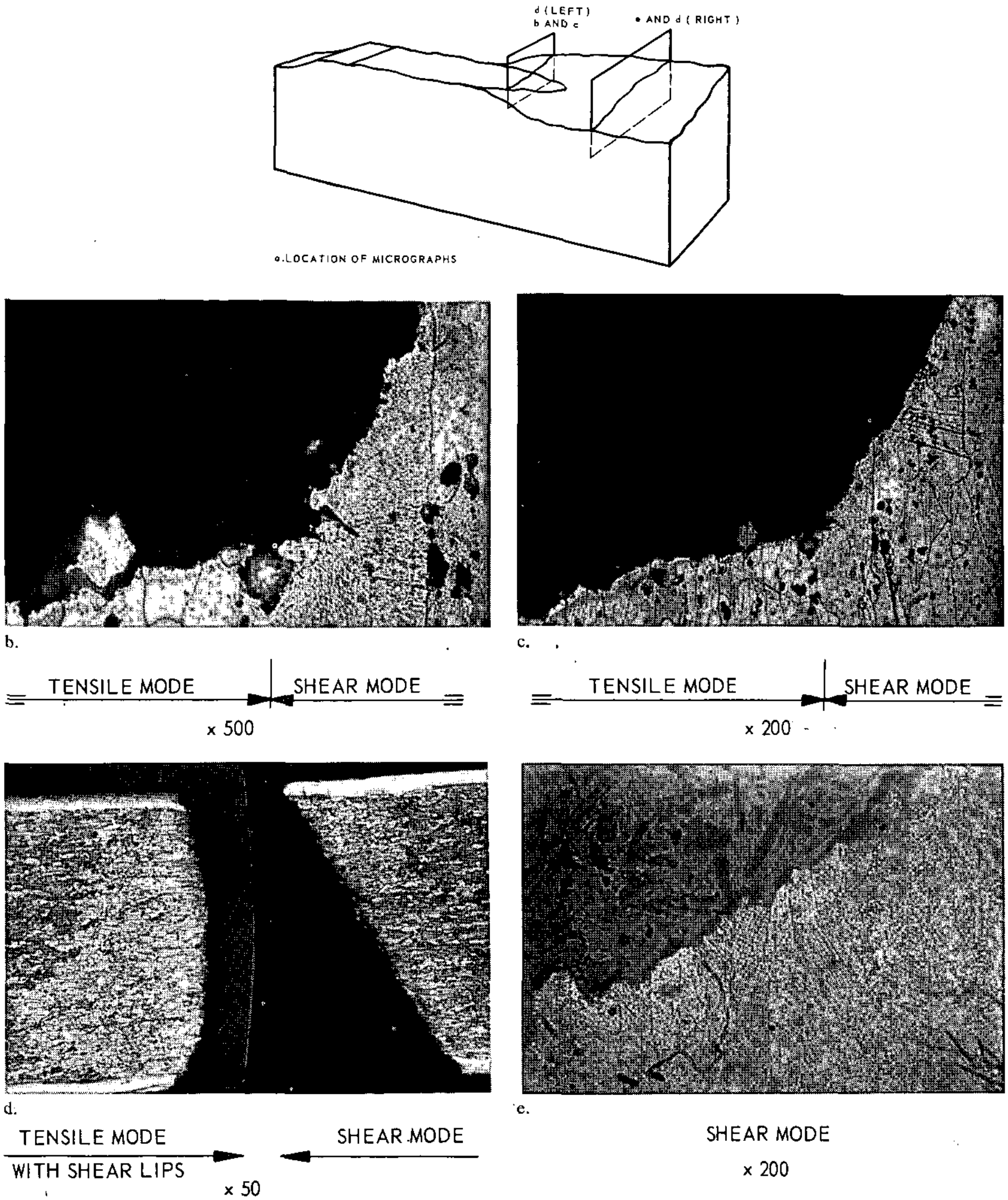

Fig. 16 The transition.

ness effect might be caused by differences of the material properties on testing conditions. The static properties presented in section 2.1 hardly allow an explanation of the thickness effect, since the thicker sheets, exhibiting the higher crack rates. Thinner have somewhat superior static properties than the thinner sheets, for both strength ($S_{0.2}$ and S_u) and elongation.

With respect to the testing conditions the only difference was the frequency which was slightly dependent on sheet thickness and stress amplitude, see section 2.3. The thicker sheets being tested at somewhat higher frequencies, showed the higher crack rates. However, the small frequency effect on crack propagation found in ref. 6, would predict the opposite trend. Consequently the thickness effect cannot be related to the loading frequencies.

It has been suggested by Liu (ref. 9) and Irwin (ref. 10) that the transition from the tensile mode to the shear mode has to be associated with a transition of the state of stress at the tip of the crack from plane strain to plane stress. This suggestion was further evaluated in ref. 8, employing shear stress distributions on slip planes through the tip of the crack. It was made plausible there that plane strain will promote the tensile mode and that plane stress will promote the shear mode. At the specimen surface the state of stress will obviously be one of plane stress. At the interior of the material around the tip of the crack there will be approximately a state of plane strain, the more so if the plastic zone is small. For an increasing size of this zone a change from plane strain to plane stress will occur in that region. The gradual development of the transition starting with shear lips at the free surface is a strong indication of a correlation of the shear mode fracture with plane stress. Such shear lips are not only found for large macrocracks since in ref. 8 they were found in unnotched 2024-T3 sheet specimens (bare material) for very small cracks (say $l < 1$ mm).

In the previous section it was concluded as a broad trend from the test results that the sheet thickness effect on the crack rate disappears after the transition has been completed, i.e. $l > l_{tr}$. Assuming that the plastic zone is then fully in a state of plane stress through the full thickness of the sheet this result seems to be plausible. Before the transition point has been reached the plastic zone at the specimen surfaces will be larger than at the interior of the sheet. This has been schematically indicated in fig. 17. Along the crack front there is a variation of the size of the plastic zone and of the state of stress. It is reasonable to assume that for a certain crack length and a certain stress amplitude (and mean stress) the change from approximately plane stress at the surface to approximately plane strain at the interior of the sheet will occur over a distance along the crack front which may be supposed to be independent of the sheet thickness. Consequently the central part of the crack front where the state of stress is one of plane strain will be larger

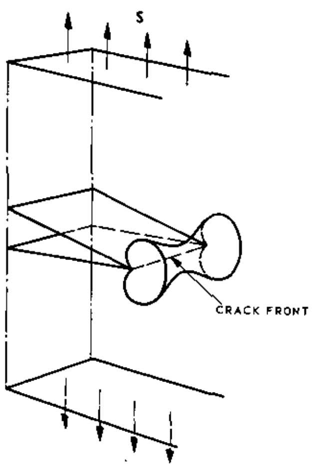

Fig. 17 Plastic zone at the tip of the crack.

for the thicker sheet. A sheet thickness effect on the crack rate then requires that a state of plane strain will induce a higher crack rate.

In ref. 8 starting from asymptotic solutions for the stress distribution around the tip of the crack and employing the Tresca yield criterion the following relations were obtained for the size of the plastic zone, p:

$$p = Cl\left(\frac{S}{S_y}\right)^2, \quad \begin{array}{l} C = 0.60 \text{ for plane stress} \\ C = 0.31 \text{ for plane strain} \end{array} \qquad (1)$$

In this relation S is the stress loading the specimen and S_y is the yield stress. The size of the plastic zone was defined by πp^2 = area of plastic zone. In view of plastic deformations occurring in the crack tip region the size and the shape of the plastic zone cannot accurately be calculated, but it is thought that eq. (1) based on the elastic stress distribution will still give a rough estimate of the size of the plastic zone. It is thought that the result of eq. (1), indicating that the plastic zone for plane strain will be approximately twice as small as for plane stress, will be approximately correct.

In ref. 8 crack growth was interpreted as a geometric consequence of dislocation movements in the crack tip region and it was pointed out that the efficiency of the conversion of slip into crack extension was dependent on the tensile stress "over the tip of the crack". In the case of plane strain the plastic zone is smaller than for plane stress as shown above. As a consequence the leveling-off of the stress peak at the tip of the crack will be less effective and although the shear stresses driving the dislocations are smaller for plane strain (see ref. 8) the former effect, i.e. the higher peak stress, could be the predominant factor explaining the thickness effect as found in the present investigation. This explanation obviously has a tentative character.

In ref. 9 Liu suggested that a state of plane stress along the whole crack front should be obtained if the size of the plastic zone, p, is equal to half the sheet thickness, t. If at the same time the transition would be completed this implies that $p = \frac{1}{2}t$ for $l = l_{tr}$, which can be checked with eq. (1) and the present test results. An alternative suggestion is that the transition will be completed when the shape of the plastic zone, which in fig. 17 is indicated as some sort of a hyperboloid has become fully cylindrical and that this will occur at a constant size of the plastic zone. With eq. (1) Liu's suggestion implies that

$$\frac{l_{tr}}{t}\left(\frac{S}{S_y}\right)^2$$

should be independent of the sheet thickness and the stress, whereas the latter suggestion implies that $l_{tr}(S/S_y)^2$ should be independent of these two variables. Both quantities have been plotted in fig. 18 as a function of t for $S = S_a$, $S = S_{max}$ and $S = S_{max}^{\frac{2}{3}} \cdot S_a^{\frac{1}{3}}$ respectively.

The latter S-value was derived from an empirical relation for the crack rate presented in ref. 1. Fig. 18 shows that an independence of the stress is neither obtained for $S=S_a$ nor for $S=S_{max}$ which is not an unexpected result, since both S_a and S_{max} will affect the amount of plastic deformation and the crack rate. For $S=S_{max}^{2/3}S_a^{1/3}$ both quantities plotted vertically in fig. 18 are approximately independent of S. It should be emphasized that this is an empirical result. Whether it could be obtained as a result of an analytical study would have to be further investigated. In figs. 18a and 18b the effect of sheet thickness is easily recognized, indicating that both Liu's suggestion and the one presented above oversimplify the actual situation. It could be said that the effect of sheet thickness is smaller in fig. 18b than in fig. 18a showing that the latter suggestion is somewhat better representing the plastic straining around the tip of the crack. It would be interesting to study this problem for a zero mean stress, since the correlation between the crack behaviour and the calculated stresses is apparently much more complex for a non-zero mean stress. This was clearly

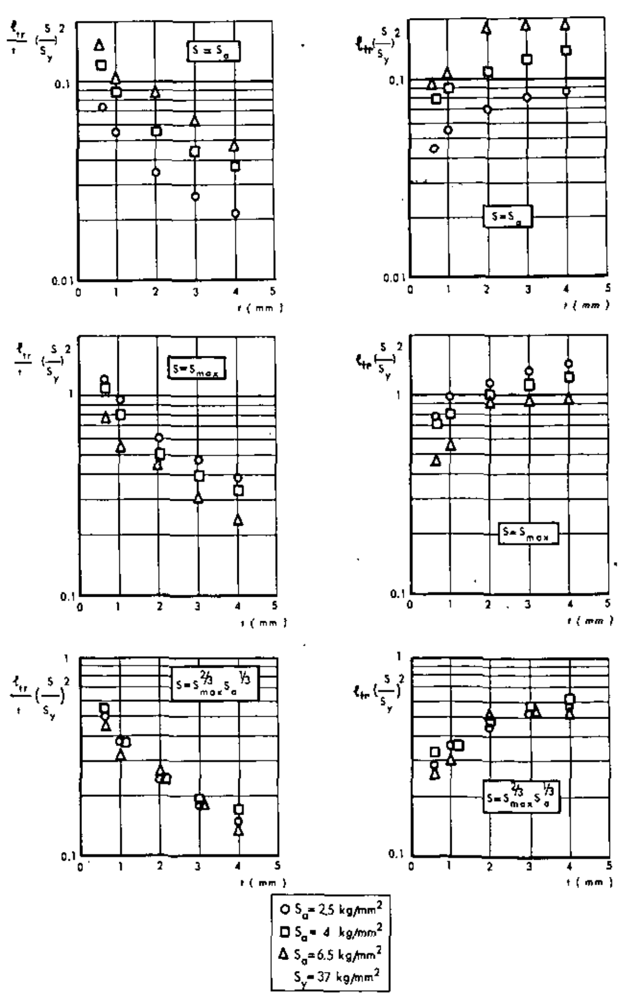

Fig. 18 Two functions for the transition point as affected by sheet thickness.
$\bigcirc S_a = 2.5$ kg/mm² $\quad \triangle S_a = 6.5$ kg/mm²
$\boxdot S_a = 4$ kg/mm² $\quad S_y = 37$ kg/mm²

illustrated in ref. 1 where it was tried to correlate the crack rate with the so-called stress intensity factor for crack propagation tests carried out at various mean stresses.

5 Conclusions

An experimental investigation on the influence of sheet thickness on the crack propagation in 2024-T3 alclad sheet leads to the following conclusions:

1. For the sheet thicknesses investigated (0.6, 1, 2, 3 and 4 mm) the crack propagation was faster in the thicker material, see figs. 2, 3 and 4.
2. Comparison with other investigations shows that the same is true for other aluminium alloys.
3. At a particular crack length the fracture surface shows a transition from the tensile mode to the shear mode. The crack length at which the transition was completed was larger for a lower stress amplitude and for a larger sheet thickness.
4. Indications were obtained that the effect of sheet thickness on the crack rate mainly occurred before the transition was completed. The effect was much smaller and unsystematical after the transition.
5. The thickness effects on the crack rate and the transition are supposed to be both correlated with the change of the state of stress from plane strain to plane stress when the crack length is increasing.

6 References

[1] Broek, D. and Schijve, J., The influence of the mean stress on the propagation of fatigue cracks in aluminium alloy sheet. N.L.R. report M. 2111, April 1963.

[2] Raithby, K. D. and Bebb, M. E., Propagation of fatigue cracks in wide unstiffened aluminium alloy sheets. R.A.E. T.N. No. Structures 305, Sept. 1961.

[3] Frost, N. E. and Denton, K., Effect of sheet thickness on the rate of growth of fatigue cracks in mild steel. Journal Mech. Engineering Science 3, 4, 1961; pp. 295–298.

[4] Frost, N. E., Effect of mean stress on the rate of growth of fatigue cracks in sheet materials. Journal Mech. Engineering Science 4, 1, 1962; pp. 22–35.

[5] Donaldson, D. R. and Anderson, W. E., Crack propagation behaviour of some airframe materials. Proc. of Crack Propagation Symposium. Cranfield, Sept. 1961, Vol. II.

[6] Schijve, J., Broek, D. and de Rijk, P., The effect of the frequency of an alternating load on the crack rate in a light alloy sheet. N.L.R. report TM. M. 2092, Sept. 1961.

[7] Broek, D., de Rijk, P. and Sevenhuysen, P. J., The transition of fatigue cracks in alclad sheet. N.L.R. report M. 2100, Febr. 1962.

[8] Schijve, J., Analysis of the fatigue phenomenon in aluminium alloys. N.L.R. Tech. Report M. 2122, April 1964.

[9] Liu, H. W., Discussion to a paper of W. Weibull in Proceedings of the Crack Propagation Symposium, Cranfield Sep. 1961, Vol. II pp. 514–517.

[10] Irwin, G. R., Fracture mode transition for a crack traversing a plate. Journal of Basic Engineering Trans. ASME 82 (1960) June, pp. 417–425.

C.C.L. Class. G 042

REPORT NLR-TR M. 2134

The effect of heat treatment on the propagation of fatigue cracks in light alloy sheet material

by

D. BROEK, J. SCHIJVE and A. NEDERVEEN

Summary

The effect was studied of artificial aging (up to and beyond maximum hardness, both with and without prior solution heat treatment) on the crack propagation in 2024-T3 alclad sheet. All heat treatments caused a noticeable increase of the rate of crack propagation, which was correlated with a decrease of ductility. The correlation is discussed and relevant data from the literature are summarized.
Some implications of the results for the curing cycle of adhesive bonding and for aerodynamic heating of structures are briefly indicated.

Contents

This investigation has been performed under contract with the Netherlands Aircraft Development Board (N.I.V.).

List of Symbols

kc	— kilocycle = 1000 cycles
$2l$	— crack length, see fig. 4
n	— number of load cycles
n_l	— number of load cycles to obtain a crack of length l
S_a	— stress amplitude
S_m	— mean stress
S_u	— ultimate stress
$S_{0\cdot2}$	— 0.2% yield stress
δ	— elongation after failure in static test

1 Introduction

For aluminium alloys used in aircraft structures the static properties are controlled by the type of heat treatment. Depending on the type of alloy the producer employs natural or artificial aging procedures. Heating of an aircraft structure may lead to unintentionally prolonged aging. For instance, adhesive bonding may involve a curing cycle of $\frac{1}{2}$–1 hour at a temperature of 150–200°C. Longer heating times at a lower temperature may occur due to aerodynamic heating during supersonic flight. At Mach 2, which is approximately the upper speed limit for an aluminium alloy structure, heating times of several thousands of hours at a temperature of say 130°C are to be considered. The effect of such additional aging treatments on the static properties and the fatigue limit at room and elevated temperatures have been published in the literature. However, little is known about the influence on crack propagation although such data are essential for judging fail-safe characteristics. Since artificial aging does affect the ductility of the material one might expect an influence on crack propagation rates. In the present investigation fatigue crack propagation tests were performed on 2024 sheet specimens subjected to various artificial aging treatments to explore their influences on growth rates of the cracks. Relevant data from the literature are summarized and some implications for the above mentioned problems are indicated.

2 The aging characteristics of the alloy tested

2.1 *Determination of the aging curves by hardness measurements*

From a sheet of 2024-T3 alclad material of 2 mm thickness (solution heat treated, cold rolled, naturally aged) 45 specimens were cut to a size of 20 × 30 mm. The specimen edges were ground with wet silicon carbide abrasive paper of grit size 600 and subsequently heat treated according to the following scheme.

specimen number	solution heat treatment	aging temperature
45	50 hours at 495°	room temperature (naturally aged)
1 through 17	50 hours at 495°	165°C
18 through 35	50 hours at 495°	195°C
36 through 44	none (as delivered condition)	195°C

Specimens 1 through 35 and 45 were solution heat-treated in an electrical air-circulation furnace and quenched in water. Specimens 1 through 35 were brought into the aging furnace (also electrical air-circulation) within 1 hour after quenching. The remaining specimens (36 through 44) were aged at 195°C without prior solution heat-treatment, i.e. the material in the naturally aged condition (T3) were further aged artificially.

When a specimen was taken from the aging furnace its edges were again lightly treated with wet 600 abrasive paper in order to remove excessive oxide layers, and immediately afterwards hardness measurements were carried out four times or more (room temperature) by means of a Vickers-micro-hardness

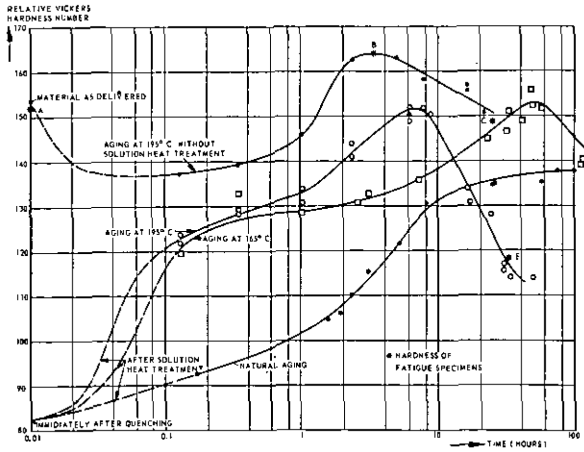

Fig. 1 Aging curves.

tester (Leitz manufacture) with a loading weight of 0.5 kg (1.1 lb). The measurements had to be carried out on the edges in view of the presence of the cladding layers.

Specimen 45 was aged at 20°C after quenching, and from time to time its hardness was determined until natural aging had continued for 100 hours.

The results of the hardness measurements are plotted in fig. 1. Each data point is the average result of at least four measurements. The aging curves are of a shape very similar to that of curves found in the literature (refs. 1, 2, 3).

2.2 *The microstructure of an aged 2024 alloy (refs. 1, 2 and 4)*

From the precipitation hardened aluminium alloys the binary Al-4% Cu has been most extensively investigated. It appears that the precipitation phenomenon in the 2024 alloy (Al-4.5% Cu-1.5% Mg) occurs in a similar way as in the Al-4% Cu alloy, since the precipitation also starts with coherent zones in the form of platelets. Also the aging curves show a great similarity with those of Al-4% Cu. A summary of the various phases of the precipitation for the latter alloy is given below.

After solution heat treatment and quenching an unstable super-saturated solution has been obtained, the copper being solved in the aluminium matrix. During subsequent aging at room temperature or artificial aging precipitation of the copper takes place. At moderate aging temperatures (i.e. below 160°C) the first precipitates to be found (by X-ray diffraction methods) are the Guinier-Preston zones type I, or G.P.I zones. G.P.I zones appear as segregates of copper atoms at the {100} planes. The zones are only one atom plane thick. By further aging they are replaced by regions, Guinier-Preston zones type II or G.P.II zones, with an ordered arrangement of copper and aluminium atoms which are a few unit cells thick.

The lattice of the Guinier-Preston zones, which have the form of platelets, remains continuous with that of

TABLE 1

Heat treatment of fatigue specimens and resulting static properties (averages of two tests)

Series	Heat treatment by NLR: Solution treatment time (hours)	Solution treatment temp (°C)	Aging time (hours)	Aging temp (°C)	0.2% yield stress $S_{0.2}$ kg/mm²	0.2% yield stress $S_{0.2}$ ksi	Ultimate tensile stress S_u kg/mm²	Ultimate tensile stress S_u ksi	elongation % of 2″ gauge length	Relative vickers Hardness*) (kg/mm²)	Type of precipitate (see Sect. 3.2)	Remarks
A	none, *material as delivered*		none		*37.5*	*58.5*	*48.3*	*69.0*	*18.5*	*154*	G.P.I *and* G.P.II	Condition T3
B	none		3.25	195	47.4	67.5	50.2	71.5	7.5	156	G.P.II	Critically aged
C	none		24	195	42.0	60.0	47.6	68.0	7	149	G.P.II and θ'	Overaged
D	50	495	6	195	40.0	57.0	46.9	67.0	9	151	G.P.II with some θ'	Critically aged
E	50	495	30	195	31.2	44.5	39.5	56.5	8	118	θ'	Overaged

*) hardness number obtained from fatigue specimens.

the matrix: the precipitate is coherent. Nevertheless, the two lattices do not fit perfectly, thus inducing elastic distortions of the lattice of the matrix. These coherency strains, involving coherency stresses are considered to be mainly responsible for the hardening of the alloy. The coherency stresses between the matrix and the precipitate increase as the precipitate grows, which will finally lead to a partial breaking away. This facilitates structural rearrangements within the precipitate to a more stable form called θ', which is semi-coherent with the matrix. The phase θ' is the forerunner of the equilibrium precipitate θ ($CuAl_2$) which forms during still further aging. θ is non-coherent, i.e. it is actually the second phase. At high aging temperatures precipitation may start with the immediate formation of G.P.II or θ'.

In general during natural aging only Guinier-Preston zones are formed, whereas during artificial aging the maximum hardness is attained in the presence of both G.P.II and θ'. The θ particles, which are visible through the optical microscope, are found only after extensive aging at high temperature, when on the aging curve the hardness has passed its peak value and is decreasing as a function of aging time (over-aging).

3 Heat treatment of the fatigue specimens

3.1 *Processing and resulting properties*

All specimens were cut from sheets in the T-3 condition, as delivered by the manufacturer. Series A was tested in this condition, while series B to E were given a second heat treatment by the NLR, involving artificial aging at 195°C. Series D and E were solution heat-treated before this aging, whereas series B and C were not. Artificial aging occurred to maximum hardness (critically aged) for series B and D and to an overaged condition for series C and E. Aging times and temperatures are specified in table 1 which also gives the resulting static properties. Hardness values obtained from the fatigue specimens and plotted in fig. 1 are in good agreement with the aging curves presented in section 2.1.

It appears from table 1 that the heat treatment has about the same effect on the tensile strength as it has on hardness values; i.e. the ultimate tensile strength is high for the critically aged condition and drops off at over-aging. As compared with the material as delivered all heat treatments result in an important drop of ductility and in all cases the ratio between yield strength and tensile strength is higher than for the T-3 condition.

3.2 *The microstructure of the specimens*

With the optical microscope it is virtually impossible to reveal G.P. zones or θ'. In general, it is difficult to examine aluminium alloys in the aged condition with the optical microscope. Fig. 2 shows the structures of static tests specimens after they had been loaded to failure. Slip lines are easily recognized. Although the

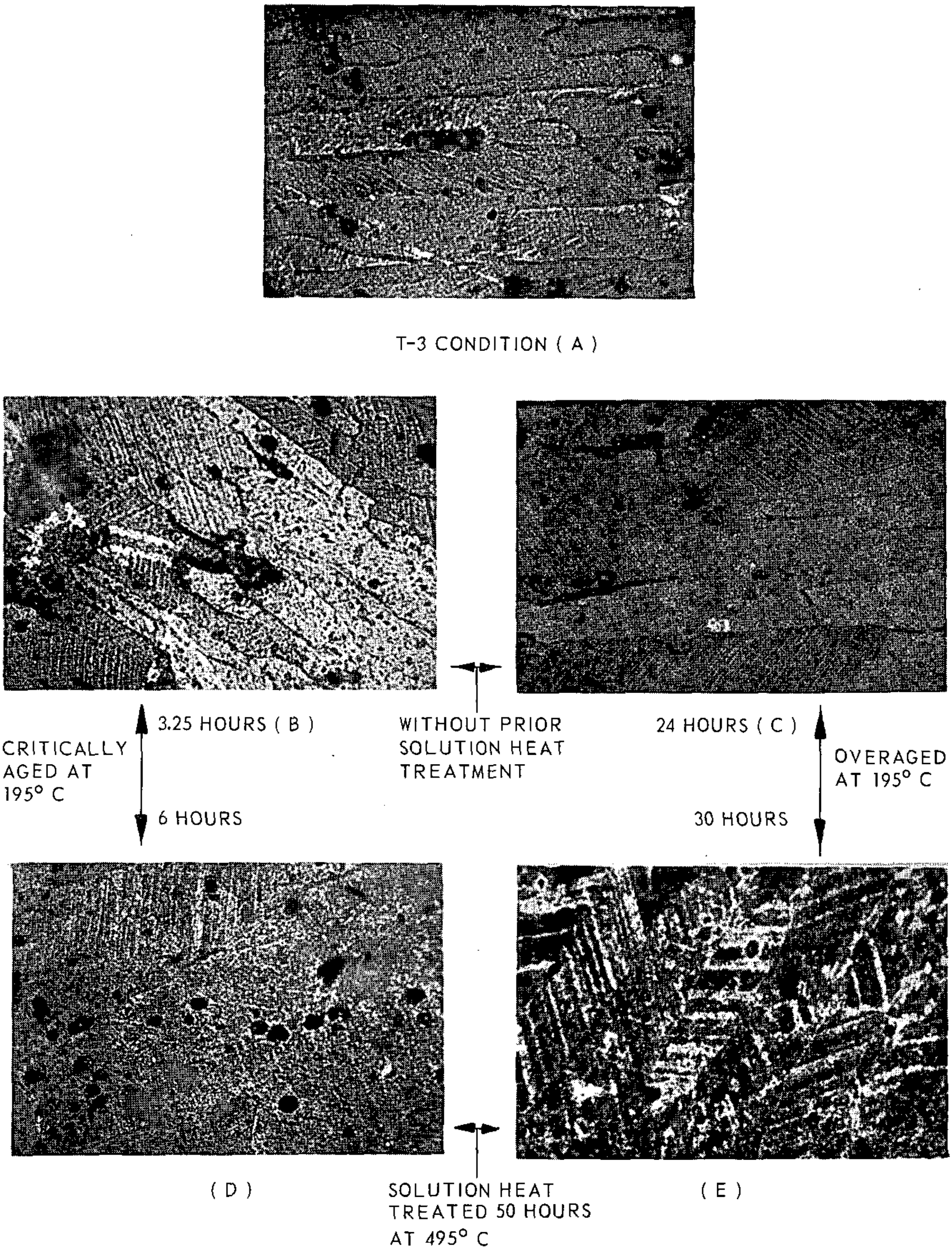

Fig. 2 Static test specimens after testing; etched, 500 ×.

information to be drawn from the micrographs is limited, a certain similarity of the structures of series A and B can be noted. The same applies to the structures of series C and D, whereas the structure for series E is different from the others.

A similar trend can be observed in fig. 3, showing the

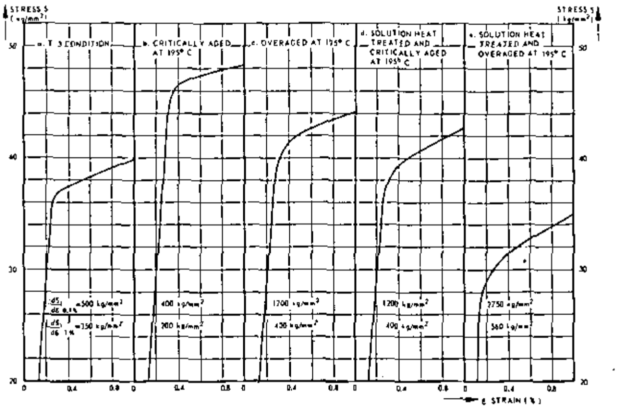

Fig. 3 Stress-strain curves of static test specimens.

first part of the stress-strain curves. There are again similarities between A and B and between C and D, E giving again a different result. The strain-hardening rate at low values of the plastic strain (up to 1%) is relatively low for series A and B, higher for series C and D, while series E shows the maximum hardening rate (see also the numerical values indicated in fig. 3 for plastic strain values of 0.1% and 1%).

The low hardening rate in series A and B should probably be associated with the presence of G.P. zones. In the literature (refs. 5 and 6) it has been argued that dislocations have to cut through G.P. zones in view of their small distances. If the stress is high enough for making this possible, subsequent dislocation movements will occur more easily and that would explain the relatively low hardening rate. It is therefore assumed that the precipitates for A and B are mainly G.P. zones, viz. G.P. II for series B in view of the aging temperature (195°C) and both G.P. I and G.P. II for series A. The presence of G.P. I for series A is deduced from fig. 1, which shows that the T3 condition (series A) exhibits the so-called reversion phenomenon (drop in hardness, see ref. 1) during aging at 195°C. The reversion is assumed to be due to the resolution of G.P. I during the beginning of artificial aging.

When the G.P. zones are growing they are partly transformed into θ'. It then becomes more difficult for dislocations to cut through the precipitates in view of the latter's increasing size. Bowing between the precipitates is facilitated by the larger distances between the precipitates. Also by-passing of the precipitates by cross-slip will be easier. The bowing mechanism will leave dislocation loops around the precipitates. As a consequence of the above, dislocation interactions will increase and this would explain an increased hardening rate (refs. 5 and 6). It is assumed that for test series C and D G.P. II zones and θ' precipitates were present. Probably the amount of θ' was not yet high for series D since this material was at peak hardness (fig. 1), whereas much θ' will lead to overaging.

For series E, which was overaged to a greater extent than series C (see fig. 1), the precipitate is supposed to be largely in the θ'-phase. The distance between the precipitates was increased so much that dislocation movements between the precipitates are fairly easy. Moreover the coherency strains will have diminished and thus a relatively low yield strength is obtained. The relatively high strain-hardening rate indicates that the precipitates still exert a considerable influence on the dislocation motions.

4 Details of fatigue tests

The specimens were cut to a size of 100 × 280 mm with the latter dimension parallel to the direction of rolling. The specimens were provided with a sharp central notch (fig. 4). The notch consisted of a hole and two saw cuts made by means of a jeweller's fret saw. The dimensions of the notch are shown in fig. 4. After the heat treatment a number of line markings in longitudinal direction were inscribed in the surface at spacings as indicated in fig. 4. The specimens were heat treated three at a time (in a way also indicated in the figure) in order to assure similar and simultaneous heating and quenching. After the heat treatment the specimen side with the scribe line markings was lightly polished to facilitate crack-propagation observations.

The specimens were loaded in axial tension in a vertical Schenck pulsator type PVQ-002S of six-tons capacity. This machine is of the mechanical resonance type. Crack-propagation records were made by counting the number of cycles necessary to extend the crack over the distance between each two successive scribe-line markings.

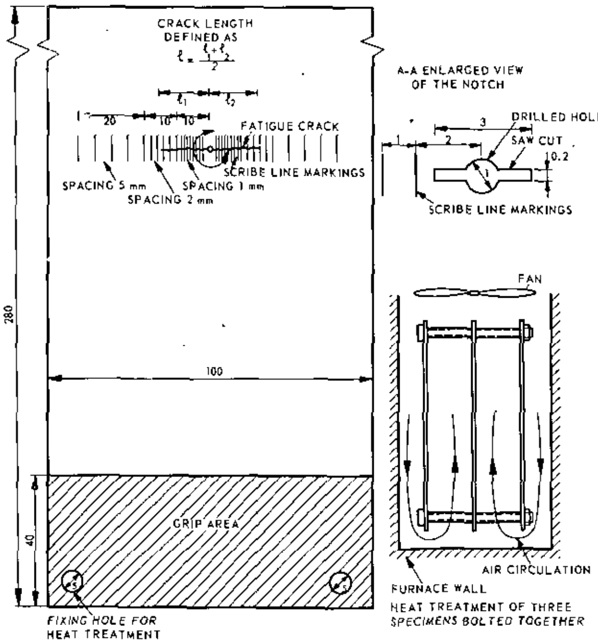

Fig. 4 Specimen for fatigue tests.

TABLE 2

Crack propagation records for $S_a = 2.5$ kg/mm²
$S_m = 8$ kg/mm² 1 kc = 1000 cycles
$S_a = 2.5$ kg/mm² $\bar{n}$ = average value of three specimens

l	A) T-3 condition				B) Critically aged without sol. heat tr.				C) Overaged without sol. heat tr.				D) Critically aged after sol. heat tr.				E) Overaged after sol. heat tr.			
(mm)	$n_{(kc)}$			$\bar{n}$	$n_{(kc)}$			$\bar{n}$	$n_{(kc)}$			$\bar{n}$	$n_{(kc)}$			$\bar{n}$	$n_{(kc)}$			$\bar{n}$
	B_2	B_{15}	B_{24}	(kc)	A_{52}	A_3	B_{22}	(kc)	A_{36}	A_{88}	A_{121}	(kc)	B_{13}	B_9	B_3	(kc)	A_{32}	A_{94}	A_{118}	(kc)
2	0	0	0	0	0	0	0	0	0	0	0	0	0	0	0	0	0	0	0	0
3	90.0	102.8	130.3	107.7	81.4	54.2	99.5	78.4	64.4	73.4	87.4	75.1	64.0	118.4	67.0	83.1	52.8	49.4	50.8	51.0
4	136.8	142.0	194.4	157.7	110.2	86.7	127.3	108.1	87.9	105.8	114.6	102.8	91.0	179.0	105.4	125.1	77.0	79.8	74.2	77.0
5	170.7	177.5	234.7	194.3	131.5	113.1	152.0	132.2	113.1	132.0	140.9	128.7	113.2	212.3	128.0	151.2	99.6	104.2	95.2	99.4
6	196.5	194.5	258.3	216.4	147.6	129.5	169.0	148.7	130.6	146.3	158.2	145.0	130.9	231.1	143.9	168.6	116.4	123.0	108.8	116.1
7	211.2	211.0	273.1	231.8	158.5	140.0	180.9	159.8	141.1	159.3	170.8	157.1	141.9	245.9	156.1	181.3	126.9	135.7	118.0	126.9
8	235.7	224.5	290.9	250.4	168.8	150.6	190.5	169.9	151.7	170.9	181.7	168.1	152.4	256.9	163.7	191.0	136.9	147.9	127.8	137.5
9	248.8	236.0	301.2	262.0	175.4	157.2	197.5	176.7	158.8	178.4	188.6	175.3	161.5	266.1	175.5	201.0	142.5	155.0	133.3	143.6
10	257.2	246.0	312.6	271.9	181.5	162.8	201.4	181.9	165.2	183.1	195.4	181.2	167.6	273.3	181.3	207.4	149.8	162.1	139.6	150.5
12	273.8	259.0	330.9	287.9	191.2	172.2	212.0	191.8	176.7	193.9	206.1	192.2	180.8	286.8	192.8	220.1	158.7	173.6	150.8	161.0
14	289.1	273.0	345.0	302.4	198.3	179.4	220.9	199.5	185.3	201.9	214.0	200.4	188.0	287.1	201.0	225.4	166.2	183.2	159.3	169.6
16	300.3	283.0	355.3	312.9	203.1	184.4	224.6	204.0	190.6	206.4	219.6	205.5	194.7	295.1	208.1	233.0	171.3	189.7	166.0	175.6
18	309.3	293.0	363.3	321.9	207.2	188.7	229.0	208.3	196.0	210.5	225.0	210.5	199.8	302.1	214.4	238.8	175.4	195.3	172.2	180.9
20	316.1	299.5	370.5	328.7	210.2	192.5	231.9	211.5	199.4	213.6	228.5	213.8	204.7	307.8	219.2	243.9	178.5	199.6	176.1	184.7
25	328.6	311.2	381.0	340.3	214.8	196.2	236.8	215.9	205.9	218.6	234.5	219.7	212.3	316.5	227.3	252.0	183.3	206.7	182.9	190.9
30	334.2	315.9	385.9	345.3	217.4	199.0	239.4	218.6	209.1	221.4	238.1	222.9	216.0	320.4	231.8	256.1	185.2	210.7	187.0	194.3
35	336.1	317.9	388.4	347.5	218.2	199.9	240.4	219.8	210.2	222.3	239.3	227.3	216.8	321.7	233.3	257.3	185.3	211.9	188.1	198.8

TABLE 3

Crack propagation records for $S_a = 4$ kg/mm²
$S_m = 8$ kg/mm² 1 kc = 1000 cycles
$S_a = 4$ kg/mm² $\bar{n}$ = average value of three specimens

l	A) T-3 condition				B) Critically aged without sol. heat tr.				C) Overaged without sol. heat tr.				D) Critically aged after sol. heat tr.				E) Overaged after sol. heat tr.			
(mm)	$n_{(kc)}$			$\bar{n}$	$n_{(kc)}$			$\bar{n}$	$n_{(kc)}$			$\bar{n}$	$n_{(kc)}$			$\bar{n}$	$n_{(kc)}$			$\bar{n}$
	B_7	B_{12}	B_{25}	(kc)	A_{62}	A_8	A_{87}	(kc)	A_{38}	A_{97}	A_{109}	(kc)	B_{19}	B_{14}	B_{10}	(kc)	A_{44}	A_{101}	A_{123}	(kc)
2	0	0	0	0	0	0	0	0	0	0	0	0	0	0	0	0	0	0	0	0
3	18.1	31.7	24.7	24.8	18.2	12.1	15.9	15.4	15.7	13.4	13.7	14.3	15.5	17.9	18.0	17.1	12.9	17.3	16.5	15.6
4	30.7	44.2	36.1	37.0	26.7	22.0	24.2	24.3	23.0	23.9	21.4	22.8	25.5	27.1	29.6	27.4	21.7	25.7	25.3	24.2
5	43.6	55.5	47.5	48.9	33.7	27.2	30.5	30.5	30.8	40.7	29.3	33.6	32.9	33.3	37.7	37.9	31.1	33.7	34.6	33.1
6	52.2	65.4	59.8	59.1	38.1	32.0	35.5	35.2	36.4	45.8	34.8	39.0	39.1	38.7	43.1	40.3	36.1	39.9	40.4	38.8
7	60.5	74.2	65.4	66.7	41.7	35.6	38.8	38.7	39.8	49.0	38.4	42.4	43.4	42.7	47.6	44.6	40.1	44.6	45.5	43.4
8	67.4	80.3	70.5	72.7	45.1	39.0	41.8	41.9	43.5	52.0	41.6	45.7	47.2	45.7	51.1	48.0	43.7	48.2	49.1	47.0
9	74.1	84.7	74.3	77.7	47.1	41.1	44.0	44.1	46.0	54.5	43.7	48.1	50.3	48.3	53.8	50.8	46.1	50.9	51.9	49.6
10	78.0	88.9	78.0	81.6	48.9	42.9	45.8	45.9	48.1	56.5	45.8	50.1	52.5	50.5	56.7	53.2	48.4	53.7	54.4	52.2
12	85.2	96.6	84.2	88.7	52.0	46.2	48.6	48.9	51.5	60.2	49.5	53.7	56.8	54.4	59.9	57.0	52.2	58.1	58.6	56.3
14	90.5	103.9	88.4	94.3	54.0	48.7	50.6	51.1	54.5	62.8	52.1	56.5	59.8	57.4	63.5	60.2	55.1	61.7	61.9	59.6
16	93.6	107.7	91.5	97.6	55.8	50.3	52.2	52.8	56.5	64.9	54.0	58.5	62.3	59.5	66.0	62.6	57.2	64.4	64.4	62.0
18	97.0	111.1	94.2	100.8	57.1	51.7	53.4	54.1	58.1	66.3	55.3	59.9	64.2	61.5	68.3	64.7	58.8	66.7	66.3	63.9
20	99.7	113.4	95.8	102.9	58.1	52.6	54.2	54.9	59.4	67.5	56.4	61.1	65.7	62.8	69.8	66.1	59.9	68.4	67.5	65.3
25	103.1	117.0	98.4	106.2	59.5	54.0	55.3	56.3	61.0	69.3	58.0	62.8	67.7	64.9	70.6	67.7	61.7	70.9	69.2	67.3
30	104.2	118.4	99.5	107.4	60.4	54.6	55.9	56.9	61.7	70.2	58.6	63.5	68.7	65.6	71.1	68.5	62.1	71.8	69.9	67.9
35	104.5	118.7	99.8	107.7	60.7	54.9	56.1	57.2	62.0	70.5	58.7	63.7	68.9	65.8	71.2	68.6				

TABLE 4

Crack propagation records for $S_a = 6.5$ kg/mm²
$S_m = 8$ kg/mm² 1 kc = 1000 cycles
$S_a = 6.5$ *kg/mm²* $\bar{n}$ = *average value of three specimens*

l	A) T-3 condition				B) Critically aged without sol. heat tr.				C) Overaged without sol. heat tr.				D) Critically aged after sol. heat tr.				E) Overaged after sol. heat tr.			
(mm)	$n_{(kc)}$			$\bar{n}$	$n_{(kc)}$			$\bar{n}$	$n_{(kc)}$			$\bar{n}$	$n_{(kc)}$			$\bar{n}$	$n_{(kc)}$			$\bar{n}$
	B_5	B_{16}	B_{20}	(kc)	A_{50}	A_{12}	A_{106}	(kc)	A_{45}	A_{105}	A_{117}	(kc)	B_{26}	B_8	A_5	(kc)	A_{34}	A_{96}	A_{112}	(kc)
2	0	0	0	0	0	0	0	0	0	0	0	0	0	0	0	0	0	0	0	0
3	6.5	8.3	7.3	7.4	7.8	9.6	5.0	7.5	5.1	7.6	3.9	5.5	5.9	5.5	5.7	5.7	2.9	5.9	5.5	4.8
4	11.8	13.6	12.8	12.7	10.4	12.3	8.0	10.2	7.7	10.7	6.5	8.3	9.7	8.9	9.5	9.4	6.5	8.5	8.5	7.8
5	17.2	20.4	18.8	18.8	13.0	15.0	10.1	12.7	10.4	13.1	9.1	10.9	13.2	12.1	12.8	12.7	9.1	11.3	11.5	10.6
6	21.0	25.8	22.5	23.1	15.0	16.5	12.1	14.5	12.4	14.8	11.1	12.8	16.2	14.8	15.4	15.5	11.0	13.5	13.7	12.7
7	24.1	30.8	25.2	26.7	16.2	17.5	13.5	15.7	14.0	16.2	12.7	14.3	19.0	17.1	17.1	17.7	12.5	14.8	15.5	14.3
8	26.7	33.9	28.6	29.7	17.5	19.0	14.8	17.1	15.5	17.3	14.0	15.6	21.8	18.3	18.8	19.6	13.6	16.3	16.9	15.6
9	28.5	36.3	30.8	31.9	18.3	19.6	15.6	17.8	16.4	17.8	14.9	16.4	23.7	19.4	20.4	21.2	14.5	17.4	17.9	16.6
10	29.7	38.2	32.6	33.5	18.9	20.2	16.4	18.8	17.2	18.4	15.4	17.0	25.5	20.4	21.2	22.4	15.1	18.2	18.8	17.4
12	31.9	40.8	35.3	36.0	19.9	21.2	17.5	19.5	18.3	19.4	16.5	18.1	28.5	22.1	22.7	24.4	16.1	19.4	20.1	18.5
14	33.2	42.3	37.5	37.7	20.5	21.9	18.2	20.2	19.1	20.1	17.2	18.8	30.1	23.1	23.7	25.6	16.8	20.1	21.0	19.3
16	33.9	43.3	38.7	38.6	20.8	22.3	18.7	20.6	19.6	20.5	17.6	19.2	31.3	23.9	24.2	26.5	17.1	20.6	21.4	19.7
18	34.4	43.9	39.5	39.3	21.1	22.6	18.9	20.9	20.0	20.8	18.0	19.6	31.9	24.4	24.6	26.9	17.4	20.8	21.7	20.0
20	34.8	44.3	40.0	39.7	21.2	22.8	19.1	21.0	20.3	21.1	18.2	19.9	32.3	24.7	24.9	27.3	17.4	21.0	21.8	20.1
25	35.2	44.7	40.7	40.2	21.4	23.0	19.4	21.3	20.6	21.4	18.5	20.2	32.7	25.0	25.2	27.6	17.4	21.2	22.0	20.2
30	35.2	44.9	40.9	40.3					20.7	21.5	18.5	20.3	32.8	25.0	25.2	27.7				
35																				

All fatigue tests were carried out at a positive mean stress of 8 kg/mm² (11.4 ksi). For each of the conditions A, B, C, D en E nine tests were carried out, viz. three tests at each of the stress amplitudes 2.5, 4 and 6.5 kg/mm² (3.6, 5.7 and 9.3 ksi). One of the three specimens which had been heat treated simultaneously, was tested at each of the three stress amplitudes, in order to avoid as far as possible a systematical influence of slight differences in heat treatment.

5 Test results

5.1 *Present results*

Records of the crack propagation were started at the moment the crack had reached the first scribe line marking (see fig. 4). This moment was considered as the actual start of the test. The aim of this procedure was to avoid an influence of the notch. (The number of cycles for crack initiation and early crack propagation might be affected by slightly different notches.)

Numerical test results are given in tables 2, 3 and 4. The crack-propagation curves have been plotted in figs. 5, 6 and 7; each curve is the average result of three tests. From these figures it follows that all heat treatments B–E (applied in addition to the T3 condition) caused an acceleration of crack-propagation. Although treatment B seems to be less unfavourable than C, D and E it cannot be said that the differences are large. For the latter three treatments the differences as shown in figs. 5, 6 and 7 are non-systematic. On the average the heat treatments reduced the crack propagation life with 25% to 50%, i.e. there was an average increase of crack rate with 50% to 100%.

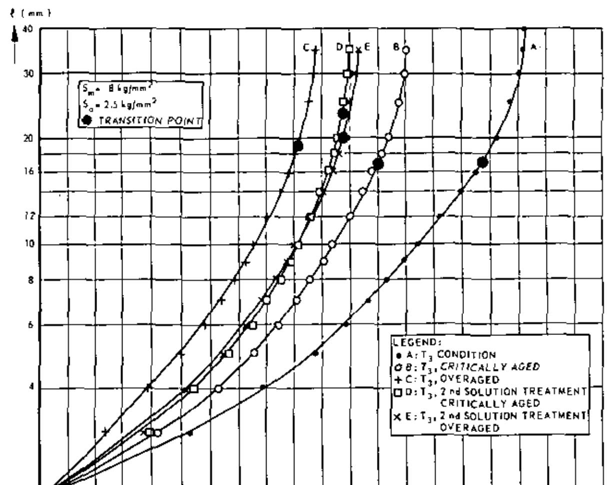

Fig. 5 Crack-propagation curves for $S_a = 2.5$ kg/mm²

5.2 *Results of other investigations*

Systematical investigations on the influence of heat treatment on the growth of fatigue cracks are very scarce. In ref. 7 some results are given of crack-propagation tests on 2024-T8 and 2024-T3 bare sheet (The T-8 condition is solution heat treated, cold rolled and artificially aged; the T-3 condition is solution heat treated, cold rolled and naturally aged). Only two

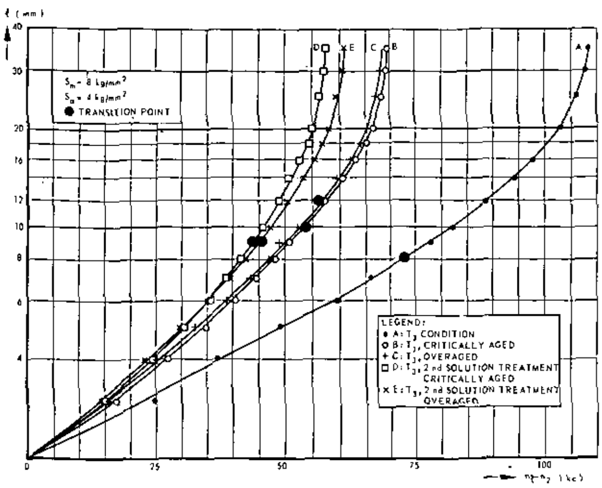

Fig. 6 Crack-propagation curves for S_a = 4 kg/mm².

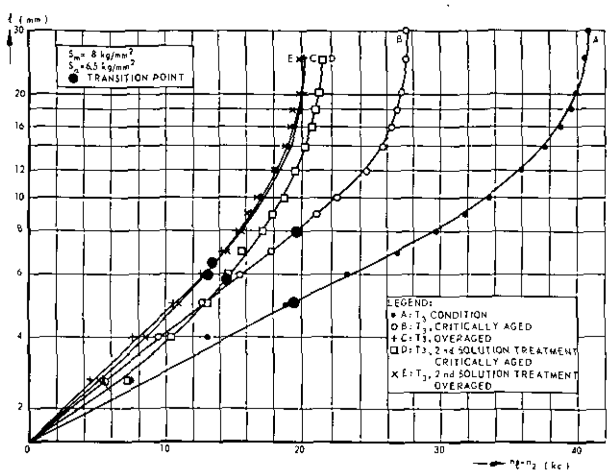

Fig. 7 Crack-propagation curves for S_a = 6.5 kg/mm²

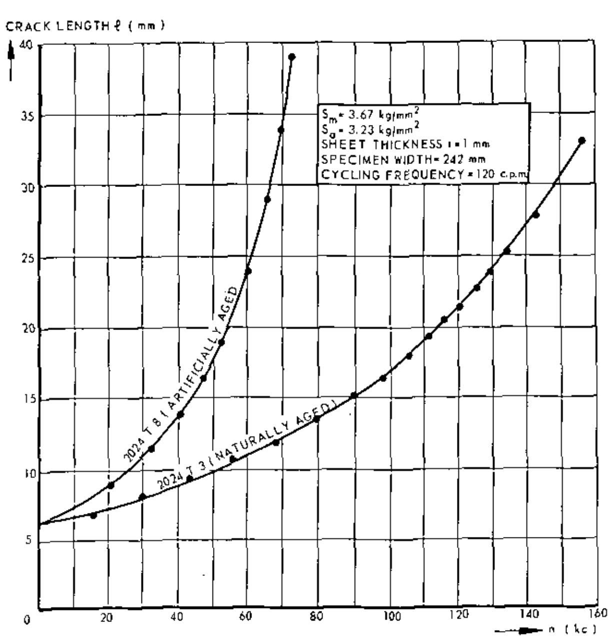

Fig. 8 Crack-propagation of 2024 bare sheet in the artificially and naturally aged conditions (ref. 7).

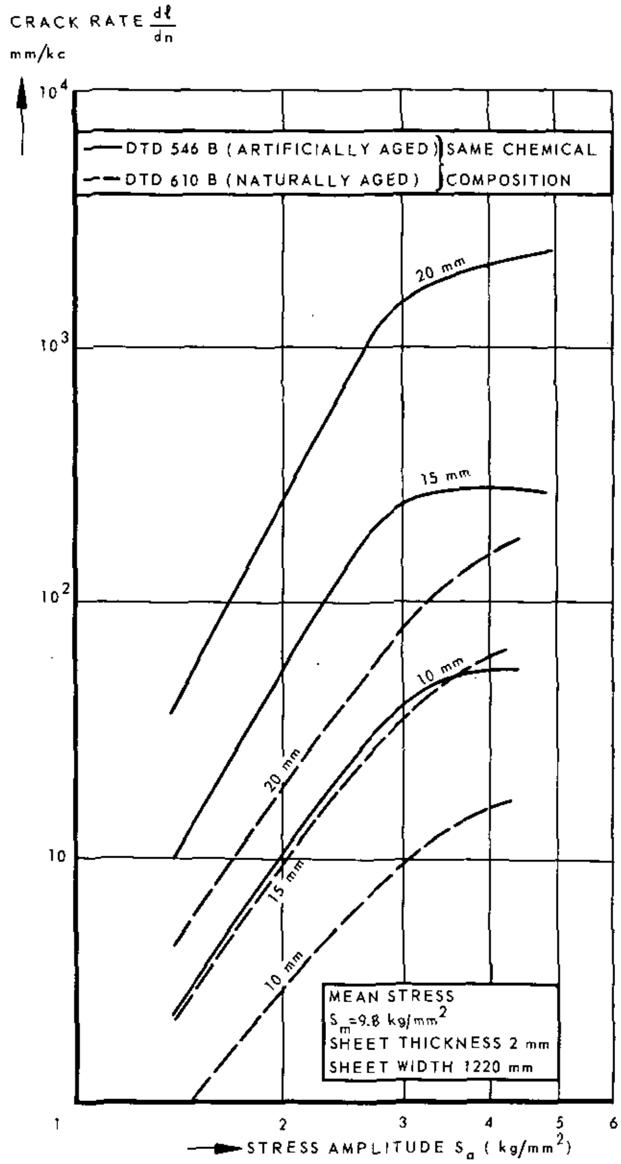

Fig. 9 The crack rate of two alloys (comparable to 2024 after different heat treatments) (ref. 8).

tests were presented for which all other parameters influencing crack-propagation (sheet thickness, sheet width, cycling frequency and stresses) were the same. The results of these two tests are plotted here in fig. 8. Crack-propagation is faster in the artificially aged alloy than in the naturally aged alloy.

If the effect of heat treatment on the crack rate is considered as an effect of ductility some more results may be quoted for aluminium-copper alloys. In ref. 8 a comparison was made between a DTD 610B (equivalent to 2024) naturally aged alloy and an artificially aged alloy of the same composition DTD 546B. A summary of the results is given here in fig. 9 in terms of the crack-propagation rate, i.e. the crack extension per cycle (or kilocycle; 1 kc = 1000 cycles). It appears from fig. 9 that the crack rate in the artificially aged alloy is 2 to 10 times larger than in the naturally aged alloy.

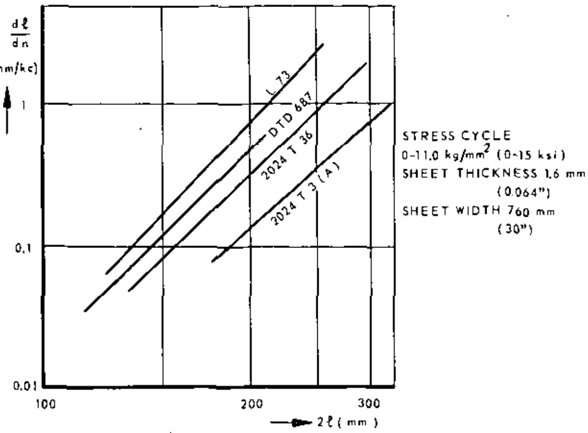

Alloy	Type	Static properties: $S_{0.1}$ (kg/mm²)	S_u (kg/mm²)	$S_{0.1}/S_u$	δ (2″G.L.)
L73	AlCu	42.6	46.1	0.92	10%
DTD 687	AlZn	49.4	54.5	0.91	12%
2024T36	AlCu	41.0	50.4	0.81	14%
2024T3(A)	AlCu	35.2	48.0	0.73	19%

Fig. 10 Crack rate results of Harpur (ref. 9) for various Al alloys.

A comparison of different alloys was also made by Harpur (ref. 9). His results for three Al Cu alloys (2024 type) and one Al Zn alloy (7075 type) are presented in fig. 10, again as the crack rate as a function of crack length. These results pertain to large cracks and high crack rates. The effect of the ductility, see the elongation and the ratio between yield limit and ultimate stress indicated in the figure, is systematic and the same as noted above, i.e. cracks grow faster in the less ductile material.

An extensive comparison of the crack rates in 2024-T3 and 7075-T6 was made in ref. 10, including references to similar comparisons in the literature. The crack rate in the less ductile 7075-T6 material was considerably larger (about four times) than in the 2024-T3 material. The effect of ductility on the crack rate was already indicated in ref. 10.

5.3 *Fractographical observations*

Some observations were made on the so-called transition phenomenon (ref. 11), i.e. the rotation of the fracture surface from a plane perpendicular to the sheet surface to a plane at 45° to it, or in other words from the tensile mode to the shear mode. The point at which this transition is completed is defined as the transition point. The transition points are indicated in figs. 5, 6 and 7. The rate of crack propagation dl/dn at the moment of the transition is tabulated in table 5. It appears from this table that for the T-3 condition the transition occurs at a constant crack rate independent of stress amplitude. This is a confirmation of previous observations (refs. 10, 12 and 13) where the same value $dl/dn \sim 0.2$ mm/kc was found. The heat treatments B–E have delayed the transition to a higher crack rate which is also approximately constant and practically the same for all these heat treatment conditions, viz. $dl/dn \sim 0.5$ mm/kc.

TABLE 5

The rate of crack propagation at the transition.

S_a (kg/mm²)	Crack rate at the transition (dl/dn; mm/kc): T-3 Condition	Condition B	Condition C	Condition D	Condition E
2.5	0.22	0.46	0.61	0.62	0.60
4	0.19	0.47	0.53	0.40	0.47
6.5	0.21	0.60	0.60	0.59	0.62

Since all heat treatments B–E resulted in almost the same ductility it might be concluded that there is a correlation between the transition (or the crack rate for the transition) and the ductility.

6 Discussion

6.1 *The ductility effect*

The results of the present investigation clearly suggest a correlation between the ductility of the material and the crack-propagation rate. A low ductility promotes faster crack growth. The correlation is confirmed by results of the literature summarized in section 5.2. A tentative explanation for the correlation will now be given.

In ref. 14 crack propagation in fatigue was outlined as a geometrical consequence of dislocation movements at the tip of the crack, whereas the efficiency of the conversion of slip into crack extension was shown to depend on the tensile stress opening the crack. In the less ductile material one should expect a smaller plastic zone and smaller slip movements. Nevertheless, the crack extension per cycle is larger than in the more ductile material. It is thought that this is due to the higher tensile stress in the crack tip region, which is a consequence of the smaller plastic zone. The leveling-off of the stress peak is less effective and apparently this predominates over the smaller slip movements. In this respect it is noteworthy that in ref. 10 the effect of mean stress on crack-propagation was more significant for the less ductile 7075-T6 alloy than for the 2024-T3 alloy.

In section 5.3 it was pointed out that the transition of the fracture surface from the tensile to the shear mode occurred at a higher crack rate for the less ductile material. Liu (ref. 15) has suggested that this transition is associated with the transition of a state of plain strain at the tip of the crack to a state of plane stress. Considerable thought on this point has been given in refs. 13 and 14. Although a fully satisfactory picture could not be obtained from a quantitative point of view, it appeared that the transition of the state of stress was closely related to the size of the plastic zone. If two sheets of the same thickness loaded at the same stress amplitude and mean stress are considered it is clear that a certain size of the plastic zone will require a larger crack length in the less ductile sheet material. Figs. 5 to 7 confirm that the crack length at the transition of the fracture surface is somewhat larger for the specimens with the heat treatments B to E than for the specimens in the T3 condition (treatment A). This larger crack length and the lower ductility then explain the higher crack rate at the transition point for the conditions B to E.

The present results do not allow a conclusion as to whether crack propagation for a certain sheet thickness (the crack rate depends on the sheet thickness, see ref. 13) and for a certain fatigue load is depending on the ductility only. In figs. 5 to 7 the heat treatment B gave slightly lower crack rates than treatments C to E although the ductility was not better. Nevertheless it is concluded that the ductility has a pronounced influence.

From the discussion in section 3.2 it follows that the ductility is related to the state of precipitation. This relation is understood only qualitatively and it is difficult to forecast whether aluminium alloys with better crack propagation properties can be developed without sacrificing their ductility and strength properties.

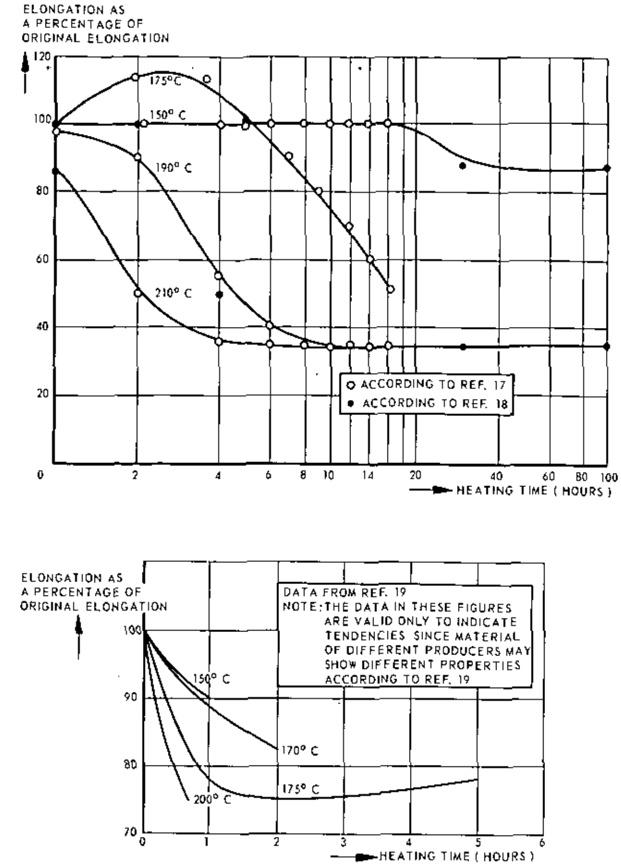

Fig. 11 The influence of different heating times on the elongation of two aluminium alloys.

6.2 *Technical implications of the results*

In the introduction the curing cycle for adhesive bonding and aerodynamic heating were mentioned as examples of heating a structure which could involve aging of its material. In view of the considerable effect of ductility on propagation one might ask how the ductility is affected by the heating mentioned above. Some relevant data of the literature have been reproduced in fig. 11 for both 2024-T3 and 7075-T6 material.

Due to the curing cycle for adhesive bonding, say a few hours at 165°C, the 2024-T3 material will probably not experience a loss of ductility. However, for the 7075-T6 material a noticeable decrease of ductility has to be anticipated and one should recognize the fact that this might adversely affect the crack-propagation properties. Such an effect can easily be determined since crack-propagation tests as described in this report are easily carried out and do not ask much time.

For supersonic aircraft exposed to aerodynamic heating for long times fig. 11a shows that the ductility of 2024-T3 material at 150° will decrease after about 20 hours. It is expected that also at 130°C a decrease of ductility, although requiring much longer soaking times, has to be anticipated. This temperature will probably be high enough for further aging, although overaging need probably not be feared. One could say that the aerodynamic heating will transform the material from the T3 (naturally aged) into the T8 condition (artificially aged).

For the Mach 2 supersonic aircraft aluminium alloys in the artificially aged condition will still be used. Chemical compositions will be somewhat different, i.e. the copper contents will be changed and other elements in small quantities will be added. The purpose of this is to improve the stability of static properties after long soaking times and to obtain better creep properties. One of these materials is RR58 (British designation, French designation A.U.2GN) for which crack-propagation data were recently published by Lachenaud (ref. 16). He studied the effects temperature and frequency have on the crack propagation in RR58 sheet specimens with a central slit and part of his results could be directly compared with results of the present investigation for $S_m \pm S_a = 8 \pm 6.5$ kg/mm^2 ($R = S_{min}/S_{max} = 0.1$, which applies to all results of ref. 16). The comparison is made in table 6, which gives some further data on the material, its ductility and the test circumstances. The table shows that the ductility of RR58 is lower than for 2024-T3 (condition A), whereas it is much like that of 2024-T8. The fatigue life for extending the crack from 5 mm to 20 mm, (last column of table 6), for RR58 is ap-

TABLE 6

Crack propagation in RR58 (ref. 16) compared with results from the present study

Material	Condition	Ductility		Cycles (kc) for growth of
		$S_{0.2}/S_u$	$\delta(\%)$	$2l = 5$ mm to $2l = 20$ mm at 8 ± 6.5 kg/mm^2
2024 (present study)	A (naturally aged)	0.78	18.5	28.8
	B (critically aged)	0.94	7.5	19.3
	C (overaged)	0.88	7	13.5
	D (critically aged)	0.85	9	16.2
	E (overaged)	0.79	8	14.3
RR58 (ref. 16)	Artificially aged	0.86	10	13.6

Data on RR58: Chemical composition: 2.4% Cu, 1.6% Mg, 1.1% Ni, 1.65% Ni, 1.65% Fe and remainder Al.
Average properties $S_{0.2} = 37$ kg/mm^2 (52.6 ksi), $S_u = 43$ kg/mm^2 (61.1 ksi) and $\delta = 10\%$.
Test data for RR58: Sheet width 100 mm, sheet thickness 1.5 mm, test frequency 2000 cpm, test temperature 20°C.
The same test data apply to the present study apart of the sheet thickness, which was 2 mm instead of 1.5 mm.

proximately half the life for 2024-T3 and equal to the lower values of the group B to E. Although this comparison is an isolated case, no more data being available, it is expected on the basis of the present study that the crack-propagation properties of the aluminium alloys for the supersonic transport will be inferior to those of the conventional 2024-T3 material, in view of their limited ductility.

7 Conclusions

From an experimental investigation on the influence of heat treatment on the fatigue crack-propagation in 2024-T3 alclad sheet the following conclusions can be drawn.

1. Further artificial aging of the material to or beyond maximum hardness reduces the crack-propagation life to an amount in the order of 50%.
2. A new solution heat treatment and subsequent artificial aging to or beyond maximum hardness reduce the crack propagation to approximately the same amount. This implies that the fatigue crack-propagation properties of the 2024 alloy in the T-8 condition should be far inferior to those of the T-3 condition. This was confirmed by some incidental results from other investigations.
3. The curing cycle for adhesive bonding will probably not affect the crack-propagation properties of the 2024-T3 alloy, but it may adversely affect the crack-propagation characteristics of the 7075-T6 alloy.
4. It must be expected however that aerodynamic heating, will accelerate the crack-propagation in the 2024-T3 alloy.
5. For precipitation hardened aluminium alloys a decrease of the ductility is associated with a reduction in crack-propagation lives.

8 References

[1] Hardy, H. K., Heal, T. J., Report on precipitation. Progress in Metal Physics 5, Ed. by B. Chalmers and R. King, London, Pergamon, 1954.

[2] Hardy, H. K., The ageing characteristics of binary aluminium-copper alloys. The Journal of the Inst. of Metals **79**, 5, July 1951, pp. 321–369.

[3] Calvet, J., Martinod, H., La réversion, cause d'un affaiblissement passage de certains alliages d'aluminium soumis à un echauffement. La Recherche Aéronautique 1960, V.79 pp. 27–34.

[4] von Gerold, V., Die atomistischen Vorgänge in übersättigten Mischkristallen. Aluminium, **37**, 9, Sep. 1961, pp. 583–586.

[5] DewHughes, D., Robertson, D., The mechanism of hardening in aged aluminium-copper alloys. Acta Metallurgica, **8**, 3 (March 1960), pp. 156–167.

[6] Price, R. J., Kelly, A. The plastic deformation of age-hardened aluminium alloys. Acta Metallurgica **10**, 10 (Oct. 1962), pp. 980–982.

[7] Donaldson, D. R., Anderson, W. E., Crack-propagation behaviour of some airframe materials. Proceedings of the Crack-Propagation Symposium Cranfield, Sep. 1961, Vol. II, p. 375.

[8] Raithby, K. D., Bebb, M. E., Propagation of fatigue cracks in wide unstiffened aluminium alloy sheets. R.A.E. rep. TN.No. structures 305, Sep. 1961.

[9] Harpur, N. F., Material selection for crack resistance. Proceedings of the Crack-Propagation Symposium Cranfield, Sep. 1961, Vol. II, p. 442.

[10] Broek, D., Schijve, J., The influence of the mean stress on the propagation of fatigue cracks in light alloy sheets. N.L.R. report M.2111, Jan. 1963.

[11] Broek, D., de Rijk, P., Sevenhuysen, P. J., The transition of fatigue cracks in alclad sheets. NLR-TR M.2100, Nov. 1962.

[12] Schijve, J., Broek, D., de Rijk, P., The effect of the frequency of an alternating load on the crack rate in a light alloy sheet. N.L.R. report M.2092, Sep. 1961.

[13] Broek, D., Schijve, J., The effect of sheet thickness on the fatigue crack-propagation in a light alloy sheet. N.L.R. Report M.2129, April 1963.

[14] SCHIJVE, J., Analysis of the fatigue phenomenon in aluminium alloys. N.L.R. report M.2122, April 1964.

[15] LIU, H. W., Discussion in the Proceedings of the Crack Propagation Symposium, Cranfield, Sep. 1961, Vol. II, p. 514.

[16] LACHENAUD, R., Fatigue strength and crack-propagation in AU 2 GN alloy as a function of temperature and frequency, ICAF-AGARD Symposium, Rome 1963 (to be published).

[17] NOCK, J. A., Reheating of 24S and 75S aluminium sheet. The Iron Age, 25 Dec. 1947.

[18] DUNSBY, A. J., Some experiments on the effect of time at temperature on the room temperature reversed bending fatigue characteristics and on the tensile strength of 24S-T alclad aluminium alloy. Nat. Aeron. Establishment. Mech. Eng. Rep. MS-102. Nat. Res. Council of Canada. N.R.C. No. 5927, Ottawa, August 1960.

[19] NIEUWENHUIZEN, M. P., Influence of reheating on the mechanical properties of aluminium alloys. Fokker report SP-40, Jan. 1963.

C.C.L. Class.: G 042

REPORT NLR-TR M.2138

The effect of temperature and frequency on the fatigue crack propagation in 2024-T3 Alclad sheet material

by

J. SCHIJVE and P. DE RIJK

Summary

Tests were carried out at 20°C and 2000 cpm, at 150°C and 2000 cpm and at 150°C and 20 cpm. Results indicate a temperature effect as well as a frequency effect. Crack extension due to creep was considered, a few provisional results being presented. Results are analysed and compared with relevant data from the literature.

Contents

List of symbols, abbreviations and units

cpm	— cycles per minute
	— kilocycle = 1000 cycles
kg/mm²	— 1 kg/mm² = 1.422 ksi, 1 ksi = 0.703 kg/mm²
l	— crack length
mm	— 1 mm = 0.04″, 1″ = 25.4 mm
n	— number of cycles
n_l	— number of cycles to obtain a crack of length l
NLR	— National Aero- and Astronautical Research Institute, Amsterdam
R	— stress ratio = S_{min}/S_{max}
S	— stress
S_a	— stress amplitude (gross stress)
S_m	— mean stress (gross stress)
S_{min}	— minimum stress (gross stress)
S_{max}	— maximum stress (gross stress)
S_u	— ultimate stress
$S_{0.2}$	— yield stress
δ	— elongation

1 Introduction

In the present research crack propagation tests were carried out on 2024-T3 Alclad sheet specimens at the following temperature/frequency combinations: 20°C/2000 cpm, 150°C/2000 cpm and 150°C/20 cpm. In a previous study (ref. 9) the effect of frequency on crack propagation in 2024-T3 Alclad sheet material was investigated at room temperature. It was found that the crack rate at 20 cpm was approximately 20 to 30% larger than at 2000 cpm. A satisfactory explanation of this result could not be given. Since one might think that creep in the crack tip region was contributing to this frequency effect a larger frequency effect had to be expected at a higher temperature. This was one reason for performing crack propagation tests at 150°C at the same frequencies mentioned before, viz. 20 and 2000 cpm.

This investigation has been performed under contract with the Netherlands Aircraft Development Board (N.I.V.).

In a concurrent study (ref. 2) on the effect of heat treatment it was found that artificial ageing in general involved a decrease of ductility and, associated with this decrease, the material exhibited higher crack propagation rates. Since 150°C is high enough for further ageing of 2024-T3, the crack rate may be adversely affected by raising the temperature to 150°C. All tests at this temperature were preceded by a presoaking under load for 100 hours at 150°C, the load being the mean load of the tests (S_m = 7 kg/mm²).

Although 2024-T3 (naturally aged) does not seem to be a competitive material for the Mach-2 transport, 2024-T8 (artificially aged) may be so in spite of its lower ductility which is associated with increased crack propagation rates (ref. 2).

It was thought that the results of the present tests might be elucidating with respect to the potential field of application of the 2024 alloy.

This report presents the results of the test, their evaluation and some fractographical observations. A comparison is made with relevant data from the literature. The contribution of creep to crack growth is considered and results of a few exploratory tests on crack growth under creep conditions are presented. It is tried to give a tentative explanation for the trends observed.

2 Experimental details

2.1 *Material and type of specimen*

All specimens were cut from 2024-T3 Alclad sheet material with a thickness of 2 mm (0.08″). The static properties of the material were (averages of 8 tests): S_u = 48.3 kg/mm² (68.7 ksi), $S_{0.2}$ = 37.1 kg/mm² (52.8 ksi) and δ = 18.9% (2″ gage length).

The type of specimen was the same as for several previous NLR investigations (e.g. refs. 1, 2 and 9), i.e. a sheet specimen with a small severe central notch for rapid crack initiation. The dimensions are shown in fig. 1. The specimens were locally polished and provided with fine line markings to facilitate the recording of the crack growth. The spacings of the markings are also indicated in fig. 1.

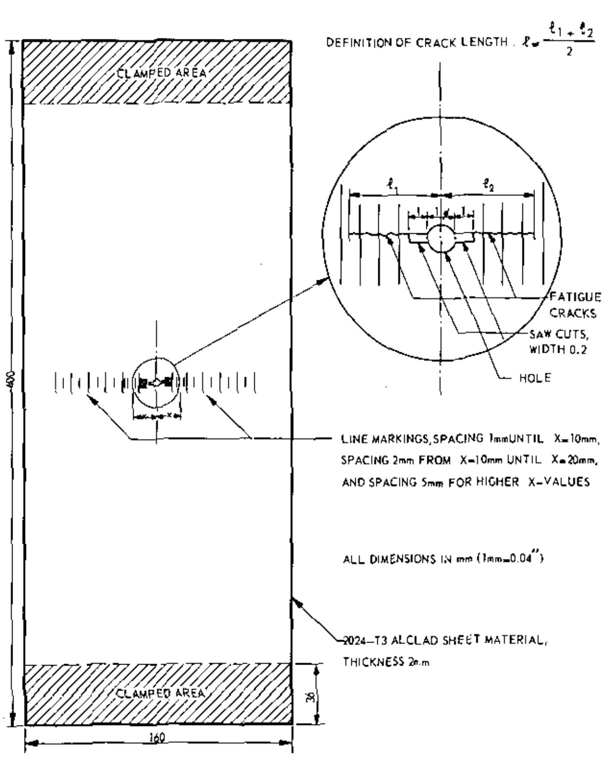

Fig. 1 Sheet specimen for crack propagation.

2.2 *Testing technique*

The specimens were tested in a horizontal Schenck pulsator, type PPD 6 with a capacity of six tons. The machine has a quick drive and a slow drive. With the quick drive the machine is of the resonance type (mechanical excitation). The frequency then depends slightly on the stiffness of the specimen and the load amplitude. Usually the frequency is in the order of 2000 cpm.

The low frequency is obtained with a reversible screw drive. The frequency, which depends on the load amplitude and the adjustment of the machine, is in the order of 20 cpm. The same clampings and dynamometer are used as for the quick drive. For the quick drive the wave form of the load is purely sinusoidal, whereas for the slow drive this form is triangular.

The specimens were axially loaded at a mean stress of 7 kg/mm² (10 ksi). The following test circumstances were adopted.

Temperature (°C)	Frequency (appr.; cpm)	Stress amplitudes kg/mm² (ksi)
20	2000	2.5 (3.6), 4.0 (5.7), 6.5 (9.3)
150	2000	ditto
150	20	ditto

In general each type of test was carried out three times.

Heating at 150°C was achieved by circulating hot air in a box surrounding the specimen. A hot air generator was connected to the box by two flexible insulated tubes thus forming a closed air circuit. The thermostatic temperature control allowed deviations from the desired temperature of ± 2°C at most. The hot air box was provided with a double glass window at one side in order to allow observation of the crack growth.

At the high frequency the propagation of the crack was recorded by noting the number of applied load cycles each time that a tip of a crack reached a scribe line marking. This was done for both cracks in a specimen (see fig. 1) at one side of the specimen only. The same procedure was adopted for the low frequency, except for S_a = 2.5 kg/mm². In view of the long dura-

TABLE 1

Crack propagation records for $S_a = 2.5$ kg/mm²

$n_l - n_3$ is the number of cycles for extending the crack from a length of 3 mm to a length of l mm

Temp.	20°C				150°C					150°C		
Freq.	2000 cpm				2000 cpm					20 cpm		
specimen	A13	A35	A114	mean	A2	A16	A74	A51	mean	A53	A39	mean
l (mm)	$n_l - n_3$ (kc)											
3	0	0	0	0	0	0	0	0	0	0	0	0
4	70.7	44.0	37.1	62.6	37.4	55.7	79.8	27.9	50.2	25.4	31.9	28.6
5	117.3	87.2	114.6	105.3	66.7	90.3	122.8	53.2	83.2	44.5	53.8	49.2
6	148.3	109.9	144.3	134.2	87.1	110.2	145.1	74.2	104.1	56.9	70.1	63.5
7	172.9	124.3	161.6	152.9	100.9	124.9	160.5	87.6	118.5	69.3	76.2	72.8
8	188.7	141.8	181.1	170.5	109.5	139.4	174.4	98.3	130.4	81.4	83.1	82.3
9	205.3	152.2	195.7	184.4	118.7	149.5	182.4	108.2	139.7	91.4	95.7	87.3
10	215.7	161.5	205.6	194.6	125.6	157.0	191.6	116.9	147.7	93.5	103.9	98.7
12	238.5	181.1	225.0	214.9	136.9	170.4	204.5	127.7	159.9	104.1	113.1	108.6
14	254.3	197.4	240.7	230.8	147.2	180.4	214.2	138.0	169.9	110.3	120.2	115.2
16	266.8	208.8	253.7	243.1	154.9	188.2	222.8	146.3	178.0	116.4	126.3	121.3
18	276.5	219.5	266.8	254.3	161.4	195.6	229.5	153.4	185.0	122.2	127.8	125.0
20	285.4	228.5	276.7	263.5	167.4	201.4	234.8	159.0	190.6	127.2	137.7	132.4
25	304.1	243.8	294.7	280.9	177.3	212.5	245.7	169.3	201.2	135.6	146.7	141.1
30	316.7	253.5	307.8	292.7	184.7	218.6	253.8	176.9	208.5	141.4	151.7	145.6
35	324.5	258.8	315.1	299.5	189.6	225.2	258.7	181.8	213.8	146.0	155.7	150.8
40	328.9	264.6	319.3	304.3	193.4	229.2	261.9	184.9	217.3	149.5	158.5	154.0
45	331.2	267.0	321.7	306.6	195.3	231.3	264.1	187.0	219.4	150.8	160.1	155.5
50	332.5	268.1	323.0	307.9	196.4	232.6	255.2	188.0	220.5	151.9	161.2	156.5
55	332.7	268.5	323.1	308.1	—	233.0	265.5	—	—	152.2	161.5	156.9
60										152.2		
80	332.7	268.6	323.2	308.2	197.0	233.0	265.5	188.4	220.9	152.2	161.5	156.9

TABLE 2

Crack propagation records for $S_a = 4$ kg/mm²

$n_l - n_3$ is the number of cycles for extending the crack from a length of 3 mm to a length of l mm

Temp.	20°C				150°C				150°C		
Freq.	2000 cpm				2000 cpm				20 cpm		
specimen	A71	A124	A67	mean	A10	A58	A76	mean	A19	A27	mean[1])
l (mm)	$n_l - n_3$ (kc)										
3	0	0	0	0	0	0	0	0	0	0	0
4	14.2	14.9	14.6	14.6	12.8	12.2	13.3	12.8	12.5	4.3	8.4
5	31.4	30.3	25.8	29.2	22.0	22.5	23.6	22.7	20.1	10.1	15.1
6	39.8	38.0	34.6	37.4	29.0	29.9	31.8	30.2	26.0	16.2	21.1
7	49.0	45.4	41.7	45.3	33.8	35.4	36.5	35.2	29.8	19.4	24.6
8	56.2	51.6	47.3	51.7	38.4	39.8	40.6	39.6	33.5	23.5	28.5
9	61.8	57.0	52.6	57.1	42.2	43.4	45.1	43.6	35.9	26.3	31.1
10	66.3	61.4	56.9	61.5	45.3	46.6	48.8	46.9	37.7	28.6	33.1
12	75.0	69.6	63.1	69.2	50.8	52.2	54.3	52.4	42.4	32.6	37.5
14	81.0	75.7	68.5	75.1	54.1	57.7	56.0	57.3	45.7	36.0	40.8
16	86.2	80.4	72.7	79.8	58.0	61.9	63.6	61.1	48.1	38.0	43.1
18	91.8	84.2	76.3	84.1	60.8	65.3	66.8	64.3	50.2	40.5	45.3
20	94.2	87.3	79.5	87.0	63.1	68.4	69.4	67.0	52.2	42.0	47.1
25	98.7	92.6	84.7	92.0	67.0	72.7	74.8	71.5	55.4		50.3
30	101.2	95.0	87.3	94.5	69.5	75.5	77.6	74.2	56.9		51.8
35	102.5	96.3	88.6	95.8	71.0	77.3	79.1	75.8	58.8		53.7
40	103.2	96.9	89.5	96.5	71.9	78.2	79.8	76.6	59.6		54.5
45	103.6	97.2	89.8	96.8	—	—	80.3	—	60.1		55.0
50	103.7	—	89.9	—	—	—	80.4	—	60.3		55.2
55											
60									60.3		55.2
80	103.7	97.9	89.9	97.2	72.3	78.7	80.5	77.2	60.3		55.2

[1]) In this column the mean value for $l > 20$ mm was obtained by adopting the increments of $n_l - n_3$ for specimen no. A19.

TABLE 3

Crack propagation records for $S_a = 6.5$ kg/mm^2
$n_l - n_3$ is the number of cycles for extending the crack from a length of 3 mm to a length of l mm

Temp.	20°C				150°C				150°C			
Freq.	2000 cpm				2000 cpm				20 cpm			
specimen	A47	A79	A119	mean	A29	A42	A81	mean	A7	A104	A48	mean[1]
l (mm)	$n_l - n_3$ (kc)											
3	0	0	0	0	0	0	0	0	0	0	0	0
4	7.6	5.8	6.9	6.8	5.2	4.0	5.5	4.9	4.3	3.3	2.4	3.3
5	14.6	12.6	12.6	13.3	10.5	8.4	9.5	9.5	7.8		5.0	6.4
6	19.8	19.9	19.2	19.6	13.4	11.4	13.4	12.7	10.1		7.2	8.6
7	23.7	26.6	22.5	24.3	15.6	13.2	15.8	14.9	11.8		8.6	10.2
8	27.4	29.7	27.3	28.1	18.6	15.4	17.6	17.2	13.1		9.8	11.4
9	30.2	32.4	29.2	30.6	19.8	17.4	19.2	18.8	14.4		10.9	12.6
10	31.9	34.5	31.9	32.8	22.1	18.5	20.6	20.4	15.2		12.1	13.6
12	34.2	37.4	34.9	35.5	24.7	20.9	22.3	22.6	16.7	15.8	13.5	15.1
14	36.2	40.4	36.9	37.8	26.6	22.6	23.9	24.4	18.0	16.8	15.0	16.5
16	37.4	41.9	37.9	39.1	28.0	23.9	25.0	25.6	19.3	17.9	16.3	17.8
18	38.2	42.9	38.7	39.9	28.9	24.9	25.8	26.5	20.0	18.6	16.8	18.4
20	38.8	43.6	39.4	40.6	29.6	25.8	26.6	27.9	20.7		17.5	19.1
25	39.6	44.5	40.5	41.5	30.7	27.0	27.6	28.4	21.7		18.6	20.1
30	40.1	44.9	40.7	41.9	31.3		27.9		22.3		19.2	20.7
35	40.2	45.1							22.7		19.4	21.0
40	40.3	45.3							22.9		19.6	21.2
45									22.9		19.6	21.2
50										21.6	19.7	
55												
60												
80	40.4	45.4	40.9	42.2	31.8	28.2	28.4	29.5	23.0	21.6	19.7	21.3

[1] The imcomplete data for specimen no. A104 were disregarded for calculating the mean values.

tion of these tests, recording of the crack growth was done automatically. At specific intervals of time (a usual period being 3 hours) pictures of the specimen were made with a Robot camera. With the aid of a mirror a cycle counter of the machine was simultaneously photographed. Pictures were made at the moment that the load was at its maximum to obtain a maximum of crack opening .The crack growth records were deduced from the film after completion of the tests.

All specimens tested at 150°C were presoaked under load at that temperature for 100 hours, the load corresponding to the mean stress of the tests ($S_m = 7$ kg/mm^2). For tests, which were interrupted overnight, the specimen remained under the mean load and the test temperature. In general, tests at the high frequency were completed in one day, whereas tests at the low frequency lasted from 2 days to 2 weeks.

3 Test results

3.1 *Crack propagation*

The high frequencies obtained in the tests for the three stress amplitudes 2.5, 4 and 6.5 kg/mm^2 were approximately 2150 cpm, 2200 cpm and 2220 cpm respectively. The low frequencies for the three amplitudes were 17 cpm, 11 cpm and 7.5 cpm respectively. For convenience of the discussion the high and the low frequencies are indicated throughout the report by the nominal values of 2000 and 20 cpm respectively.

The crack propagation records are compiled in tables 1, 2 and 3. Although the central notch initiates two cracks in each specimen, the two cracks are considered as one central crack growing simultaneously at its two crack tips. The crack length l for such a crack is defined in fig. 1. The total crack length from tip to tip is $2l = l_1 + l_2$. In general the differences between l_1 and l_2 were very small. The crack propagation records start from $l = 3$ mm (or $2l = 6$ mm). Since the width of the central notch is 3 mm the effect of the notch on the crack growth will have vanished for $2l \geqslant 6$ mm.

An impression of the scatter can be obtained from the tables 1–3 and from table 4. In the latter table the fatigue life from $l = 3$ mm to final failure is split up in three intervals, viz. $l = 3$ to $l = 5$, $l = 5$ to $l = 10$ and $l = 10$ to finale failure. For each interval the fatigue lives and the scatter are presented. The table does not indicate any consistent influence on the scatter from either the crack interval, the stress amplitude or the testing temperature. The scatter is low, as is usual for macro-crack propagation.

The mean crack propagation results for each group of similarly tested specimens, given in tables 1–3, were

TABLE 4

Scatter of the crack propagation life for three crack propagation intervals
Frequency 2000 cpm

Crack propagation interval	S_a (kg/mm²)	Temp. (°C)	Crack propagation life[1]) (kc)	Scatter interval[2]) (%)	Median of previous column
	2.5	20	87.2, 114.6, 117.3	28	
		150	53.2, 66.7, 90.3, 122.8	84	
$l = 3$ mm to $l = 5$ mm	4	20	25.8, 30.3, 31.4	19	20%
		150	22.0, 22.5, 23.6	7	
	6.5	20	12.6, 12.6, 14.6	15	
		150	8.4, 9.5, 10.5	22	
	2.5	20	74.3, 92.0, 98.4	27	
		150	63.7, 58.9, 66.7, 68.8	15	
$l = 5$ mm to $l = 10$ mm	4	20	31.1, 31.1, 34.9	12	14%
		150	23.3, 24.1, 25.2	8	
	6.5	20	19.3, 21.9, 17.3	24	
		150	10.1, 11.1, 11.6	14	
	2.5	20	107.1, 116.6, 117.0	9	
		150	71.5, 71.4, 76.0, 73.9	6	
$l = 10$ mm to final fracture	4	20	33.0, 36.5, 37.4	12	14%
		150	27.0, 32.1, 31.7	17	
		20	9.0, 10.9, 8.5	25	
	6.5	150	9.7, 7.8, 9.7	21	

[1]) For $l = 3$ mm to $l = 5$ mm life values are given in increasing order of magnitude. For the other two intervals the sequence of the corresponding specimens is the same as for the former interval.

[2]) The scatter interval is defined as the difference between the maximum and the minimum values in the previous column divided by the mean value of the previous column.

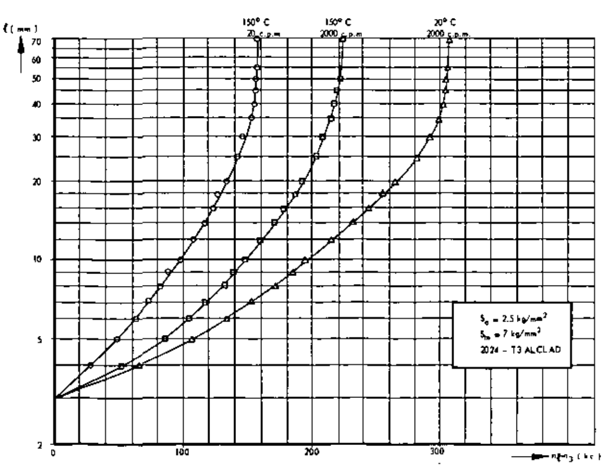

Fig. 2 Influence of the temperature and the frequency on the crack propagation ($S_a = 2.5$ kg/mm²)

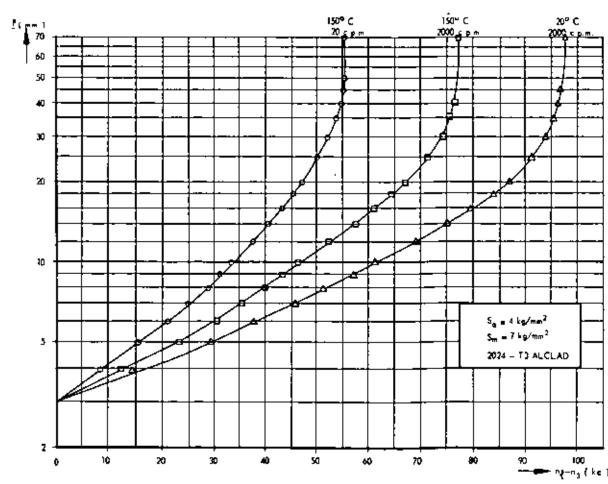

Fig. 3 Influence of the temperature and the frequency on the crack propagation ($S_a = 4$ kg/mm²)

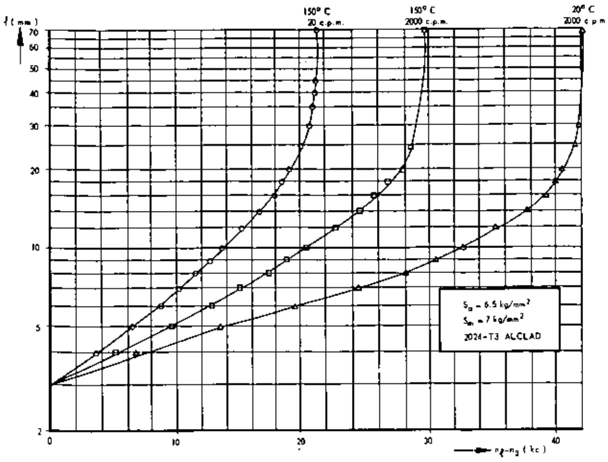

Fig. 4 Influence of the temperature and the frequency on the crack propagation ($S_a = 6{,}5$ kg/mm²)

plotted in figs. 2, 3 and 4 for the three S_a-values respectively. The trends of the figures are the same, i.e. crack propagation at 2000 cpm is faster at 150°C than at 20°C and secondly crack propagation at 150°C is faster for the lower frequency. For the crack propagation life from $l = 3$ mm to $l = 20$ mm (the latter value corresponds to 25% cracked area) the results are summarized in table 5. The table shows that the temperature rise from 20°C to 150°C reduces the crack propagation life with an amount of approximately 30% and lowering the frequency from 2000 cpm to 20 cpm gives a reduction of another 30%.

TABLE 5

Crack propagation life for extending the crack from $l = 3$ mm to $l = 20$ mm, as affected by temperature and frequency

S_a	Temperature effect			Frequency effect		
(kg/mm²)	n_{20}–n_3 (kc)		reduction	n_{20}–n_3 (kc)		reduction
	20°C	150°C	(%)	2000 cpm	20 cpm	(%)
2.5	263.5	190.6	28	190.6	132.4	31
4	87.0	67.0	23	67.0	47.1	30
6.5	40.6	27.9	31	27.9	19.1	32

Crack rates dl/dn were calculated for each specimen as average crack rates over the interval l_i to l_{i+1}, where l_i successively takes the values of the first column of tables 1–3. The crack rates were plotted against $l = \frac{1}{2}(l_i + l_{i+1})$ and curves were drawn through the data points. These curves were collected in figs. 5, 6 and 7. The figures confirm the trends of figs. 2–4 and table 5. In addition they shown that the temperature effect and the frequency effect are at a maximum for smaller values of the crack length. Both effects are disappearing at higher values of the crack length and the crack rate. For the three stress amplitudes this occurs at approximately the same value of the crack rate, which is about 4 mm/kc. The corresponding value of l is obviously larger for the smaller stress amplitude.

3.2 *Fractographical observations*

On a macro-scale the fracture surface shows the so-called transition phenomenon (ref. 9). During crack propagation the crack front is slightly curved and approximately perpendicular to the growing direction.

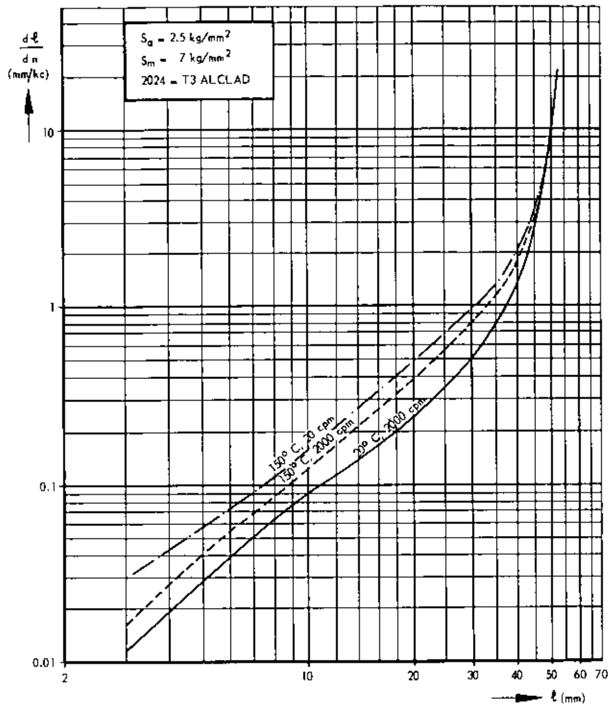

Fig. 5 The crack rate as a function of the crack length for $S_a = 2.5$ kg/mm²

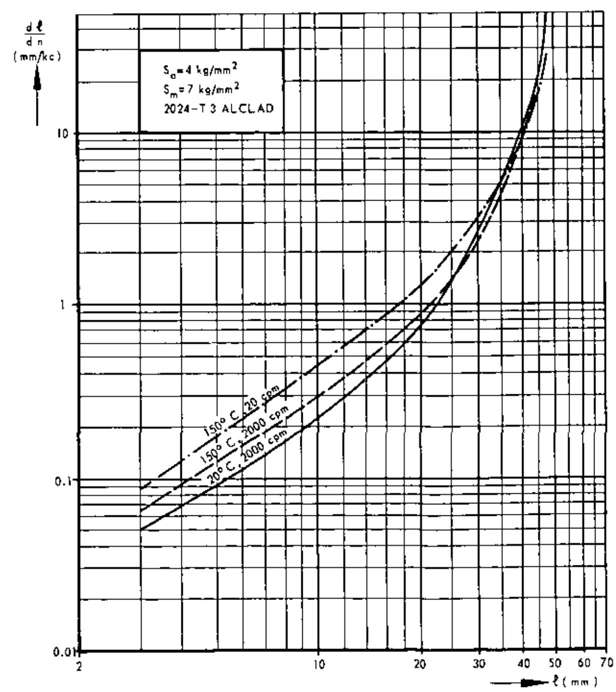

Fig. 6 The crack rate as a function of the crack length for $S_a = 4$ kg/mm²

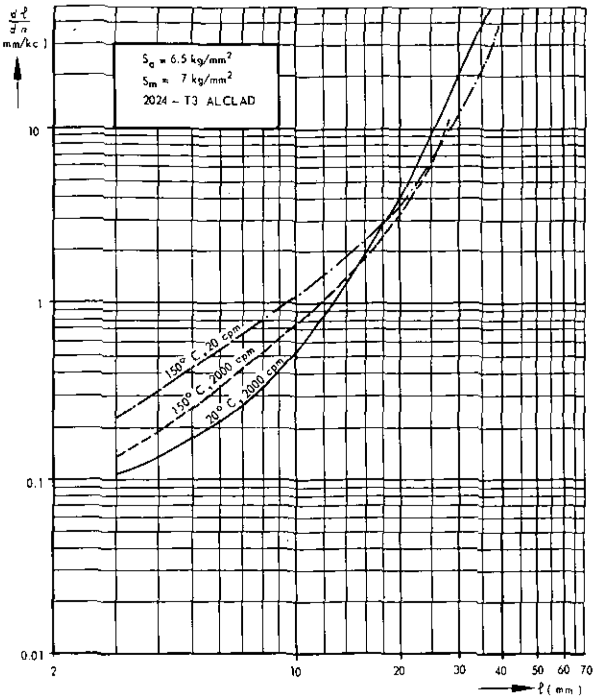

Fig. 7 The crack rate as a function of the crack length for $S_a = 6.5$ kg/mm²

Initially the fracture surface is perpendicular to the loading direction (90°-mode). Shear lips (45°-mode) are formed at the two surfaces of the specimen, and they are becoming broader as the crack is growing. When they have a width of half the specimen thickness, the 90°-mode has terminated and either a single shear or a double shear fracture surface is the result. The end of the 90°-mode (at the center of the specimen) was indicated as the transition point in previous NRL publications (e.g. refs. 1, 2 and 9).

In the present test series the development of shear lips was clearly noticed on the specimens tested at room temperature. However, in the specimens tested at 150°C, although the transition of the 90°-mode to the 45°-mode did occur, the shear lips did not so clearly develop, i.e. the boundary between the shear lips and the central 90°-mode of the fracture was less distinct and it was practically impossible to indicate the transition point. This applies to the specimens tested at both the high and the low frequencies. The impression was obtained that the 90°-mode extended to a greater crack length than in specimens tested at 20°C; however, in view of the vagueness of the transition point this observation cannot be expressed quantitatively.

It is noteworthy that the tests at room temperature reported in ref. 9 and also carried out at 2000 cpm and 20 cpm on specimens of the same material, have shown a clear transition at both frequencies. The 90°-mode was somewhat more extensive at the lower frequency.

On a micro-scale growth lines could be observed with a spacing approximately equal to the crack extension per cycle. The growth lines indicate the successive positions of the crack front and confirm that growth occurs in each load cycle as found previously (refs. 9 and 10). On the specimens tested at room temperature the growth lines were easily visible in the cladding layer while their observation in the core material was more difficult. This is in agreement with previous experience (ref. 9). On the specimens tested at 150°C the growth lines in the core occurred more abundantly and could easily be observed irrespective of the loading frequency.

Cross sections of fractured specimens loaded at $S_a = 4$ kg/mm² were prepared for microscopic examination. The plane of the section was parallel to the sheet surface and approximately 0.5 mm below that surface (sheet thickness 2 mm). The fracture was transcrystalline in all cases. Obvious differences between 20°C and 150°C, and 20 cpm and 2000 cpm were not found. The impression was obtained that the fracture path at 150°C for both the low and the high frequencies showed some correlation with crystal planes, a tendency which was practically absent at 20°C.

3.3 *Ageing*

All specimens tested at 150°C were presoaked under load at that temperature for 100 hours before testing. During the test itself this heating was continued, which for the test at the low frequency implied an additional time at temperature of about 50 to 300 hours. The heating may be regarded as an artificial ageing of the naturally aged 2024-T3 material. Specimens for static tensile tests were cut from several crack propagation specimens after the fatigue testing had been completed. The static properties are compiled in table 6. Surprisingly enough the table does not indicate any noticeable change of these properties. Some trends of the effect of heating 2024-T3 on its properties as found in the literature are briefly mentioned below.

TABLE 6

The effect of soaking at 150°C and fatigue loading on the static properties

Testing conditions			Static properties¹) after fatigue testing		
Temp.	Freq.	S_a (kg/mm²)	$S_{0.2}$ (kg/mm²)	S_u	δ (2″g.l.)
150°C	20 cpm	2.5	36.5	48.6	17.5%
		6.5	36.4	48.2	17%
	2000 cpm	2.5	36.2	48.3	18%
20°C	2000 cpm	2.5	36.9	48.2	18%
Virgin sheet material			37.1	48.3	19%

¹) Mean values of 4 test results obtained from two pairs of tensile test specimens cut from two different crack propagation specimens.

It is generally found that 2024-T3 (naturally aged) exposed to a temperature of 150°C (~300°F) is not a stable material (refs. 3, 5, 8, 11 and 12). Its room-temperature static properties vary as a function of the heating time. The reversion phenomenon was observed in refs. 3 and 8 while overageing was found to occur after 1 month of heating (ref. 8). Unfortunately the quantitative agreement between data of different sources is not always good. For instance a 100 hours heating period induces an increase of S_u and a decrease of δ according to ref. 8, a negligidale effect on S_u and δ according to refs. 5 and 11 and a decrease of S_u and an increase of δ according to ref. 12. It is thought that these disagreements are a result of different rates of the ageing process, which might be caused by differences of the initial state of the material (amount of strain hardening) and differences in chemical composition. In ref. 3 the alloys 2024 (4.4% Cu and 1.5% Mg) and 2014 (4.1% Cu and 0.7% Mg) exhibited qualitatively the same ageing trends, but quantitatively there were noticeable differences. The conclusion to be drawn is that 2024-T3 is not a stable material at 150°C. Even at somewhat lower temperature the material does not seem to be fully stable (refs. 3 and 8). It is thought that in the present test series the structure of the material was affected by the heating at 150°C. Probably some resolution of GP I zones and some growth of GP 2 zones may have occurred, in spite of the absence of any noticeable change of the static properties at room temperature.

4 Comparison with results of other investigations

Only a few systematic studies of the effect of frequency and temperature on crack propagation in aluminium alloys could be found in the literature.

With respect to the frequency a previous NLR investigation at room temperature was reported in ref. 9. Recently Lachenaud (ref. 6) has published results of an investigation carried out at 150°C. A few isolated results mentioned in the literature will not be considered.

In the NLR test series at 20°C, also performed on 2024-T3 Alclad sheet material the average crack rates for $S_a = 2.4$, 3.3 and 5.5 kg/mm² respectively ($S_m =$ 8.2 kg/mm²) were approximately 30% higher at 20 cpm as compared with crack rates at 2000 cpm. This is quantitatively the same result as found in the present tests at 150°C.

Lachenaud*) carried out tests at 150°C employing two frequencies, viz. 2000 cpm (also on a Schenck machine) and 20 cycles per hour = 0.3 cpm (special test set-up, trapezoid wave form). The latter frequency is extremely low for a fatigue test. The material RR58 was especially developed for high temperature service. Chemical composition and average room temperature properties are indicated in fig. 8. Lacheaud observed a considerable frequency effect, the crack rate at 0.3 cpm being approximately 2.5 times as large as that at 2000 cpm. Some of his results and those of the present and the earlier NLR test series are compared in fig. 8 by plotting the ratio, v, between the average crack rate at a certain frequency and the average crack rate at 2000 cpm as a function of the period of the load cycle (which is the inverse of the frequency). The ratio v can be considered as a relative crack rate, viz. relative to the crack rate at 2000 cpm. The crack rates were averaged over certain intervals of crack growth (indicated in fig. 8), since Lachenaud presents his results in this way. The upper limit of the intervals is $2l = 20$ mm and as

RESULTS OF:	TEMP. (°C)	MATERIAL	S_m (kg/mm²)	S_{max} (kg/mm²)	CRACK GROWTH INTERVAL $2l$ (mm)	SPECIMEN SIZE (mm) WIDTH	SPECIMEN SIZE (mm) THICKNESS
△ LACHENAUD	150	RR 58	R = 0.1	16, 20	5 - 20	100	1.5
○ PRESENT REPORT	150	2024 - T3	7	9.5, 11, 13.5	6 - 20	160	2
□ NLR M.2092	20	2024 - T3	8.2	10.6, 11.5, 13.7	8 - 20	160	2

RR 58. COMPOSITION 2.4% Cu, 1.6% Mg, 1.1% Ni, 1.65% Fe, REMAINDER Al, ARTIFICIALLY AGED, AVERAGE PROPERTIES $S_u = 43$ kg/mm², $S_{0.2} = 37$ kg/mm², $\delta = 10\%$

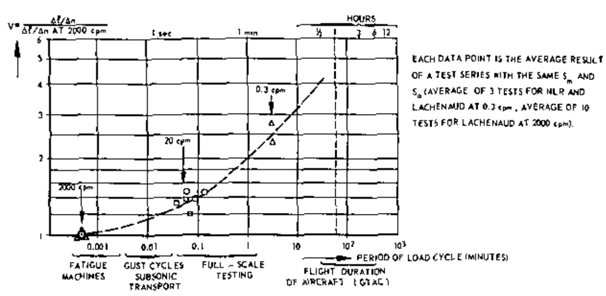

Fig. 8 The effect of frequency on the crack rate in RR58 and 2024-T3 alclad sheet material. Results of Lachenaud (ref. 6) and the NLR (ref. 9 and the present test series).

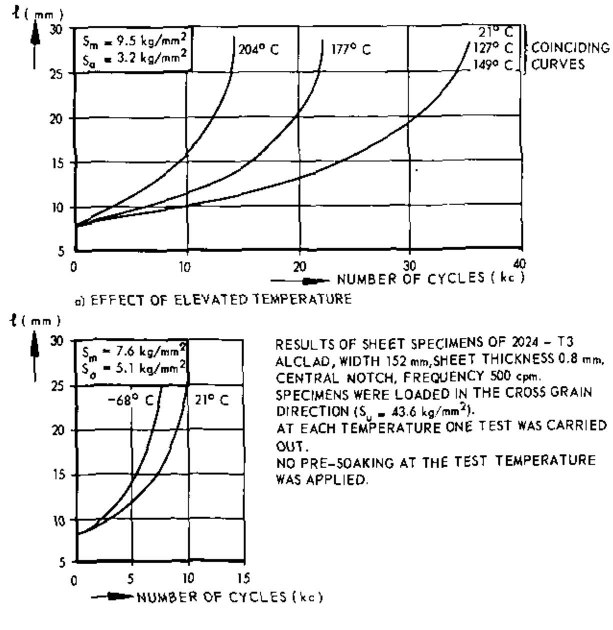

Fig. 9 The effect of temperature on the crack propagation in 2024-T3 Alclad Results of Cristensen (ref. 4).

*) Results of Lachenaud presented in ref. 6a are superseded by those of ref. 6, which gives more information and covers a larger number of tests than ref. 6a.

indicated in the previous chapter for such small macrocracks the frequency effect is maximum.

Fig. 8 shows that despite the differences in testing conditions a consistent trend is noticeable, viz. increasing crack rates for larger periods of the load cycling (lower frequencies). In ref. 6 data for tests on specimens with a width of 50 mm and for the average crack rate for crack extension from $2l = 5$ mm to $2l = 10$ mm are also given. They quantitatively confirm the trend of fig. 8.

The effect of temperature on the crack propagation in aluminium alloy sheet material was also studied by Christensen (ref. 4) and Lachenaud (ref. 6).

The results of Christensen for 2024-T3 Alclad are reproduced in fig. 9. Contrary to the present investigation Christensen did not find a faster crack propagation at 149°C. It should be noted that he did not presoak his specimens before testing. The duration of his tests was in the order of one hour. At 177°C and 204°C crack propagation was faster than at room temperature. Curiously enough the crack rate at a sub-zero temperature (−68°C) was also slightly faster than at room temperature.

Lachenaud's results for RR58 obtained at a stress ratio $R = 0.1$ have been plotted in fig. 10 and for comparison results of the present investigation interpolated for $R = 0.1$ ($S_m = 7$ kg/mm^2, $S_a = 5.73$ kg/mm^2) were added. It is surprising that Lachenaud observes an improvement of the crack propagation life, i.e. the life at 150°C is some 30% larger than the life at room temperature. The present study and the results of Christensen for the temperature effect showed the opposite trend. Fig. 10 further shows that at room temperature the crack propagation life for 2024-T3 was about 60% larger than for RR58, whereas at 150°C the crack propagation life for 2024-T3 was about 30% shorter than for RR58.

5 Crack propagation due to creep

In a recent study (ref. 7) van Leeuwen considered time-dependent plastic deformation and its relation with creep and fatigue. Starting from the Manson-Coffin relation he derived analytic functions for the frequency effect under cyclic loading. Crack growth is obviously a result of plastic deformation, but the conditions are extreme, i.e. the plastic deformation occurs in a small area under a highly inhomogeneous stress distribution and the material has no stable structure. There is some empirical evidence available on crack growth under constant load. Although this evidence is very limited it might shed some light on the relation between the frequency effect on crack growth and the time dependent character of plastic deformation.

Three preliminary tests on crack growth under constant load, $S = 20$ kg/mm^2, were carried out by the NLR at three different temperatures. The same specimens as for the fatigue crack propagation tests were used. The time involved in crack growth from $l = 12$ mm to $l = 20$ mm has been plotted in fig. 11. From the graph one derives that at 150°C 30 hours are required for such a crack extension. In the present fatigue tests S_{max} was much lower than 20 kg/mm^2. A few results on the influence of stress on crack growth under a creep loading at a temperature of 204°C (400°F) were published by Christensen (ref. 4) and are reproduced here in fig. 12. From this figure it follows that at a stress corresponding to the S_{max}-values used in the crack propagation tests the crack growth under creep loading may be in the order of 100 times slower than at $S = 20$ kg/mm^2. If this would approximately apply to 150°C as well, a time in the order of 3000 hours

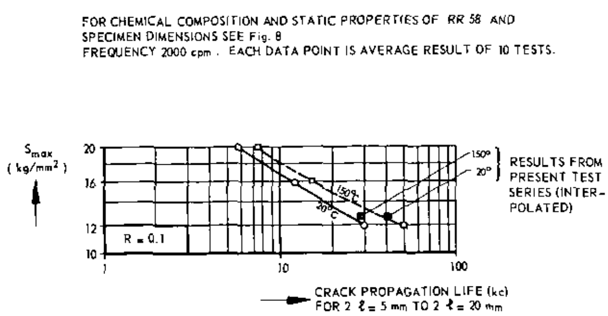

Fig. 10 The effect of temperature on the crack propagation in RR58. Results of Lachenaud (ref. 6).

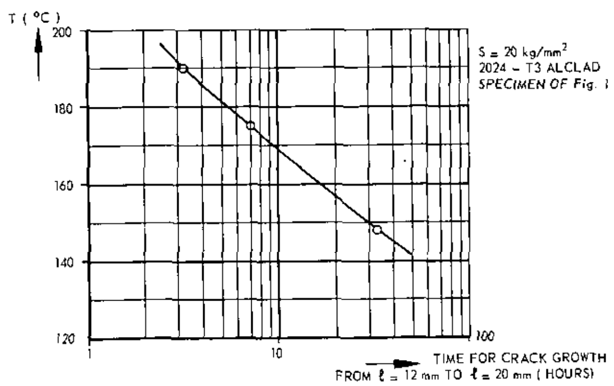

Fig. 11 Effect of temperature on crack growth under creep loading (unpublished NLR results).

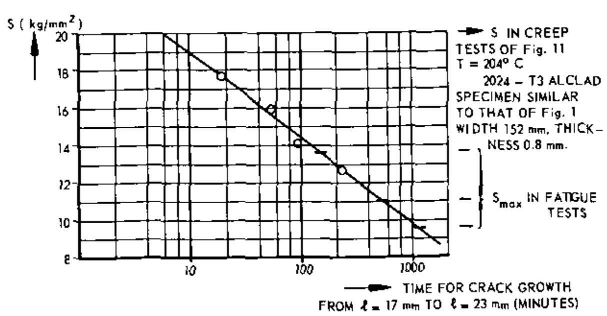

Fig. 12 Effect of stress on crack growth under creep loading. Results of Cristensen (ref. 4).

would be required for crack growth from $l = 12$ mm to $l = 20$ mm under a constant load at stresses corresponding to the S_{max}-values of the present test series. The same amount of crack growth under fatigue loading at the low frequency required testing times of 23, 15 and 9 hours for the three S_{max}-values adopted. This is some orders of magnitude less than the 3000 hours required by creep.

For a comparison of the loading times during the fatigue tests and the creep tests the different circumstances should be considered. During the fatigue test the stress is varying between S_{min} and S_{max} instead of being constant at S_{max}. Although one might speculate that this will further decrease the contribution of creep to crack growth no empirical evidence seems to be available for aluminium alloys to answer this question. Secondly the mode of fracture is not necessarily the same for fatigue and creep. Microscopic specimens were prepared from the creep specimen tested at 150°C and the fatigue specimen tested at the same temperature, the highest amplitude ($S_a = 6.5$ kg/mm^2 and $S_{max} = 13.5$ kg/mm^2) and the low frequency. In the creep specimen grainboundary separations had formed in the neighbourhood of the crack at small values of the crack length (low crack growth rate and therefore a long time at a high stress level). An example is shown in fig. 13. The impression from the microscopic examination was that the crack was partly intercrystallyne although its growth mainly occurred in a transcrystalline way. In the fatigue specimen no grain boundary separations were found and the crack was certainly transcrystalline. Although there are probably differences between the fracture modes for creep and fatigue at the temperatures of present interest a more specialized study would be required to indicate these differences. This was beyond the scope of the present investigation. If there are differences it might again be speculated that the combined effect of fatigue and creep will be less than additive.

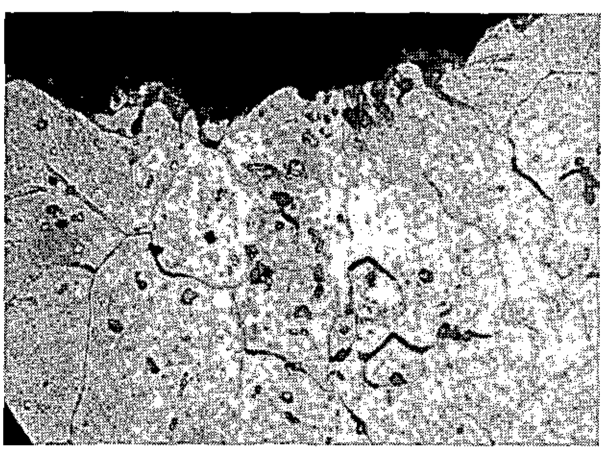

Fig. 13 Micrograph (400 ×) of the specimen tested at 150°C under a constant loading ($S = 20$ kg/mm^2) showing grain boundary separations near the main crack (at top of photo).

In view of the large discrepancy between the time under load in the present crack propagation tests and the time required for the same amount of crack growth in a creep test it is now tentatively concluded that the crack growth in the present test series was primarily caused by the cyclic character of the loading, i.e. it was due to fatigue rather than creep. This is substantiated by fig. 11 which shows a large temperature effect on crack growth under creep loading, whereas the present test series show a small effect of temperature on fatigue crack growth, since the crack rate at 150°C was only 30% higher than a at room temperature.

6 Discussion

Three outstanding features of the previous chapter are:

(1) In the 2024-T3 alloy the fatigue crack propagation mechanism at 150°C seems to be different from the mechanism operating at room temperature, although it is still mainly due to the cyclic nature of the load rather than being due to creep. (2) For the RR58 material a rise of temperature from 20°C to 150°C has a favourable effect on the crack rate, whereas for the 2024-T3 material the opposite applies. (3) In 2024-T3 Alclad the crack propagation at 20 cpm was approximately 30% faster than at 2000 cpm at both room temperature and 150°C. Some more thoughts on these questions are presented in this chapter and it will be tried to arrive at a tentative explanation.

The following aspects seem to be important:

(a) Fatigue is a consequence of cyclic slip and this also applies to the growth of fatigue cracks. The crack rate depends on the amount of cyclic slip in the crack tip region and on the conversion of cyclic slip into crack extension. The latter depends on the tensile stress in the crack tip region. These views on crack growth are more extensively evaluated in ref. 10.

(b) An important difference between 2024-T3 at room temperature and at 150°C is that GP 1 zones are present at room temperature and probably not or to a lesser extent at 150°C.

(c) An important difference between 2024-T3 at 150°C and RR58 at 150°C is that in the former material the precipitates (mainly GP II) are less stable than in the latter one. In 2024-T3 ageing at 150°C will lead to a lower ductility whereas ageing in the RR58 will not occur, or far less extensively, since this material has been artificially aged at 200°C by the manufacturer. The static properties of RR58 are fairly stable up to heating periods of 1000 hours (refs. 6a en 13). The ageing of the 2024-T3 at 150°C may be further enhanced by cyclic slip. The size of the plastic zone at the tip of the crack can be estimated with eq. (B32) of ref. 10 and considering the crack rates as found in the present test series it was calculated that the number of cycles during which a point along the crack path is in the plastic zone until it is reached by the crack front is in the order of 4000 to 1000 cycles for $l = 3$ to 10 mm. Although the number will further decrease for higher l-values the crack will always meet with material which has seen many cycles of plastic deformation.

(d) In a fully stable material the effect of a temperature rise on crack propagation will be twofold, viz. (1) in general the yield stress will decrease allowing more levelling off of the peak stress at the tip of the crack and (2) thermal activation will increase the amount of cyclic slip. The former will cause a deceleration of the crack, whereas the latter will have an accelerating effect, see aspect (a) above.

The results of the RR58 material will be considered first, since this is the more stable material. Aspect (d) then seems to be applicable. The lower crack rate at 150°C (see fig. 10) can be attributed to the lower yield stress at that temperature, allowing a lower peak stress at the tip of the crack, and the frequency effect at 150°C (see fig. 8) can be attributed to the thermal activation of slip. For the latter, interactions with precipitated zones may be important.

In the more unstable 2024-T3 material the phenomena are more complex. The frequency effect is the same at 20°C and 150°C. Now it is difficult to think of a time-dependent mechanism which is independent of temperature. It is therefore suggested that different mechanisms are responsible for the frequency effects at the two temperatures, which is confirmed by the fractographic observations. The activation energy for the mechanism causing the frequency effect at 150°C should be larger than for the mechanism causing the frequency effect at room temperature in order to yield the same quantitative frequency effect. In view of what has been said under aspects (b) and (c) above it is though that the frequency effect is associated with GP I zones at room temperature and with GP II zones (and the absence of GP I) at 150°C. It will not be tried here to speculate in any further detail on these mechanisms but it may be said that these zones do not have a great stability at the temperatures concerned.

The temperature effect in the 2024-T3 material is tentatively attributed to the change of the state of precipitation, i.e. to the resolution of GP I and the growth of GP II at 150°C. Both the time at temperature (150°C) and the amount of cyclic slip were not very much different for the specimens tested at the low and the high frequencies. These two factors may be responsible for the change of the state of precipitation. The change will be associated with a decreased ductility which usually causes an increased crack rate (ref. 2) as a consequence of a less effective levelling-off of the peak stress at the tip of the crack.

It has to be pointed out once again that the above discussion has a tentative character. One also should keep in mind that the temperature effect and the frequency effect on the crack rate, both found to be approximately 30% for the 2024-T3 material in the present test series, although being systematic, are in fact fairly small.

7 Conclusions

In the present report results are reported from fatigue crack propagation tests on 2024-T3 Alclad sheet specimens, tested at a mean stress of 7 kg/mm² and stress amplitude of 2.5, 4 and 6.5 kg/mm². Tests were carried out at (1) 2000 cpm and 20°C, (2) 2000 cpm and 150°C and (3) 20 cpm and 150°C. The frequencies 2000 cpm and 20 cpm are nominal values; in the tests the high frequencies were slightly larger than 2000 cpm and the low frequencies somewhat lower than 20 cpm. A few exploratory tests were performed on crack growth at elevated temperature under constant load (creep conditions). Relevant information from the literature was summarized. The following results and conclusions were obtained.

1. For crack propagation up to a crack length $2l = 40$ mm (specimen width 160 mm) the crack propagation at a frequency of 2000 cpm was 30% faster at 150°C than at room temperature. At a temperature of 150°C it was another 30% faster at 20 cpm than at 2000 cpm. The temperature effect and the frequency effect both decreased and finally vanished at higher values of the crack length.
2. Fractographic observations indicated that the fracture mechanism was affected by the temperature rise from 20°C to 150°C. At the latter temperature the transition from the tensile mode to the shear mode was less pronounced, and microscopic growth lines, indicating the successive positions of the crack front, were better visible.
3. Heating of the sheet material at 150°C for periods up to 400 hours did not noticeably change its room temperature static properties. Despite this result the state of precipitation at 150°C is not a stable one.
4. Results of Lachenaud for the artificially aged alloy RR58 showed a frequency effect at 150°C which was consistent with the present results. However, contrary to the present results and those of Christensen for 2024-T3, the crack propagation in RR58 at 150°C was slightly slower than at room temperature.
5. Crack growth at 150°C under a constant load is possible; however, it occurs so slowly that the fatigue crack propagation at 20 cpm and 150°C has

still to be ascribed to the cyclic character of the load rather than to creep.

6. A few exploratory tests indicated a large increase of the crack growth rate under constant loading when the temperature increased.
7. The trends observed were tentatively related to the unstable structure of the 2024-T3 material.

8 References

[1] Broek, D. and Schijve, J., The effect of sheet thickness on the fatigue crack propagation in 2024-T3 Alclad sheet material. NLR Report M.2129, April 1963.

[2] Broek, D., Schijve, J. and Nederveen, A., The effect of heat treatment on the propagation of fatigue cracks in light alloy sheet material. NLR Report M.2134, May 1963.

[3] Calvet, J. and Martinod, H., La réversion, cause d'un affaiblissement passager de certains alliages d'aluminium soumis à un échauffement. La Recherche Aéronautique, No. 79, p. 27, 1960.

[4] Christensen, R. H., Prediction of cumulative fatigue-crack growth under complex environments. Douglas Engineering Paper no. 1461, Oct. 1962.

[5] Dunsby, J. A., Some effects of time at temperature on 24 S-T aluminium alloy. Canadian Aero. Journal, vol. 7, 1961, p. 201. Also N.R.C. Report MS-102, 1960.

[6] Lachenaud, R. and Jaillon, P., Influence de la fréquence et de la température sur la vitesse de propagation des criques en fatigue. Sud-Aviation, Procès-Verbal No. 26.712/4, Sep. 1964.

[6a] Lachenaud, R., Fatigue strength and crack propagation in AU2GN alloy as a function of temperature and frequency. ICAF-AGARD symposium, Rome, April 1963, Pergamon Press, p. 77.

[7] Van Leeuwen, H. P., Frequency effects in fatigue. AGARD Structures and Materials Panel. Working Paper S-22, Addendum I, May 1964.

[8] Nock, Jr. J. A., Reheating of 24S and 75S aluminum sheet The Iron Age, Dec. 25, 1947.

[9] Schijve, J., Broek, D. and de Rijk, P., The effect of the frequency of an alternating load on the crack rate in a light alloy sheet. NLR Report M.2092, Sep. 1961. See also: Advances in Aeronautical Sciences, vol. 3, p. 387, Pergamon Press, 1961.

[10] Schijve, J., Analysis of the fatigue phenomenon in aluminium alloys. NLR-TR M.2122, April 1964.

[11] Stickley, G. W. and Anderson, H. L., Effects of intermittent versus continuous heating upon the tensile properties of 2024-T4, 6061-T6 and 7075-T6 alloys. NACA Tech. Memo 1419, Aug. 1956.

[12] Strength of Metal Aircraft Elements. MIL-Handbook-5, March 1961.

[13] Hiduminium RR58 sheet. The high strength sheet for high temperatures. Pamphlet of High Duty Alloys Ltd.

C.C.L. Class. G 042: G 311

REPORT NLR-TR M.2142

The effect of the sheet width on the fatigue crack propagation in 2024-T3 Alclad material.

by

J. Schijve, A. Nederveen and F. A. Jacobs

Summary

The size effect on crack propagation was studied with sheet specimens of 2024-T3 Alclad. Values of the width were 80, 160, 300 and 600 mm, sheet thickness 3 mm, mean stress 8 kg/mm^2 and stress amplitudes 2.5, 4 and 6.5 kg/mm^2. Results are compared with the theory of the stress intensity factor and the Weibull theory. Practical implications of the results are indicated.

Contents

List of symbols

C	— correction factor for specimen width
C_1, C_2, C_3	— constants
dl/dn	— crack rate
k	— stress intensity factor
k_W	— stress intensity factor for Weibull test
l	— half crack length, see fig. 1
l_{tr}	— crack length at transition from tensile to shear mode fracture
m	— constant
n	— number of cycles
r, θ	— polar co-ordinates from tip of crack
R	— stress ratio $= S_{min}/S_{max}$
S	— stress
S_a	— stress amplitude (gross stress in specimen)
S_m	— mean stress (gross stress in specimen)
S_{max}	— maximum stress of cycle (gross stress in specimen)
S_{min}	— minimum stress of cycle (gross stress in specimen)
S_{net}	— net stress in specimen, based on uncracked area
$S_{0.2}$	— yield stress
S_u	— ultimate stress
w	— half width of specimen, see fig. 1
β	— constant
δ	— elongation
kc	— kilocycle = 1000 cycles

1 kg/mm^2 = 1,422 psi, 1000 psi = 0.703 kg/mm^2
1 mm = 0.04″, 1″ = 25.4 mm

1 Introduction

One of the principal factors determining the safety of an aircraft with respect to fatigue is the rate of propagation of fatigue cracks. At present it is common practice to perform ad-hoc fatigue tests on prototype structures and to study the crack propagation in these tests. The information obtained will be used for establishing maintenance and inspection procedures for the aircraft in service. In the design stage of the

This investigation has been performed under contract for the Netherlands Aircraft Development Board (NIV)

aircraft it is one of the aims of the designer to secure that crack rates will be as low as possible. For this purpose he has to consider the stress levels in his structure, the type of material and the type of structure. The NLR has recently performed several test series to investigate the effect of various parameters on fatigue crack growth in aluminium alloys, such as the mean stress, the type of alloy and heat treatment, the sheet thickness, the frequency and the temperature. In the present test series the influence of the width of a sheet on the crack propagation is studied.

The amount of crack propagation data in the literature is steadily increasing. Unfortunately, the dimensions of the specimens are different for most investigations. With respect to the effect of the specimen width on the results obtained two more or less obvious assumptions can be made:

1. The crack rate in millimeters per cycle is independent of the specimen width (for the same crack length)
2. The crack growth per cycle as a percentage of the specimen width is independent of this width (for the same percentage cracked area).

In the present test series fatigue crack propagation in 2024-T3 Alclad sheet material was recorded in specimens with a width of 80 mm, 160 mm, 300 mm and 600 mm, respectively (3.15", 6.3", 11.8" and 23.6"). The mean stress was 8 kg/mm² (11.4 ksi) and the stress amplitudes were 2.5, 4 and 6.5 kg/mm² (3.6, 5.7 and 9.2 ksi). The report gives a presentation and evaluation of the crack propagation data. Secondly, a comparison is made with predictions according to the theory of the stress intensity factor and the Weibull theory. Test results available in the literature are reviewed. Finally, some attention is paid to the practical implications of the results.

2 Experimental details

2.1 *The material and the specimens*

The specimens were cut from 2024-T3 Alclad sheet material with a thickness of 3 mm (0.125"). The nominal composition of the core material is: 4.5% Cu, 1.5% Mg, 0.6% Mn, remainder Al. The mechanical properties were determined with eight specimens in the longitudinal direction of the sheet and one specimen in the transverse direction. The results are given in the table below:

2024-T3 Alclad	$S_{0.2}$		S_u		δ (2" gage length)
	kg/mm²	ksi	kg/mm²	ksi	
Long. direction (average)	35.8	50.9	47.8	68.0	16.5%
Trans. direction	35.3	50.2	47.6	67.7	18%

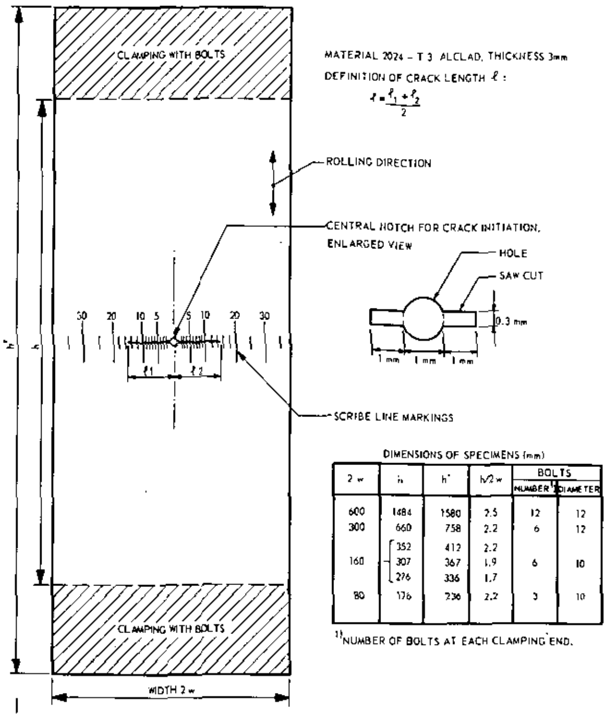

DIMENSIONS OF SPECIMENS (mm)

2w	h	h'	h/2w	BOLTS NUMBER[1]	BOLTS DIAMETER
600	1484	1580	2.5	12	12
300	660	758	2.2	6	12
160	352	412	2.2	6	10
	307	367	1.9		
	276	336	1.7		
80	176	236	2.2	3	10

[1] NUMBER OF BOLTS AT EACH CLAMPING END.

Fig. 1 Dimensions of the specimens.

Specimens of four different sizes were tested. The dimensions are shown in fig. 1. The characteristic dimension is the specimen width. The four values of the width are 600 mm, 300 mm, 160 mm and 80 mm (23.6", 11.8", 6.3" and 3.15"). Each specimen was provided with a sharp central notch for crack initiation. The notch consisted of a hole (diameter 1 mm) and two saw cuts (depth 1 mm). Line markings were inscribed on the cladding to facilitate recording of the crack growth, see fig. 1. The same type of specimen was previously used in several NLR investigations on fatigue crack propagation.

The sheet material available for the present investigation was limited to two sheets of 350 x 122 centimeters. Instead of limiting either the number or the size of the largest specimens it was decided to cut the smaller specimens from the larger ones after the latter had been tested. It was then possible to have eight specimens of the largest size. Moreover, there was an additional advantage, viz. the risk of a variation of crack propagation properties is obviously smaller if specimens are cut from larger ones. The mapping of the specimens in the two sheets is shown in figs 2a and 2b. The smaller specimens were located in the central part of the larger specimens (i.e. in the shadow of the growing crack) in order to secure that the stresses in the material of the smaller specimens had been relatively low in the preceding tests on the larger specimens from which they were cut.

2.2 *Testing procedures*

For all specimens the mean stress S_m was 8 kg/mm² (11.4 ksi). Tests were carried out at stress amplitudes

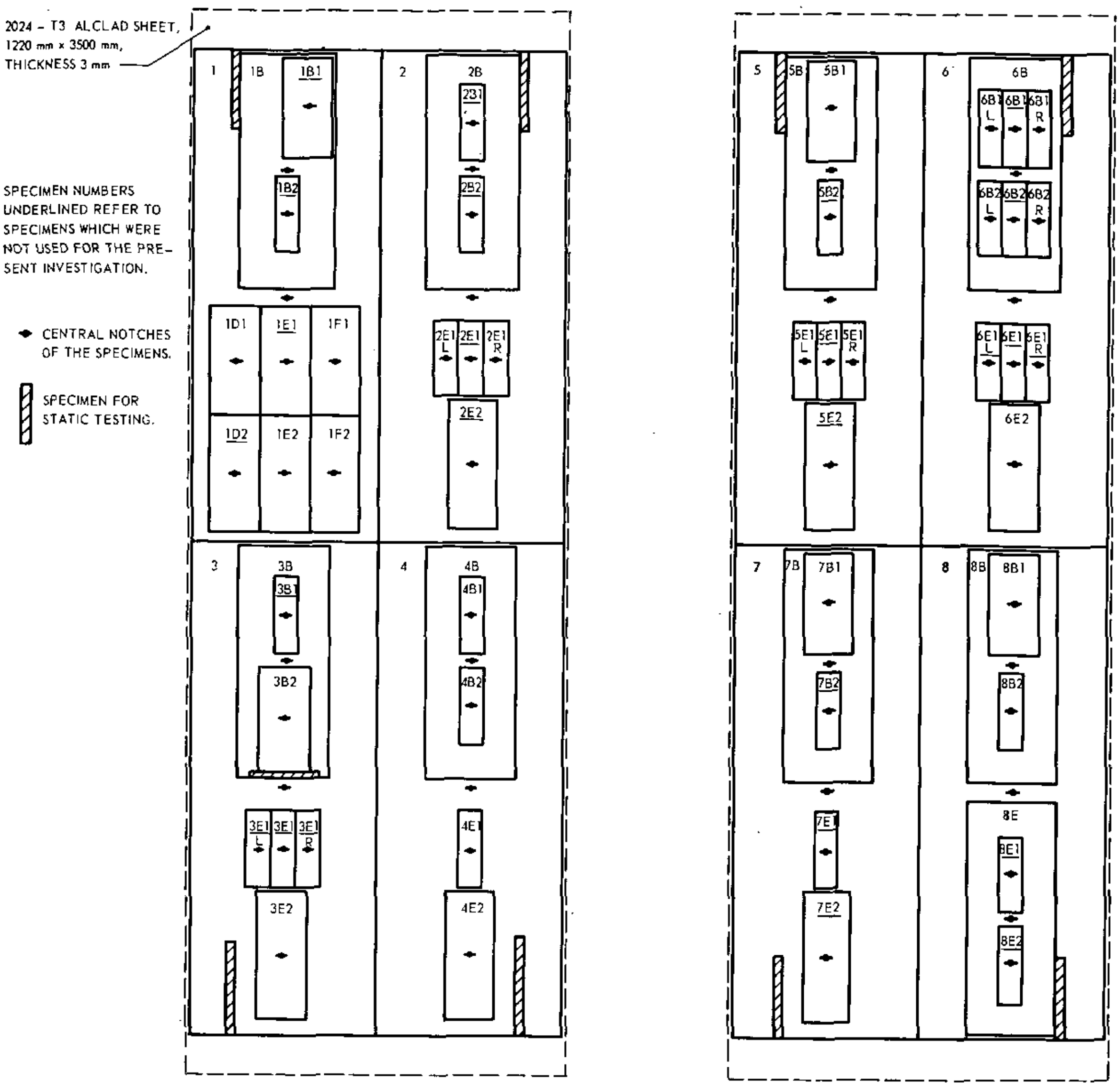

Fig. 2 Mapping of the specimens in the two sheets. Fig. 2a First sheet. Fig. 2b Second sheet.

$S_a = 2.5$ kg/mm^2, $S_a = 4$ kg/mm^2 and $S_a = 6.5$ kg/mm^2 (3.56, 5.69 and 9.24 ksi, respectively), usually three tests at each stress amplitude.

All specimens were tested in the same fatigue machine, viz. a 50 tons Amsler hydraulic pulsator, at a frequency of 250 cycles per minute. The ends of the specimen were clamped with bolts between two steel plates (thickness 10 mm each, height 140 mm). These plates were connected to the machine by a simple lever mechanism for securing a homogeneous load transmission into the specimen. Strain gage measurements on a specimen with the largest width ($2\ w = 600$ mm), which were carried out before the central notch was made, indicated a fully satisfactory stress distribution in the specimen.

For the smallest specimens (width 80 mm) the loads were fairly low for application by a 50 tons machine. Therefore two specimens of this type were tested in parallel, see fig. 3. If one of the two specimens broke it was replaced by a dummy specimen and testing was continued.

Strain gage measurements were made during each crack propagation test for checking the dynamic load. For the largest specimens (width 600 mm) the strain gages were bonded to the specimen itself near the clamping. The gages could therefore be used in the first part of the test only when the crack growth had not yet noticeably affected the stress distribution near the clamping. For the specimens of the other sizes a strain gage bridge was bonded on the element connecting the lever system to the fatigue machine. The gages were first calibrated statically.

3 Test results

3.1 *Crack progagation data*

The results of all specimens are compiled in tables 1, 2 and 3 by presenting the number of cycles (Δn) involved

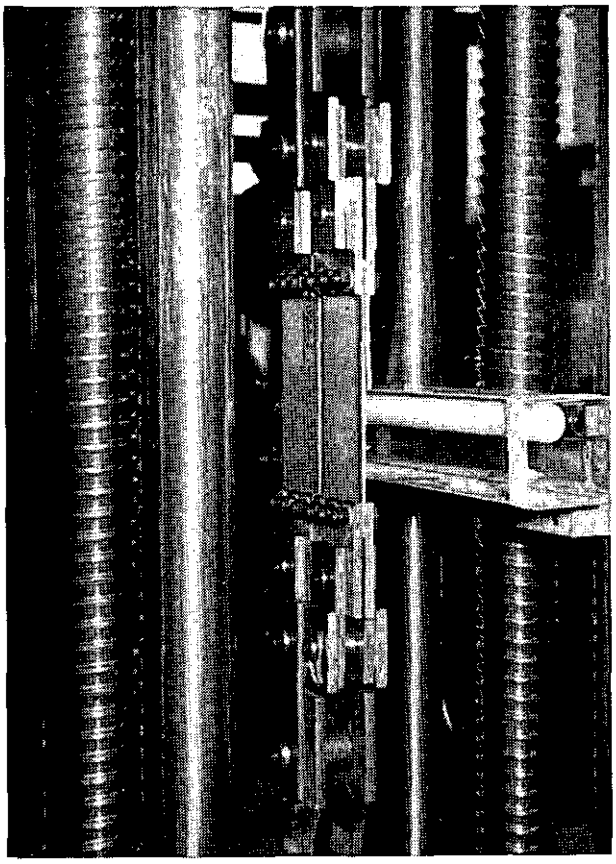

Fig. 3 Two specimens with a width of 80 mm tested in parallel.

in the growing of the crack through successive small crack length intervals (from l_i to l_j). The Δn values are the averages for the two cracks in one specimen. The tables also give the mean results ($\bar{\Delta n}$) for one group (usually three) of similarly tested specimens. The $\Sigma\,\bar{\Delta n}$ values yield the average crack propagation curves which were plotted in figs 4, 5 and 6.

From the $\bar{\Delta n}$ values the average crack rates were calculated as:

$$\mathrm{d}l/\mathrm{d}n = (l_j - l_i)/\bar{\Delta n}\ .$$

These crack rates were plotted as a function of the crack length $l = \frac{1}{2}(l_i + l_j)$ in figs 7, 8 and 9.

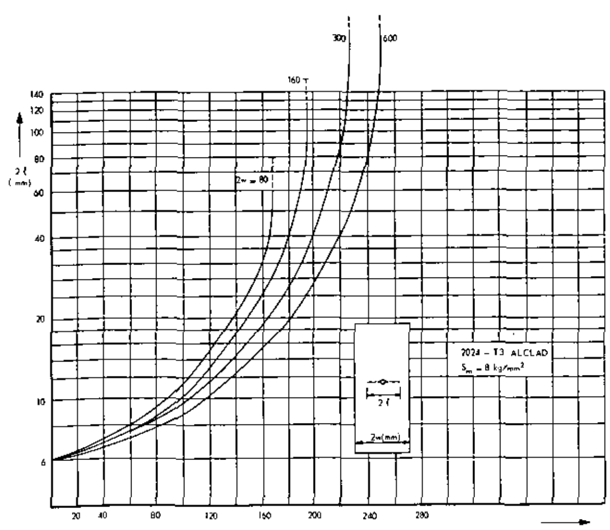

Fig. 4 Avarage crack propagation curves at S_a = 2.5 kg/mm^2.

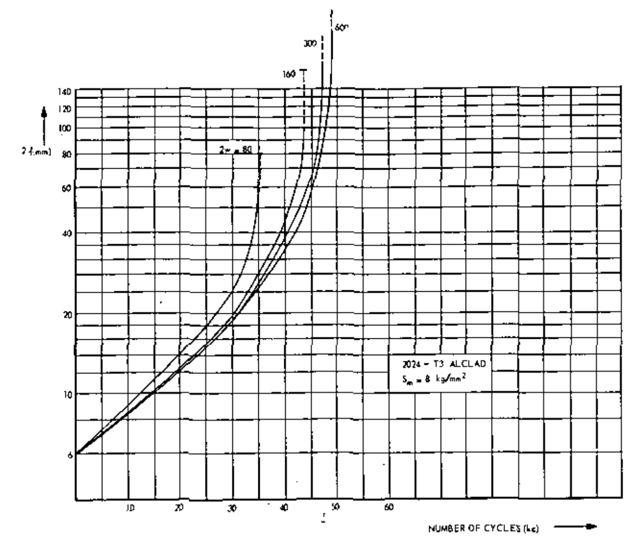

Fig. 5 Average crack propagation curves at S_a = 4 kg/mm^2.

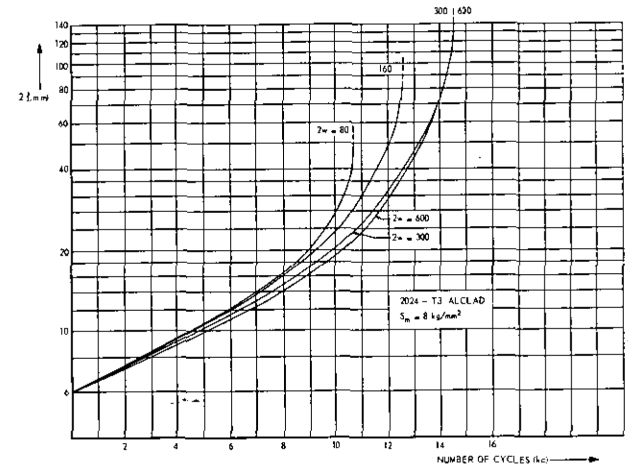

Fig. 6 Average crack propagation curves at S_a = 6.5 kg/mm^2.

3.2 *Fractographic observations*

The fatigue cracks start growing in a plane perpendicular to the loading direction, which will be called the tensile mode of fracture. During its growth the fracture develops shear lips at the two sheet surfaces and finally the crack is growing in either single or double shear. This is more extensively described elsewhere (see for instance refs 3, 4 and 5). The crack length at which the tensile mode terminates in the centre of the sheet is indicated by l_{tr} and this marks the point at which the transition from the tensile mode to the shear mode was completed. Values of l_{tr} have been compiled in table 4, which shows that l_{tr} does not depend on the sheet width. It should be noted that measurements of l_{tr} are not particularly accurate in view of the gradual transition from the tensile mode to the shear mode.

Although after the transition single shear was more frequently observed than double shear, the latter was not at all rare. Also, it occurred that double shear was followed at greater crack lengths by single shear. If double shear persisted the direction of crack growth deviated slightly from the normal to the loading direction, the angle of deviation being approximately 9°. Such a deviation did not occur for a single shear crack.

4 Discussion

4.1 *The trends of the test results*

The crack propagation curves in figs 4, 5 and 6 show a small, but consistent effect of the specimen width; the crack was growing faster in the smaller specimen. However, the effect is almost negligible for the smaller

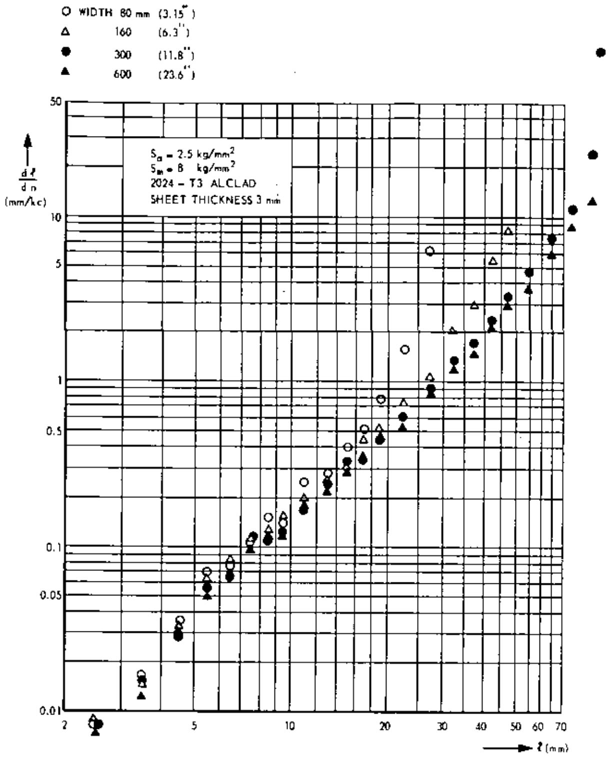

Fig. 7 The crack rate as a function of crack length for S_a = 2.5 kg/mm².

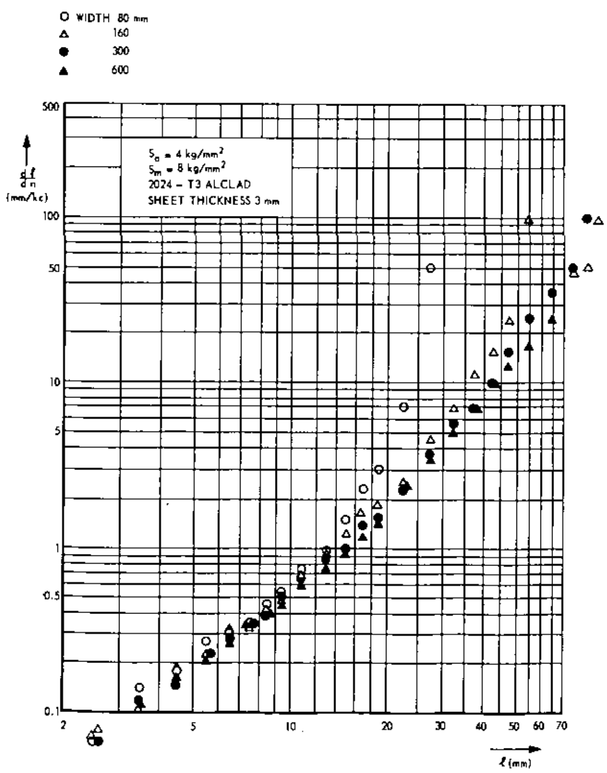

Fig. 8 The crak rate as a function of the crack length for S_a = 4 kg/mm².

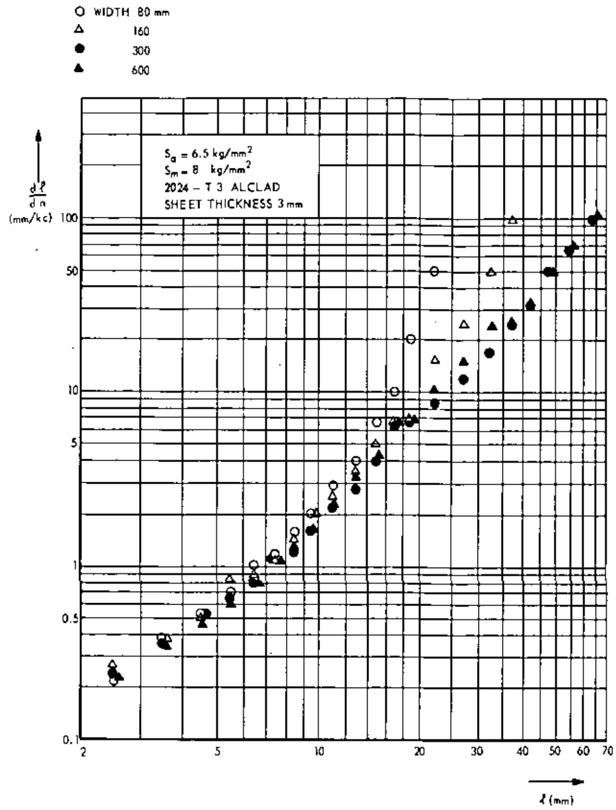

Fig. 9 The crack rate as a function of the crack length for S_a = 6.5 kg/mm².

values of the crack length. A better appreciation can be obtained from figs 7, 8 and 9, which confirm that the crack rate is almost independent of the specimen width for small cracks, while for large values of the crack length the crack rate is higher in the smaller specimen. The latter result could obviously be anticipated, but the former one might be surprising according to some theoretical predictions. In the following sections the trends of the present results are compared with the trends as predicted by a few theories published in the literature.

4.2 *Theory of the stress intensity factor*

For a material which remains elastic the stress field around a crack in an infinite sheet was known as early as 1913 (ref. 9). From the exact solution an asymptotic solution, which is valid in the immediate vicinity of the tips of the crack only, can be derived. Contrary to the exact solution the asymptotic solution allows an analytic presentation which is easily evaluated and appreciated. For an infinite sheet loaded in tension perpendicular to the crack the asymptotic solution is:

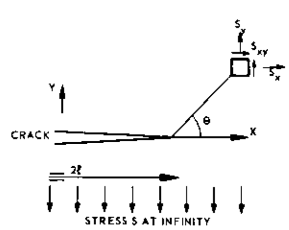

$$S_y = S\sqrt{l}\sqrt{\frac{1}{2r}}\cos\frac{\theta}{2}\left(1+\sin\frac{\theta}{2}\sin\frac{3\theta}{2}\right) \quad (1)$$

$$S_x = -S+S\sqrt{l}\sqrt{\frac{1}{2r}}\cos\frac{\theta}{2}\left(1-\sin\frac{\theta}{2}\sin\frac{3\theta}{2}\right) \quad (2)$$

$$S_{xy} = S\sqrt{l}\sqrt{\frac{1}{2r}}\cos\frac{\theta}{2}\sin\frac{\theta}{2}\cos\frac{3\theta}{2} \quad (3)$$

These equations in a somewhat different form were published by Sneddon (ref. 21). Since the stresses in the tip region are high, the constant term ($-S$) in eq. (2) can be neglected and the eqs (1), (2) and (3) may generally be written as

$$S_{x_ix_j} = k\sqrt{\frac{1}{2r}}f_{ij}(\theta) \quad (4)$$

with the stress intensity factor $k = S\sqrt{l}$

Equations (4) and (5) imply that for arbitrary values of S and l the (elastic) stress field around the tip of the crack is completely described by the stress intensity factor k.

Similar equations have been published for several configurations of cracked specimens and various types of loading. They are summarized in ref. 1. However, a general solution for a sheet specimen of finite width as used in the present investigation is not available. A comparable case is the infinite sheet with a number of collinear cracks. Exact solutions were independently derived by Westergaard (ref. 25) and Koiter (ref. 11). The asymptotic solution (valid for small values of r) is:

$$S_{x_ix_j} = k\sqrt{\frac{1}{2r}}f_{ij}(\theta) \quad (6)$$

with the same $f_{ij}(\theta)$ as in eq. (4), for $2w$ = infinite, and

$$k = C\,S\sqrt{l} \quad \text{with} \quad C = \left(\operatorname{tg}\frac{\pi l}{2w}\Big/\frac{\pi l}{2w}\right)^{\frac{1}{2}} \quad (7)$$

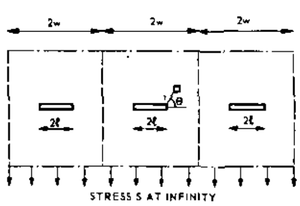

The factor C was derived by Irwin (ref. 10). The factor should be considered as a correction factor for the finite width of the specimen, showing how much the stresses are larger than for the case $2w$ = infinite.

The stress intensity factor k was introduced by Irwin for fracture toughness problems. It was adopted by Paris et al. (refs 14, 15 and 16) for fatigue crack propagation. Starting from the idea that k describes the stress field around the tip of the crack, Paris assumes that k alone is controlling the rate of crack propagation

$$\frac{dl}{dn} = f(k) \quad (8)$$

The asymptotic solutions (eqs 1–8) lose their validity when plastic deformations occur at the tip of the crack. Therefore the applicability of eq. (8) will probably be better if the plastic zone is small. It can be easily shown that the size of this zone is approximately proportional to $lS^2/S_{0.2}^2 = k^2/S_{0.2}^2$ (see for instance eqs B31 and B32 of ref. 20). In other words, the usefulness of eq. (8) will probably be better if the stresses are low as compared with the yield stress $S_{0.2}$. This applies to fatigue crack propagation in the low-ductility aluminium alloys. The usefulness of eq. (8) was clearly confirmed by Paris and his co-workers for aluminium alloys and was further shown in other investigations (refs 2, 4 and 8). The majority of data was obtained, however, in tests for which either $S_m = 0\,(R = -1)$ or $S_{min} = 0\,(R = 0)$. For an arbitrary R-value one should ask whether S_{max} or S_a has to be substituted for S in defining the stress intensity factor. Test results have shown (refs 4 and 8) that neither of these two choices leads to a general applicability of eq. 8. This is confirmed by the present test results in fig. 10. It was empirically shown (refs 2 and 4) that eq. (8) does hold if results for the same R-value are compared, although the function $f(k)$ depends on the value of R. For a constant R-value the ratio between S_{max} and S_a is constant and the ratio between k_{max} (k for $S = S_{max}$) and k_a (k for $S = S_a$) is also constant. In other words if for constant R-values eq. (8) holds for k_{max} it automatically holds for k_a. For a constant R-value there is also a constant ratio between k_{max} and k_{min} (k for $S = S_{min}$), and k_{max} (or k_a) and R fully describe the stress field around the tip of

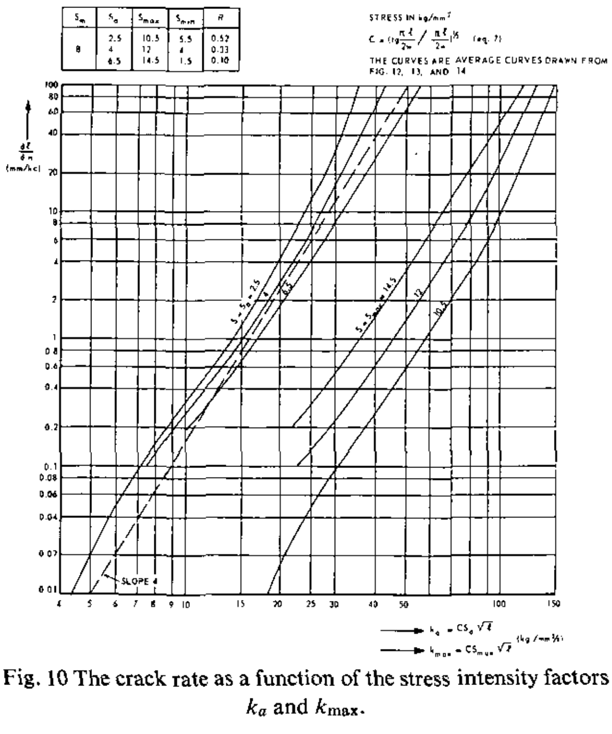

Fig. 10 The crack rate as a function of the stress intensity factors k_a and k_{max}.

the crack, at both S_{max} and S_{min}. The result that eq. (8) does hold for a constant R-value is then considered as a further confirmation of the applicability of the concept of the stress intensity factor.

The implications of eq. (8) for the effect of sheet width on the crack rate should be deduced from eqs (6) and (7). The correction factor C (eq. 7) has been plotted in fig. 11 as a function of the relative crack length l/w. Crack growth data were obtained up to a maximum of $l/w \sim 0.7$ for the lowest S_a. For the majority of data l/w was sufficiently small to yield a correction factor C which is only a few percent above unity. This implies that, according to the concept of the stress intensity factor a negligible effect of the sheet width on the crack rate should be expected, except for large l/w values. This is clearly confirmed in figs 7, 8 and 9. In figs 12, 13 and 14 dl/dn has been plotted as a function

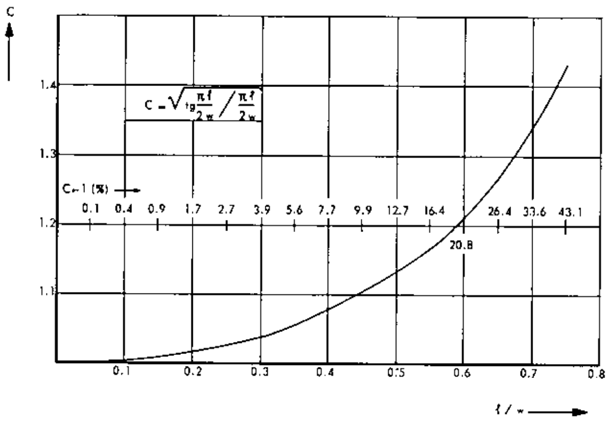

Fig. 11 The correction factor for the effect of sheet width.

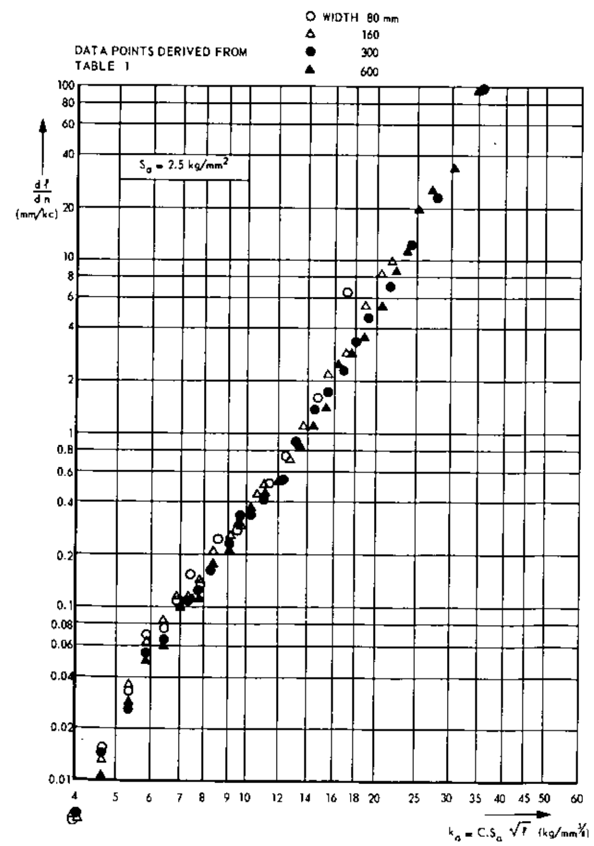

Fig. 12 The crack rate as a function of the stress intensity factor for $S_a = 2.5$ kg/mm².

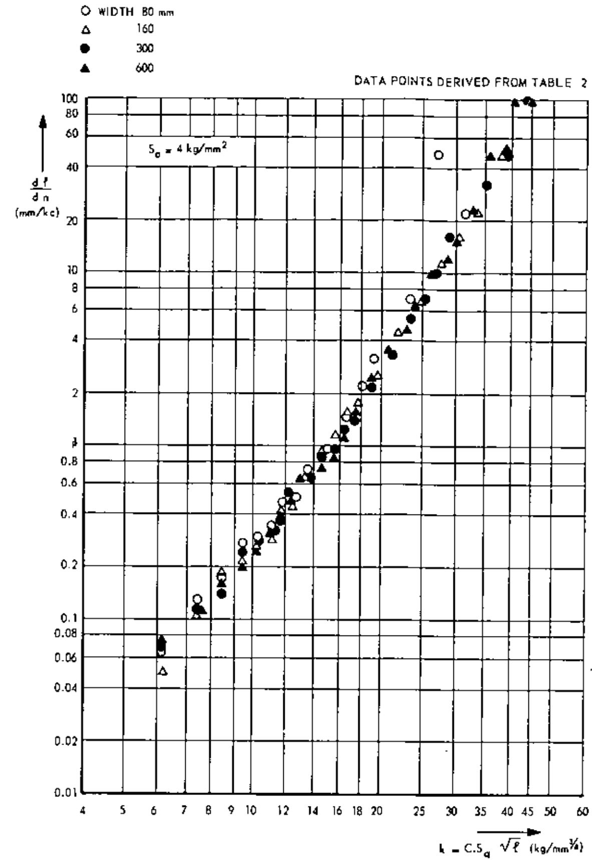

Fig. 13 The crack rate as a function of the stress intensity factor for $S_a = 4$ kg/mm².

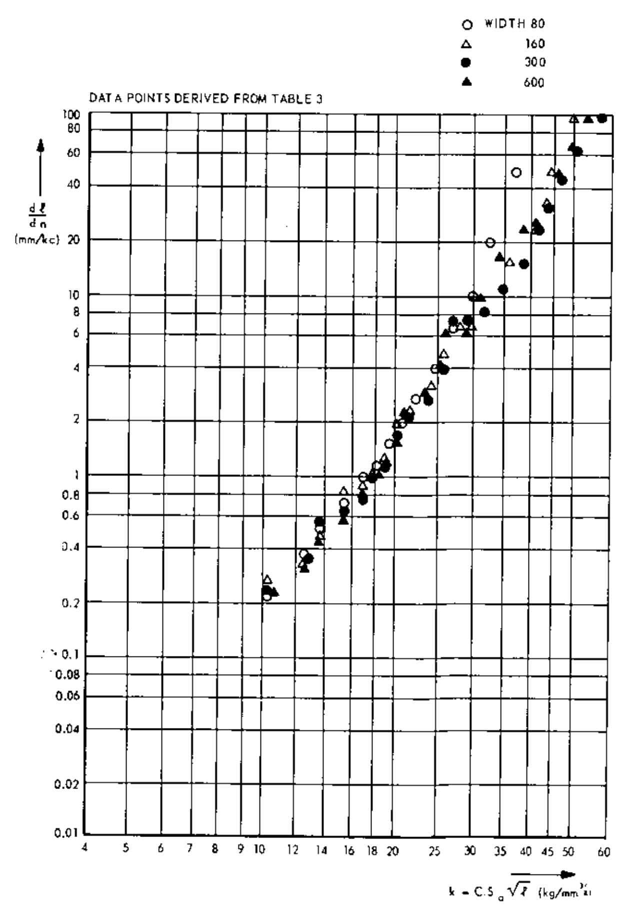

Fig. 14 The crack rate as a function of the stress intensity factor for $S_a = 6.5$ kg/mm².

of the stress intensity factor including the correction factor C (eq. 7). If the correction factor had not been applied these graphs would have looked like figs 7, 8 and 9, respectively (since $\log S_a\sqrt{l} = \log S_a + \frac{1}{2}\log l$). The much better convergence to a single curve in figs 12, 13 and 14 as compared with figs 7, 8 and 9, respectively, shows that the application of the correction factor C implies a noticeable improvement of the correlation, which in itself can be considered as a substantiation of the usefulness of the stress intensity factor concept.

Another indication of the validity of the stress intensity factor concept offered by the present tests stems from the fractographic observations. The *transition of the fracture surface from the tensile mode* to the shear mode occurred for a certain stress amplitude at a crack length, l_{tr}, which did not depend on the specimen width (table 4 and section 3.2). This transition is associated with a change from a state of plane strain to a state of plane stress (see ref. 20) and since the stress distribution around the tip of a crack according to the stress intensity factor is so little dependent on the sheet width, l_{tr} should indeed be independent of this width.

4.3 *The NACA theory*

In ref. 13 Mc Evily and Illg proposed a theory based on the idea that a crack may be replaced by an elliptic hole with the major axis equal to the crack length and some "effective" tip radius. For this hole an "effective" stress concentration factor K_e is calculated adopting the Neuber correction for stress gradient effects. It is then assumed that the crack rate is a function of the product of K_e and the net stress S_n on the cracked specimen, or in other words a function of the effective peak stress at the tip of the crack. This idea in a somewhat different way was also adopted by Welbourne (ref. 24).

It has been shown (refs 2, 16 and 17) that this theory will lead to approximately the same results as the stress intensity factor theory, i.e. if test results satisfy one of the two theories they will also approximately satisfy the other one. The present authors then prefer the use of the stress intensity factor in view of its more rational background.

4.4 *The Weibull theory*

Starting from some fairly arbitrary assumptions, Weibull (refs 22 and 23) arrives at the conclusion that the crack rate, expressed as $d(l/w)/dn$, as a function of l/w should obey the relation

$$d(l/w)/dn = C_1 S^{\beta}/(1-l/w)^{\beta} \qquad (9)$$

C_1 and β being constants. In other words the crack propagation on a non-dimensional basis (l/w) should be independent of the specimen size. This conclusion and the relation in eq. (9) are checked in figs 15, 16 and 17 by plotting $d(l/w)/dn$ against $1-l/w$ on a double-log scale. According to eq. (9) all the curves in each figure should coincide, and they should be straight lines. Both trends are contradicted by the graphs. On a non-dimensional basis (l/w) the crack rate is considerably faster in the larger specimens.

Weibull has reported results of tests on 2024-T3 Alclad sheet specimens tested at $R=0$ for which the stress was decreased during the crack propagation in order to have a constant net stress (S_{net}) on the uncracked area. Since $S = S_{net}\,(1-l/w)$ eq. (9) then predicts a constant crack rate which he indeed found. For such a test the stress intensity factor k_w is:

$$\begin{aligned} k_w = C\,S\sqrt{l} &= \left(\frac{\operatorname{tg}\pi l/2w}{\pi l/2w}\right)^{\frac{1}{2}} S_{net}(1-l/w)\sqrt{l} = \\ &= \frac{S_{net}\sqrt{w}}{\sqrt{\pi/2}}(1-l/w)(\operatorname{tg}\pi l/2w)^{\frac{1}{2}} = \\ &= C_2\,w^{\frac{1}{2}} f(l/w) \end{aligned} \qquad (10)$$

Values for the function $f(l/w)$ are tabulated below.

l/w	0.1	0.2	0.3	0.4	0.5	0.6	0.7
$f(l/w)$	0.36	0.46	0.50	0.51	0.50	0.47	0.42

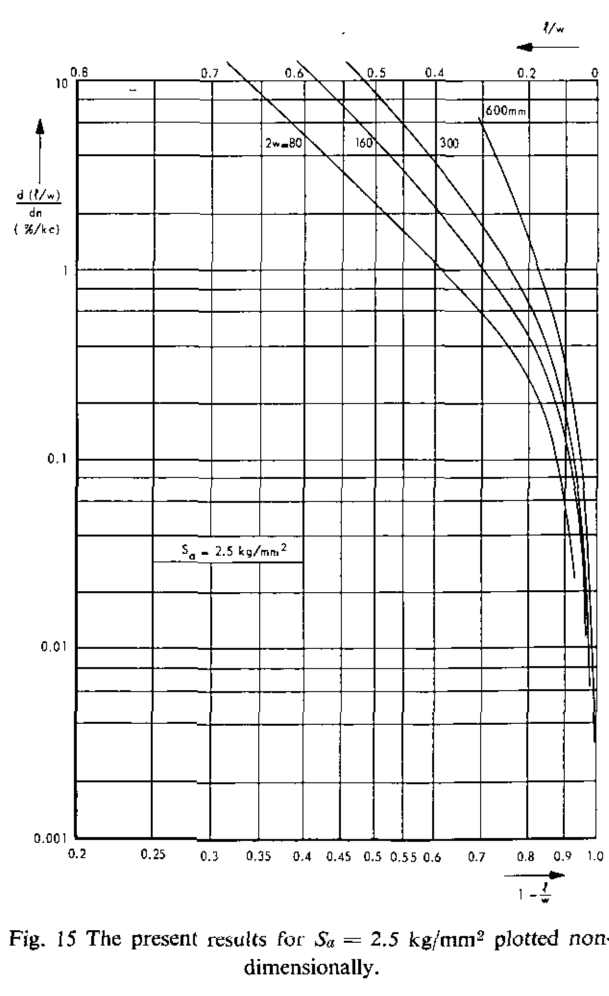

Fig. 15 The present results for $S_a = 2.5$ kg/mm² plotted non-dimensionally.

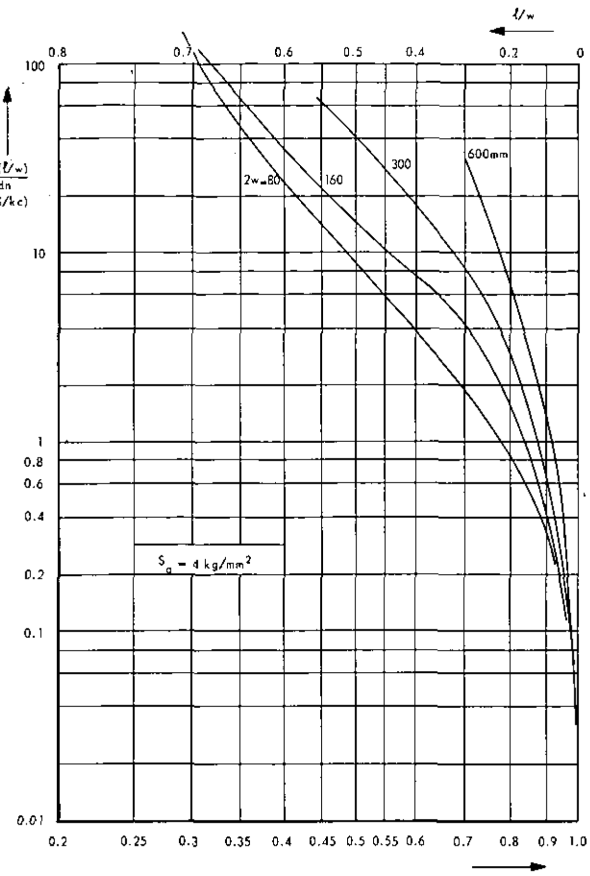

Fig. 16 The present results for S_a = 4 kg/mm² plotted non-dimensionally.

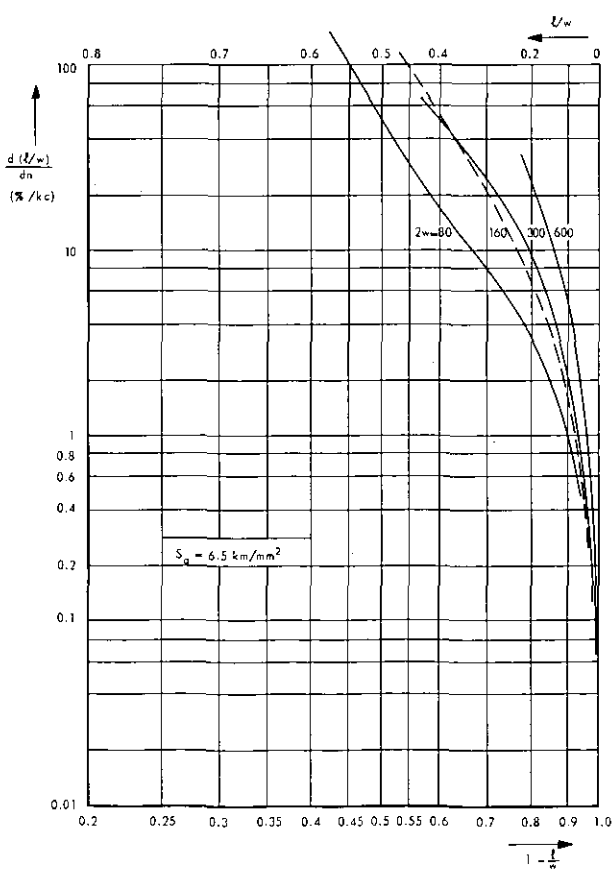

Fig. 17 The present results for S_a = 6.5 kg/mm² plotted non-dimensionally.

Weibull considers relatively large cracks in the range from 20% to 60% of the sheet width and in this range the variation of $f(l/w)$ is very small, viz. 0.46 to 0.51. Consequently, k is approximately constant and an approximately constant crack rate is predicted by the stress intensity factor concept. A similar reasoning was presented by Barrois (ref. 2) using a width correction proposed by Dixon (see section 4.5) instead of eq. (7), whereas Liu (ref. 12) showed the compatibility between the Weibull results and the stress intensity factor concept in a slightly different way.

Similar tests ($R \neq 0$) as performed by Weibull were carried out at this laboratory (ref. 3). The crack rate did not appear to be fully constant, but varied in accordance with $f(l/w)$ as tabulated above, i.e. it showed a weak maximum at $l/w = 0.4$.

Although it now seems that it is not necessarily curious that Weibull found a constant crack rate in his tests, it is surprising that he found $\mathrm{d}(l/w)/\mathrm{d}n$ at the same l/w to be independent of w, which is fully contradicted by the present test results (figs 15, 16 and 17). In ref. 2 Barrois has pointed out that, if eq. (8) is of the form

$$\mathrm{d}l/\mathrm{d}n = C_3 k^m \,, \tag{11}$$

the width effect as found by Weibull requires $m=2$ which easily follows if eq. (10) is substituted into the above relation. He also showed that $m=2$ was indeed the most satisfactory value for Weibull's crack propagation data, whereas $m=4$, a value also proposed by Paris (ref. 15) was in better agreement with results of other investigations. Fig. 10 shows that eq. (11) with $m=4$ is a reasonable approximation for the present results (with C_3 depending on R, see section 4.2).

The present section will be completed with a summary of the differences in testing circumstances between Weibull's tests and the present investigation. (1) Weibull performed his tests with a decreasing load amplitude to maintain a constant net stress. The decrease was applied stepwise, i.e. after certain amounts of crack extension, and this might have had a decelerating effect on the crack growth (refs 18 and 19). This effect might have been larger for the larger specimen in view of the larger plastic zone for the same l/w. (2) Weibull's tests were performed at $R=0$ for one value of S_{max} only, viz. $S_{max,net} = 12$ kg/mm². (3) His specimens were smaller (width 22.8, 45.5, 68.5 and 170.6 mm; present test series 80, 160, 300 and 600 mm). (4) Weibull considered relatively large cracks (large l/w values). (5) Barrois (ref. 2) indicated that Weibull's crack rates were low as compared with those of others, which may be explained by the first item mentioned above.

4.5 *Correction factors for the sheet width*

In section 5.2 the Irwin correction factor C, eq. (7), was presented as a factor indicating the stress-increasing effect around the tip of the crack, caused by the finite width of the sheet. Other factors have been proposed in the literature and were recently discussed by Dixon (ref. 7) and Barrois (ref. 2). It turns out that the Irwin factor and a factor proposed by Dixon (ref. 7) are practically the same and according to measurements of Dixon should be preferred over some other proposed factors. The Dixon factor reads

$$C=(1-l^2/w^2)^{-\frac{1}{2}} \tag{12}$$

4.6 *Test results from other investigations*

Systematic investigations on the effect of sheet width on crack propagation are far from abundant. The results of Weibull were already discussed in section 4.4. Another investigation was performed by Mc Evily and Illg (ref. 13) on sheet specimens and some information on stiffened panels was presented in ref. 19. Mc Evily and Illg performed tests on specimens of bare 2024-T3 and 7075-T6 sheet material with two different sizes, viz. width 2" and width 12" ($\sim$50 mm and $\sim$300 mm, respectively). The tests were performed at zero stress ratio ($R=0$ or $S_{\min}=0$). From the tables in ref. 13 the average crack rates in the intervals $2l=0{,}2-0.3$, $0.3-0.4$, $0.4-0.5$, $0.5-0.6$, $0.6-0.8$ and $0.8-1.0$ inches were calculated and plotted in fig. 18 as a function of the mean crack length of the intervals. This is the same procedure as adopted for the present tests in figs 7, 8 and 9 (see section 3.1). Data points in fig. 18 are average results of two tests. Fig. 18 shows larger and less systematic differences between the two sizes. At low values of the crack length there is a tendency for higher crack rates in the larger specimen which is opposite to the trend of the present investigation. For larger values of the crack length the reversed tendency is observed for several values of $S_{\max}$ but not for all values, whereas this was more clearly noticed in the present investigation. Although the differences in the crack rates of the large and the small specimens in fig. 18 in general do not exceed a facor 1.5, they are not fully consistent with the present investigation.

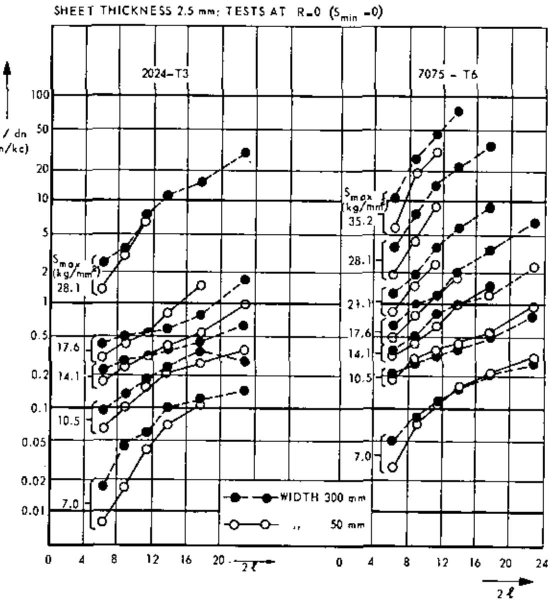

Fig. 18 Crack rates observed in NACA tests (ref. 13) on aluminium alloy sheet specimens of different widths.

In ref. 19 a comparison was made between the crack rates in stiffened panels with widths of 3 and 11 stringer pitches, pitch 130 mm. The material of the skin and the hat stringers was 7075-T6. The comparison could be made for one load amplitude only ($S_a \sim 3$ kg/mm²). The crack rates dl/dn at $l=20$ mm and $l=40$ mm were practically the same in the panels with 3 and 11 stringers. This should not be an unexpected result by now, since the effect of width for an unstiffened panel is small if not negligible. Hence, if the crack in an unstiffened panel is unconscious of the width of the panel in which it is growing it might well be expected that a stiffening will further stimulate this unconsciousness.

4.7 *Concluding remarks*

From the previous sections it may be concluded that the effect of sheet width on the crack propagation rate (in millimeters per cycle) is small and practically negligible as long as the crack length is not too large, say not larger than 30% of the sheet width. This seems to be a conclusion of practical significance, since it implies that in adopting crack rate data from other sources one need not worry about a size effect. Secondly, it implies that crack propagation data obtained on structural panels will apply to the complete structure into which the panel is integrated (provided that loading conditions are the same).

The main reason for focussing attention on the concept of the stress intensity factor was that this concept has a rational background, that it is confirmed by experimental evidence and that it describes quite well the small width effect as found in the present investigation. In other words, one might flatter oneself that this effect is reasonably well understood which is a prerequisite for generalizing the conclusions in the preceding paragraph.

Although the width effect on fatigue crack propagation is small, generalizing of data from various sources is not justified in view of several other parameters which systematically affect the crack rate. Recent investigations of this laboratory on sheet material of aluminium alloys have shown a considerable influence of the mean stress S_m (or the stress ratio R) (ref. 4), and systematic influences of the ductility (ref. 6) and the sheet thickness (ref. 5). Crack rates were consistently higher in the alloy heat-treated to a high strength and a low ductility and also systematically higher in the thicker sheet material. Finally, crack propagation tests on 2024-T3 Alclad sheet material from six different manufacturers (results still to be published) have also revealed consistent differences to a maximum ratio of about two, although the static properties were virtually the same.

In view of the foregoing it should be recommended to perform some crack propagation tests in the case when crack rate data are required for a certain project, and to perform these tests on the material which actually will be used, i.e. the same thickness, the same heat-treatment, the same manufacturer etc. Such tests can be performed on simple specimens as used in the present investigation and although the width should not be too small a width in the order of 160 mm may be sufficient. This procedure will be more reliable than borrowing crack rate data from the literature and need not be costly. Some extrapolation of the data so obtained to other values of S_m and S_a can be made by adopting the trends such as found in ref. 4, or, if R is kept constant, by employing the stress intensity factor. It even seems worthwhile to standardize a sheet specimen for the above purpose. A specimen with a width of 160 mm, a length of 400 mm and a central notch as shown in fig. 1 is proposed here as a compromise for size, although it is recognized that the actual dimensions are not too important for the purpose considered.

5 Conclusion

Crack propagation tests on 2024-T3 Alclad specimens with widths of 80, 160, 300 and 600 mm were carried out at $S_m=8$ kg/mm^2 and $S_a=2.5$, 4 and 6.5 kg/mm^2. The results and a comparison with crack propagation theories have led to the following conclusions:

1. The effect of the sheet width on the crack propagation rate (in millimeters per cycle) was small and practically negligible as long as the crack was not larger than about 30% of the sheet width.
2. The small effect of the sheet width was well predicted by the stress intensity factor concept. It was in complete disagreement with Weibull's theory.
3. It is thought that the first conclusion will apply to other aluminium alloys and also to stiffened panels of these alloys. This may be important with respect to panel testing for an actual aircraft structure.
4. Although the width effect seems to be relatively unimportant for fatigue-crack propagation in aluminium alloy sheet material generalizing of crack propagation data is not always justified in view of other parameters than the sheet width, such as the mean stress, the sheet thickness, the loading frequency, the heat treatment and the manufacturer. Recent tests have shown systematic influences of these factors.
5. For design purposes, it should be recommended to perform some simple crack propagation tests, rather than adopting crack rate data from the literature.

6 References

[1] Bahar, L. J., Beer, F. P., Erdogan, F., Paris, P.C., Sih, G. C. and Tuncel, O., Fracture Mechanics Research at Lehigh University, 1960-61. Document D6-7960.

[2] Barrois, W., Critical study on fatigue crack propagation. AGARD Report 412, June 1962.

[3] Broek, D., de Rijk, P. and Sevenhuysen, P. J., The transition of fatigue cracks in alclad sheet. NLR-TR M.2100, Nov. 1962.

[4] Broek, D. and Schijve, J., The influence of the mean stress on the propagation of fatigue cracks in aluminium alloy sheet. NLR-TR M.2111, Jan. 1963.

[5] Broek, D. and Schijve, J., The effect of sheet thickness on the fatigue-crack propagation in 2024-T3 Alclad sheet material. NLR-TR M.2129, April 1963.

[6] Broek, D., Schijve, J. and Nederveen, A., The effect of heat treatment on the propagation of fatigue cracks in light alloy sheet material. NLR Report M.2134, May 1963.

[7] Dixon, J. R., Stress distribution around edge slits in a plate loaded in tension; the effect of finite width of plate. NEL Report No. 13, Nov. 1961.

[8] Donaldson, D. R. and Anderson, W. E., Crack propagation behaviour of some airframe materials. Proc. Propagation *Symposium, Cranfield 1961, Vol. II, p. 375.*

[9] Inglis, C. E., Stress in a plate due to the presence of cracks and sharp corners. Trans. Inst. of Naval Architects, Vol. 55, part 1, p. 219, 1913.

[10] Irwin, G. R., Fracture. Encyclopaedia of Physics, Vol. VI, p. 565. Springer-Verlag, 1958.

[11] Koiter, W. T., An infinite row of collinear cracks in an infinite elastic sheet. Ingenieur-Archiv, Vol. 28, p. 168, 1959.

[12] Liu, H. W., Fatigue crack propagation and the stresses and strains in the vicinity of a crack. Appl. Mat. Research, Vol. 3, p. 229, Oct. 1964.

[13] Mc Evily, A. J. and Illg, W., The rate of fatigue-crack propagation in two aluminium alloys. NACA TN 4394, Sept. 1958.

[14] Paris, P. C., Gomez, M. P. and Anderson, W. E., A rational analytic theory of fatigue. The Trend in Engineering, vol. 13, p. 9, 1961.

[15] Paris, P., The growth of cracks due to variations in load. Doctor Thesis, Leligh University, 1962.

[16] Paris, P. and Erdogan, F., A critical analysis of crack propagation laws. Trans. ASME, Series D., Vol. 85, p. 528, Dec. 1963.

[17] Schijve, J., Broek, D. and de Rijk, P., The effect of the frequency of an alternating load on the crack rate in a light alloy sheet. NLR Report M.2092, Sep. 1961.

[18] Schijve, J., Broek, D. and de Rijk, P., Fatigue crack propagation under variable-amplitude loading. NLR Report M.2094, Dec. 1961.

[19] Schijve, J., Fatigue crack propagation in light alloy sheet material and structures. Advances in Aero. Sc., vol. 3, p. 387, Pergamon Press, 1962.

[20] Schijve, J., Analysis of the fatigue phenomenon in aluminium alloys. NLR-TR M. 2122, April 1964.

[21] Sneddon, I. N., The distribution of stress in the neighbourhood of a crack in an elastic solid. Proc. of the Royal Soc. of London, Series A., Vol. 18, p. 229, 1946.

[22] Weibull, W., The propagation of fatigue cracks in light-alloy plates. SAAB TN 25, Jan. 1954.

[23] Weibull, W., The effect of size and stress history on fatigue crack initiation and propagation. Proc. Crack Propagation Symposium, Cranfield 1961, Vol. II, p. 271.

[24] Welbourne, E. R., An analysis of fatigue crack propagation in sheet material using familiar concepts. Current Aero. Fatigue Problems, Proc. Rome Symposium 1963, p. 265, Pergamon Press 1965.

[25] Westergaard, H. M., Bearing pressure and cracks. J. of Appl. Mech., Trans. ASME, Vol. 61, p. A49, 1939.

TABLE 1

Crack propagation records for $S_a = 2.5$ kg/mm^2

width (mm)				80					160		
specimen	6B2L	6B2R	6BIL	6BIR			7B1	3E2	6E2		
$l_i - l_j$ (mm)			Δn (kc)		$\overline{\Delta n}$ (kc)	$\Sigma\overline{\Delta n}$ (kc)		Δn (kc)		$\overline{\Delta n}$ (kc)	$\Sigma\overline{\Delta n}$ (kc)
2– 3	154.2	161.4	84.0	142.3	135.7	—	111.2	136.5	150.0	132.5	—
3– 4	51.4	60.2	61.5	69.2	60.6	60.6	39.4	104.8	66.5	70.2	70.2
4– 5	29.2	20.8	23.7	38.3	28.0	88.6	21.6	28.4	31.8	27.2	97.4
5– 6	10.4	22.0	13.8	16.2	14.3	102.9	11.2	18.1	16.5	15.3	112.7
6– 7	10.5	15.9	13.6	12.6	13.2	116.1	10.7	12.5	11.6	11.6	124.3
7– 8	10.4	7.9	7.2	10.0	8.9	125.0	8.4	8.5	9.9	9.0	133.3
8– 9	6.7	2.9	6.5	8.6	6.2	131.2	7.1	8.0	8.8	8.0	141.3
9–10	6.1	7.3	6.5	9.0	7.2	138.4	5.2	8.1	6.2	6.5	147.8
10–12	9.6	7.0	8.3	8.7	8.4	146.8	8.5	9.5	11.1	9.7	157.5
12–14	7.1	6.5	6.6	8.2	7.1	153.9	6.3	7.7	7.9	7.1	164.6
14–16	4.4	5.3	4.7	5.4	4.9	158.8	5.3	7.1	7.2	6.6	171.2
16–18	3.0	3.9	4.1	4.5	3.9	162.7	3.9	4.6	5.2	4.5	175.7
18–20	2.4	3.2	2.1	2.9	2.6	165.3	3.5	4.2	4.0	3.9	179.6
20–25	3.0	2.9	3.1		3.0	168.3	5.8	7.7	6.9	6.8	186.4
25–30	0.8	1.0	0.7		0.8	169.1	3.4	5.0	4.9	4.4	190.8
30–35							2.1	1.9	2.9	2.3	193.1
35–40							1.4	1.9	1.8	1.7	194.8
40–45							0.7	1.1	1.0	0.9	195.7
45–50							0.5	0.8	0.5	0.6	196.3
50–60								0.5		0.5	196.8

Crack propagation records for $S_a = 2.5$ kg/mm^2

width (mm)			300					600		
specimen	3B	6B	7B			3	6	7		
$l_i - l_j$ (mm)		Δn (kc)		$\overline{\Delta n}$ (kc)	$\Sigma\overline{\Delta n}$ (kc)		Δn (kc)		$\overline{\Delta n}$ (kc)	$\Sigma\overline{\Delta n}$ (kc)
2–3	153.6	153.2	134.0	124.6	—	148.9	139.9	171.7	151.9	—
3–4	92.2	45.9	68.2	68.8	68.8	99.5	98.3	53.6	87.1	87.1
4–5	33.9	33.9	41.3	36.3	105.1	32.7	29.0	31.5	32.1	119.2
5–6	17.0	19.9	18.2	18.4	123.4	23.0	18.5	19.8	20.4	139.6
6–7	15.4	14.9	—	15.2	138.7	15.1	14.6	20.4	16.5	156.1
7–8	8.1	8.8	—	8.4	147.1	9.4	7.3	12.2	9.7	165.8
8–9	8.2	9.0	9.3	8.8	155.9	8.3	8.4	8.6	8.4	174.2
9–10	6.9	9.0	6.9	7.6	163.5	8.9	7.2	8.0	8.0	182.2
10–12	11.4	10.6	12.3	11.4	174.9	11.1	10.0	10.0	10.4	192.6
12–14	9.4	9.3	9.8	8.0	182.9	9.4	8.8	8.2	8.8	201.4
14–16	5.4	8.1	4.6	6.0	188.9	6.7	7.1	7.1	7.0	208.4
16–18	5.9	—	5.9	5.9	194.8	6.2	4.7	6.0	5.6	214.0
18–20	4.6	—	4.6	4.6	199.4	4.4	4.3	4.4	4.4	218.4
20–25	8.0	—	9.0	8.5	207.9	9.2	8.2	9.0	8.8	227.2
25–30	5.4	5.6	5.2	5.4	213.3	5.8	5.4	5.2	5.5	232.7
30–35	3.1	3.9	3.7	3.6	216.9	4.1	3.8	4.2	4.0	236.7
35–40	2.6	2.8	3.0	2.8	219.7	3.1	3.5	3.0	3.2	239.9
40–45	2.0	2.2	2.0	2.1	221.8	3.0	2.0	1.8	2.1	242.0
45–50	1.5	1.5	1.5	1.5	223.3	1.6	1.5	2.0	1.7	243.7
50–60	1.9	2.4	2.0	2.1	225.4	2.9	2.5	2.4	2.6	246.3
60–70	1.3	1.3	1.3	1.3	226.7	1.9	1.7	1.6	1.7	248.0
70–80	0.8	0.9	0.7	0.8	227.5	1.3	0.8	1.3	1.1	249.1
80–90	0.4	0.4	0.4	0.4	227.9	0.9	0.8	0.8	0.8	249.9
90–100	0.15	0.1	0.1	0.1	228.0	0.6	0.4	0.5	0.5	250.4
100–120	0.1	0.1		0.1	228.1	0.5	0.4	0.4	0.4	250.8
120–140						0.3	0.1	0.4	0.3	251.1
140–160						0.1	0.1	0.1	0.1	251.2

TABLE 2

Crack propagation records for $S_a = 4$ kg/mm²

width (mm)	80						160					
specimen	5EIL	5EIR	2EIL	2EIR			3B2	5B1	1F2	1E2		
$l_i - l_j$ (mm)	Δn (kc)				$\overline{\Delta n}$ (kc)	$\Sigma\overline{\Delta n}$ (kc)	Δn (kc)				$\overline{\Delta n}$ (kc)	$\Sigma\overline{\Delta n}$ (kc)
2–3	18.9	21.7	10.9	13.6	16.2	—	21.4	15.2	12.9	19.0	17.1	—
3–4	6.8	9.8	6.5	6.5	7.1	7.1	9.8	10.2	10.5	7.6	9.5	9.5
4–5	5.3	6.7	5.8	5.5	5.8	12.9	4.3	4.8	5.9	6.3	5.3	14.8
5–6	4.1	3.1	3.4	4.0	3.7	16.6	4.2	5.7	3.4	4.8	4.5	19.3
6–7	3.2	4.1	3.2	3.3	3.4	20.0	3.5	2.3	3.5	3.5	3.2	22.5
7–8	3.1	3.2	2.8	2.3	2.8	22.8	2.1	2.8	5.3	2.5	3.2	25.7
8–9	2.4	2.2	2.1	2.2	2.2	25.0	1.9	2.4	2.5	2.6	2.4	28.1
9–10	2.0	3.0	1.9	1.7	2.0	27.0	1.9	2.5	3.1	1.9	2.3	30.4
10–12	3.0	2.8	2.5	2.3	2.7	29.7	2.6	3.3	2.5	3.3	2.9	33.3
12–14	2.0	2.6	2.0	1.9	2.1	31.8	2.1	2.3	1.6	2.3	2.1	35.4
14–16	1.4	1.3	1.4	1.2	1.3	33.1	1.5	2.0	1.2	1.8	1.6	37.0
16–18	0.8	1.2	1.0	0.6	0.9	34.0	1.1	1.5	0.6	1.5	1.2	38.2
18–20	0.6	0.6	0.7	0.5	0.6	34.6	0.9	1.2	1.2	1.2	1.1	39.3
20–25	0.8	0.8	0.7	0.6	0.7	35.3	1.5	2.4	2.0	1.7	1.9	41.2
25–30		0.2	0.1	0.1	0.1	35.4	1.1	1.2	1.1	0.9	1.1	42.3
30–35							0.6	0.8	0.8	0.6	0.7	43.0
35–40							0.4	0.4	0.5	0.4	0.4	43.4
40–45							0.2	0.3	0.3	0.3	0.3	43.7
45–50							0.2	0.2	0.2	0.1	0.2	43.9
50–60							0.1	0.1	0.1		0.1	44.0

Crack propagation records for $S_a = 4$ kg/mm²

width (mm)	300					600				
specimen	1B	2B	5B			1	2	5		
$l_i - l_j$ (mm)	Δn (kc)			$\overline{\Delta n}$ (kc)	$\Sigma\overline{\Delta n}$ (kc)	Δn (kc)			$\overline{\Delta n}$ (kc)	$\Sigma\overline{\Delta n}$ (kc)
2–3	14.8	13.2	18.5	15.5	—	13.4	13.0	12.6	13.0	—
3–4	9.7	9.4	7.0	8.7	8.7	9.4	9.5	8.4	9.1	9.1
4–5	6.4	7.6	6.4	6.8	15.5	5.7	6.4	5.6	5.9	15.0
5–6	5.1	3.2	4.5	4.3	19.8	4.9	4.6	5.3	4.9	19.9
6–7	3.6	3.7	3.3	3.5	23.3	3.7	3.4	3.8	3.6	23.5
7–8	3.3	2.7	2.8	2.9	26.2	2.8	2.7	2.8	2.8	26.3
8–9	3.1	2.5	2.3	2.6	28.8	2.3	2.6	2.9	2.6	28.9
9–10	1.7	1.5	2.5	1.9	30.7	2.1	2.1	2.2	2.1	31.0
10–12	3.1	3.2	3.0	3.1	33.8	2.8	3.2	3.6	3.2	34.2
12–14	2.5	2.2	2.2	2.3	36.1	2.6	2.5	2.9	2.7	36.9
14–16	2.2	1.9	2.1	2.1	38.2	2.1	2.2	2.3	2.2	39.1
16–18	1.4	1.5	1.3	1.4	39.6	1.7	1.6	1.6	1.6	40.7
18–20	1.6	1.2	1.2	1.3	40.9	1.1	1.4	1.4	1.3	42.0
20–25	2.3	2.1	2.2	2.2	43.1	2.0	2.3	2.4	2.2	44.2
25–30	1.5	1.3	1.3	1.4	44.5	1.4	1.4	1.5	1.4	45.6
30–35	0.9	0.8	0.9	0.9	45.4	0.9	0.9	1.1	1.0	46.6
35–40	0.8	0.7	0.7	0.7	46.1	0.6	0.6	0.8	0.7	47.3
40–45	0.4	0.5	0.6	0.5	46.6	0.4	0.5	0.6	0.5	47.8
45–50	0.4	0.3	0.3	0.3	46.9	0.3	0.4	0.4	0.4	48.2
50–60	0.5	0.4	0.4	0.4	47.3	0.6	0.5	0.6	0.6	48.8
60–70	0.3	0.3	0.2	0.3	47.6	0.3	0.4	0.4	0.4	49.2
70–80	0.2	0.2	0.1	0.2	47.8	0.2	0.2	0.3	0.2	49.4
80–90	0.1	0.1		0.1	47.9	0.15		0.2	0.2	49.6
90–100						0.1		0.1	0.1	49.7
100–120						0.1		0.1	0.1	49.8

TABLE 3

Crack propagation records for $S_a = 6.5$ kg/mm^2

width (mm)	80						160					
specimen	4E1	8B2	4B1	4B2			4E2	8B1	1F1	1D1		
$l_i - l_j$ (mm)			Δn (kc)		$\overline{\Delta n}$ (kc)	$\Sigma\overline{\Delta n}$ (kc)			Δn (kc)		$\overline{\Delta n}$ (kc)	$\Sigma\overline{\Delta n}$ (kc)
2–3	4.8	4.7	3.8	5.2	4.6	—	3.6	3.3	4.0	3.6	3.6	—
3–4	2.8	2.9	2.7	1.8	2.6	2.6	2.7	2.7	3.0	2.6	2.8	2.8
4–5	1.9	1.8	1.8	2.0	1.9	4.5	1.7	1.7	2.6	2.0	2.0	4.8
5–6	1.4	1.4	1.6	1.2	1.4	5.9	1.6	1.2	0.6	1.1	1.2	6.0
6–7	1.2	1.0	0.9	0.9	1.0	6.9	1.2	1.1	1.0	1.0	1.1	7.1
7–8	0.8	0.8	0.7	0.8	0.8	7.7	0.9	0.9	0.8	0.8	0.9	8.0
8–9	0.7	0.8	0.6	0.5	0.6	8.3	0.8	0.5	0.8	0.6	0.7	8.7
9–10	0.5	0.4	0.5	0.5	0.5	8.8	0.6	0.5	0.5	0.5	0.5	9.2
10–12	0.7	0.8	0.7	0.7	0.7	9.5	0.9	0.9	0.9	0.7	0.8	10.0
12–14	0.4	0.5	0.4	0.5	0.5	10.0	0.7	0.6	0.6	0.4	0.6	10.6
14–16	0.3	0.3	0.3	0.2	0.3	10.3	0.6	0.4	0.5	0.3	0.4	11.0
16–18	0.2	0.1	0.2	0.2	0.2	10.5	0.4	0.3	0.3	0.3	0.3	11.3
18–20	0.1	0.1	0.1	0.1	0.1	10.6	0.3	0.3	0.3	0.2	0.3	11.6
20–25	0.1		0.1	0.1	0.1	10.7	0.5	0.4	0.4	0.3	0.4	12.0
25–30							0.3	0.3	0.4	0.2	0.3	12.3
30–35							0.2	0.2	0.1	0.2	0.2	12.5
35–40							0.2		0.1	0.1	0.1	12.6
40–45							0.1		0.05	0.05	0.05	12.65

Crack propagation records for $S_a = 6.5$ kg/mm^2

width (mm)	300					600			
specimen	4B	8B	8E			4	8		
$l_i - l_j$ (mm)		Δn (kc)		$\overline{\Delta n}$ (kc)	$\Sigma\overline{\Delta n}$ (kc)		Δn (kc)	$\overline{\Delta n}$ (kc)	$\Sigma\overline{\Delta n}$ (kc)
2–3	4.8	4.5	3.2	4.2	—	4.7	4.7	4.7	—
3–4	3.1	3.1	2.2	2.8	2.8	3.4	2.5	2.9	2.9
4–5	1.8	1.8	2.0	1.9	4.7	1.8	2.6	2.2	5.1
5–6	1.6	1.5	1.6	1.6	6.3	1.6	1.8	1.7	6.8
6–7	1.3	1.3	1.4	1.3	7.6	1.2	1.2	1.2	8.0
7–8	0.8	0.9	0.9	0.9	8.5	1.0	0.8	0.9	8.9
8–9	0.8	0.8	0.8	0.8	9.3	0.7	0.7	0.7	9.6
9–10	0.5	—	0.6	0.6	9.9	0.6	0.5	0.6	10.2
10–12	0.9	—	1.0	0.9	10.8	1.1	0.8	0.9	11.1
12–14	0.7	0.7	0.6	0.7	11.5	0.5	0.6	0.6	11.7
14–16	0.5	0.4	0.5	0.5	12.0	0.5	0.5	0.5	12.2
16–18	0.4	0.3	0.3	0.3	12.3	0.4	0.2	0.3	12.5
18–20	0.3	0.3	0.4	0.3	12.6	0.3	0.3	0.3	12.8
20–25	0.6	0.5	0.6	0.6	13.2	0.5	0.4	0.5	13.3
25–30	0.4	0.3	0.4	0.4	13.6	0.3	0.3	0.3	13.6
30–35	0.3	0.2	0.3	0.3	13.9	0.2	0.1	0.2	13.8
35–40	0.2	0.2	0.2	0.2	14.1	0.2	0.2	0.2	14.0
40–45	0.15	0.15	0.15	0.15	14.25	0.15	0.15	0.15	14.15
45–50	0.1	0.1	0.1	0.1	14.35	0.1	0.1	0.1	14.25
50–60	0.15	0.15	0.15	0.15	14.5	0.15	0.15	0.15	14.4
60–70	0.1		0.1	0.1	14.6	0.1	0.1	0.1	14.5

TABLE 4

Effect of specimen width on the crack length at which the transition from tensile mode to shear mode is completed (l_{tr}).

Width (mm)	80	160	300	600		
S_a (kg/mm^2)		l_{tr} (mm)			Mean[1] l_{tr}	dl/dn[2] (mm/kc)
2.5	20	19	20.5	20	20	0.6
4	13	10.5	11.5	12	12	0.7
6.5	8	7.5	7.5	8	8	1.2

[1]) mean for all values of the specimen width. [2]) crack rate corresponding to the crack length in the preceding column.